INFORMATION TO USERS

This manuscript has been reproduced from the microfilm master. UMI films the text directly from the original or copy submitted. Thus, some thesis and dissertation copies are in typewriter face, while others may be from any type of computer printer.

The quality of this reproduction is dependent upon the quality of the copy submitted. Broken or indistinct print, colored or poor quality illustrations and photographs, print bleedthrough, substandard margins, and improper alignment can adversely affect reproduction.

In the unlikely event that the author did not send UMI a complete manuscript and there are missing pages, these will be noted. Also, if unauthorized copyright material had to be removed, a note will indicate the deletion.

Oversize materials (e.g., maps, drawings, charts) are reproduced by sectioning the original, beginning at the upper left-hand corner and continuing from left to right in equal sections with small overlaps. Each original is also photographed in one exposure and is included in reduced form at the back of the book.

Photographs included in the original manuscript have been reproduced xerographically in this copy. Higher quality 6" x 9" black and white photographic prints are available for any photographs or illustrations appearing in this copy for an additional charge. Contact UMI directly to order.

UMI

A Bell & Howell Information Company
300 North Zeeb Road, Ann Arbor MI 48106-1346 USA
313/761-4700 800/521-0600

UNIVERSITY OF OKLAHOMA

GRADUATE COLLEGE

SURFACTANT BEHAVIOR IN THE MECHANISMS OF INK REMOVAL FROM SECONDARY FIBER IN FLOTATION DEINKING

A Dissertation

SUBMITTED TO THE GRADUATE FACULTY

in partial fulfillment of the requirements for the

degree of

Doctor of Philosophy

By

ACHILLE E. RIVIELLO, JR.

Norman, Oklahoma

1997

SURFACTANT BEHAVIOR IN THE MECHANISMS OF INK REMOVAL FROM SECONDARY FIBER IN FLOTATION DEINKING

A Dissertation APPROVED FOR THE

SCHOOL OF CHEMICAL ENGINEERING AND MATERIALS SCIENCE

BY

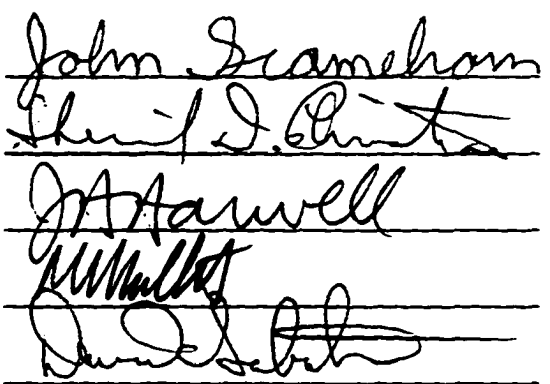

This work is dedicated to the memory of Dr. Felix Sebba (1911-1989), professor of chemical engineering at Virginia Polytechnic Institute and State University, who was my mentor and dear friend.

ACKNOWLEDGMENTS

When pursuing a goal as far reaching as a dissertation, one inevitably encounters a myriad of people without whom completion of the task would have been impossible. I would like to take a moment to enumerate just a few of these people. Of course, I would like to express my appreciation to Dr. John Scamehorn, my chief advisor, for his guidance, patience, and support throughout my near-tenure stay at the University of Oklahoma. Thanks are also due to Dr. Sherril Christian for his contributions as my coadvisor and solution thermodynamics drill instructor, to Dr. Uli Nollert for his insight into image analysis techniques, and to Drs. Jeff Harwell and David Sabatini for their input and for sitting on my committee. Several other professors who did not sit on my committee also aided my in my search for solutions to the numerous challenges I faced with my work: Dr. Robert White for his help with novel approaches to HPLC, Dr. Arnulf Hagen for discussions on hydrosiliation and silane bonding, and Dr. Richard Taylor for his insight into chemical equilibria and metal/ligand binding properties. Others that have directly helped me in my work include Rong Wang (GC/MS) and Wei-Li Yuan (AFM).

Many students and lab mates also played important and/or memorable roles in my years in the chemical engineering department. This quite lengthy list includes (but is by no means limited to): Bruce Roberts, Jeff Lapota, Cheryl Haskins, Bita Young, Hatice Gecol, Diego Acosta, Obe Bhummasobhana, Ahmadali Tabatabai,

Ahmed Ali, Luke Kitiyanan, Jerry Newman, Leon Grossman, Christy Crow, Yanick Blanche, and Emmanuel (Jim) Faisant. Those listed can take guesses as to whether he/she falls into the "important role" or 'memorable role" category.

Of course, nothing would get done in the department without the blessings of the staff. Big "thank you's" to Donna, Shirly, Sherry, Susan, Larry, Chris, and my very good friend, Rick Wheeler. Other miscellaneous acknowledgments are heaped upon Tony and Debra Ong, Danny Fallis of Tall Tales fame, Soul Shaker (Matt, Ty, Danny, and Barry), Chris Boline, John Ressmeyer, Mark and Rita Loeffler, Corbyn Roberts, and Kim Son Restaurant for making my years in Norman pleasurable/tolerable/interesting--take your pick.

Financial support for this work was provided by the TAPPI Foundation, a National Science Foundation Grant CBT 8814147, and an Applied Research Grant from the Oklahoma Center for the Advancement of Science and Technology. In addition, support was received from the industrial sponsors of the Institute for Applied Surfactant Research including Akzo Nobel, Amway Corporation, Colgate-Palmolive, Dow Chemical Company, DowElanco, E. I. DuPont de Nemours & Co., Henkel Corporation, ICI Surfactants, Kerr-McGee Corporation, Lever Brothers, Lubrizol Corporation, Nikko Chemicals, Phillips Petroleum Company, Pilot Chemical Company, Reckitt and Coleman, Shell Development Company, Sun Chemical Corporation, and Witco Corporation.

To my parents and sister, I would like to express special gratitude for their support, love, and confidence. Finally, to my dearest wife-to-be, Julie: thanks for putting up with me.

TABLE OF CONTENTS

TABLE OF CONTENTS (Continued)

LIST OF TABLES

LIST OF FIGURES

LIST OF FIGURES (Continued)

LIST OF FIGURES (Continued)

FIGURE Page

LIST OF FIGURES (Continued)

LIST OF HISTOGRAMS

ABSTRACT

To date, the majority of the research into ink removal from secondary fiber by the flotation deinking method has centered about empirical research, and the fundamental mechanisms have not been well understood. In this study, the underlying mechanisms of "collector chemistry" are elucidated and found to be complex combinations of the ink particle interactions stemming from the nature of the surfactant/calcium relationship. While previous investigators employed long chain fatty acid surfactants typically used in industrial applications, this study focuses on two medium chain-length fatty acids (sodium octanoate and sodium dodecanoate) and a comparable chain-length sulfate (sodium dodecyl sulfate) so as to be able to observe the system behavior below the K_{sp} of the surfactant/calcium complex. By investigating the adsorption isotherms of the surfactants on both model inks and fibers, the associated zeta potentials, the aggregation characteristics of the model ink, and the flotation of the ink and fibers, the fundamental mechanisms were found to be adsorptive rather than precipitative. This mechanistic understanding could translate into more efficient surfactant formulations for the flotation deinking process. In addition to the aforementioned investigations, a new technique was developed to simultaneously measure paper brightness and dirt count using an image analyzer.

Also, a new class of polymeric reverse phase high performance liquid chromatography (HPLC) packings was developed.

CHAPTER 1

THE MECHANISMS OF COLLECTOR CHEMISTRY IN FLOTATION DEINKING

In this study, the mechanisms of ink particle agglomeration and the subsequent flotation in the deinking process for recycling of waste paper were investigated. A model ink (carbon black), and medium chain-length surfactants (sodium octanoate, sodium dodecanoate, and sodium dodecyl sulfate) were employed in an attempt to elucidate the fundamental mechanisms of collector chemistry. Experimental data from adsorption isotherms, zeta potential measurements, and model flotations, combined with knowledge of the solubility product constant of surfactant-calcium precipitates support the mechanism of co-adsorption of the surfactant and calcium ions on the carbon being responsible for the aggregation and subsequent flotation of the carbon rather than bulk phase precipitation of the surfactant. Disparities in flotation efficiency of the carbon between the carboxylates and the sulfate indicate fundamental differences in the flotation mechanism of the two classes of surfactants, probably due to the different molecular structure of the dissimilar hydrophilic groups and their interactions with the calcium ion.

Keywords: Deinking, flotation, collector chemistry, surfactants.

1.1 INTRODUCTION

Since the issue of the patent to Henkel in 1908 [1] for "paper detergents" for the removal of ink from paper, the topic of secondary fiber recycling has attracted much attention, from both the scientific community and the general public. The basic process, practiced on a large commercial scale only since World War II, is often compared to laundering [2]. In the United States, nearly 36 million tons of secondary fiber were recovered in 1993 [3], representing an 80% increase since 1985, and the figures are projected to reach 50 million tons by the year 2000 [4]. Legislative quotas on the use of secondary post-consumer fiber have caused the industry to reconsider its approach to the removal of ink from the secondary fiber sources. Improved deinking technology has allowed more recycled fiber use in papermaking processes while maintaining or improving quality of the final product [5]. Flotation deinking, which is well established in Europe and Japan, has been gaining popularity with North American deinking mills and has helped to increase the efficiency of recycling of diverse sources of secondary fiber into more valuable products. At the same time, many chemical additives used in secondary fiber recovery have been reformulated or used differently in order to accommodate new technologies [6].

Whereas washing deinking has historically been the predominant method of ink removal in North America, many mills are incorporating the technology of flotation deinking into two-stage washing/flotation (hybrid) systems for increased

efficiency and higher grade end products. Washing deinking is particularly effective in the removal of small particles (less than 15 μm) while the flotation technique is more effective in the removal of larger particles or aggregates of particles. Unlike the washing process, flotation deinking is only mildly sensitive to ink particle size and relies on the agglomeration of the ink particles into hydrophobic aggregates that can be preferentially removed by forced-air flotation [5]. Though traditional flotation deinking employs anionic surfactants, nonionic surfactant formulations for flotation and washing deinking have become commonplace.

1.2 COLLECTOR CHEMISTRY

The induced aggregation of the ink particles and improved attachment to air bubbles is often referred to as "collector chemistry". This general term traditionally implies the use of an anionic surfactant, usually a sparingly water-soluble carboxylate salt such as sodium stearate, and a "collector" ion, such as calcium, to impart the desired properties to the ink particles. Several theories as to the mechanism of the surfactant/calcium/ink interaction have been forwarded.

In one investigation, Hornfeck [1] proposed the existence of an electrostatic calcium bridge that is formed between the moderately negative surface of the ink particle and the anionic head group of the carboxylate surfactant. According to this theory, the hydrophobic tail of the surfactant is then free to interact with the

hydrophobic portions of other such electrostatically bridged surfactants, thus causing ink particle aggregation due to hydrophobic bonding. Particle and aggregate attachment to air bubbles was explained by insertion of the hydrophobic tails of the electrostatically bound surfactant molecules into the air phase of the rising air pocket. The theory did not address the possibility of bilayer formation or of a lying-down orientation of the surfactant molecules, both of which are possible geometries of adsorbed surfactants.

Larsson et al. [7, 8] studied the zeta potential and flotation efficiency as a function of the addition of calcium ion concentration to model ink dispersions in the presence of sodium stearate. The investigators observed that the absolute value of the negative zeta potential of the ink particles decreased with increasing calcium concentration while flotation efficiency increased. Microscopic analysis of the ink particle revealed precipitated calcium distearate adhering to the surface of the ink. From these observations, the authors concluded that precipitation of the calcium dicarboxylate was necessary to create a micro-encapsulation of the ink particles causing aggregation, hydrophobicity, and subsequent flotation. It should be noted, however, that all of the experiments in that study were conducted with surfactant and calcium concentrations at least two orders of magnitude above the solubility product constant (K_{sp}) of the calcium distearate. A subsequent study [9] supported this precipitation mechanism, but again the surfactant employed (sodium oleate) did not

allow observation of behavior below the K_{sp} due to the extremely low solubility of the calcium di-surfactant complex. Conditions under which no surfactant precipitate is present were not considered in those studies.

The present study was carried out using a model ink, carbon black, instead of a real ink that may consist of varying pigments and binders. Also, neither cellulose fibers, fillers, or coatings were present in the experiments. This simplified system was selected to elucidate the mechanisms of collector chemistry without interference from extraneous variables. A complementary study is ongoing to investigate collector chemistry and aggregation behavior in flotation deinking systems using actual waste paper. While the present study is concerned only with model systems, the increasing popularity of water-based flexographic inks due to environmental and health concerns actually increases the applicability of these fundamental studies to realistic industrial problems. Flexographic inks of this type are composed of a pigment, usually carbon black, that is dispersed in water with the use of water-soluble carboxylic derivatives. These dispersants double as binders and are usually composed of resins which are usually homo- and co-polymers of esters of acrylic and methacrylic acids. The carboxylic group content is appreciable. Under basic pH conditions, such as those prevalent in deinking systems, the dried binders hydrolyze and resume their role as dispersants [10]. The pigment, then, exists as a suspension of carbon black--very similar to the model systems being investigated in this study.

1.3 EXPERIMENTAL

The carbon black was supplied by Cabot and was Type 400R, a pigment commonly used in the manufacture of many varieties of inks [11]. The nominal particle size was stated by the manufacturer to be 25 nm, but the stable aggregates of carbon averaged approximately 1 μm. The supplier-provided BET surface area was 96 m^2/g. Due to a relatively high concentration of ionic salts originally present in the carbon, it was necessary to remove the salts by washing the carbon. The carbon was mixed with distilled, deionized water in the ratio of 1:4, agitated thoroughly, centrifuged, and the water decanted off. The procedure was repeated three times, which was sufficient to reduce the Ca^{2+} concentration in the rinse water to less than 0.1 ppm. The concentration of Ca^{2+} in an untreated sample of 1.0 g of carbon mixed with 10 mL of water was 600-700 μM.

The surfactants employed for these investigations were sodium octanoate (hereafter referred to as C8), sodium dodecanoate (C12), and sodium dodecyl sulfate (SDS). Schematics of the chemical structure of the three surfactants are illustrated in Figure 1.1. The C8 and C12 were purchased from Sigma Chemical Company with a purity of greater than 99%. The electrophoresis grade SDS was provided by Fisher Scientific and also had a purity of greater than 99%. The calcium chloride was obtained from Fisher and was oven-dried for 12 hours at 90°C just prior to making the stock solutions due to the chemical's hygroscopic nature. Adjustments of the pH

were made with Fisher-Brand Certified N/20 NaOH. All of the above materials were used without further purification. The water used for the experiments was distilled and deionized.

Zeta potentials were determined using a Zeta Meter Model 3.0. The potential across the cell was adjusted as a function of the ionic strength (specific conductance) of the sample so as to avoid thermal overturn associated with overpotentials. The measurements were taken at a constant temperature of 30°C.

Adsorption isotherms were obtained at 30°C using the solution depletion method; 1.0 g of carbon was mixed with 10 mL of solution, allowed to equilibrate for three days with occasional agitation, and centrifuged. The surfactant and calcium concentrations in the supernatant liquid were analyzed. Solubility product constant (K_{sp}) values were determined by mixing known concentrations of surfactant and calcium together, cooling the solutions to force to precipitation, heating the solution to 30°C, and allowing them to equilibrate under thermostatted conditions. This procedure was necessary to avoid the possibility of supersaturated solutions. The supernatant liquid was then analyzed for the residual concentrations of surfactant and calcium. Calcium concentrations were measured by atomic absorption spectroscopy (AA). Determination of the surfactant concentrations was accomplished by high pressure liquid chromatography (HPLC) with an electrical conductivity detector. The SDS and C12 were analyzed employing a bicratic step-change solvent scheme (water-

rich/methanol-rich mobile phases) on octadecyl and octyl reverse phase silica columns, respectively. The C8 analysis employed similar solvent programming but used a special poly (lauryl methacrylate) reverse phase silica developed specifically for this system [12].

A Hallimond flotation cell [13], illustrated in Figure 1.2, was employed for the model flotations of the carbon. Instead of the 50 μm opening and the magnetic stirrer described in the literature for gas introduction and dispersion, a 0.5 inch diameter, medium-grit fritted glass disk was fused at the point of gas introduction to act as a sparger. A Cole-Parlmer flowmeter was used to regulate the gas flow rate to 60 mL per minute, and the duration of flotation was 5.0 minutes in all cases. The flow rate was selected to allow substantial flotation in a reasonable amount of time while only gently agitating the suspension and avoiding unrepresentative carryover of the carbon. Compressed nitrogen was used as the flotation gas.

The general procedure for the flotation experiments began with adding 70 mL of water to 0.05 g of carbon black. The calcium and/or surfactant was then added in the form of pre-prepared stock solutions, the pH was adjusted to 9.0 or 11.0, and more water was added to bring the total volume to 80 mL. The moderately basic pHs were selected to conform with the conditions of traditional deinking operations. The suspension was thermostatted at 30°C for 30 minutes. The sample was then decanted into the Hallimond tube and flotation was immediately commenced. Following the

5.0 minutes allotted for flotation, the top fraction, consisting of carbon entrained in the froth and the carbon carried over the division and deposited into the side tube by the froth breakage, was drained by removing the stopper in the bottom of the side tube and collected in a sample bottle. The unfloated fraction was then collected. Both samples were filtered through three preweighed FisherBrand glass fiber filter circles with a nominal pore size of 2.0 μm. Three filter papers were employed to minimize the loss of fine particles. The filter papers were oven dried, and the amount of floated and unfloated carbon was determined gravimetrically. The mass balances closed within 5% in all cases.

1.4 RESULTS AND DISCUSSION

The present investigations centered about the effect of the calcium and surfactant concentration on adsorption of the additives and on the zeta potential and flotation efficiency of the carbon in relation to the precipitation phase boundaries of the calcium di-surfactant complexes. In surfactant systems below the critical micelle concentration (CMC) where no micelles are present, this phase boundary corresponds to conditions where the K_{sp} is exactly satisfied. For systems comprised of a divalent cation, such as Ca^{2+}, and a monovalent anionic surfactant, the concentration-based K_{sp} is defined as follows:

$$K_{sp} = [Ca^{2+}]\,[\text{surfactant}]^2 \qquad \{1\}$$

where the bracketed values represent the concentration of the species in a solution in equilibrium with the calcium disurfactant precipitate. The CMC values for the surfactants employed in this investigation are 350,000 μM for C8, 27,000 μM for C12, and 8300 μM for SDS [14], and surfactant concentrations remained below the CMC for all experiments. In all of the adsorption and zeta potential experiments, the concentrations of the calcium and surfactant remained below the K_{sp} value (no surfactant precipitation). No significant effect of pH was observed between pH 9 and 11; therefore, only data at a pH of 9 are presented. The complete sets of data can be found elsewhere [15].

The concentration-based K_{sp} values of the calcium dicarboxylate species were experimentally determined to be 1.5×10^{-6} M^3 for C8 and 1.0×10^{-12} M^3 for C12. These values compare well to those reported in the literature [16]. For the experimental conditions, the concentration-based K_{sp} of the calcium di(dodecyl sulfate) was previously determined to be 6.0×10^{-10} M^3 (activity-based K_{sp} is 5.0×10^{-10} M^3) [17]. Knowledge of the K_{sp} values allowed experimental conditions to be defined to insure that precipitation did not occur in the adsorption experiments.

Adsorption isotherms on carbon were generated for all species of surfactants as well as for ionic calcium. Figure 1.3 illustrates the adsorption isotherms for C8, C12, and SDS on washed carbon at 30°C and a pH of 9. Due to the larger hydrophobic group having greater attraction to the carbon surface through

hyerophobic bonding, the C12 has a greater affinity for the carbon than does the C8 in accordance with Traub's Rule [18],. Equilibrium surfactant adsorption studies have shown that four distinct regions are observable in the isotherms of many systems involving hyrdrophilic substrates [19-21]. At low surfactant concentration, a proportionality between adsorption and equilibrium concentration is observed. This region physically corresponds to monomeric surfactant adsorption on the surface without significant association or aggregation of adsorbed surfactant. This region is referred to as the Henry's Law region or Region I. A sharp increase in the slope of the isotherm defines the onset of Region II and is usually indicative of associative adsorption of the surfactant into aggregates (either monolayers or bilayers) due to hydrophobic tail-tail interactions. Region III corresponds to a decrease in the slope of the isotherm compared to Region II. At concentrations above the CMC, adsorption remains constant, even when the surface is not completely covered. This is know as Region IV or the plateau adsorption region. Above the CMC, the surfactant monomer concentration is approximately constant and additional added surfactant forms more micelles as described by the pseudo-phase separation model for micelle formation [21]. It is possible that the surface may become saturated and adsorption become invariant with concentration below the CMC if the tendency to adsorb is high. Conversely, sometimes Region III or even Region II can be absent and a Region I to IV or II to IV transition at the CMC can be observed. Surfactant adsorption on

hydrophobic surfaces, such as carbon, has not been as well studied as that on hydrophilic substrates [21]. For adsorption onto carbon, slope changes, especially those initiating and terminating Region II, and may not be well defined because of the high affinity of the surfactant hydrophobe for the substrate in Region I; i.e., the relative favorability of the environment in a surface aggregate of surfactants for the surfactant hydrophobe compared to that in Region I is expected to be less for a hydrophobic surface than for a hydrophilic surface.

The adsorption isotherms at 30°C for C8, C12, and SDS are shown in Figure 1.3. Adsorption above the CMC is nearly constant for C12 and SDS while the Region IV was not measured for C8 because of the extremely high CMC. For all three surfactants, a Region I to II is not observed, but the slope of the adsorption isotherm becomes lower prior to the CMC for the C8 and C12 which is consistent with a Region II to III transition. However the C8 adsorption seems to approach a constant value at a fairly low concentration well below the CMC. This adsorption level is less than half the maximum adsorption of the C12. Assuming similar physically adsorbed configurations of the C8 and C12 on the carbon surface (molecules lying flat or in bilayers), it is obvious that the surface is not saturated with adsorbed C8 when the adsorption isotherm levels off. A mechanism consistent with these results is a horizontal or laying down configuration of the adsorbed C8. One reason that the C12 shows higher molar adsorption is that the C8 may not be

adsorbing on low energy regions of the surface at the concentrations attained while the C12 may adsorb on these surface patches due to the greater hydrophobic interactions. Surface heterogeneity is the basis of this explanation. Another effect could be the formation of surface aggregates of C12 on surface patches where the C8 is adsorbing in nonaggregated form. These two explanations are not mutually exclusive and may both contribute to the observed adsorption differences. It is important to note that calcium is not present in these systems. As will be shown, calcium ions can dramatically affect adsorption levels and probably the configuration of the adsorbed surfactant.

The approximate adsorption corresponding to saturation of the entire surface by either a monolayer or a bilayer can be calculated from the area of a single adsorbed surfactant molecule. Adamson [20] reports a value of 20.5 $Å^2$ for a carboxylate molecule adsorbed in close-packed perpendicular orientation on surfaces such as carbon black while Rosen [22] suggests 50 $Å^2$ for the sulfate . Using these values, monolayer coverage of 1.0 m^2 of the carbon would require 8.1 $\mu moles/m^2$ of the carboxylate and 3.2 $\mu moles/m^2$ for the sulfate. Bilayer coverage would result in the doubling of these values. The C8 and SDS adsorption isotherms approach values of approximately 1.1 and 2.0 $\mu moles/m^2$, respectively. While the C12 does not reach an adsorption plateau in the range of concentrations studied, its maximum surface coverage, measured just below the CMC, was 2.6 $\mu moles/m^2$. These values are all

well below estimated full monolayer coverage and are consistent with non-associative adsorption onto hydrophobic surfaces.

Figure 1.4 depicts the adsorption of Ca^{2+} on the carbon in the absence of surfactants and shows the affinity of the Ca^{2+} for the carbon to be of similar magnitude to that of the surfactants. The calcium ions are attracted by the negatively charged sites on the carbon surface which result from oxidation. Adsorption of this type is purely electrostatic and non-associative. Noting that the ionic radius of a Ca^{2+} ion is 0.99Å [23], the maximum coverage of the carbon surface by the adsorbed Ca^{2+} observed in these experiments is 0.60% of close-packed monolayer coverage. The slope of the curve in Figure 1.4 is nearly 1, which, along with the sparse coverage and non-associative nature of the adsorption, indicates that Henry's Law is obeyed in this concentration region. The similarity in the magnitudes of the calcium and surfactant adsorptions would imply that the surfactant adsorption is non-associative and, thus, driven by hydrophobic interactions of the tail with the carbon substrate.

Adsorption of the surfactants in the presence of varying initial concentrations of Ca^{2+} is shown in Figures 1.5-1.7. The designation of "$[Ca^{2+}]$ = 600-700 μM" refers to the calcium naturally present when using unwashed carbon. In all experiments, the concentration of the surfactant and calcium remain below the K_{sp} of the calcium di-surfactant precipitates. For all cases, increasing initial concentrations of Ca^{2+} leads to increased adsorption of the surfactant. As is shown in Figure 1.8,

increasing initial concentrations of surfactant cause increased adsorption of Ca^{2+} on the carbon, presumably as the cations associate with exposed anionic surfactant head groups. Similar results are observed all systems studied. This type of cooperative adsorption is common with ionic surfactants in the presence of oppositely charged ions and is due to diminished electrostatic repulsion among the head groups of the surfactants by association of the counterion. This binding is not a precipitative process. Results from these experiments allow calculation of the ratio of surfactant to calcium adsorbed onto the carbon, which is as high as 96:1. Because the model proposing electrostatic binding of the anionic surfactant to the carbon surface via the calcium ion [1] would result in a surfactant to calcium adsorption ratio of 1:1 or less, the calcium bridge theory is not likely to be predominating mechanism for surfactant adsorption on the carbon. The series of results presented in Figures 1.5-1.8 demonstrates typical synergistic coadsorption of the surfactants with calcium; i. e., calcium enhances surfactant adsorption and the surfactants enhance calcium adsorption.

The zeta potential of a particle is directly related to its tendency to aggregate [20] and is an estimation of the electrical potential of a particle at the shear layer of adsorption as determined by its electorphoretic mobility. The zeta potential of carbon black in water with a pH of 9 is approximately -28 mV. The net negative charge on the otherwise hydrophobic carbon is probably due to surface oxidation. For some

systems, there is a potential determining ion, usually H^+ or OH^- (expressed as pH), the concentration of which will affect the zeta potential of the particle and may even cause charge reversal. The potential determining ions actually reversibly incorporate into the structure of the solid rather than simply adsorbing onto the surface. The point at which the zeta potential is zero as a function of the pH is called the point of zero charge (PZC). For carbon black in water, the PZC was determined to be approximately 2.3.

Figure 1.9 illustrates the zeta potential of the carbon black as a function of initial surfactant concentration with no calcium present. The surfactants have essentially no effect on the measured zeta potential even though the adsorbed molecules carry a negative charge. This lack of zeta potential modification may be due to counterion binding of the associated sodium ions to the relatively small amount of surfactant adsorbed to the surface. However, as is shown in Figures 1.10-1.12, when Ca^{2+} is added to the system, the zeta potential of the carbon particles decreases dramatically for all surfactants, regardless of the surfactant type or concentration. Since experiments could not be performed without precipitation of the surfactant at higher Ca^{2+} concentrations for the C12 system, only the data for $[Ca^{2+}]$=100 μM is reported. For systems with surfactant present, the zeta potential is observed to be a function only of the calcium ion concentration and is not substantially affected by the surfactant structure or concentration within the ranges

studied in this investigation. Interestingly, surfactant addition actually causes a reduction in the magnitude of the zeta potential of the carbon when calcium ions are present. This effect may reflect the synergistic cooperative adsorption of the calcium as depicted in Figure 1.8. Because the zeta potential can be directly related to the aggregation potential of particles, it might be assumed that agglomeration of the carbon is independent of the surfactant type and concentration. However, a concurrent investigation [28], has shown that aggregation of carbon particles is a strong function of surfactant type due to the calcium/surfactant interaction. While the carboxylate surfactant (C8) studied in the concurrent investigation promoted agglomeration, the SDS retarded aggregation despite similar zeta potential trends.

In order to relate the adsorption and zeta potential data to collector chemistry mechanisms, it was necessary to correlate the results to a performance variable. This was accomplished by measuring the percent carbon flotation in a Hallimond flotation tube as a function of surfactant and calcium concentrations as is illustrated in Figures 1.13-1.15. It must be stressed that the surfactant and Ca^{2+} concentrations listed in the figures represent initial, rather than equilibrium, concentrations. In all cases, adsorption of both the surfactant and Ca^{2+} occur. However, the solution/substrate ratio is 160 times greater than in the adsorption experiments, so the equilibrium concentrations of the surfactant and calcium are only slightly less than the initial concentrations. The initial concentrations of surfactant necessary to produce bulk

phase precipitation for the cases of initial Ca^{2+} concentrations of 100 and 1000 μM are presented in Table 1.I and are designated by the vertical lines on Figures 1.13-1.15. These values corrected for the adsorptive losses of surfactant and calcium using the adsorption isotherms.

For the carboxylates, efficient carbon flotation is achieved at relatively low surfactant concentrations for both Ca^{2+} concentrations. The C12 exhibits maximum flotation at a concentration of only approximately 125 μM for both calcium concentrations while the C8 system shows flotation maximums at 3000 μM of surfactant. It is important to note that maximum flotation efficiency of the carbon occurs well below the K_{sp} for the C8 and at or just above the K_{sp} for the C12 system series of experiments. These results demonstrate that bulk phase precipitation is not necessary for efficient flotation. The flotation efficiency increases with the decreases in zeta potential depicted in Figures 1.10 and 1.11, which also indicates that the mechanisms of collector chemistry are adsorptive-based rather than precipitative-based. The SDS system, on the other hand, does not exhibit flotation of the carbon greater than that of the blank runs despite the diminished zeta potential values and bulk phase precipitation. This discrepancy indicates that the SDS is not an effective surfactant for collector chemistry and suggests that the carboxylates possess some feature that causes flotability of the carbon even in the absence of precipitation.

A concurrent study [24] showed trends for agglomeration of carbon in the presence of C8, SDS, and Ca^{2+} to be similar to those for the carbon flotation. Experiments conducted below the K_{sp} of the calcium-disurfactant complexes exhibited significant aggregation of the carbon for the C8/Ca^{2+} system, while the SDS acted to disperse the particles despite the zeta potential reductions caused by added calcium ions. The results showed that bulk phase precipitation was not necessary for agglomeration and suggested that the carboxylate molecules complex in a cooperative adsorption (rather than precipitative) mechanism to cause aggregation. Extrapolation of theories from biological systems in which vesicles are caused to aggregate due to calcium/carboxylate binding lead to a proposed aggregation mechanism involving calcium bridging between carboxylate molecules adsorbed in a tail-down orientation on adjacent carbon particles.

Consideration of the results presented in this investigation leads to the conclusion that even though both the carboxylates and the SDS exhibit synergistic coadsorption of the surfactant and the calcium ions, only the former class of surfactants interacts with the calcium to cause carbon particle aggregation and attachment to the air-water interface of rising bubbles. Figure 1.16 schematically illustrates this proposed scenario. While calcium ions may electrostatically adsorb onto oxidized sites on the carbon causing decreased surface charge, association of the divalent cation with the head group of the carboxylate may create localized regions of

hydrophobicity which may aid in the attachment of the carbon particles to the gas/water interface of a rising bubble. The sulfate of the SDS molecule does not seem to possess this ability. These differences in flotation and aggregation performance may be a function of the geometry of the head groups of the surfactants in question. The tetrahedral structure of the sulfate has three oxygens and is likely to be more hydrophilic than the trigonal planar (two oxygens) carboxylate when associated with the Ca^{2+}.

1.5 CONCLUSIONS

In the traditional collector chemistry system, cooperative adsorption of surfactant and calcium ions occurs. Both carboxyated and sulfated surfactants readily adsorb on the carbon surface, presumably with a tail-down or lying down orientation. Calcium also adsorbs onto the carbon and is responsible for the diminished zeta potential regardless of the surfactant type or concentration. Enhanced flotation of carbon occurs, however, only with carboxylates and not with the SDS. The experiments were conducted below the K_{sp} of the calcium di-carboxylate complexes and reveal precipitation is not necessary to achieve flotation. A theory of cooperative adsorption between the carboxylate and the calcium ion that creates regions of hydrophobicity on the carbon is proposed.

1.6 REFERENCES

1. Hornfeck, K., Conservation & Recycling, **10** (2/3): 125 (1987)
2. Borchardt J. K., Colloids and Surfaces A, **88** (1): 13 (1994).
3. Mulligan, D. B., Prog. Paper Recycl., **4** (1): 12 (1995).
4. Anon. Paper Recycl., **5** (9): 5 (1994).
5. Harrison, A., Pulp and Paper, **63** (3): 60 (1989).
6. Basta, N., Gilges, K., and Ushio, S., *Chem Eng.* , **98** (3): 45 (1991).
7. Larsson, A., Stenius, P, and Ödberg, L. *Svensk Papperstidning*, **87** (18): R165 (1984).
8. Larsson, Larsson, A., Stenius, P, and Ödberg, L. *Svensk Papperstidning*, **87** (18): R158 (1984).
9. Johansson, B., Wickman M., and Ström, G., *J. Pulp Pap. Sci.*, **22** (10): J381 (1996).
10. Dorris, G. M., and Nguyen, N., *J. Pulp Pap. Sci.*, **21** (2): J55 (1995).
11. Cabot Corporation, Technical Report S-127, 1987.
12. Riviello, Jr., A. E., Scamehorn, J. F., and. O'Haver, J. H., "A Novel Technique for the Production of Customized HPLC Packings", submitted to *Journal of the American Oil Chemists' Society.*

13. Fuerstenau, D. G., Metzger, P. H., and Steele, D. D., *Eng. and Min. J.*, 158 (3): 93 (1957).

14. Mukerjee, P and Mysels, K. J., *Critical Micelle Concentrations of Aqueous Surfactant Systems*, Department of Commerce, U. S. Government: Washington, D. C., 1970.

15. Riviello, Jr., A. E., Ph. D. Thesis, University of Oklahoma, 1997.

16. Irani, R. R. and Callis, C. F., *J. Phys. Chem.*, **64** (11): 1741 (1960).

17. Stellner, K. L., and Scamehorn, J. F., *Langmuir*, **5** (1): 70 (1989).

18. Traube, I. *Annals*, **265**, 27 (1891).

19. Somasundaran, P, and Fuerstenau, D. W., *J. Phys. Chem.*, **70** (1): 90 (1966).

20. Adamson, A. W. *Physical Chemistry of Surfaces, Fifth Edition*, John Wiley & Sons, Inc., New York, 1990.

21. Harwell, J. H. and Scamehorn, J. F., "Adsorption from Mixed Surfactant Systems" in *Mixed Surfactant Systems*, Marcel Dekker, Inc., New York, 1993.

22. Rosen, M. J., Surfactants and Interfacial Phenomena, 2nd ed., Wiley, New York (1989).

23. Brady, J. E. and Humiston, G. E., *General Chemistry: Principles and Structure, Third Edition*, John Wiley & Sons, New York, 1982.

24. Faisant, E., Riviello, Jr., A. E., Scamehorn, J. F., and Christian, S. D., *Size Characterization of Model Ink Aggregates in Flotation Deinking Collector Chemistry*, submitted to TAPPI Journal.

Table 1.I. Initial surfactant concentrations resulting in precipitation for flotation experiments.

	Initial [Surfactant] (μM) required for precipitation for:	
Surfactant	$[Ca^{2+}]$=100 μM	$[Ca^{2+}]$=1000 μM
C8	122,475	38,700
C12	155	62
SDS	2522	835

Figure 1.1. The Structure of the surfactants: A) Sodium Octanoate, B) Sodium Dodecanoate, C) Sodium Dodecyl Sulfate

A)

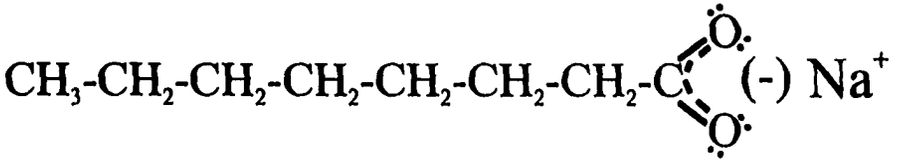

B)

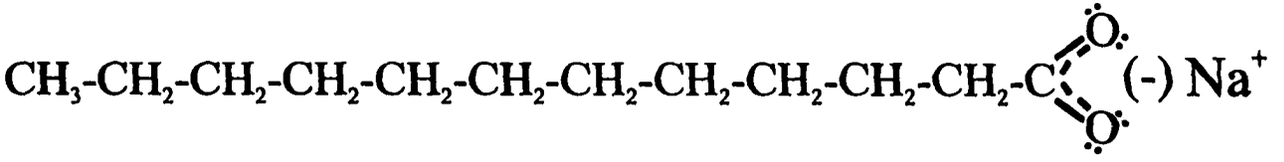

C)

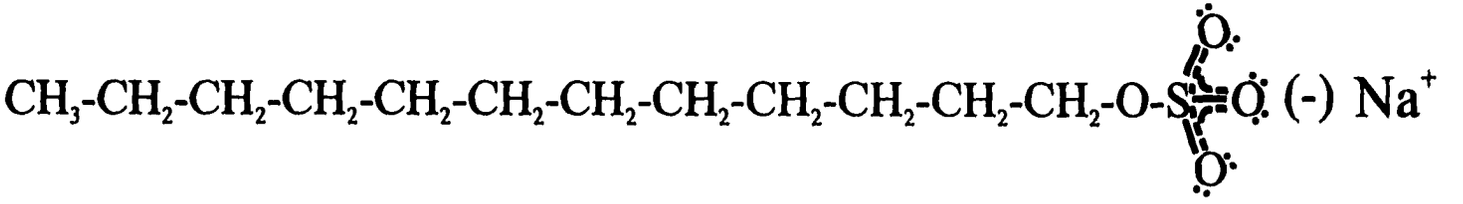

Figure 1.2. The Hallimond flotation tube

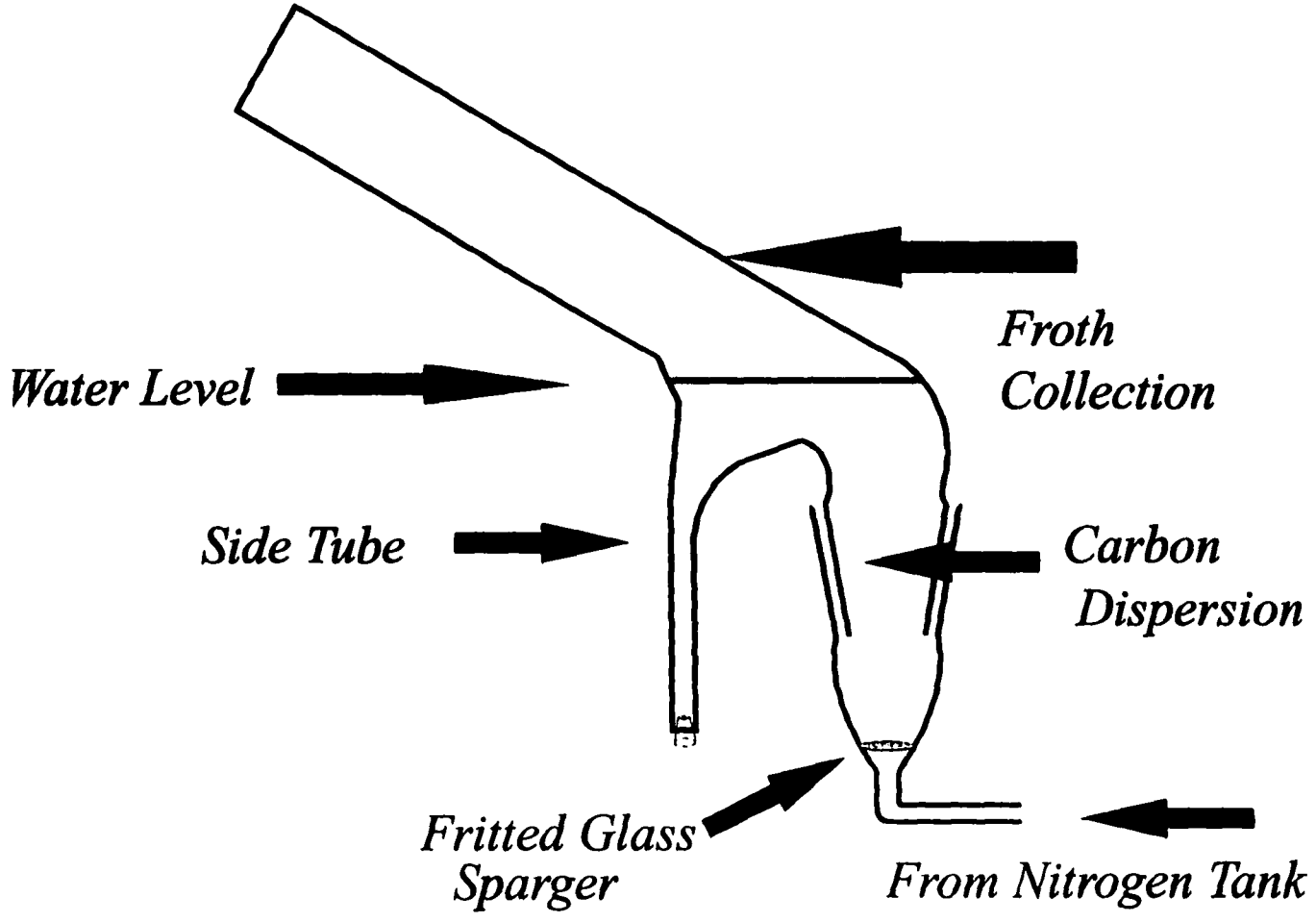

Figure 1.3. Adsorption of C8, C12 and SDS on Carbon. [Ca++]=0 uM.

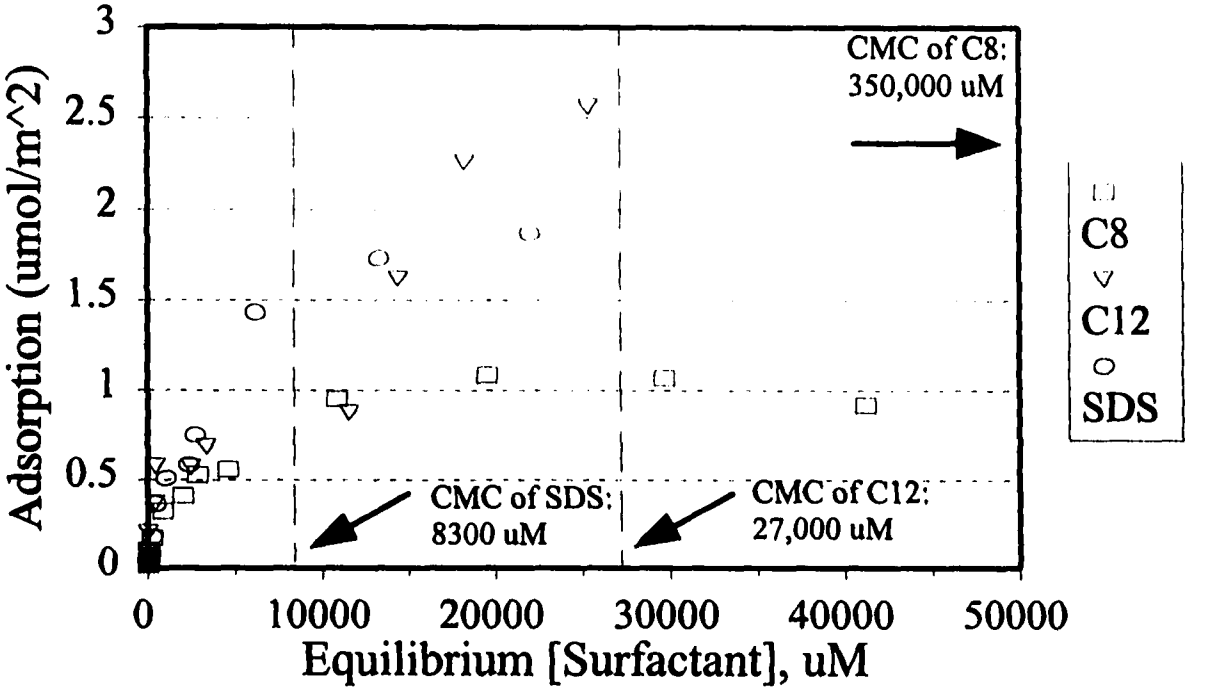

Figure 1.4. Adsorption on Carbon.

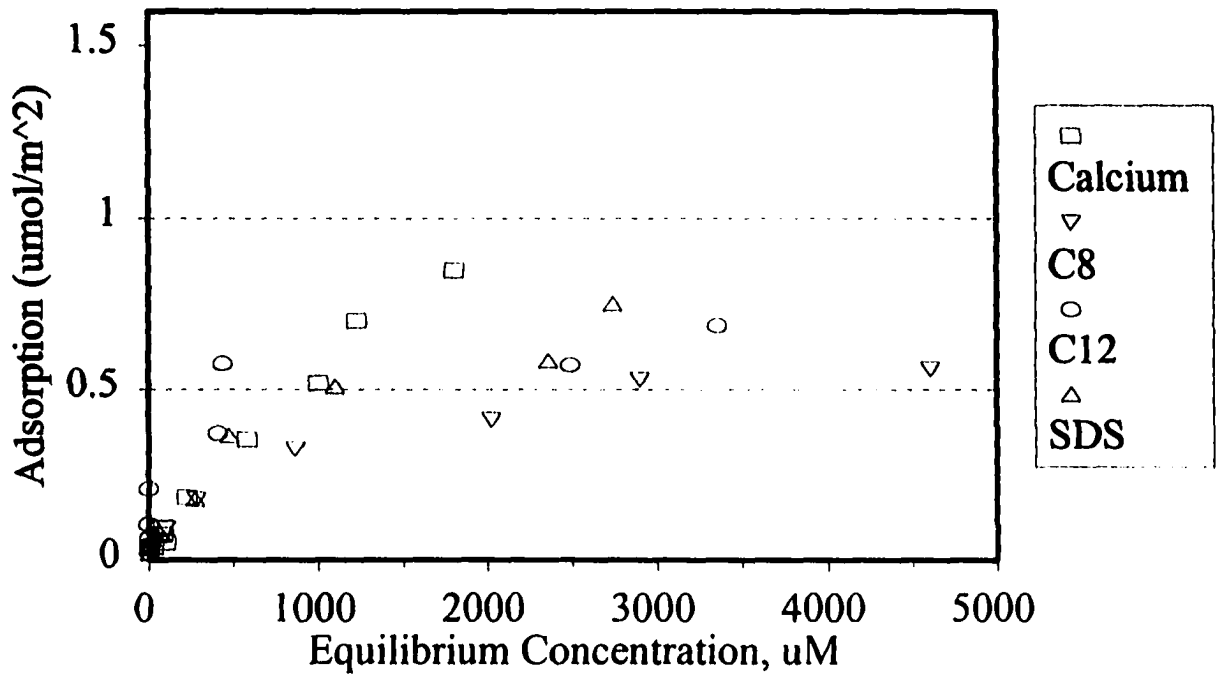

Figure 1.5. C8 Adsorption on Carbon.
[Ca++]=Variable

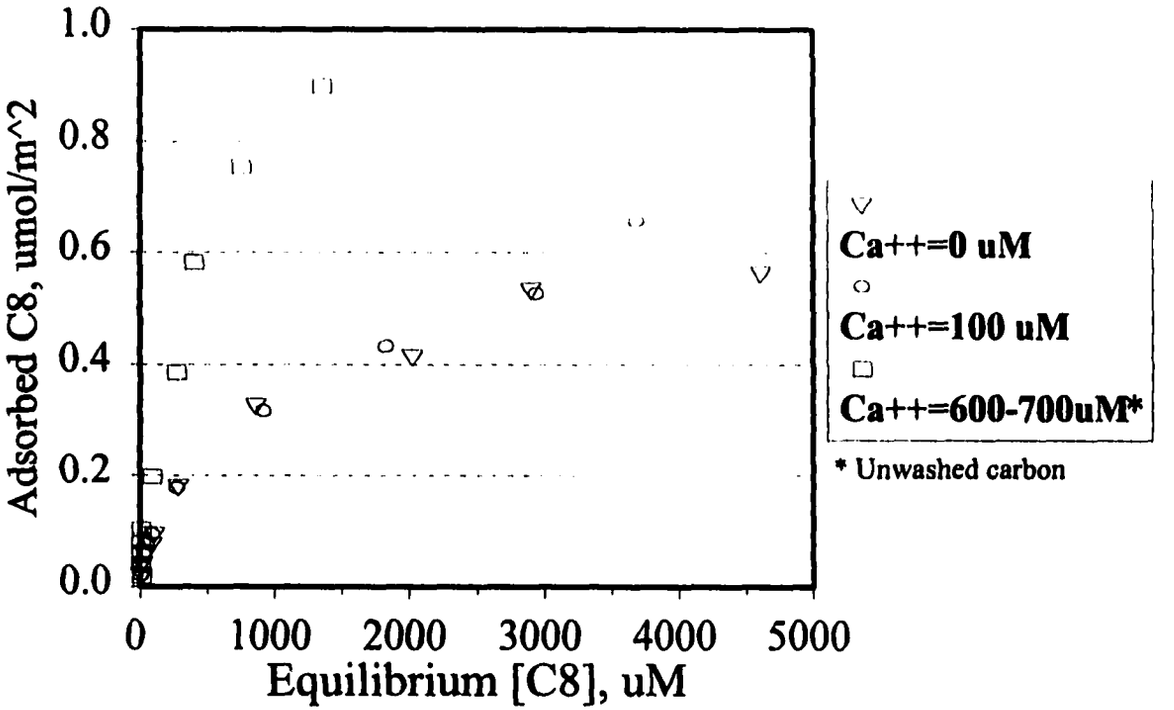

Figure 1.6. C12 Adsorption on Carbon. [Ca++]=Variable.

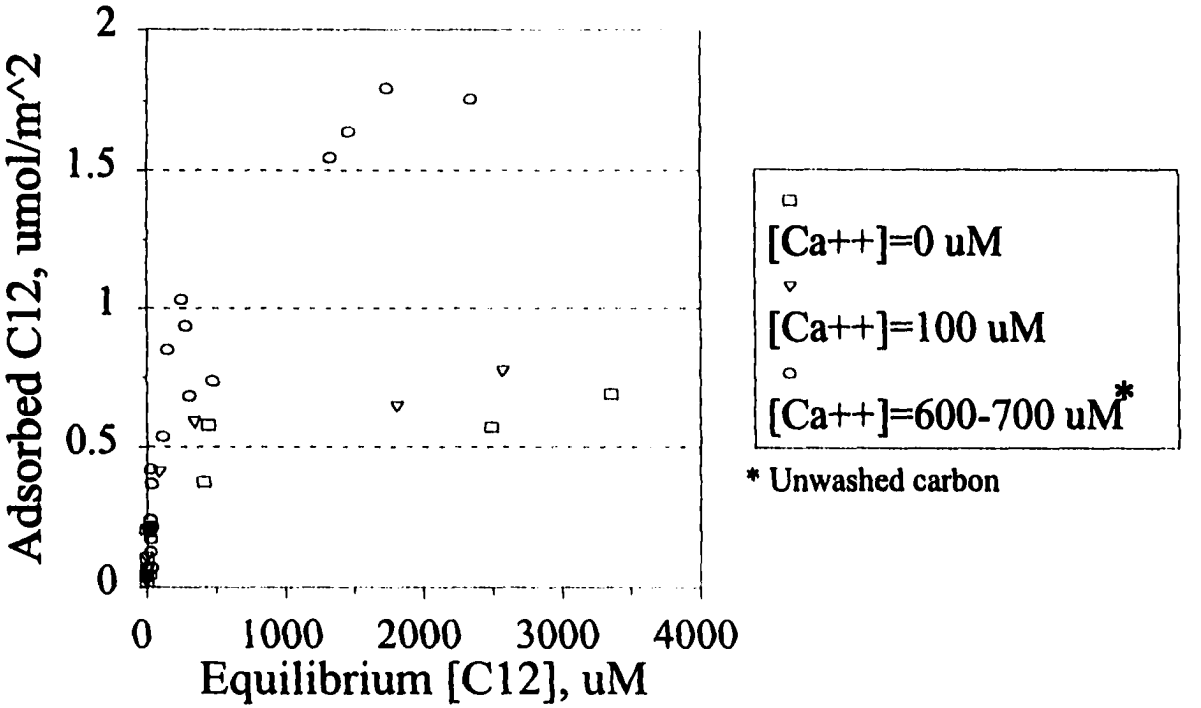

Figure 1.7. SDS Adsorption on Carbon. [Ca++]=variable.

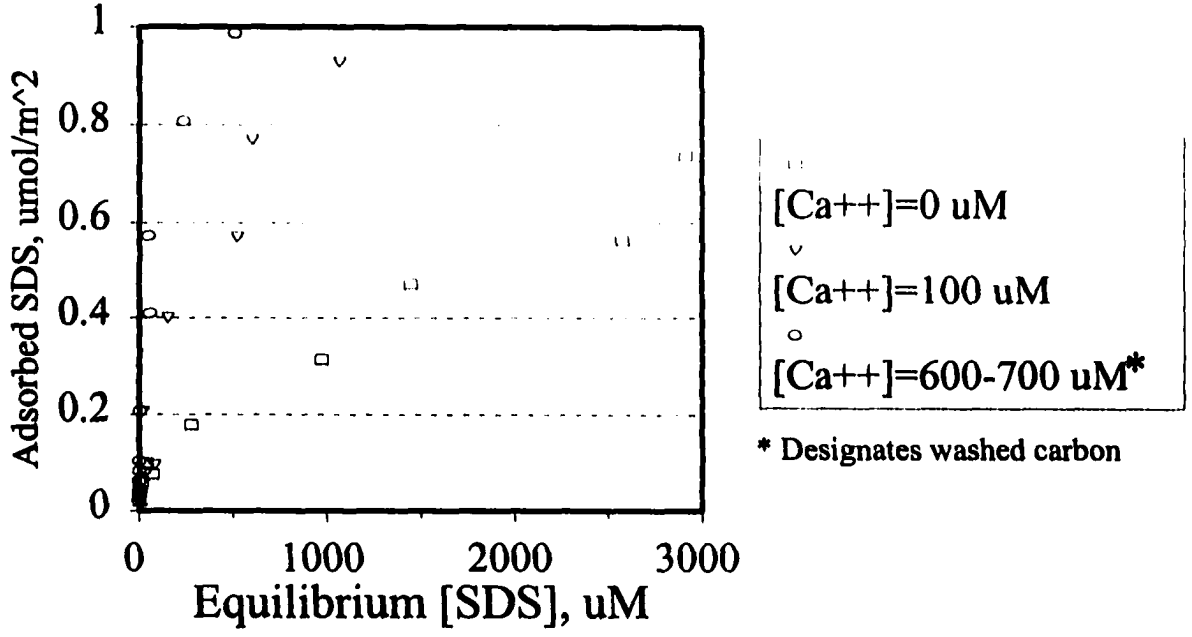

Figure 1.8. Calcium Adsorption on Carbon Black vs. Initial [SDS]. Initial [Ca++]=100 uM

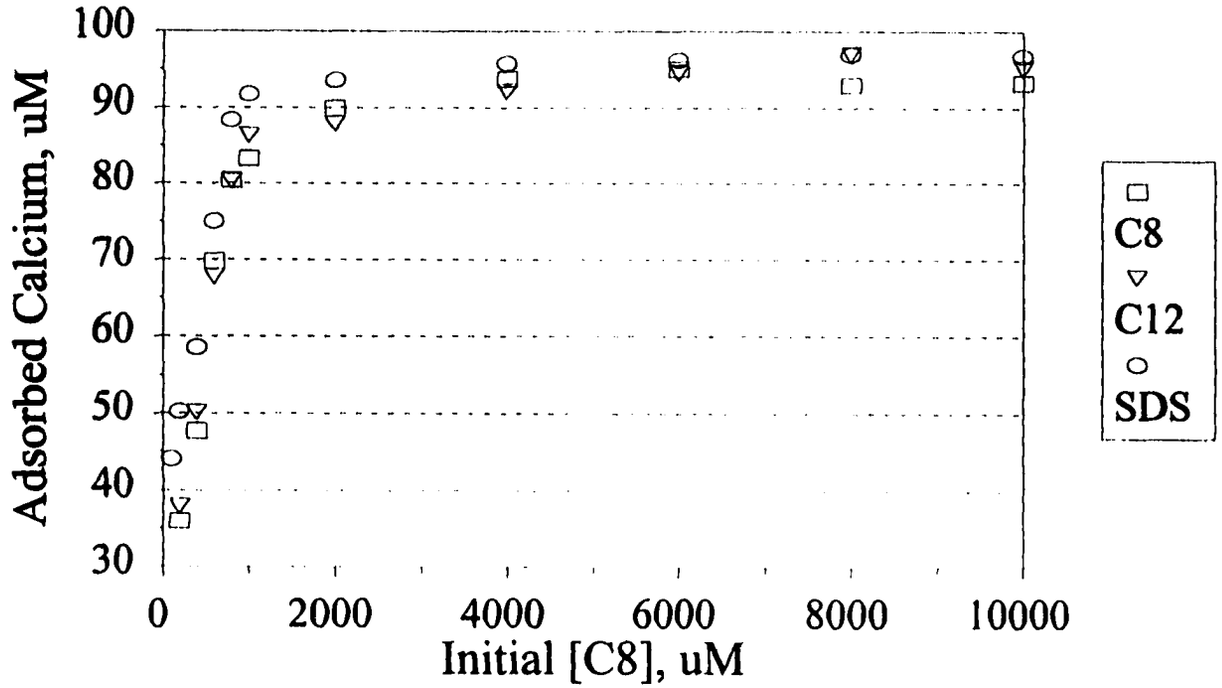

Figure 1.9. (-) Zeta Potential of Carbon Black vs. Surfanctant Concentration

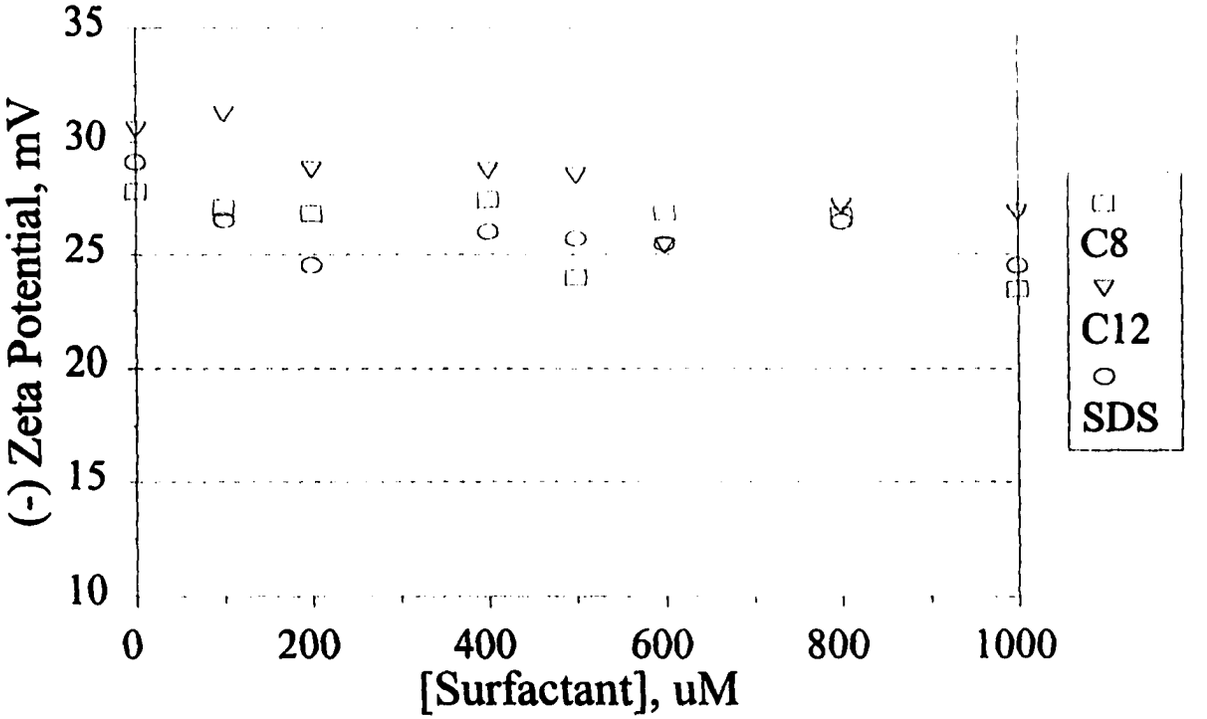

Figure 1.10. (-) Zeta Potential of Carbon vs. [Ca++]; [C8]=Variable.

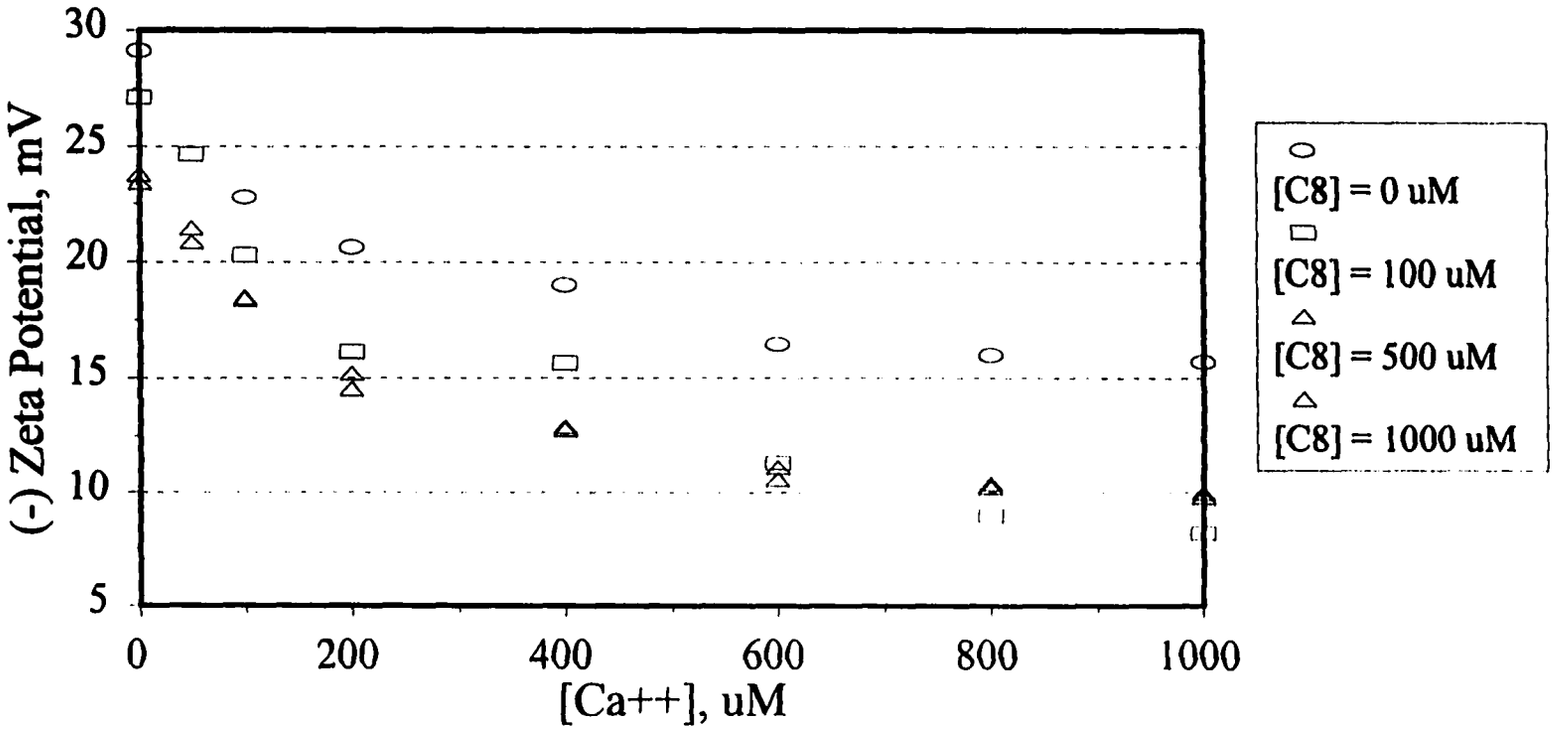

Figure 1.11. Zeta Potential of Carbon vs. [Ca++]; [C12] = 100 uM

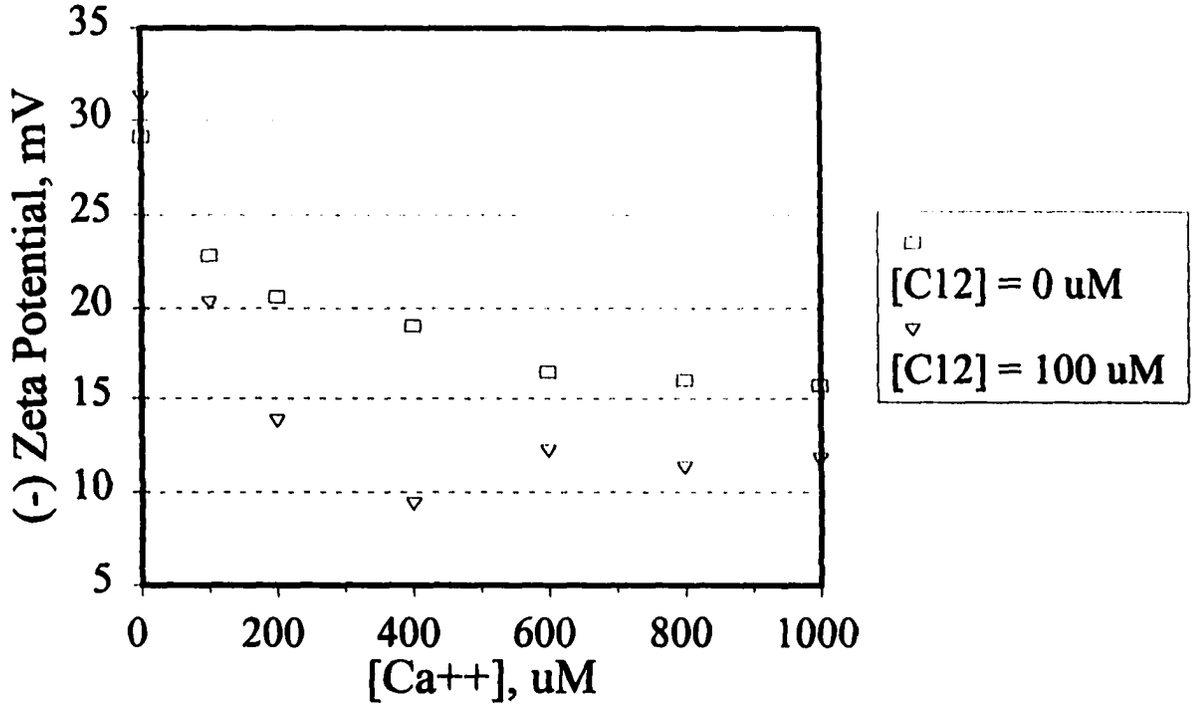

Figure 1.12. Zeta Potential of Carbon vs. [Ca++]; [SDS]=Variable

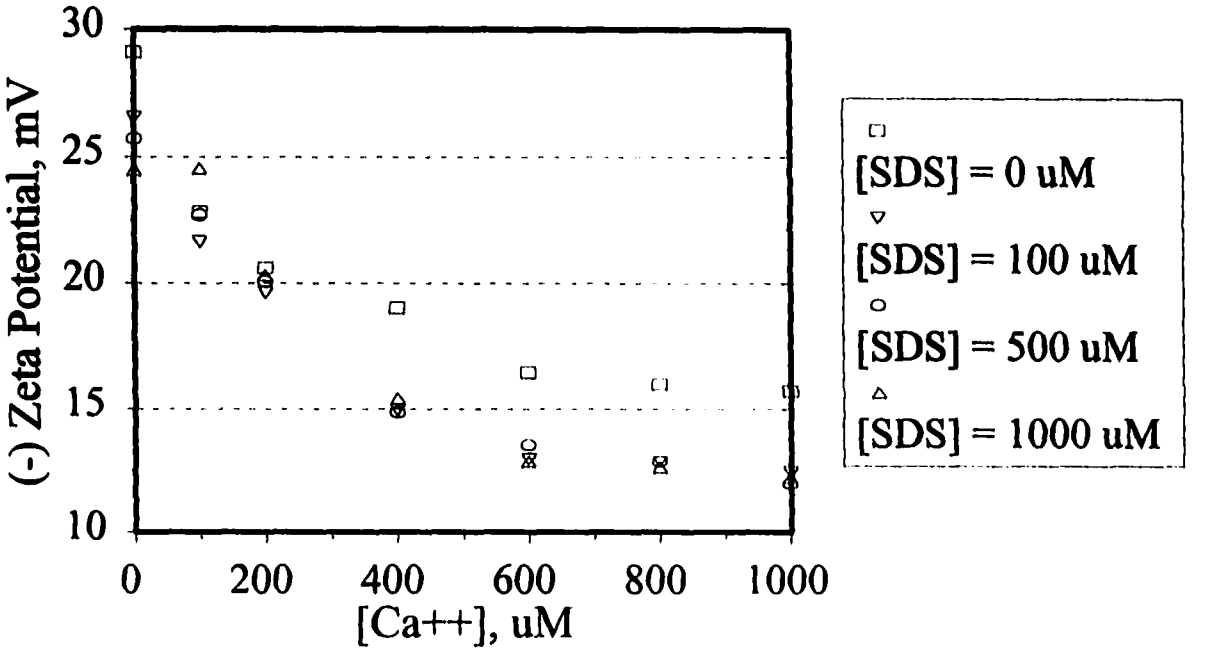

Figure 1.13. Carbon Flotation vs. [C8]

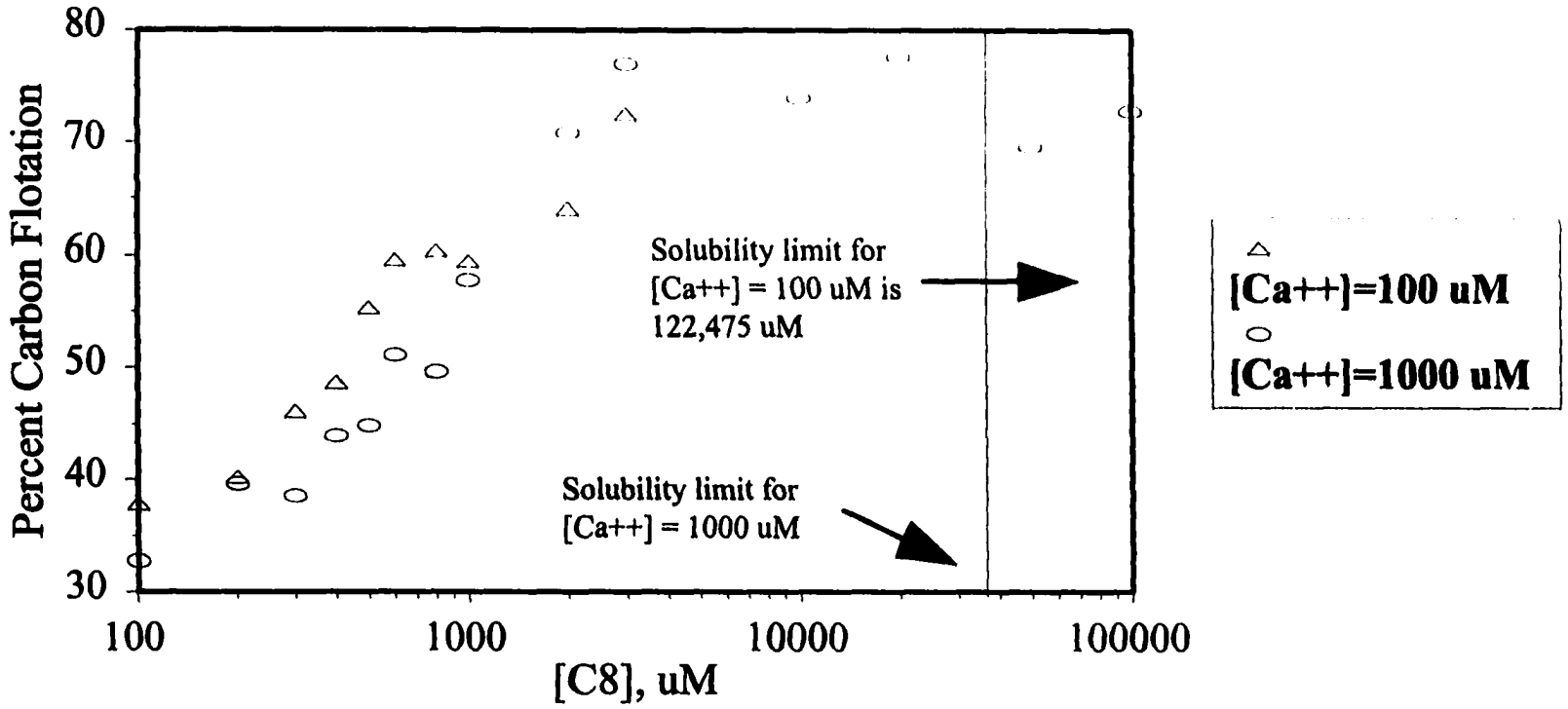

Figure 1.14. Carbon Flotation vs. [C12]

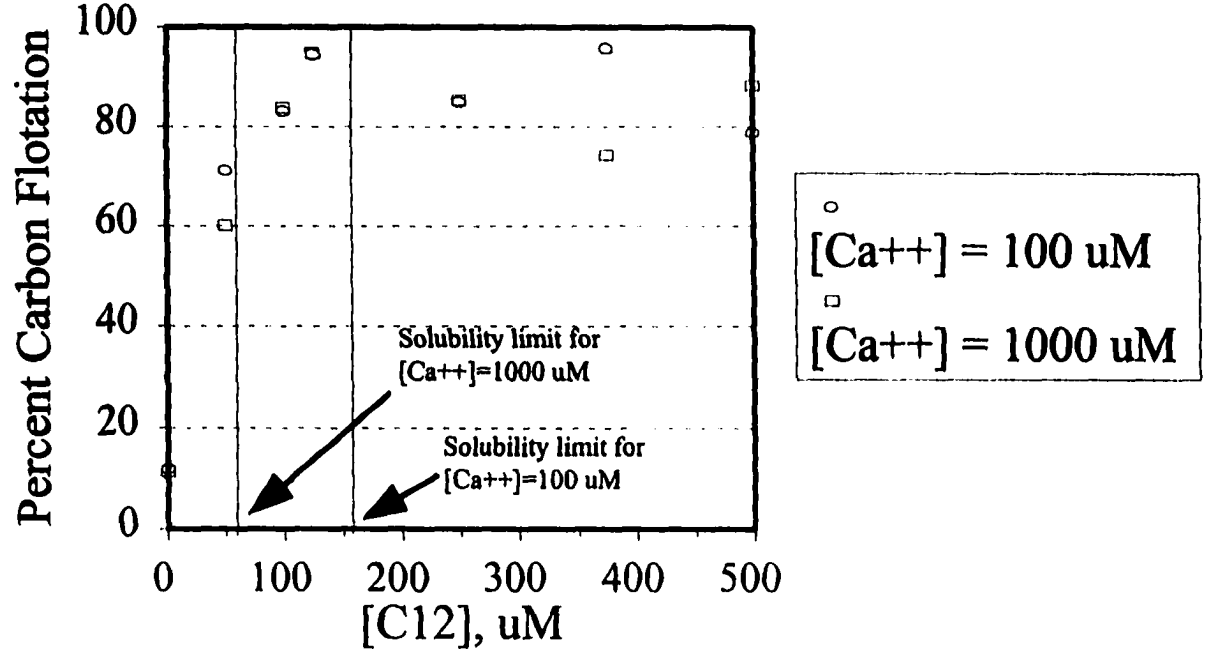

Figure 1.15. Carbon Flotation vs. [SDS]

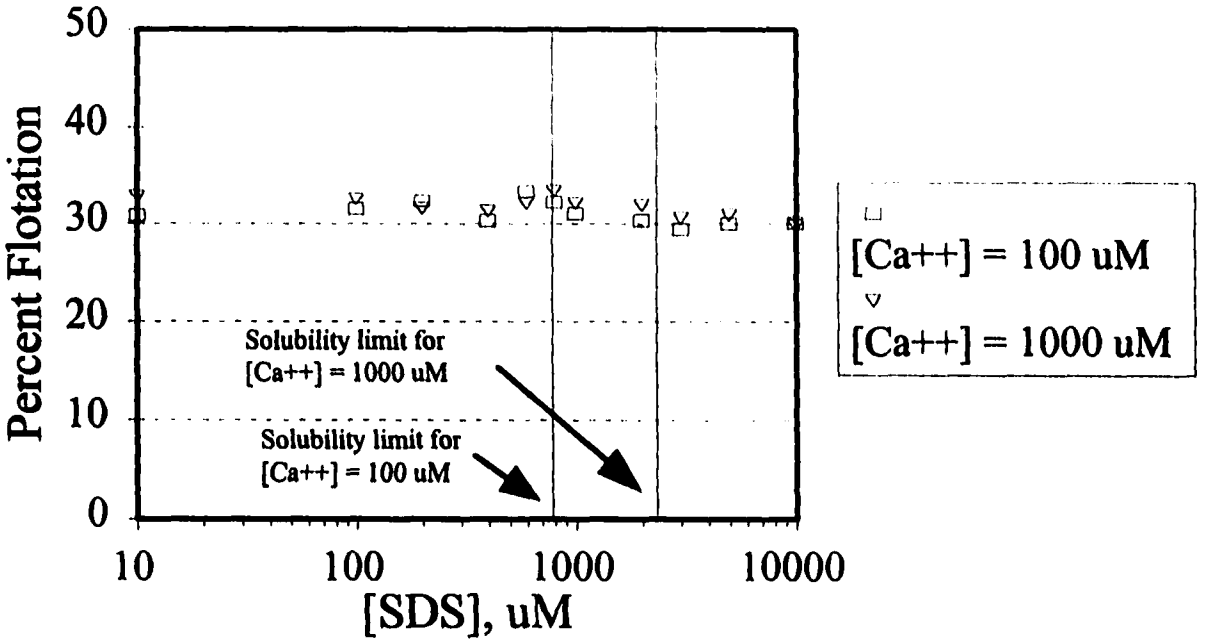

Figure 1.16. Schematic of the collector chemistry mechanism depicting the association of the calcium ions with the adsorbed carboxylate..

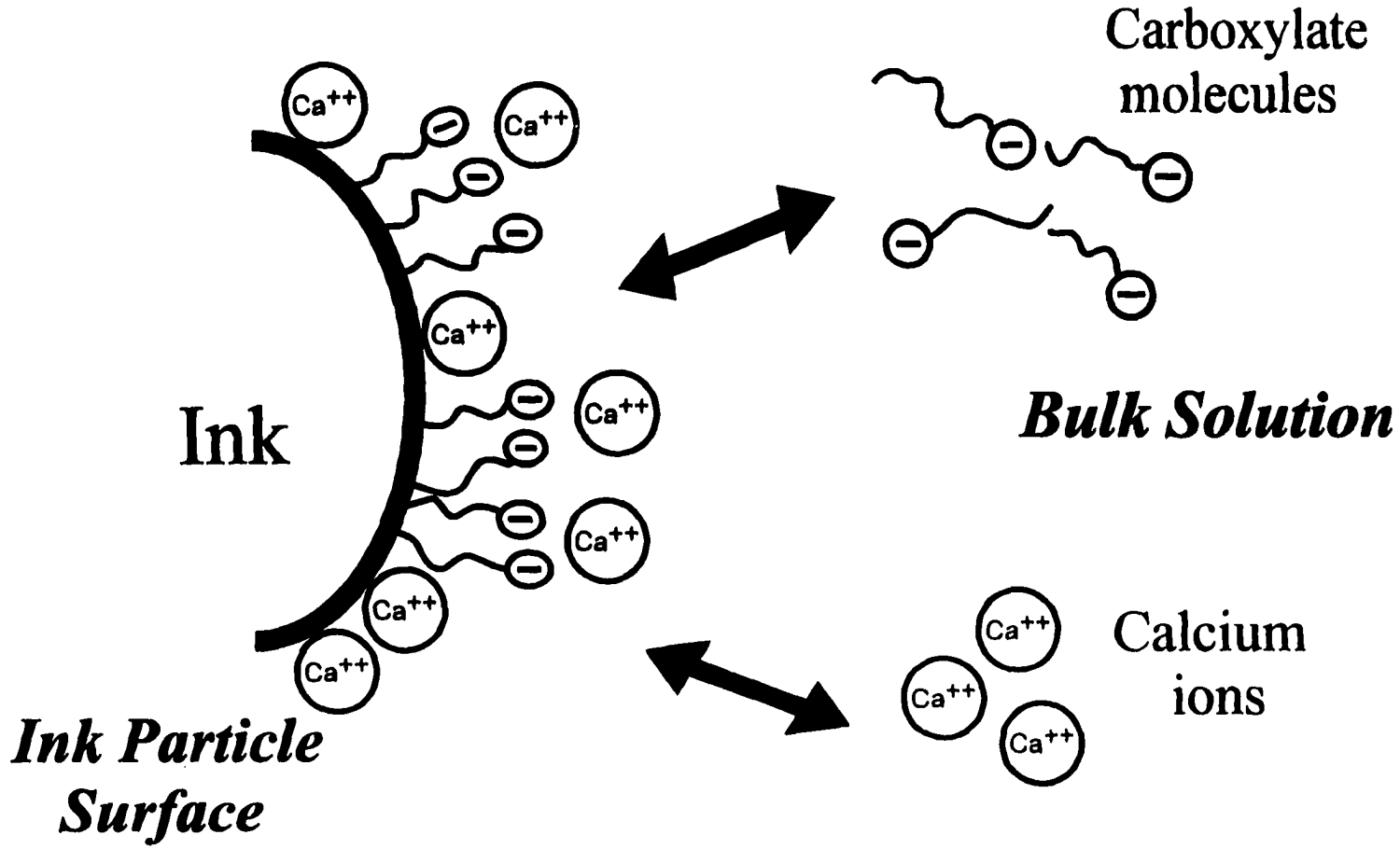

CHAPTER 2

SIZE CHARACTERIZATION OF MODEL INK AGGREGATES IN FLOTATION DEINKING COLLECTOR CHEMISTRY

In this investigation, the effect of calcium and surfactant (sodium dodecyl sulfate and sodium octanoate) concentrations on carbon particle aggregation in flotation deinking systems is described. Surfactant type is shown to be of prime importance in the agglomeration of the particles. This study provides support for the mechanisms of the flotation process being based on the coadsorptive behavior of the carboxylate with the calcium and on carboxylate-calcium bridging as opposed to precipitation of a calcium disurfactant species. The alkyl sulfate did not exhibit this association with the calcium and, instead, acted to disperse the carbon particles despite diminished zeta potentials in the presence of calcium.

Keywords: Deinking, Flotation, Collector Chemistry, Surfactant, Ink Particle Size, Image Analysis.

2.1 INTRODUCTION

Deinking is the process of removing the ink from reusable paper fiber. This general operation, practiced on a large commercial scale only since World War II, is often compared to the laundering process [1]. In fact, the original 1908 Henkel patent [2] for the process referred to the chemicals that were employed as "paper detergents". In 1993, nearly 36 million tons of secondary fiber were recovered in the United States [3], representing an 80% increase since 1985, and the figures are projected to reach 50 million tons by the year 2000 [4]. Improved deinking technology over the past few years has allowed more recycled fiber to be used in papermaking processes while maintaining or improving quality of the final product [5]. Recently, technology such as flotation deinking, which is well established in Europe and Japan, has been gaining popularity with North American deinking mills and has made easier the recycling of diverse sources of secondary fiber into more valuable products. Many chemical additives used in secondary fiber recovery have been reformulated or used differently in order to accommodate new technologies [6].

Paper recycling is, in theory, a very simple process; only two steps are necessary. First, the secondary fiber source must be broken down into contaminants and recoverable fibers. Next, the contaminants must be separated from the fiber. However, the practice of recycling involves many complications [7]. Varying types and concentrations of contaminants can hamper the recycling process. Many

difficulties result from mixed furnishes of secondary fiber that may contain significantly different types of inks. For example, newsprint inks (ink Types I and II [8]), when subjected to a typical recycling process, detach from the fibers relatively easily to form individual slightly hydrophobic colloidal particles of several μm. in diameter. Photocopy (Xerographic) and laser print inks (Type III inks [8]), however, break into usually large (50-1000 μm in major axis length), essentially two dimensional platelets upon repulping in recycling conditions due to the crosslinked polymeric structure of the toner particles which comprise the ink. Individual fibers may have also been physically incorporated into the polymer matrix [9, 10]. In the recycled product, those ink particles with effective diameter of greater than approximately 50 μm., which is the accepted limit of unaided human vision, appear as visible specks in the paper [11, 12]. Those particles smaller than 50 μm. tend to diminish the brightness of the paper by imparting a gray tint to the surface [14]. Furthermore, a new generation of water-based flexographic inks further complicates matters because of the extremely small (0.3-2 μm.) and hydrophilic nature of the pigment particles. Redeposition of the pigment derived from flexographic inks onto the fibers may be detrimental to final product quality [14], though the importance of redeposition is controversial [15].

In this study, carbon particles were used as model inks to probe mechanisms, but these investigations may be directly applicable to deinking of water-based

flexographic inks, which are composed of a pigment, usually carbon black, that is dispersed in water with the use of water-soluble carboxylic derivatives. These dispersants double as binders and are usually composed of resins which are typically homo- and co-polymers of esters of acrylic and methacrylic acids. The carboxylic group content is appreciable. In basic pH conditions, such as those prevalent in deinking systems, the dried binders hydrolyze and resume their role as dispersants [16]. The pigment, then, exists as a suspension of carbon black--very similar to the model systems being investigated in this study.

The physical size of the contaminants often dictates the method of ink removal. The chemistry of the washing process of paper recycling attempts to detach the ink particles from the fiber and to disperse them as individual particles or extremely small aggregates of pigment. Removal of the ink is then accomplished by dewatering. In the ideal case of a completely homogenous dispersion of the ink and fiber, the amount of pigment removed from the system is proportional to the amount of water removed. Thus, several washing stages could remove nearly all of the contaminant. In practice, however, it is necessary that the particles or aggregates be less than 10 μm. in effective diameter, and ideally below 5 μm., so as not to be entrapped in the fiber mat that results from dewatering . In fact, for ink particles 25 μm. in size, only approximately 75% of the theoretical removal is achieved, and for

50 μm. particles, the efficiency decreases to 35% [17]. This entrapment may result in a substandard product, especially when Type III inks are present in the furnish.

The chemistry of flotation deinking, on the other hand, strives to cause the small detached ink particles to aggregate into larger agglomerates. The ink aggregates are then preferentially removed from the fiber slurry by injected air flotation. The size range of particles amenable to flotation is 10 to 150 μm., while most efficient flotation of the ink occurs when the particles or aggregates fall in the 15-50 μm. size range [5, 14]. One explanation of the ink attachment to the air bubble is that the particle-bubble collision efficiency decreases with decreasing particle diameter due to hydrodynamic considerations involving breaching of the boundary layer of the rising air bubble by the particle [14, 18, 19]. While the flotation method is more adept at removing Type III inks than is the washing method, larger two dimensional particles also are not readily floated, due to boundary layer considerations with respect to the particle geometry [20, 21]. Therefore, in the case of Type III inks, it is be beneficial to take advantage of the ability of the pulper to reduce the ink particle size and then to employ the correct chemistry to aggregate the ink into specific size ranges. Clearly, then, the size of the particle aggregates can be instrumental in the efficiency of ink removal, and a fundamental understanding of the mechanisms of this aggregation is important.

2.2 COLLECTOR CHEMISTRY

The induced hydrophobicity of the ink particles and subsequent aggregation is usually referred to as "collector chemistry". This general term typically implies the use of an anionic surfactant, traditionally a sparingly water-soluble carboxylate salt, such as sodium stearate, and a "collector" ion, such as calcium, to impart the desired properties to the ink particles.

In one investigation, Hornfeck [2] advocated the existence of an electrostatic calcium bridge that is formed between the moderately negative surface of the ink particle and the anionic head group of the carboxylate surfactant. According to this theory, the hydrophobic tail of the surfactant is then free to interact with the hydrophobic portions of other such bridged surfactants, thus causing ink particle aggregation due to hydrophobic bonding. Particle and aggregate attachment to air bubbles was explained by adsorption of the hydrophobic tails of the electrostatically bound surfactant molecules at the air-water interface of the rising air pocket. The theory did not address the possibility of bilayer formation or of a lying-down orientation of the surfactant molecules, both of which more thermodynamically favorable arrangements than the proposed tail-out structure..

Larsson et al. [14, 19] studied the change of the zeta potential and flotation efficiency as a function of the addition of calcium ions to model ink dispersions in the presence of sodium stearate. The investigators observed that the absolute value of the

negative zeta potential of the ink particles decreased with increasing calcium concentration. The trend was shown to nearly mirror the increase in flotation efficiency of the model ink as a function of the same variables. Microscopic analysis of the ink particle revealed precipitated calcium distearate adhering to the surface of the ink. From these observations, the authors concluded that precipitation of the calcium dicarboxylate was necessary to create a micro-encapsulation of the ink particles causing aggregation, hydrophobicity, and subsequent flotation. It should be noted, however, that all of the experiments in that study were conducted with surfactant and calcium concentrations at least two orders of magnitude above the solubility product constant (K_{sp}) of the calcium distearate. A subsequent study [22] supported this precipitation mechanism, but again the surfactant employed (sodium oleate) did not allow observation of behavior below the K_{sp} due to the extremely low solubility of the calcium di-surfactant complex. Conditions under which no surfactant precipitate is present were not considered in these studies.

Riviello et al. [23] investigated the mechanism of collector chemistry by employing medium chain length carboxylates and sodium dodecyl sulfate as the surfactants. The investigators studied adsorption isotherms of sodium caprylate, sodium laurate, and sodiium dodecyl sulfate on carbon black particles, as well as zeta potentials and flotation efficiency of the carbon as a function of surfactant and calcium concentrations. The concentrations of the surfactants and calcium were

varied so that the solubility product was exceeded in some cases and not exceeded in other experiments so that the effect of the presence of surfactant precipitate could be investigated. In the study, the flotation efficiency of the model ink peaked well below the K_{sp} of the calcium di-surfactant complexes and, in the case of the carboxylates, actually diminished slightly following precipitation. Adsorption of the surfactant and calcium were shown to be cooperative, while the magnitude of the zeta potential of the carbon particles was depressed by the calcium ions regardless of the surfactant concentration. It was proposed that the surfactant adsorbs tail-down on the surface of the carbon particles, and the calcium strongly associates with the anionic head groups. This orientation of carboxylate adsroption on carbon black from aqueous solutions is supported in the literature [24-26]. Hydrophobicity was thought to be induced by the structure of the calcium dicarboxylate complex and allowed preferential flotation of the carbon. While electrical double layer compression was achieved by calcium alone, the carboxylate-calcium association was necessary to achieve flotation.

The current investigation continues the work of Riviello et al. [23] and further investigates the coadsorption of surfactant and calcium and the aggregation behavior of model carbon particles below the K_{sp} of the surfactant-calcium complexes.

2.3 IMAGE ANALYSIS

Studies of aggregation phenomena require particle size measurement techniques that yield statistically valid data. One such method is the "dirt count" measurement in paper handsheets prescribed by the TAPPI Standard Test Methods [27]. This procedure, however, is quite time consuming and cannot account for those particles smaller than the limit of unaided human vision. Due to these difficulties, image analysis is quickly becoming the industry standard for particle counting and sizing.

Image analysis is the name given to the general technique of employing a computer to acquire an image of a paper sample and determine the number and size of the contaminants. The image acquisition may be either microscope-based (Figure 2.1) or scanner-based. The latter configuration is able to discern only those specks above the limit of vision (50-60 μm), while microscope-based machines are able to detect particles in the micron-size range. Configurations involving microscopes are also much more flexible, allowing the operator to choose the magnification or manipulate the illumination source, be it reflected (most common) or transmitted. Following the image acquisition, the signal may be sent to an image enhancer that allows image averaging, overlays, and background subtraction. This signal is then transferred to the computer where analysis of the image can be performed. The method of speck detection is based on the assignment of a gray value to each pixel in

the field of view. A threshold is set below which all darker portions of the image are then considered as ink specks. Pre-written software or specially written code is employed to extract the histographic information, and accurate and reproducible results are usually achieved, assuming the threshold remains constant.

Several authors [28-32] have investigated the errors associated with image analysis. Zeyer et al. [29] have concluded that if the threshold is held constant, inadequate sampling is the only source for appreciable error. The level of impurities or ink particles detected in the sample, W, expressed in ppm, can be defined by the equation

$$W = \left(\frac{\sum_{i=1}^{m} x_i}{T} \right) * 10^6 \qquad \{2.1\},$$

where m is the total number of impurities observed, x_i is the area of each detected impurity, and T is the sampled area. Juan [32] proposed a statistical method for the calculation of the sampling error in the measurement of dirt in paper as well as the minimum area required to be sampled for statistical validity. According to this study, the number of impurities detected is the variable with the greatest potential influence and determines the overall sampling error. The only assumption of the model is that the impurities in the sample obey a random Poisson distribution, which is reasonable when the physical characteristics of the process are taken into account [32]. In this

mathematical presentation, *ERR(W)*, the percent estimation of the relative error in the measurement of the level of impurities present, is defined as

$$ERR(W) = \left\{\left[1+\left(\hat{S}/\bar{x}\right)^2\right]/m\right\}^{1/2} \qquad \{2.2\},$$

where $\hat{S}$ is the square root of the estimator of the variance, and $\bar{x}$ is the estimator of the average area of impurities. A reasonable approximation of the expected error is

$$ERR(W) \approx 1/m^{1/2} \qquad \{2.3\}.$$

For the determination of the required sample size, Juan [32] proposes the following formula :

$$T \geq \mu / We_r^2 \qquad \{2.4\},$$

where T becomes the minimum area to be sampled for a given maximum relative error, e_r, (i.e., ERR(W) $\leq e_r$), and μ is the average area of impurities. Thus, Equations {2.3} and {2.4} permit the calculation of the error associated with the method of analysis and the calculation of the minimum sample size that must be scanned.

2.4 EXPERIMENTAL

2.4.1 Materials and equipment

The carbon black was supplied by Cabot and was Type 400R, a pigment commonly used in the manufacture of many varieties of inks [33]. The nominal

particle size was advertised to be 25 nm., but the stable aggregates of carbon averaged approximately 1 μm. The supplier-provided BET surface area was 96 $m.^2/g$. The surfactants employed for these investigations were sodium octanoate (hereafter referred to as C8) and sodium dodecyl sulfate (SDS). Schematics of the chemical structure of the two surfactants are illustrated in Figure 2.2. The C8 was purchased from Sigma Chemical Company with a purity of greater than 99%. The electrophoresis grade SDS was provided by Fisher Scientific and also had a purity of greater than 99%. The calcium chloride was also obtained from Fisher and was oven-dried for 12 hours at 90°C just prior to manufacturing the stock solutions due to the chemical's hygroscopic nature. pH adjustments were made with Fisher-Brand Certified N/20 NaOH. All of the above materials were used without further purification. The water used for the experiments was distilled and deionized.

Zeta potentials were determined using a Zeta Meter Model 3.0. The potential across the cell was adjusted as a function of the ionic strength (specific conductance) of the sample so as to avoid thermal overturn associated with overpotentials. The measurements were taken at a constant temperature of 30°C.

The image analysis equipment consisted of a Nikon Optifot II microscope, with reflected and transmitted light capabilities. Reflected light was chosen for the illumination. A Sola Model CVS line conditioner was installed for the microscope light source to avoid the deleterious effect of fluctuating lamp intensity [34]. The

lamp was allowed a 2 hour warm-up period prior to using the image analysis for measurement. A Hamamatsu C2400 CCD monochromatic video camera was mounted on the microscope with the use of an adapter. The image created by the camera was sent to a Hamamatsu Argus 20 image processor/camera controller with image averaging, background subtraction, and overlay capabilities. The video signal was displayed on a Sony Trinitron monitor while simultaneously being sent to a Imaging Technology, Inc. VISION*plus*-AT frame-grabber computer card that controlled the image acquisition. Version 4.1 of the Optimas imaging software was employed to manipulate the image and provide various measurements, which were controlled from the computer (Intel Pentium®, 60 MHz clock speed) CRT. The microscope stage was a worm driven, 3 x 4 inch travel, motorized stage, manufactured by Prior. Stage movement was controlled by software written for the Optimas package, thus allowing automated sample movement.

2.4.2 Methods

In the aggregation experiments 70 mL of water was added to 0.05 g of carbon black. The suspension was then homogenized using a Fisher Model 550 Sonic Dismembrator in order to insure that all large aggregates were broken and that initial particle agglomeration was constant for each suspension. Homogenization was accomplished by applying an ultrasonic frequency of 20 kHz to the suspension for

approximately 5 seconds. The calcium and/or surfactant was then added in the form of pre-prepared stock solutions, the pH was adjusted to 9.0 or 11.0, and more water was added to bring the total volume to 80 mL. The moderately basic pHs were selected to conform with the conditions of traditional deinking operations. The suspension was then thermostatted at 30°C for 30 minutes.

Instead of forming traditional handsheets for image analysis, the carbon suspensions were deposited on filter papers using a standard Büchner filter. In order to achieve a random distribution of the carbon particles and aggregates for representative sampling, two filter papers (FisherBrand glass fiber filter circles with a nominal pore size of 2 μm.) were placed on the porcelain Büchner filter. Two papers were necessary to avoid a non-random distribution due to the filter hole pattern. With standard filtration, the larger particles and aggregates tended to migrate toward the edge of the filter paper. Therefore, a glass cylinder with a diameter approximately one third that of the filter was placed on the paper and kept in place by applying pressure in a uniform manner. The suspension was then gently stirred using a glass rod so as to ensure uniformity without causing shear-induced breakage of the aggregates. Five mL of water was added to the glass cylinder, and, using a micropipette, 0.200 mL of the suspension was withdrawn from the sample and added to water. Vacuum was then immediately applied to the filter to quickly dewater the carbon and deposit it on the filter paper. This process was carried out rapidly to avoid

dissociation of the aggregates. This technique insured a random and reproducible deposition of the particles and aggregates on the filter paper. The filtered samples were then dried, and the particle size distribution was measured with image analysis.

For each sample in this investigation, particle size measurements were taken using the 5x objective of the microscope-based analysis equipment. The 5x objective was chosen because it afforded a reasonable compromise between the desire for a high magnification and a large area to be examined. With this objective, particles as small as several microns were detectable while the region of interest was large enough to allow representative sampling in a short period of time. The automated stage movement was used to scan a grid of 49 fields of view (7 by 7), and the area of each frame was approximately 1 $mm.^2$. This sampling number agrees with the work of Vidotti et al. [35], who concluded that the total number of fields counted to be scanned should be approximately 50 per sample. The data was exported to an electronic spreadsheet (Microsoft Excel) where calculations were performed.

The threshold limit was determined by viewing a region of interest and increasing the threshold until all ink specks were marked by the software. These thresholds were set at the beginning of each data gathering session and were not changed. The levels were not necessarily constant from session to session due to small differences in the intensity of the lighting, video image contrasting, and the relative gray values of the paper and the ink specks.

For this study, the statistical evaluation suggested by Juan [32] was employed to calculate the estimated overall sampling error and the minimum area required to be scanned for an error of less than 5%.

2.5 RESULTS AND DISCUSSION

In order to elucidate the fundamental aggregation behavior of ink as a function of the concentrations of the chemical additives, it was necessary to eliminate as many extraneous variables, normally present in industrial deinking operations, as possible. Therefore, the present study was carried out using a model ink, carbon black, instead of a real ink that may consist of varying pigments and binders. Also, neither cellulose fibers, fillers, or coatings were present in the experiments.

Parameters obtained from image analysis included the total number of particles, the average area and major axis length, the total area covered by the particles, and the standard deviation of the measurements. In this study, the size-relative population evolution of the aggregates with respect to the chemical additives are illustrated by three dimensional histograms. In the histograms, the overall size range of the particles is divided into smaller bins. The Z axis represents the number or area percentage of particles in each bin, the X axis represents the bins (area of the particles or equivalent diameter), and the Y axis represents the varying concentrations of calcium or surfactant.

The large number of small particles (diameter less than 50 μm.) created difficulties in tracking the average size of the particles as a function of the surfactant and calcium concentrations. The number-average size is actually an inefficient means to report particle size distribution [35]. While the particle number distributions with respect to size are important, they do not indicate the relative amounts of areas of the different sized particles that are present. Several large particles may represent a much greater area than many small particles, and, with respect to the optical qualities of the paper, the few large particles may be more important and troublesome in quality control. Therefore, it is instructive to consider the particle area distribution, or, more exactly, the relative area in each bin, rather than simply the number of particles. Histograms 2.1 and 2.2 illustrate this conclusion. The particle number distribution (Histogram 2.1) is shown to be quite different from the relative area distribution (Histogram 2.2). In fact, the largest particles represent a significant part of the total area covered by the ink, even if these particles number fewer than the small particles. A software macro, written specifically for this application, permitted the calculation of the relative areas of each of the bins. In tests of repeatability, a sample was analyzed several times, and the deviations of the average size and histogram bins were compared. In all cases, the deviation was less than 5 %, indicating that the measurement procedure was reliable.

Statistical relevance of the data gathered by the image analyzer was evaluated per the previously discussed mathematical model. Because, according to Juan's model [32], the potential error in the measurement is inversely proportional to the number of contaminants detected, the series of data with the fewest ink aggregates was employed for statistical evaluation. This data set, then, reflects the maximum error that may be attributed to the imaging techniques in this investigation. Table 2.I presents an estimation of the percentage errors associated with the chosen sample area, *ERR(W)*, and the minimum area, T_{min}., that must be sampled for a relative error of less than 5.0%, using Equations {2.3} and {2.4}. The maximum relative error is 4.15%, while the average relative error for this series is 2.81%. These values are well below the 5% error that is commonly used for statistical evaluations of this type [30]. In this series, the maximum required sampling area for the 5% relative error is 33.7 mm.^{2}, compared to approximately 49 mm.^{2} scanned in all cases in this investigation. Therefore, the data gathered by the image analysis are statistically valid.

The present investigations centered about the effect of the calcium and surfactant concentration on the particle size evolution. In all experiments, the concentrations of the calcium and surfactant remained well below the K_{sp} of the calcium disurfactant complex, and surfactant concentrations remained below the critical micelle concentration (CMC). Therefore, no bulk phase precipitation or micellization effects play a role. While experiments were performed at both pHs 9

and 11, no significant effect of pH was observed in this narrow range. Therefore, only data from the trials where pH=9 are presented. The complete sets of data can be found elsewhere [36].

The size distribution of the particles as a function of surfactant concentration is shown in Histograms 2.3-2.8 for both the SDS and the C8 with constant calcium concentrations of 0, 600, and 1000 μM. In the case of the SDS, Histograms 2.3, 2.4, and 2.5 illustrate that as the calcium concentration was increased, the relative area represented by the larger particles increased significantly at the expense of the smaller particles for the low SDS concentrations. However, as the surfactant concentration was increased with the concentration of calcium remaining constant, the relative area represented by the large particles decreased while that represented by the small particles increased. Competing mechanisms may be responsible for these trends. At the lower SDS concentrations, increasing the divalent calcium cation concentration caused compression of the electrical diffuse double layer around the negatively charged carbon particles and a decrease in the magnitude of the zeta potential (see Figure 2.3). This compression of the double layer resulted in diminishing electrostatic repulsion between the carbon particles and allowed aggregation. At higher SDS concentrations, increased adsorption of the surfactant possibly led to increased steric stabilization of the carbon suspension. Also, the surface of the

particles may have become less hydrophobic due to the very hydrophilic nature of the outward-oriented sulfate head groups.

Histograms 2.6, 2.7, and 2.8 illustrate the particle size as a function of the C8 concentration. In this case, the size of the aggregates increased significantly with increasing calcium concentration at both low and high C8 concentrations. The relative areas of the larger particles were much greater than those for SDS. At low C8 concentrations, the calcium again adsorbed to the negatively charged carbon particles, decreased the electrostatic repulsion, and contributed to aggregate formation. However, at higher concentrations of the carboxylate, dispersion of the carbon particles was not observed. In fact, much-increased agglomeration was observed, indicating some type of association between the C8 and the calcium on the carbon surface.

Histograms 2.9 and 2.10 illustrate the particle size distribution as a function of calcium concentration with a constant surfactant concentration (4000 μM). In the former histogram, due to the high SDS concentration, the particle sizes remained small in spite of the increasing calcium levels. No aggregate-inducing association occurred. However, Histogram 2.10 of the carboxylate system shows significant aggregation of the carbon at higher calcium concentrations. Again, the SDS acted to disperse the carbon while the C8 aided in agglomeration of the particles.

Histograms 2.3 through 2.10 graphically illustrate a dramatic difference in the behavior between the SDS and C8 surfactants. Two differences between SDS and C8 can be seen in the molecular structures (Figure 2.2). First, the SDS has an aliphatic, saturated hydrophobic tail composed of 12 carbons, while a 7 or 8 carbon chain (depending upon whether or not the tail is defined as containing the carbon of the carboxylic group) forms the hydrophobe of the C8. Secondly, the hydrophilic head group of the SDS is sulfate, while that of the C8 is a carboxylate. The K_{sp} of both calcium di-surfactant complexes are similar: approximately 10^{-6} for calcium dioctanoate [23, 37] and 5×10^{-10} M^2 for the calcium didodecyl sulfate [23, 38] in spite of the fact that the hydrophobic tail of the SDS is 4 (or 5) carbons longer than the C8. However, the calcium complex of a comparable-length caboxylate salt, sodium dodecanoate, has a K_{sp} of approximately 10^{-12} M^2 [37]. Therefore, the carboxylate has a greater affinity to form insoluble calcium disurfactant complexes than does the sulfate. Histograms 2.3 through 2.10 illustrate that the carboxylate also has a much greater aggregate-inducing association with the calcium than does the sulfate, even though the concentrations in all systems are well below the K_{sp} of the respective calcium disurfactant complexes.

The difference in the association of the calcium ion with the carboxylate and sulfate head groups of surfactants below the CMC may explain the difference in aggregation for the two surfactants. Both head groups tend to form resonance

structures upon dissociation in aqueous systems [39, 40], with the carboxylate having a planar geometry and the sulfate adopting a tetrahedral structure. The single negative charge is, then, distributed between the two and three pendant oxygens, respectively. Association constants for hydrogen sulfate and formic acid anions with the divalent calcium cation show that the sulfate group has a binding constant nearly one order of magnitude greater than the carboxylate group (log K=2.31 vs. 1.43) [41]. These types of values typically do not change significantly with the addition of an aliphatic hydrocarbon chain in place of the terminal hydrogen [41]. The hybridized sulfate may provide a better environment for calcium association due to its tetrahedral geometry than does the planar carboxylate. The authors are unaware of any data that has been reported on the existence of water-soluble non-dissociated calcium disurfactant complexes.

However, as previously noted, the association constants (K_{sp}) for disulfate and dicarboxylate calcium complexes show the reverse trend to that of the mono-complexed calcium species; i.e. the disulfated species is more soluble than is the corresponding dicarboxylated species, while its mono-associated form tends to form more readily. This phenomenon may be, in part, explained by the crystal structure of the calcium disurfactant species. Ordered surfactant systems, such as SDS micellar structures and the corresponding solid crystalline phases, have been compared in the literature [40, 42, 43]. In crystallized calcium dicarboxylate species, the predominant

molecular structure is that of the calcium bridging two of the carboxylate molecules via one oxygen of each head group [44]. It is likely that the calcium didodecyl sulfate bonds in a similar manner.

Calcium-carboxylate complexes of similar structure have been reported in the biological literature [45-47]. In these cases, aggregation of vesicles having carboxylic groups on the exposed surface is attributed to the association of calcium with the carboxylic groups in the same structure that predominates the precipitated phase. Even though the concentration of the carboxylic groups on the surface is high, the molecules are integrated into the vesicles and do not precipitate. Similar behavior has been observed with phosphate groups of phospholipids [48, 49], but no mention is made of sulfate-induced aggregation. The phenomenon is commonly referred to as "calcium bridging", and the scenario is quite similar to that of the tail-down adsorption of the surfactant onto the surface of carbon. The authors believe that an mechanism analogous to the aggregation behavior of the vesicles is observed with the carbon particles.

Our proposed mechanism of carbon particle aggregation is most likely a combination of calcium bridging between adsorbed carboxylate molecules augmented by diminished electrostatic repulsion caused by calcium adsorption on the carbon surface. The agglomeration does not occur with the SDS because it seems to fail to form such bridges. It is also likely that hydrophobicity of the carbon is augmented by

this molecular association. While calcium dicarboxylate species usually have only two, and sometimes no pendant oxygens with their associated lone pair electrons, calcium disulfate species of similar structure would have four pendant oxygens. These extra oxygens of the disufate species would tend to impart a more hydrophilic character to the complex than the dicarboxylate complex. This observation could explain the preferential flotation of the carbon achieved with the carboxylate as well as the fact that the K_{sp} of the calcium dicarboxylates is lower than the calcium disulfates of corresponding carbon chain length.

This bridging mechanism, combined with the previously discussed induced hydrophobicity attributed to the calcium-carboxylate structure, is hypothesized to result in the aggregation and preferential flotation of the carbon particles . Therefore, the potential for association of the surfactant that is adsorbed in a tail-down orientation with the divalent calcium cation is highly dependent upon the nature of the hydophilic head group. Bulk surfactant precipitation is not necessary for the carbon aggregation, as shown in this study or for flotation of the carbon [23]. A schematic of the proposed mechanism is illustrated in Figure 2.5.

Figures 2.3 and 2.4 illustrate the dependence of the average particle size and zeta potential of the carbon particles as a function of calcium concentration for constant SDS and C8 concentrations. In the case of the carboxylate (Figure 2.4), the increase in the average particle size nearly mirrors the decrease in the magnitude of

the zeta potential of the carbon particles. However, for the systems with SDS (Figure 2.3), the average particle size of carbon aggregates did not increase with the decreasing magnitude of zeta potential. While the magnitude of the zeta potential fell off with increasing concentrations of calcium, only the system with low concentrations of SDS exhibited an increase in average particle size as the calcium concentration was increased. In the cases where the SDS concentration was 600 μM or greater, there was no appreciable aggregation of the carbon particles in spite of the significant decrease in the magnitude of the zeta potential due to increasing calcium concentration. These results illustrate that a decrease in zeta potential is not solely responsible for the aggregation of the carbon and imply that specific surfactant-calcium interaction is integral to the mechanisms of collector chemistry and is necessary for induced hydrophobicity and agglomeration.

2.6 CONCLUSIONS

A tail-down orientation with co-operative adsorption of calcium to the head groups is hypothesized to occur in collector chemistry. The association serves to induce hydrophobicity and results in preferential flotation. The carbon particle aggregation data presented in the current investigation support the coadsorption mechanism of collector chemistry and indicate that calcium-carboxylate bridging is responsible for the agglomeration behavior with the C8. While coadsorption of the

surfactant and the calcium occurred in both the C8 and SDS systems, the sulfate lacked the strong association of the calcium with the surfactant head group to create this bridging. Though aggregation was induced by calcium alone, the SDS redispersed the particles while the carboxylate surfactant enhanced the agglomeration at concentrations significantly below the K_{sp} of the precipitating complex. Thus, the underlying mechanism of collector chemistry is coadsorptive rather than precipitative.

2.7 REFERENCES

1. Borchardt J. K., *Colloid Surf.s A*, **88** (1): 13 (1994).
2. Hornfeck, K., *Conserv. Recycl.*, **10** (2/3): 125 (1987)
3. Mulligan, D. B., *Prog. Paper Recycl.*, **4** (1): 12 (1995).
4. Anon. *Paper Recycl.*, **5** (9): 5 (1994).
5. Harrison, A., *Pulp and Paper*, 63 (3): 60 (1989).
6. Basta, N., Gilges, K., and Ushio, S., *Chem Eng.*, **98** (3): 45 (1991).
7. Estes, T. K. TAPPI Deinking Short Course, May 1995.
8. Read, B. R. , *Paper Tech. Ind.*, **26** (7): 339 (1985).
9. Johnson, D. A. and Thompson, E. V., *Tappi J.*, **78** (2): 41 (1995).
10. Dorris, G. M. and Page, M., Proceedings from *The 3rd Research Forum on Recycling*, Vancouver, BC, Canada; CPPA, Montreal (1995).
11. McKinney, W. J., *Tappi J.*, 71 (1): 128 (1988).
12. McCool, M. A. and L. Silveri, *Tappi J.*, **70** (11): 75 (1987).
13. Turvey, R. W., *Paper Tech. and Ind.*, **25**: 294 (1984).
14. Larsson, A., Stenius, P, and Ödberg, L. *Svensk Papperstidning*, **87** (18): R165 (1984).
15. Chabot, B., Daneault, C., and Dorris, G. M., *J. Pulp Pap. Sci.*, **21** (9): J296 (1995).
16. Dorris, G. M., and Nguyen, N., *J. Pulp Pap. Sci.*, **21** (2): J55 (1995).

17. Horacek, R. G., and Kronlund, N. W., *Tappi J.*, **63** (11): 135 (1980).

18. Pan, R., Paulsen, F. G., Johnson, D. A., Bousfield, D. W., and Thompson, E. V., *Tappi J.*, **79** (4): 177 (1996).

19. Larsson, A., Stenius, P, and Ödberg, L. *Svensk Papperstidning*, **87** (18): R158 (1984).

20. Schmidt, D. C., and Berg, J. C., Proceedings from *The 3rd Research Forum on Recycling*, Vancouver, BC, Canada: 227 (1995).

21. Schmidt, D. C., and Berg, J. C., *Prog. Paper Recycl.*, **5** (2): 67 (1996).

22. Johansson, B., Wickman M., and Ström, G., *J. Pulp Pap. Sci.*, **22** (10): J381 (1996).

23. Riviello, Jr., A. E., Scamehorn, J. F., Christian, S. D., and Borchardt, J. K., *Tappi J.*, submitted..

24. Bartell, F. E. and Miller, E. J., *J. Phys. Chem.*, **28**: 922 (1924).

25. Hartman, R. J., Kern, R. A., and Bobalek, E. G., *J. Coll. Sci.*, **1** (3): 271 (1946).

26. Parkash, S., *Carbon*, **12** (1):37 (1974).

27. TAPPI Standard 437 om-90, Dirt in paper and paperboard, in *TAPPI Test Methods* 1995-1995, TAPPI Press, Atlanta (1994).

28. Jordan, B. D., Nguyen, N. G., and Trépanier, R. J. R., *Tappi J.*, **76** (10): 110 (1993).

29. Zeyer, C., Venditti, R. A., Puangchinda, K. W., and Heitmann, J. A., *Tappi J.*, **78** (2): 168 (1995).

30. Zeyer, C., Venditti, R. A., and Heitmann, J. A., *Tappi J.*, **78** (2): 176 (1995).

31. Moss, C. S., *Tappi J.*, **76** (10): 117 (1993).

32. Juan, J., *Tappi J.* **79** (5): 222 (1996).

33. Cabot Corporation, Technical Report S-127, 1987.

34. Riviello, Jr., A. E., Scamehorn, J. F., Christian, S. D., and Borchardt, J. K., *Prog. Paper. Recycl.*, submitted.

35. Vidotti, R. M., Johnson, D. A., and Thompson, E. V., *Prog. Paper Recycl.*, **2** (3): 30 (1993).

36. Faisant, E., Bachelor's Thesis, CUST, Départment Génie Physique, Institut des Sciences de l'Ingénieur de Clermont-Ferrand, Clermont-Ferrand, France (1996).

37. Irani, R. R. and Callis, C. F., *J. Phys. Chem.*, **64** (11): 1741 (1960).

38. Stellner, K. L., and Scamehorn, J. F., *Langmuir*, **5** (1): 70 (1989).

39. Morrison, R. T., and Boyd, R., N., *Organic Chemistry, Second Edition*, Allyn and Bacon, Inc., Boston, 1966.

40. Coiro, V. M., Manigrasso, M., Mazza, F., and Pochetti, G. *Acta Cryst.*, **C43** (5): 850 (1987).

41. Martell, A. E. and Smith, R. M., *Critical Stability Constants, Vol. 4:*

Inorganic Ligands, Plenum Press, New York, 1977.

42. Conte, C., Di Blasi, R., Giglio, E., Parretta, A., and Pavel, N. V., *J. Phys. Chem*, **88** (23): 5720 (1984).

43. Coiro, V. M., Massa, F., and Pochetti, G., *Acta Cryst.*, **C42** (8): 991 (1986).

44. Einspahr, H., and Bugg, C. E., *Acta. Cryst.* **B37** (5): 1044 (1981).

45. Ahkong, Q. F., Fisher, D. Tampion, W, and Lucy, J. A., *Boichem. J.*, **136** (1): 147 (1973).

46. Cullis, P. R., and Hope, M. J., *Nature*, **271** (5646): 672 (1978).

47. Ortiz, A., and Gomez-Fernandez, J. C., *Chem. Phys. Lipids*, **46** (4): 259 (1988).

48. Bettelheim, F. A., *Biochim. Biophys. Acta*, **236** (3): 702 (1971).

49. Nir, S., Wilschut, J., and Bentz, J., *Biochim. Biophys. Acta*, **688** (1): 275 (1982).

Table 2.I. Calculation of the error associated with the sampling

Sample	Total Area Covered (μm^2)	Avg. Particle Area (μm^2)	Number of particles	W (ppm)	$T_{min}(mm.^2)$	ERR(W) (%)
1-1	33349.77	42.00	794	680	24.7	3.55
1-2	30877.8	30.60	1009	630	19.4	3.15
1-3	26213.79	45.11	581	535	33.7	4.15
1-4	211858.9	38.26	5537	4323	3.50	1.34
1-5	75838.44	40.62	1867	1548	10.50	2.31
1-6	55762.00	48.07	1160	1138	16.90	2.94
1-7	52346.27	25.56	2048	1068	9.57	2.21

Figure 2.1. Illustration of the image analysis system.

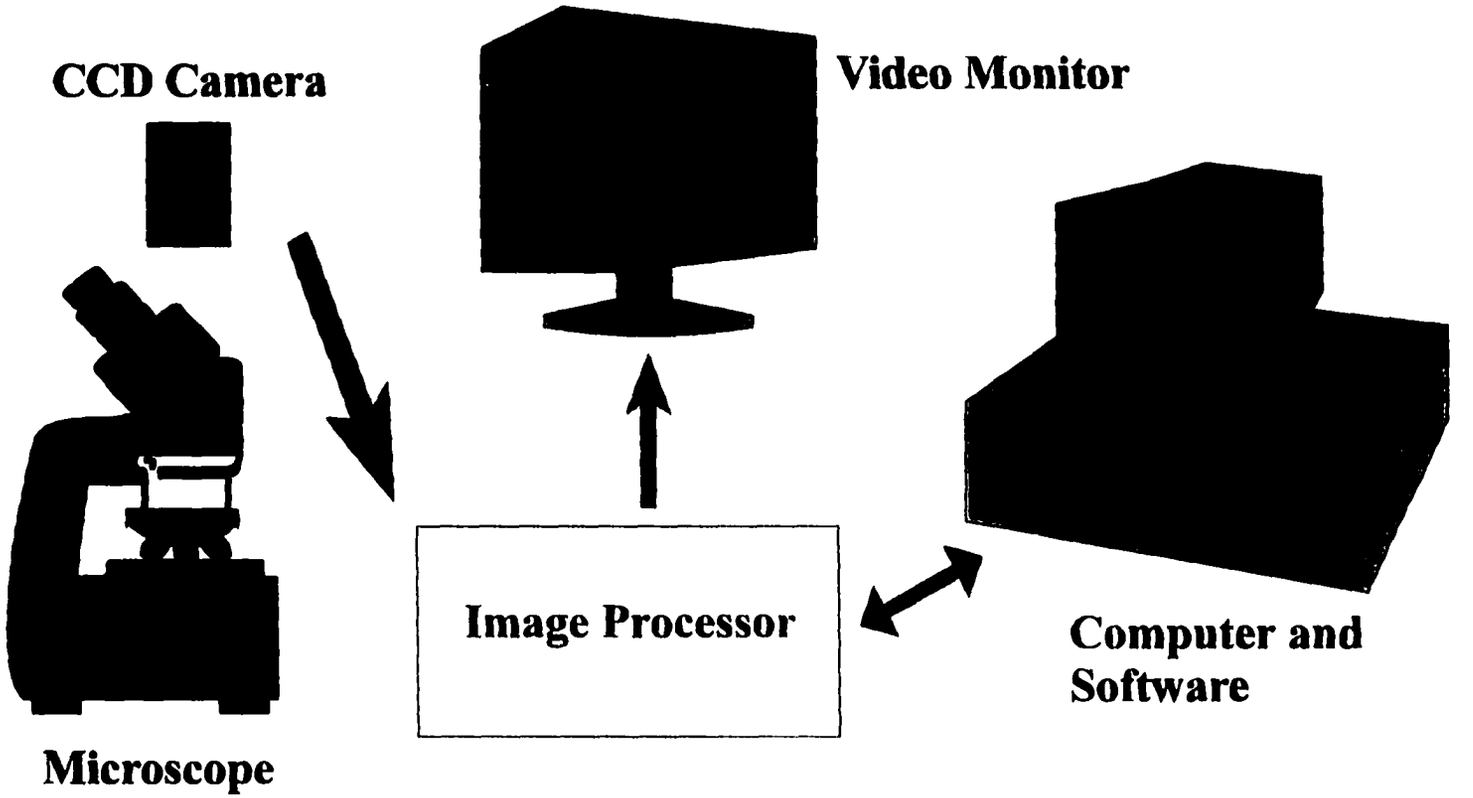

Figure 2.2. The Structure of the surfactants: A) Sodium Octanoate, B) Sodium Dodecyl Sulfate

A)

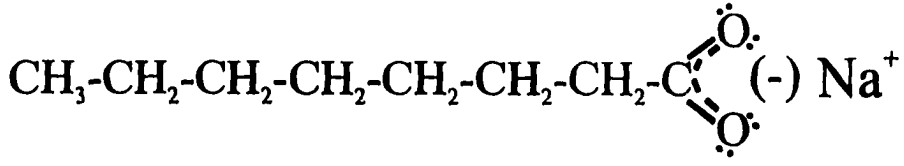

B)

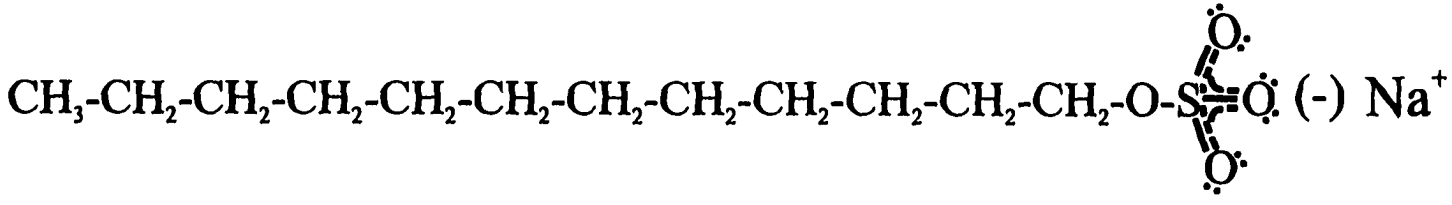

Figure 2.3. Average Particle Size and Zeta Potential for SDS

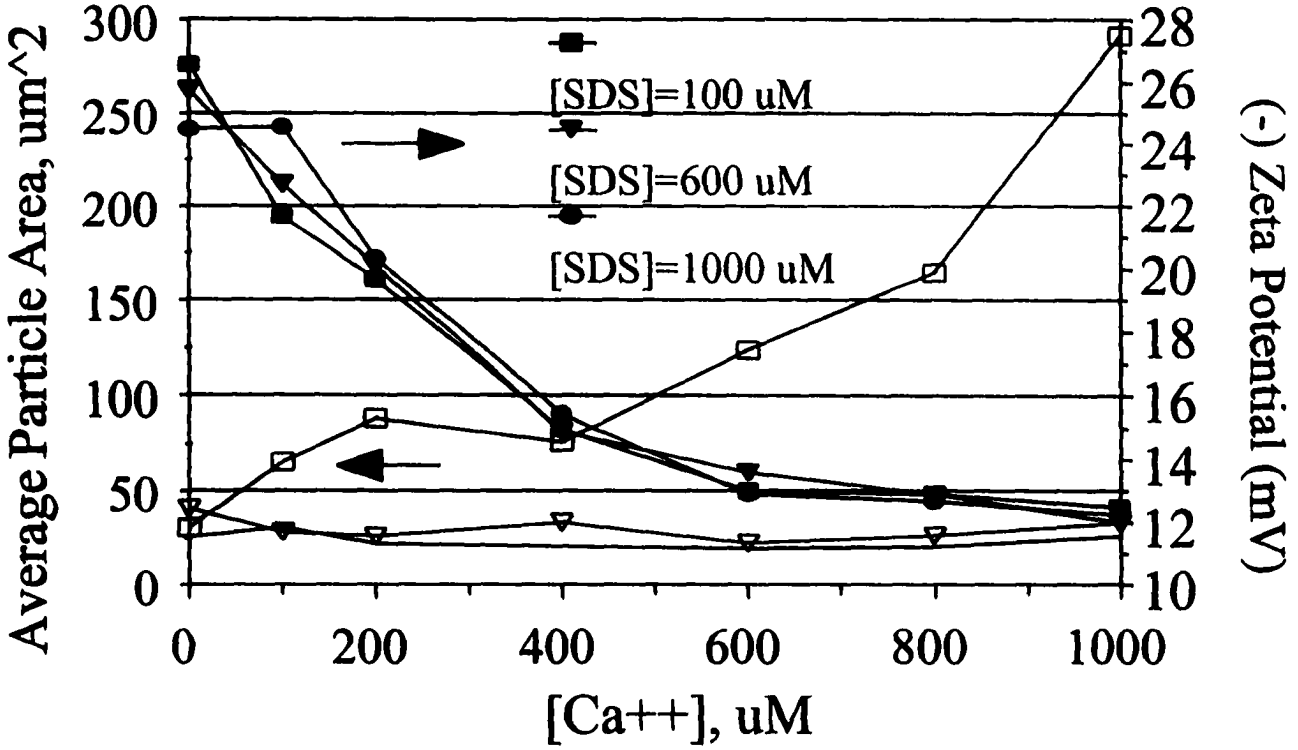

Figure 2.4. Average Particle Area and Zeta Potential for C8

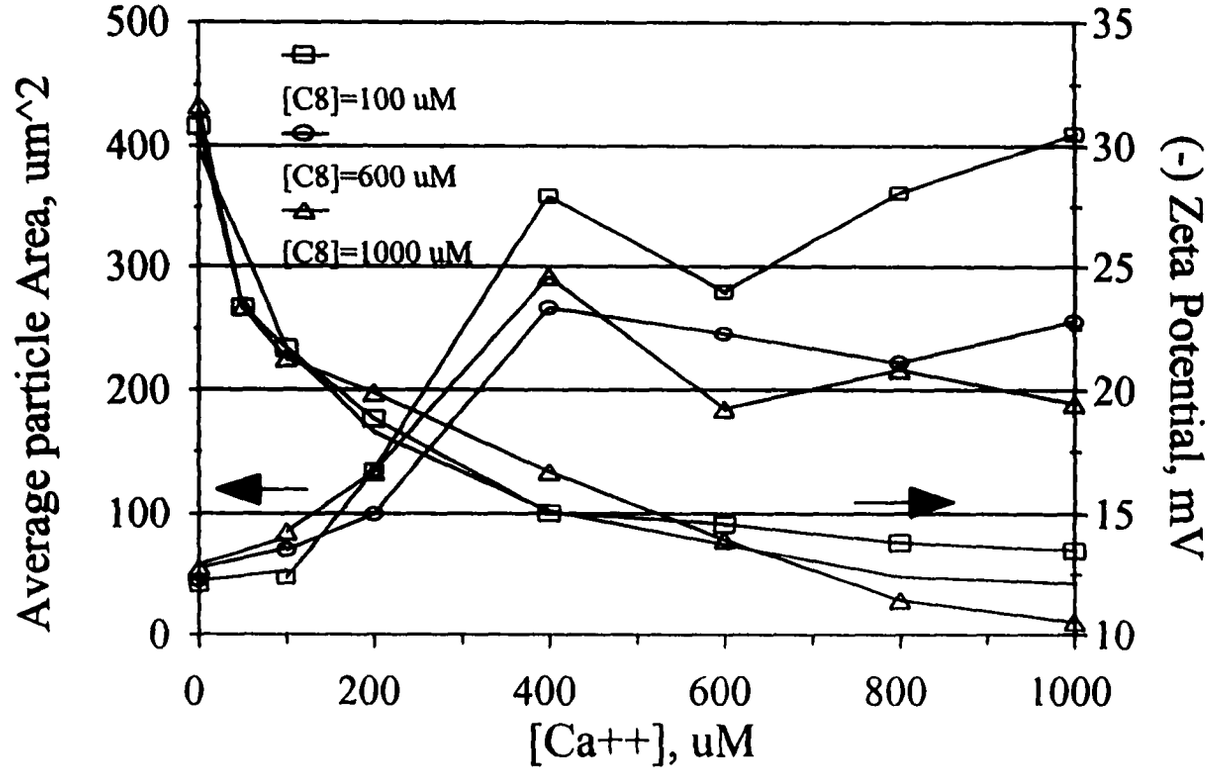

Figure 2.5. Collector chemistry mechanism

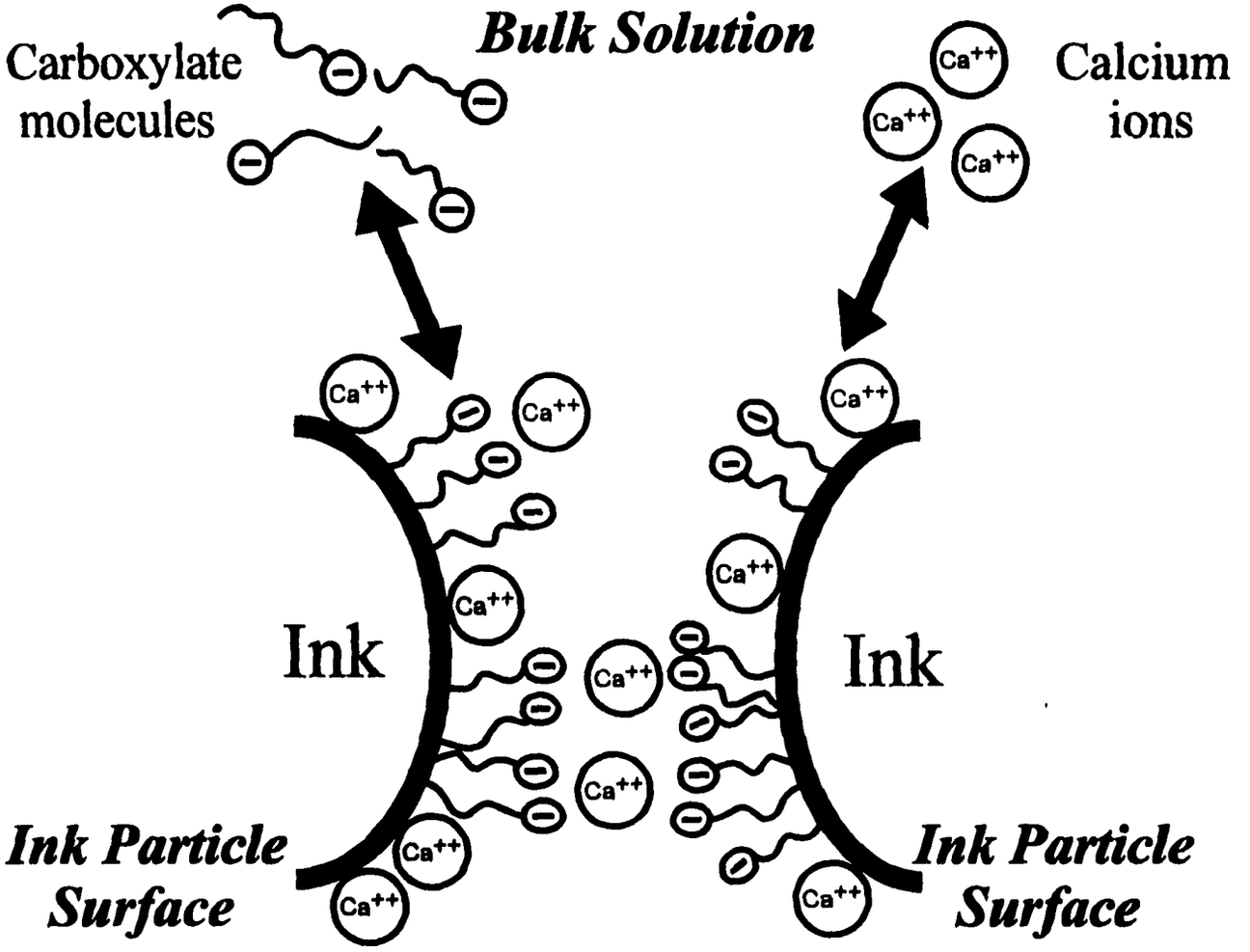

Histogram 2.1. Size distribution as a function of the C8 concentration; [Ca^{2+}]=400 μM

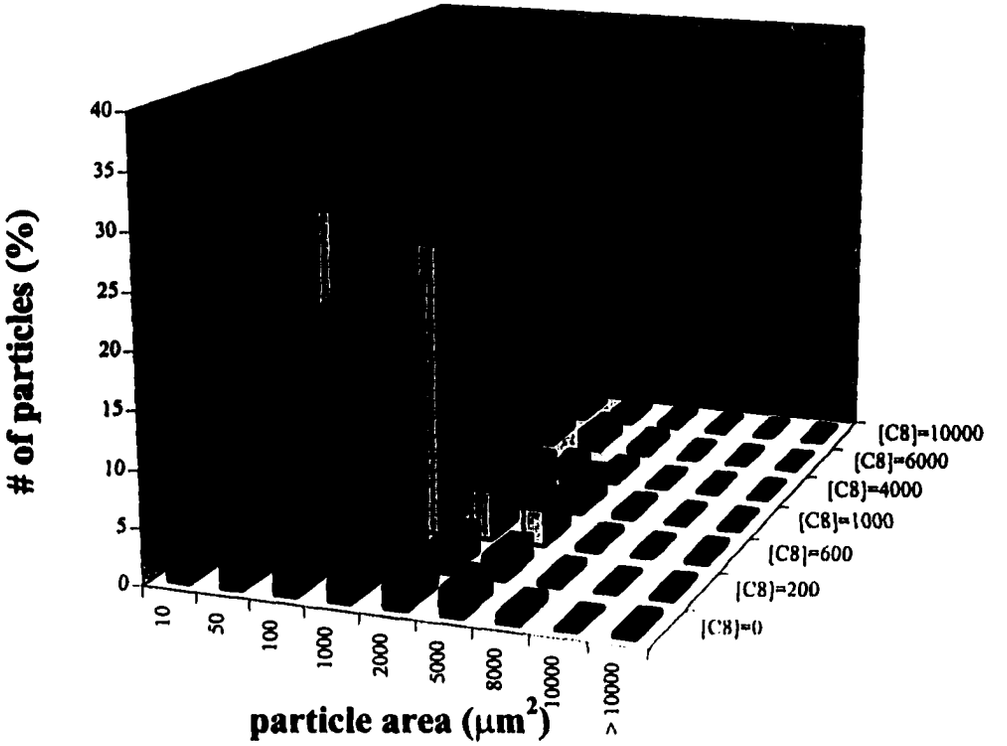

Histogram 2.2. Size distribution as a function of the C8 concentration; [Ca^{2+}]=400 μM

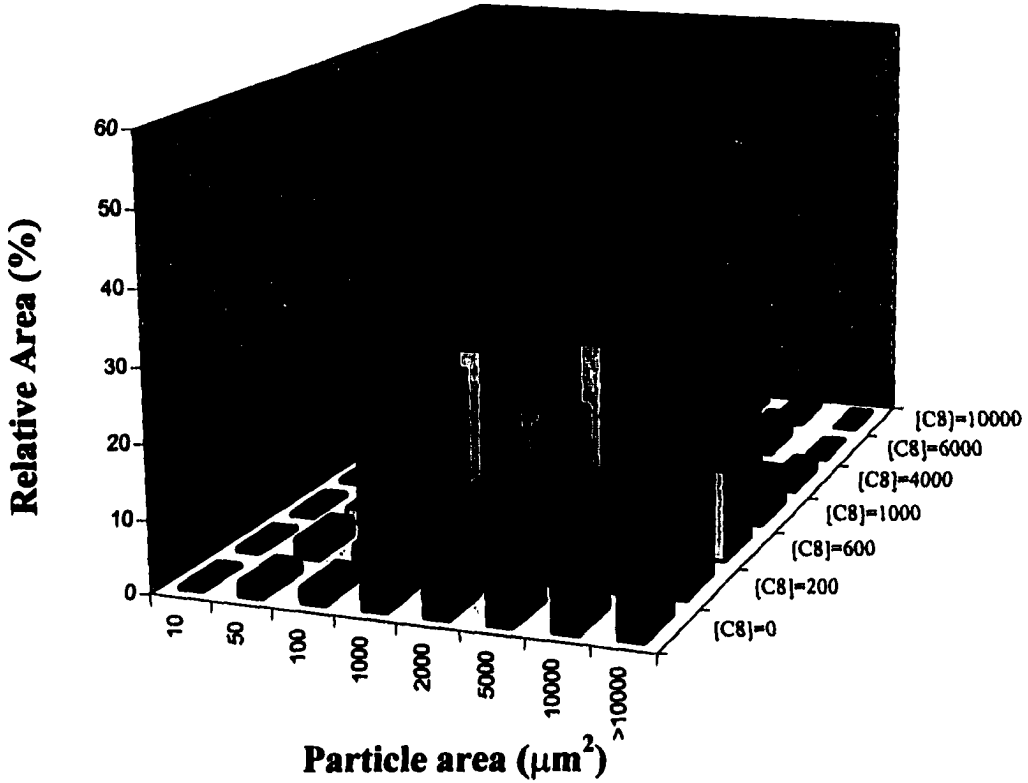

Histogram 2.3. Size Distribution as a Function of theSDS Concentration; [Ca^{2+}]=0 μM

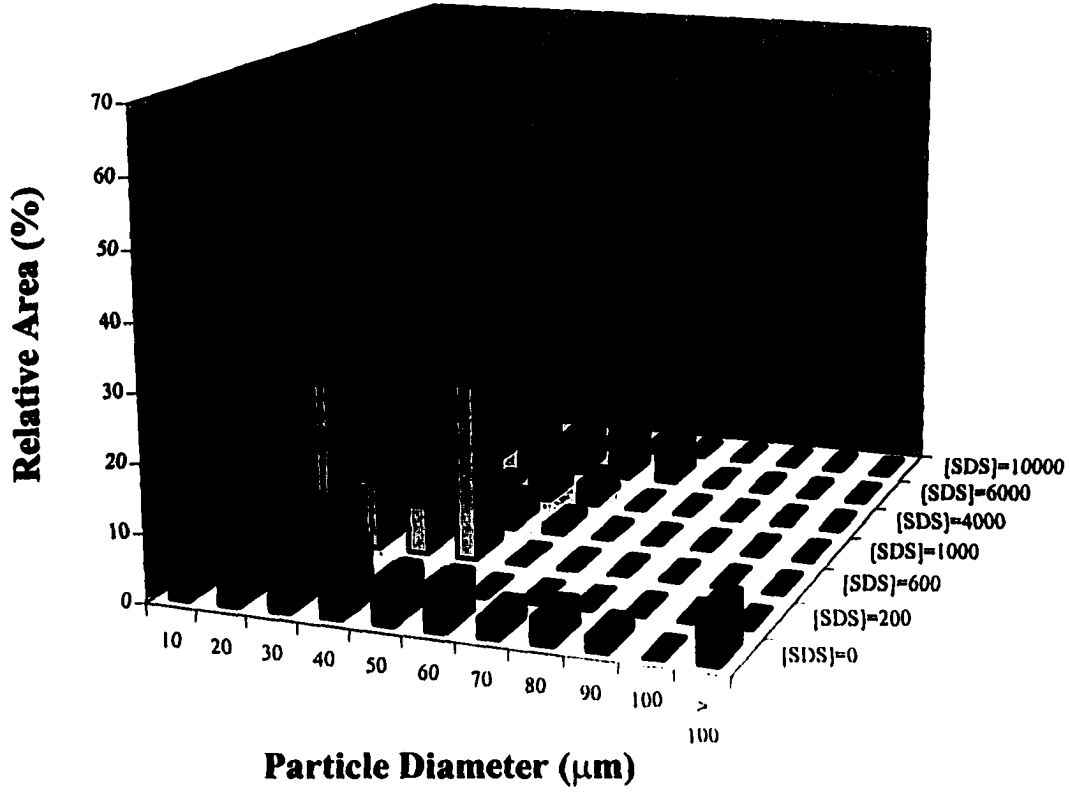

Histogram 2.4. Size Distribution as a Function of the SDS Concentration; [Ca^{2+}]=400 μM

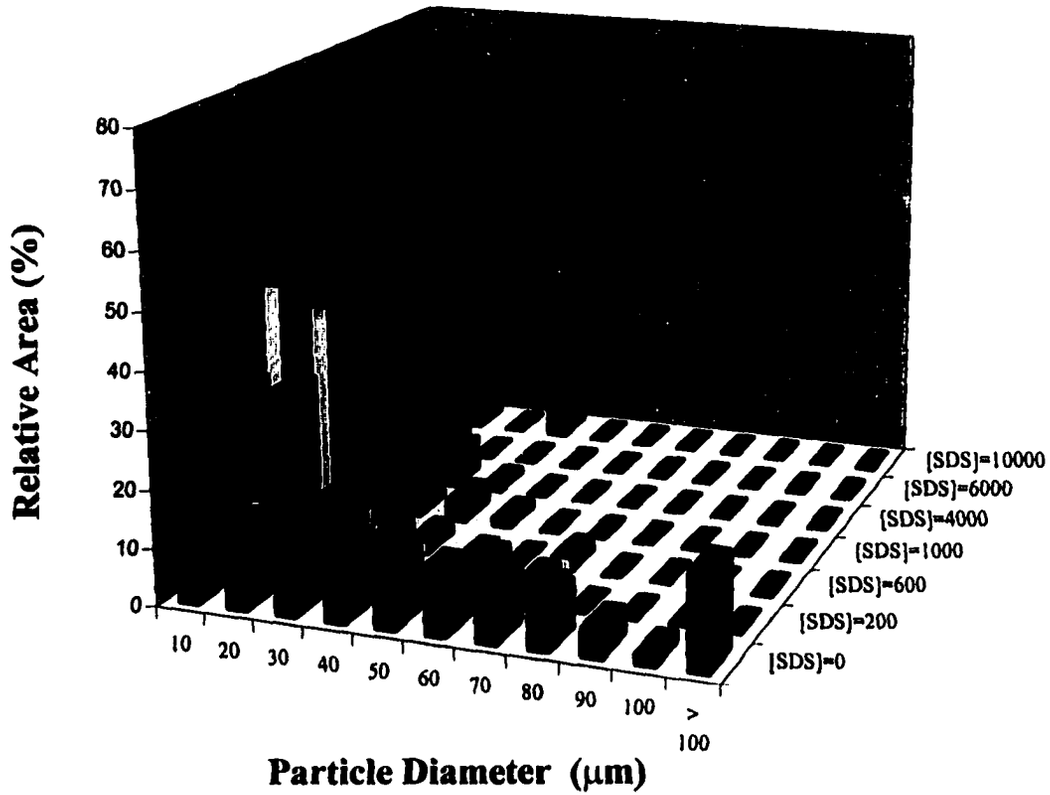

Histogram 2.5. Size Distribution as a Function of the SDS Concentration; [Ca^{2+}]=1000 μM

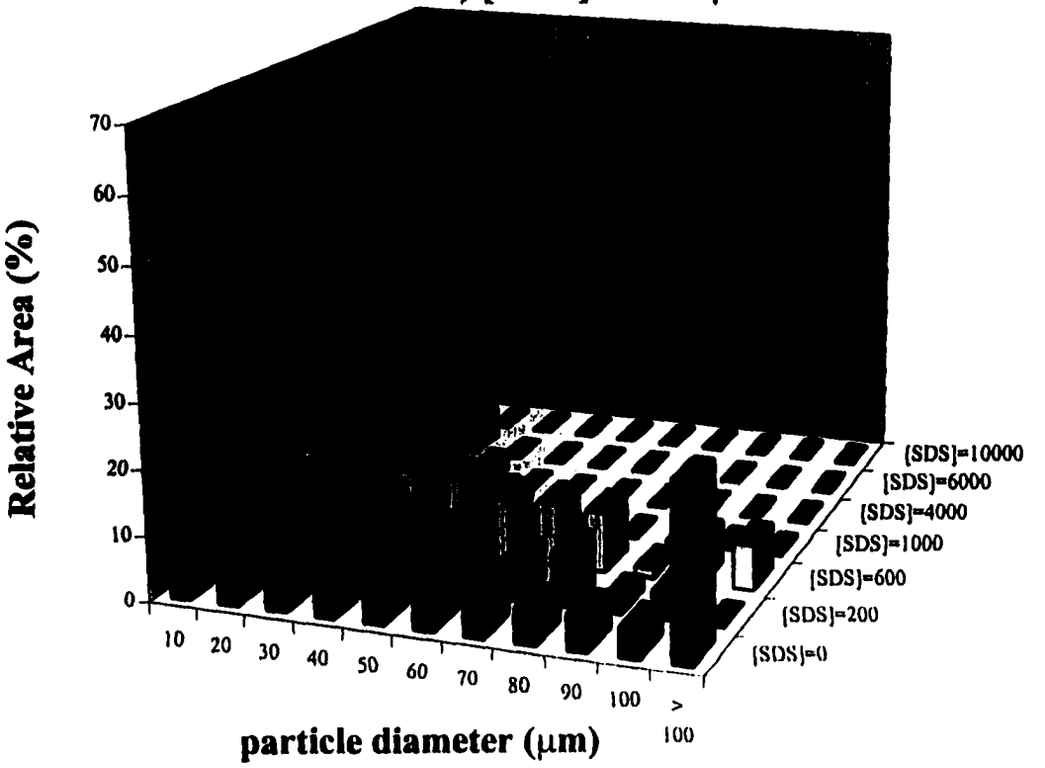

Histogram 2.6. Size Distribution as a Function of the C8 Concentration; [Ca^{2+}]=0 μM

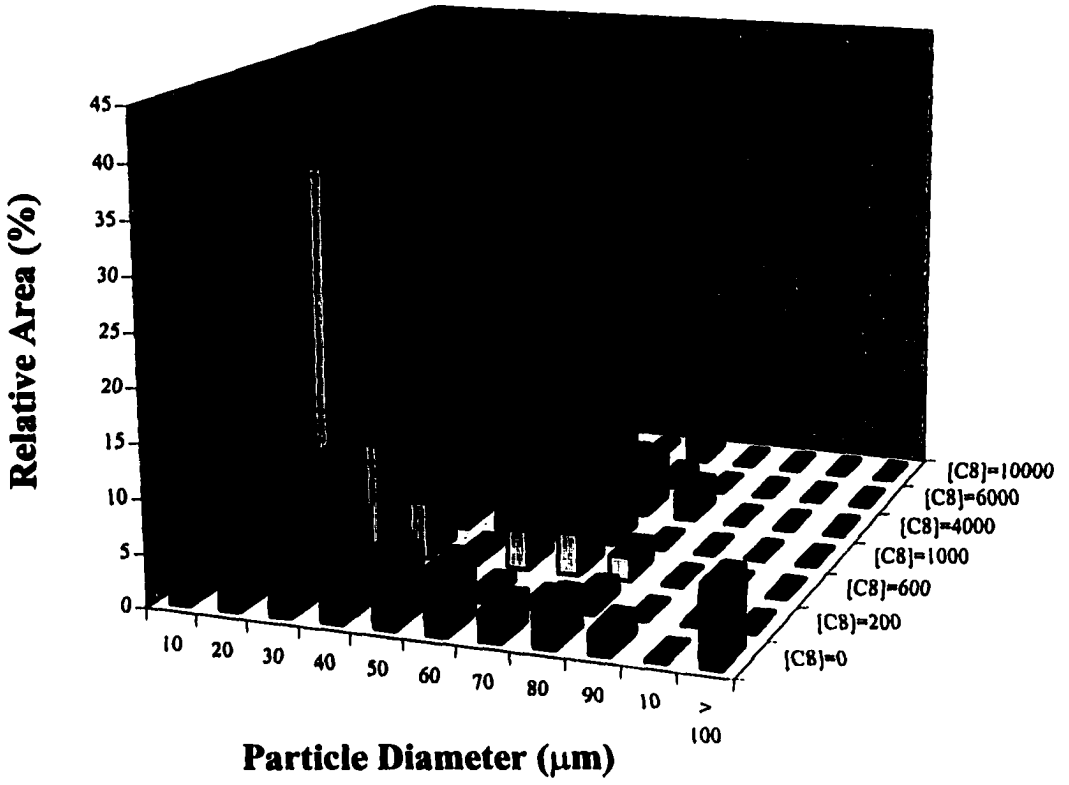

Histogram 2.7. Size Distribution as a Function of the C8 Concentration; $[Ca^{2+}]$=400 μM

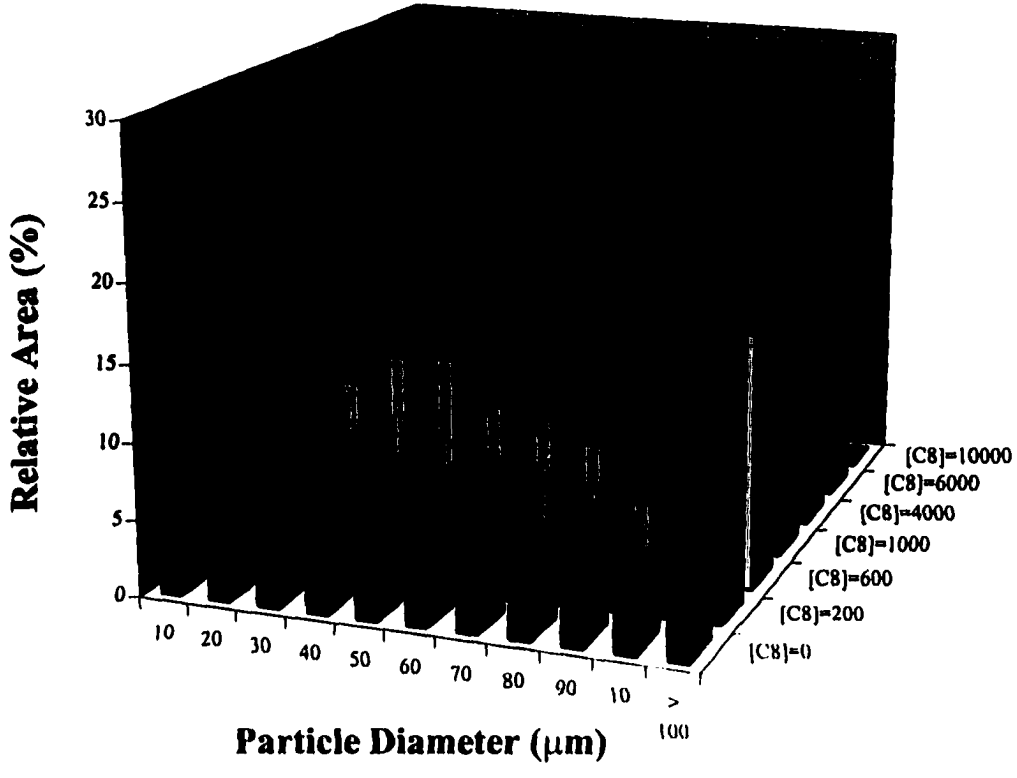

Histogram 2.8. Size Distribution as a Function of the C8 Concentration; [Ca^{2+}]=1000 μM

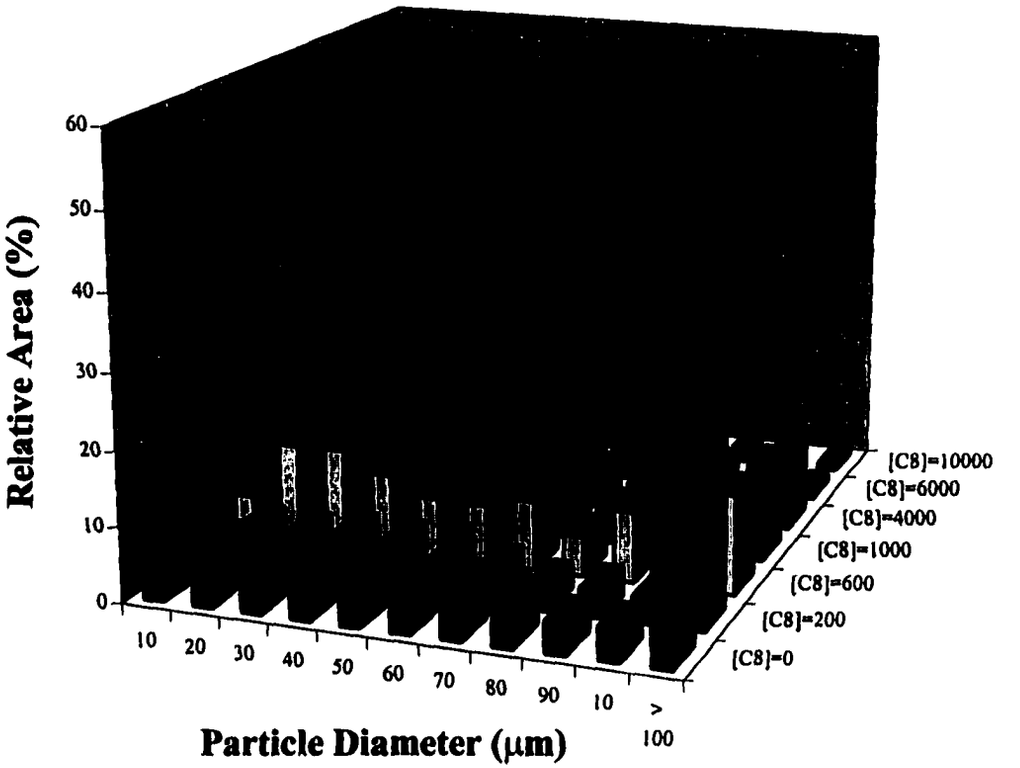

Histogram 2.9. Size Distribution as a Function of the Ca^{2+} Concentration; [SDS]=4000 μM

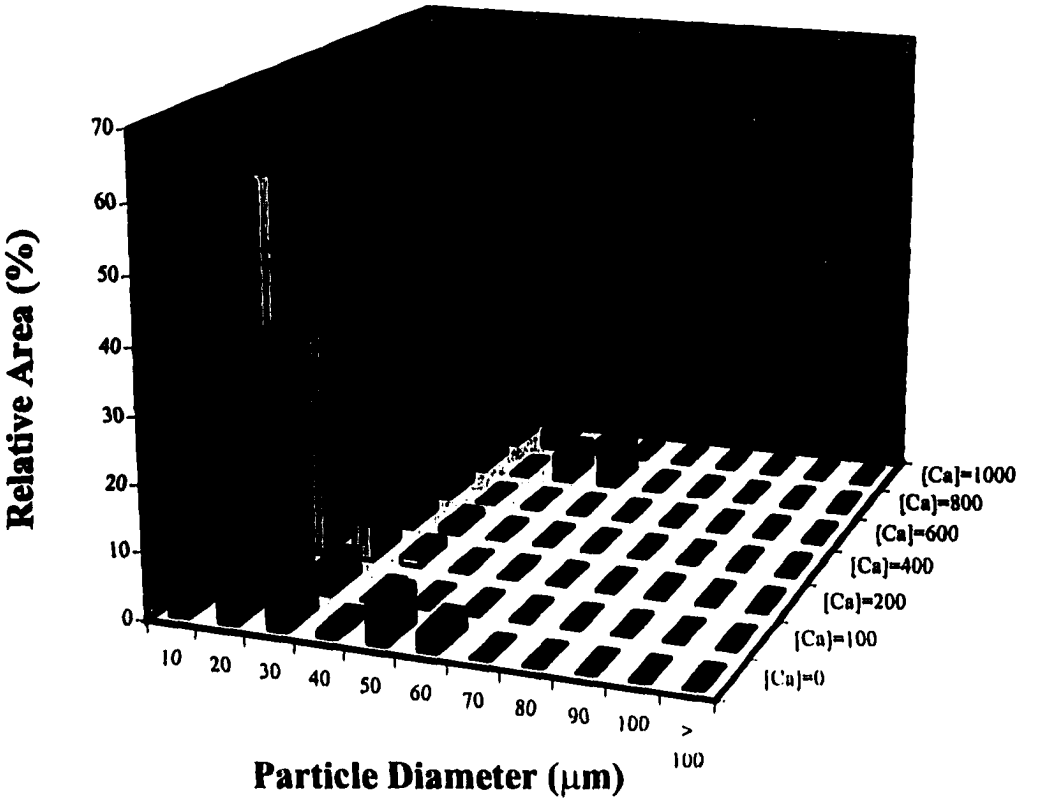

Histogram 2.10. Size Distribution as a function of the Ca^{2+} concentration; [C8]=4000 μM

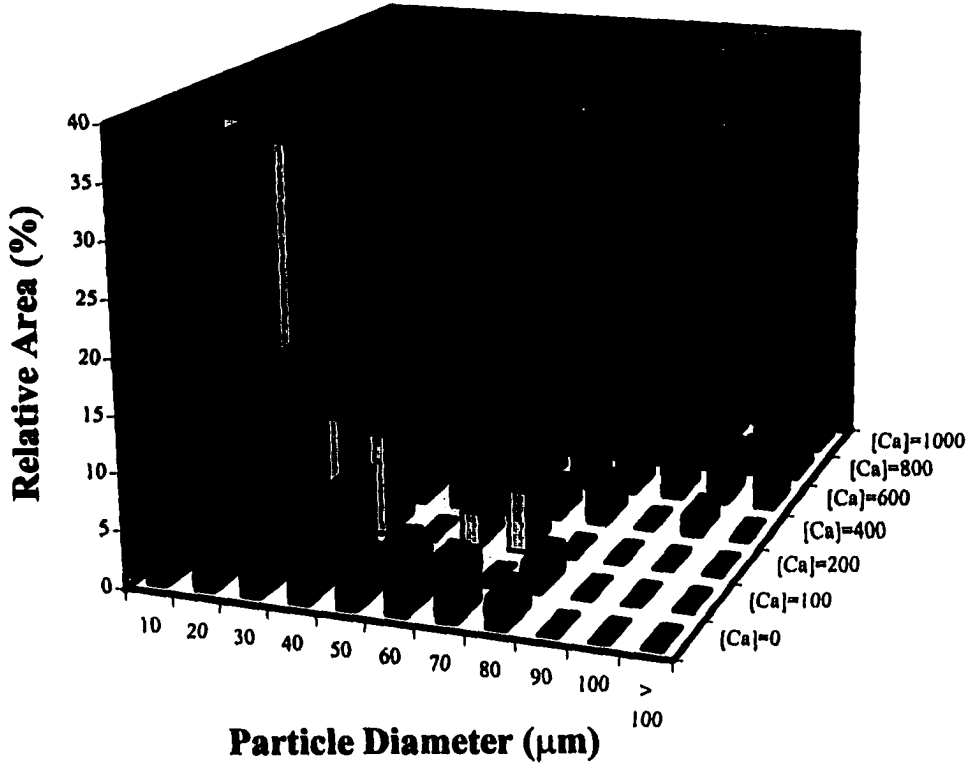

CHAPTER 3

SURFACTANT-FIBER INTERACTIONS IN FLOTATION DEINKING

In this study, the interactions of anionic surfactants with fiber and carbon and their subsequent flotation in the deinking process for recycling of waste paper were investigated. For the investigations, a model ink (carbon black), a model fiber (pulped and washed office paper), and medium chain-length surfactants (sodium octanoate and sodium dodecyl sulfate) were employed in an attempt to elucidate the fundamental mechanisms of preferential flotation of ink in ink/fiber systems. Experimental data from adsorption isotherms, zeta potential measurements, and model flotations, combined with knowledge of the solubility product constant of surfactant-calcium precipitates, indicate that even though significant adsorption of the surfactants occurs on the fiber, the fiber does not interact with the carboxylate and calcium ions in the same manner as the carbon. Effective flotation of the fiber was not observed until carboxylate concentrations at which the surface loading on the fiber was roughly equivalent to that of the carbon. Sodium dodecyl sulfate failed to

efficiently float the carbon or fiber in the concentration ranges studied. Flotations attempted in systems combining model fibers and carbon did not exhibit preferential flotation of the carbon, possibly due to carbon/fiber interaction and deposition of the carbon onto the fibers. However, preferential ink separation using the carboxylate surfactant was observed in flotations conducted with newsprint and photocopied office paper. An unanticipated behavior of negative adsorption of calcium as a function of increased carboxylate concentration was noted during the adsorption experiments of carboxylate on fiber.

Keywords: Deinking, flotation, fiber, collector chemistry, surfactants.

3.1 INTRODUCTION

Preferential flotation of ink is the fundamental objective in flotation deinking of secondary fiber in paper recycling. However, since the issue of the patent to Henkel in 1908 [1] for "paper detergents" for the removal of ink from paper, the majority of the published studies on the topic have centered on empirical investigations rather than upon the fundamental mechanisms of the process. Several theories [1-6] have been forwarded with respect to the mechanisms of "collector chemistry", a term describing the induced hydrophobicity of the ink particles and subsequent aggregation and flotation in carboxylate/calcium systems.

Riviello et al. [5] investigated the mechanism of carbon flotation by employing medium chain length carboxylates and sodium dodecyl sulfate as the surfactants. The investigation involved the measurement of adsorption isotherms of sodium octanoate, sodium dodecanoate, and sodium dodecyl sulfate on carbon black particles, as well as zeta potentials and flotation efficiency of the carbon as a function of surfactant and calcium concentrations. It was proposed that the surfactant adsorbs in a tail-down or lying-down geometry on the surface of the carbon particles, and that the calcium strongly associates with the anionic head groups without bulk phase precipitation. Flotation of the carbon was thought to be induced by the structure of the calcium dicarboxylate complex. While zeta potential reduction (and presumably electrical double layer compression) was achieved by calcium alone, the carboxylate-

calcium association was necessary to achieve flotation. A concurrent study [6] of ink aggregate size as a function of the surfactant and calcium concentration revealed that significant agglomeration occurred well below the K_{sp} of the calcium dicarboxylate complex. The aggregation mechanism was proposed to be related to calcium bridging between the head-groups of carboxylate molecules adsorbed in a tail-down orientation on the carbon particles. This interaction was proposed to be the basis for preferential flotation of ink.

Surfactant-calcium-fiber interactions in collector chemistry have received less attention than flotation of inks. Since fiber flotation must be minimized under conditions of high ink flotation, the mechanisms of surfactant and calcium interaction with fibers is important to understand. Larsson et al. [7] investigated surfactant deposition on fibers from a model calcium/carboxylate deinking system. The study found significant carboxylate retention on the fibers under conditions of high surfactant and calcium concentrations but reported that reductions in fatty acid retention could be achieved by the use of dewatering methods that did not cause filter cake formation. Turvey [8] concluded that the presence of calcium ions causes major losses in fiber stock yield in the case where print or print components are deposited on the fiber. However, the investigators found Ca^{2+} alone was not responsible for fiber flotation. Schwinger [9] demonstrated decreases in the magnitude in the zeta potential of the fibers as a function of the Ca^{2+} concentration but reported increased

fiber loss as a result of this charge reduction. Also, fiber flotation was shown to increase slightly with increasing sodium carboxylate concentrations.

While no consensus seems to have been reached with respect to the underlying mechanisms of fiber flotation, two points have been established. First, pulp fibers contain acidic groups, such as carboxylic acids and hydroxyl groups, that ionize in alkaline aqueous solutions and impart a net negative charge to the fiber surface [9-18]. Also, multivalent cations (specifically Ca^{2+}) have been found to bind extensively on the fiber surface [8, 9, 18] and can be naturally present in the system [18].

The present study was carried out using a model fiber derived from common office paper and a model ink, carbon black, which was employed in lieu of a real ink that may consist of varying pigments and binders. The objective of the study was to investigate the flotation of the fiber both without and in the presence of the model ink as a function of the adsorption characteristics and zeta potential data in an attempt to deduce the mechanisms of the preferential flotation of the carbon. A complementary study is ongoing to investigate collector chemistry, aggregation, and preferential flotation behavior in real deinking systems (pulping and deinking of waste paper). While the present study is concerned only with model systems, the increasing popularity of water-based flexographic inks due to environmental and health concerns actually increases the applicability of these fundamental studies to realistic industrial problems. Flexographic inks of this type are composed of a pigment, usually carbon

black, that is dispersed in water with the use of water-soluble carboxylic derivatives. These dispersants double as binders and are usually composed of resins which are usually homo- and co-polymers of esters of acrylic and methacrylic acids. The carboxylic group content is appreciable. Under basic pH conditions, such as those prevalent in deinking systems, the dried binders hydrolyze and resume their role as dispersants [19]. The pigment, then, exists as a suspension of carbon black--very similar to the model systems being investigated in this study.

3.2 EXPERIMENTAL

3.2.1 Materials

The fiber used in the experiments was prepared by pulping common office paper (Xerox 4200 DP 20 lb.) at 5.0% consistency for 20,000 beats at 3000 rpm in a Model D-111 TAPPI Standard Pulper manufactured by Precision Machinery Corporation (PMC). The pulp slurry was then liberally washed over a 140 mesh screen (105 μm nominal opening) to remove all fillers and extraneous ions. Washing was continued until the Ca^{2+} concentration in the supernatant was less than 0.1 ppm as determined by standard atomic absorption spectroscopy (AA) techniques. The fiber was then pressed to remove excess water and was oven dried at 50°C. The BET surface area of the dry fiber was found to be approximately 1.51 m^2/g. This

measurement was derived from a five point nitrogen adsorption isotherm using a Micromeritics ASAP 2000 surface area analyzer. These data compare well with reported values of between 1.0 and 2.2 m^2/g [20].

The carbon black was supplied by Cabot and was Type 400R, a pigment commonly used in the manufacture of many varieties of inks [21]. The nominal particle size was advertised to be 25 nm, but the stable aggregates of carbon averaged approximately 1 μm. The supplier-provided BET surface area was 96 m^2/g. Due to a relatively high concentration of ionic salts present, it was necessary to wash the carbon to remove the salts. Carbon was mixed with distilled, deionized water in the ratio of 1:4, agitated thoroughly, centrifuged, and the water decanted off. The procedure was repeated three times, which was sufficient to reduce the Ca^{2+} concentration below 0.1 ppm as measured by standard AA techniques. The concentration of Ca^{2+} in a sample of 1.0 g of carbon mixed with 10 ml of water was 600-700 μM.

The surfactants employed for these investigations were sodium octanoate (hereafter referred to as C8) and sodium dodecyl sulfate (SDS). Schematics of the chemical structure of the two surfactants are illustrated in Figure 3.1. The C8 was purchased from Sigma Chemical Company with a purity of greater than 99%. The electrophoresis grade SDS was provided by Fisher Scientific and also had a purity of greater than 99%. The calcium chloride was obtained from Fisher and was oven-

dried for 12 hours at 90°C just prior to manufacturing the stock solutions due to the chemical's hygroscopic nature. pH adjustments were made with Fisher-Brand Certified N/20 NaOH. All of the above materials were used without further purification. The water used for the experiments was distilled and deionized.

3.2.2 Methods

Zeta potentials were determined using a Zeta Meter Model 3.0. The potential across the cell was adjusted as a function of the ionic strength (specific conductance) of the sample so as to avoid thermal overturn associated with overpotentials. The measurements were taken at a constant temperature of 30°C.

Adsorption isotherms were obtained at 30°C using the solution depletion method; 1.8 g of dried fiber was mixed with 30 ml of solution, allowed to equilibrate for three days with occasional agitation, and centrifuged. The surfactant and calcium concentrations in the supernatant liquid were analyzed. Calcium concentrations were measured by standard AA techniques. Determination of the surfactant concentrations was accomplished by high pressure liquid chromatography (HPLC) with an electrical conductivity detector. The SDS was analyzed employing a bicratic step-change solvent scheme (water-rich/methanol-rich mobile phases) on an octadecyl reverse phase silica columns. The C8 analysis employed similar solvent programming but

used a special poly (lauryl methacrylate) reverse phase silica developed specifically for this system [22].

A Hallimond flotation cell [23], illustrated in Figure 3.2, was employed for the model flotations. Instead of the 50 μm opening and the magnetic stirrer described in the literature for gas introduction and dispersion, a 0.5 inch diameter, medium-grit fritted glass disk was fused at the point of gas introduction to act as a sparger. A Cole-Parlmer flowmeter was used to regulate the gas flow rate to 60 mL per minute, and the duration of flotation was, in all cases, 5.0 minutes. The flow rate was selected so as to allow substantial flotation in a reasonable amount of time while only gently agitating the suspension and avoiding unrepresentative carryover. Compressed nitrogen was used as the flotation gas.

The general procedure for the flotation experiments began with adding 70 mL of water to 0.05 g of fiber. A Fisher Model 550 Sonic Dismembrator was used to disperse the fibers by applying an ultrasonic frequency of 20 kHz to the suspension for approximately 20 seconds. In those trials involving both fiber and the model ink, 0.01 g of carbon black was then added to the system. Finally, the calcium and/or surfactant was added in the form of pre-prepared stock solutions, the pH was adjusted to either 9.0 or 11.0, and more water was added to bring the total volume to 80 mL. The basic pHs were selected to conform with the conditions of traditional deinking operations. The suspension was thermostatted at 30°C for 30 minutes. The mixture

was then decanted into the Hallimond tube, and flotation was immediately commenced. Following the 5.0 minutes allotted for flotation, the top fraction, consisting of fiber and/or carbon entrained in the froth and carried over the division and deposited into the side tube by the froth breakage, was drained by removing the stopper from the bottom of the side tube and collected in a sample bottle. The unfloated fraction was then collected. Both samples were filtered through two FisherBrand glass fiber filter circles with a nominal pore size of 2.0 μm. Two filter papers were employed to minimize the loss of fine particles. The filter papers were oven dried, and the amount of floated and unfloated matter was determined gravimetrically. The mass balances closed within 5% in all cases.

For the systems containing both fiber and carbon, a reflectance technique, similar to that used in a TAPPI brightness measuring machine, was employed to determine the amount of carbon on the filter disk sample. A HunterLab Ultrascan light transmission and reflectance analyzer that detected the intensity of 457 nm light reflected from the sample illuminated by a full spectrum source was used for these measurements. A series of filter paper disks, upon which known amounts of carbon and fiber were deposited, were analyzed, and the dependence of the reflectance on the ratio of carbon to fiber was found to be negligible for the ranges of 0.001 to 0.01 g carbon and 0.01 to 0.05 g fiber. Standard filter paper disks were then manufactured using 0.025 g fiber and varying amounts of carbon. The log of the reflectance of the

standard samples was found to be a linear function of the carbon content. From this calibration, the amount of carbon in each sample was determined.

For the flotation experiments employing newsprint and photocopied office paper, 0.4 g of uniformly printed portions of the paper were combined with 70 mL of water, and pulping was accomplished ultrasonically using a Fisher Model 550 Sonic Dismembrator to apply an ultrasonic frequency of 20 kHz to the suspension for approximately one minute. The newspaper was offset-printed, while the office paper (Xerox 4200 DP 20 lb.) was printed using a Xerox Model 5350 photocopier. The calcium and/or surfactant was then added to the paper slurry in the form of pre-prepared stock solutions, the pH was adjusted to 9.0 or 11.0, and more water was added to bring the total volume to 80 mL (0.5% consistency). The procedure for flotation was the same as with the fibers with the exception of the gas flowrate, which was raised to 100 mL/min. Reflectance was measured in the same manner as that used for the mixed fiber and carbon flotations.

Procedures for the acquisition of the data for the experiments involving carbon in the absence of fibers can be found elsewhere [5].

3.4 RESULTS AND DISCUSSION

The present investigations centered about the effect of the calcium and surfactant concentration on adsorption of the additives and on the zeta potential and

flotation efficiency of the fiber in relation to that of the carbon. In all of the adsorption and zeta potential experiments, the concentrations of the calcium and surfactant remained below the K_{sp} value (no precipitation of surfactant occurred), and surfactant concentrations remained below the critical micelle concentration (CMC) for all experiments (no micelles were present). The concentration-based K_{sp} and CMC values for the surfactants employed in this investigation are approximately 1.5 x 10^{-6} M^3 and 350,000 μM, respectively, for C8 and 6.0 x 10^{-10} M^3 and 8300 μM, respectively, for SDS [24-26]. Knowledge of the K_{sp} values allowed experimental conditions to be defined to insure that precipitation did not occur in the adsorption experiments. No significant effect of pH was observed between pH 9 and 11; therefore, only data at a pH of 9 are presented. The complete sets of data can be found elsewhere [27]. Adsorption, zeta potential, and flotation results presented for carbon in the absence of fiber are derived from a previous study [5].

Adsorption isotherms were generated for both surfactants as well as for ionic calcium. Figure 3.3 depicts the adsorption of Ca^{2+} on carbon and fiber and shows the fiber to have a much higher loading (roughly two orders of magnitude greater) of adsorbate than does the carbon, based on the dry surface area of 96 m^2/g for the carbon and 1.51 m^2/g for the fiber. However, one study [28] has reported the specific surface area of water-swollen cellulose fibers to be between 50 and 200 m^2/g. The calcium ions are attracted by the negatively charged sites on carbon surface that result

from oxidation and to the negative sites on the fiber resulting from ionization of the carboxylate and hydroxyl groups. Adsorption of this type is purely electrostatic and non-associative. Noting that the zeta potentials for the carbon and fiber in water with no additives are nearly equivalent (approximately -28 mV [5,6]), similar adsorption characteristics would be expected for electrostatic association. This supposition is illustrated for the case in which the fiber surface area is assumed to be 100 m^2/g. This observation is consistent with the fiber surface area in aqueous systems being approximately two orders of magnitude greater than the dry value.

Figures 3.4 and 3.5 illustrate the adsorption isotherms of C8 and SDS, respectively, onto fiber and carbon black. For both surfactants, the fiber has a much higher loading (roughly two orders of magnitude greater) of adsorbate than does the carbon, based on the dry surface area of 96 m^2/g for the carbon and 1.51 m^2/g for the fiber. However, assuming the surface area of the water-swollen fiber to be 100 m^2/g yields a surfactant adsorption (on a unit area basis) on the carbon which is approximately one order of magnitude greater than on the fiber. These data suggest that the surfactants have a greater affinity for the carbon than for the fiber, due to hydrophobic interactions between the surfactant tail group and the surface whether surfactant adsorption is in a flat or tail down (monolayer) orientation. The values also suggest that the C8 has a slightly greater affinity for the fiber than does the SDS, while the converse is valid for adsorption on the carbon.

Adsorption of the surfactants on the carbon and fiber in the presence of varying initial concentrations of Ca^{2+} is shown in Figures 3.6 and 3.7. In all experiments, the concentrations of the surfactant and calcium remain below the K_{sp} of the calcium di-surfactant complexes. In all cases, increasing initial concentrations of Ca^{2+} leads to increased adsorption of the surfactant. This type of cooperative adsorption is common with ionic surfactants in the presence of oppositely charged ions and is due to diminished electrostatic repulsion between the head groups of the surfactants caused by binding or coadsorption of the counterion. This binding is not a precipitative process. In most instances, adsorption of the calcium ions also increases with increasing surfactant concentration due to association with exposed head groups of the anionic surfactants. This trend is illustrated in Figure 3.8 by the data set for adsorption of the calcium on the carbon as a function of the initial C8 concentration. In this case, increasing initial concentrations of C8 causes augmented abstraction of Ca^{2+} from solution.

However, the opposite trend is observed for C8/fiber system in Figure 3.8. The concentration of free calcium ions increases as greater amounts of carboxylate become associated with the fiber; i.e., calcium adsorption decreases as carboxylate adsorption increases. This effect may be due to expulsion of calcium that is associated with the fiber. The same behavior is not observed with SDS (Figure 3.9), where synergistic coadsorption is observed for both the SDS/carbon and SDS/fiber

systems. These results indicate that there is an association between the carboxylate and the fiber surface that does not occur with the sulfate. It is not obvious why this "calcium exclusion" effect is observed.

The zeta potential is directly related to the dispersion of particles [29]. This measurement is an estimation of the electrical charge of a particle at the shear layer of adsorption as determined by its electorphoretic mobility. The zeta potential of fiber in water at a pH of 9 is approximately -27 mV. The net negative charge on the fiber surface is due to ionization of carboxylic and hydroxyl groups in the cellulose structure. For some systems, there is a potential-determining ion, usually H^+ (expressed as pH), the concentration of which will affect the zeta potential of the particle and may even cause charge reversal. The potential determining ions actually reversibly incorporate into the structure of the substrate rather than simply adsorbing onto the surface [29]. The point at which the zeta potential is zero as a function of the pH is called the point of zero charge (PZC). For fiber in water, the PZC was determined to be at a pH of approximately 3.6.

Figure 3.10 illustrates the zeta potential of the fiber as a function of initial surfactant concentration in the absence of added calcium. Both surfactants decrease the magnitude of the negative zeta potential even though the adsorbed molecules carry a negative charge. As might be predicted from the adsorption data and the observed "calcium exclusion", the C8 exhibits a greater effect on the zeta potential

than does the SDS. The carboxylate causes a change in the zeta potential of approximately 10 mV for an initial concentration of 200 μM while the sulfate has only a 5 mV effect at the same concentration. These results are likely to be another manifestation of the anomalous association between the carboxylate and the functional groups on the fiber surface. The sulfate may have a similar, but not as pronounced, interaction with the fiber that was not readily observed from the adsorption data. The effect of added calcium on the zeta potential of the fiber is shown in Figures 3.11 and 3.12. With increasing Ca^{2+} concentration, the magnitude of the zeta potential diminishes from the already reduced value resulting from the added surfactant. The effect is not a function of the surfactant concentration or type but, within the ranges studied in this investigation, is only dependent upon the Ca^{2+} concentration.

In order to determine the relative flotation of carbon compared to fiber, a Hallimond flotation tube was used to determine the flotation efficiencies for the model ink and fiber as a function of surfactant concentration. In these experiments, the initial Ca^{2+} concentration was 1000 μM. The results are presented in Figures 3.13 and 3.14 and represent experiments in which only the carbon or fiber was present. It must be stressed that the surfactant and Ca^{2+} concentrations listed in the figures represent initial, rather than equilibrium, concentrations. However, while adsorption of both the surfactant and Ca^{2+} onto the carbon and fiber occurs, the solution/substrate

ratio is at least 96 times greater than in the adsorption experiments, and the final concentration of the additives can be assumed to be approximately equal to the initial concentrations. The initial concentration levels at which precipitation is noted on the figures. Similar data were obtained for an initial Ca^{2+} concentration of 100 μM and are presented elsewhere [27].

Figure 3.13 illustrates that preferential flotation of carbon occurs at relatively low concentrations of C8 (100-1000 μM). However, at higher concentrations of the surfactant, the fiber is readily floated. This data depicts an apparent window of opportunity for preferential flotation of the carbon with respect to the carboxylate concentration. A comparison Figures 3.6 and 3.13 indicate that the fiber begins to float when the surface loading approaches 0.15 μmoles/m^2 (equilibrium concentration approximately 1000 μM) based on a fiber surface area of 100 m^2/g. By contrast, loading on the carbon slightly exceeds 0.15 μmoles/m^2 when the C8 equilibrium concentration is only 100 μM, which coincides with the concentration at which flotation begins to increase. The data for the SDS systems (Figure 3.14) reveal no substantial flotation for either the carbon or the fiber. These results indicate that the SDS is not an effective surfactant for preferential flotation and suggests that the carboxylates possess some feature that causes flotability of the carbon and fiber under different conditions.

Significant preferential flotation of carbon was not exhibited in systems containing mixtures of model inks and fibers. These results are presented in Figures 3.15 and 3.16 for initial Ca^{2+} concentrations of 1000 μM. For the C8 system, only a small difference in flotation efficiency is observed between the ink and the fiber throughout the range of concentrations studied. This series of experiments closely mimics the overall environment present in deinking of water-based flexographic inks in which flotation has been shown to be ineffective [30-32]. In both the model system and that of the repulped water-based flexographically printed paper, the major components are fiber, carboxylate, and bare pigment (carbon black). Redeposition of the pigment on the fiber has been found to be a major problem for such systems and little to no preferential flotation of the pigment is common. It is likely that similar interactions between the carbon black and the fibers in this model system are responsible for the poor separation.

At low concentrations, SDS had a slightly greater effect on the separation of the ink from the fiber (Figure 3.16) than did the C8. However, at increased concentrations of the SDS, flotation of the model ink significantly decreased. This detrimental effect of higher SDS concentrations on carbon flotation is supported by aggregation data derived from a concurrent study [6] in which SDS was shown to act as a dispersant for carbon even in relatively high concentrations of Ca^{2+}.

In light of the poor results achieved in the model systems which were expected to simulate water-based flexographic inks, printed news and office papers were pulped, and the flotation of the ink was measured. Figure 3.17 depicts the increase in reflectance of the filter pads made from the unfloated portion of the slurry over that of pads made with pulped-only slurry as a function of the C8 concentration. The initial Ca^{2+} concentration was 1000 μM. In the case where no preferential flotation occurs, the pads made from the floated portion would have the same reflectance as those made from pulped-only slurry. As the concentration of the C8 is increased, an increase in the reflectance of the unfloated fiber is observed for both the office and the newsprint. The higher reflectance values indicate that the ink has been concentrated in the floated fraction and was preferentially removed from the system. These results suggest that the lack of selective ink removal in the model ink/fiber system under conditions which should yield preferential ink flotation based on results with individual components was an anomaly, perhaps due to its similarity to the water-based flexographic ink system.

3.5 CONCLUSIONS

Preferential flotation of the ink requires specific interaction of the Ca^{2+} with the carboxylate molecules and is not observed in SDS systems. The specific interactions between the carboxylate, the Ca^{2+}, and the fiber result in decreased calcium

adsorption with increasing C8 adsorption (a "calcium exclusion" effect) and diminishing zeta potential as a function only of the C8 concentration. While both C8 and SDS readily adsorb on the fiber, the SDS does not cause flotation in the concentration ranges studied in this investigation. The C8, on the other hand, is responsible for fiber flotations at higher surfactant concentrations. The observed differences in adsorption of C8 and calcium and zeta potential for fiber and carbon are related to differences in flotation of the two particles. A concentration-based window of opportunity exists during which carbon is efficiently floated without fiber carryover.

3.5 REFERENCES

1. Hornfeck, K., Conservation & Recycling, 10 (2/3): 125 (1987)
2. Larsson, A., Stenius, P, and Ödberg, L. *Svensk Papperstidning*, **87** (18): R165 (1984).
3. Larsson, Larsson, A., Stenius, P, and Ödberg, L. *Svensk Papperstidning*, **87** (18): R158 (1984).
4. Johansson, B., Wickman M., and Ström, G., *J. Pulp Pap. Sci.*, **22** (10): J381 (1996).
5. Riviello, Jr., A. E., Scamehorn, J. F., and Christian, S. D., "The Mechanisms of Collector Chemistry in Flotation Deinking", submitted to TAPPI Journal.
6. Faisant, E., Riviello, Jr., A. E., Scamehorn, J. F., and Christian, S. D., "Size Characterization of Model Ink Aggregates in Flotation Deinking Collector Chemistry", submitted to TAPPI Journal.
7. Larsson, A, Stenius, P, and Ödberg, *Svensk Papperstidning*, **88** (3): R2 (1985).
8. Turvey, R. W., CPPA 1991 Recycling Forum, p. 123.
9. Schwinger, K and Dobias, B., CPPA 1991 Recycling Forum, p. 145.
10. Das, B. S. and Lomas, H., *Pulp. Pap. Canada*, **74** (8): 95 (1973).
11. Briggs, D. R., *J. Phys. Chem.*, **32**: 641 (1928).
12. Balodis, V., *Appita*, **21** (3): 96 (1967).
13. Lottermoser, A., *Trans. Faraday Soc.*, **31**: 411 (1935).

14. Ranby, B. G., *Disc. Faraday Soc.*, **11**: 158 (1951).

15. Kratohvil, S., Janauer, G. E. and Matijevic, E., *J. Colloid Interface Sci.*, **29**: 187 (1969).

16. Walkush, J. C. and Williams, D. G., *Tappi J.*, **57** (1): 112 (1974).

17. King, C. A. and Williams, D. G., *Tappi J.*, **58** (9): 138 (1975).

18. Been, J. and Oloman, C. W., *J. Pulp Pap. Sci.*, **21** (3): J80 (1995).

19. Dorris, G. M., and Nguyen, N., *J. Pulp Pap. Sci.*, **21** (2): J55 (1995).

20. Sjögren, P., *Nordisk Cellulosa*, 5 (3): 114 (1988).

21. Cabot Corporation, Technical Report S-127, 1987.

22. Riviello, Jr., A. E., Scamehorn, J. F., and. O'Haver, J. H., "A Novel Technique for the Production of Customized HPLC Packings", submitted to *Journal of the American Oil Chemists' Society.*

23. Fuerstenau, D. G., Metzger, P. H., and Steele, D. D., *Eng. and Min. J.*, **158** (3): 93 (1957).

24. Mukerjee, P and Mysels, K. J., *Critical Micelle Concentrations of Aqueous Surfactant Systems*, Department of Commerce, U. S. Government: Washington, D. C., 1970.

25. Irani, R. R. and Callis, C. F., *J. Phys. Chem.*, **64** (11): 1741 (1960).

26. Stellner, K. L., and Scamehorn, J. F., *Langmuir*, **5** (1): 70 (1989).

27. Riviello, Jr., A. E., Doctoral Thesis, Department of Chemical Engineering, University of Oklahoma, Norman, Oklahoma, 1997.

28. Budd, J. and Herrington, T. *Colloids Surf.*, **36**: 273 (1989).

29. Adamsom, A. W. *Physical Chemistry of Surfaces, Fifth Edition*, John Wiley & Sons, Inc., New York, 1990.

30. Dorris, G. M. and Nguyen, N., *J. Pulp. Pap. Sci.*, **21** (2): J55 (1995).

31. Chabot, C., Daneault, C. and Dorris, G. M., *J. Pulp. Pap. Sci.*, **21** (9): J296 (1995).

32. Sain, M. M., Marchildon, L., and Daneault, C., *Prog. Pap. Recycl.* **5** (1): 54 (1995).

Figure 3.1. The Structure of the surfactants: A) Sodium Octanoate, B) Sodium Dodecyl Sulfate

A)

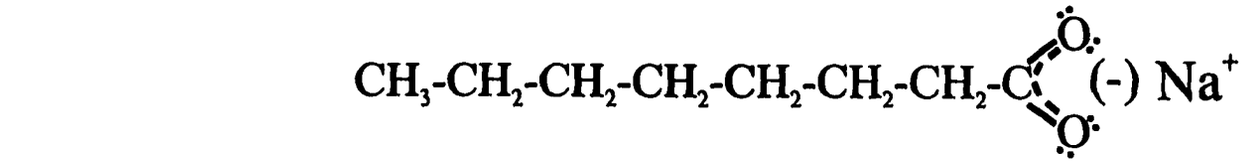

B)

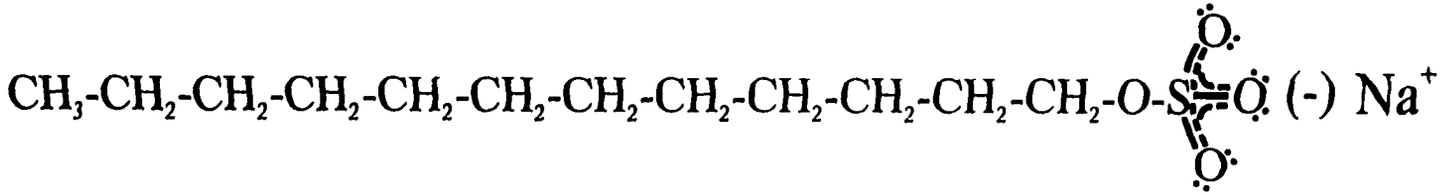

Figure 3.2. The Hallimond flotation tube

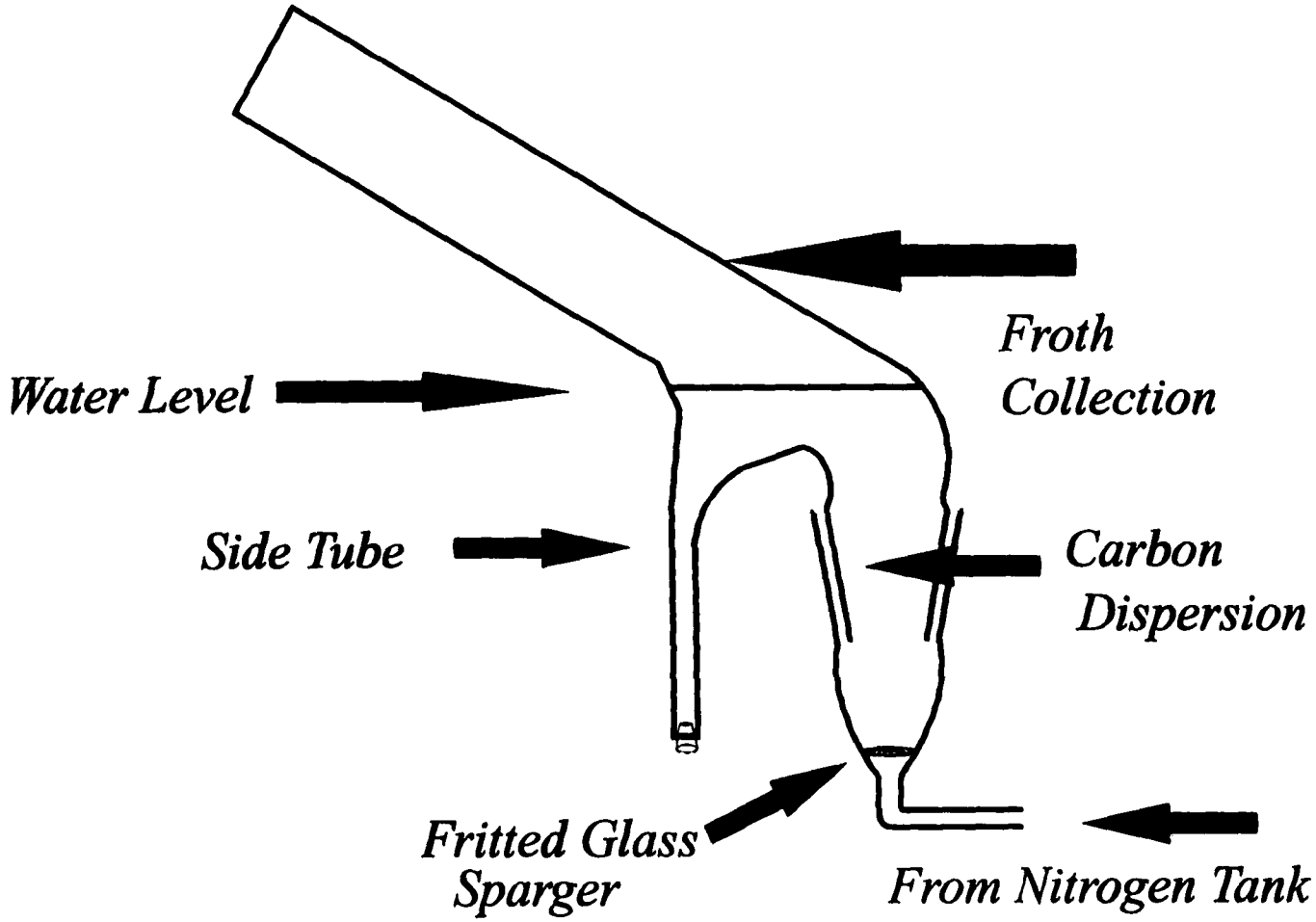

Figure 3.3. Ca++ Adsorption on Carbon and Fibers

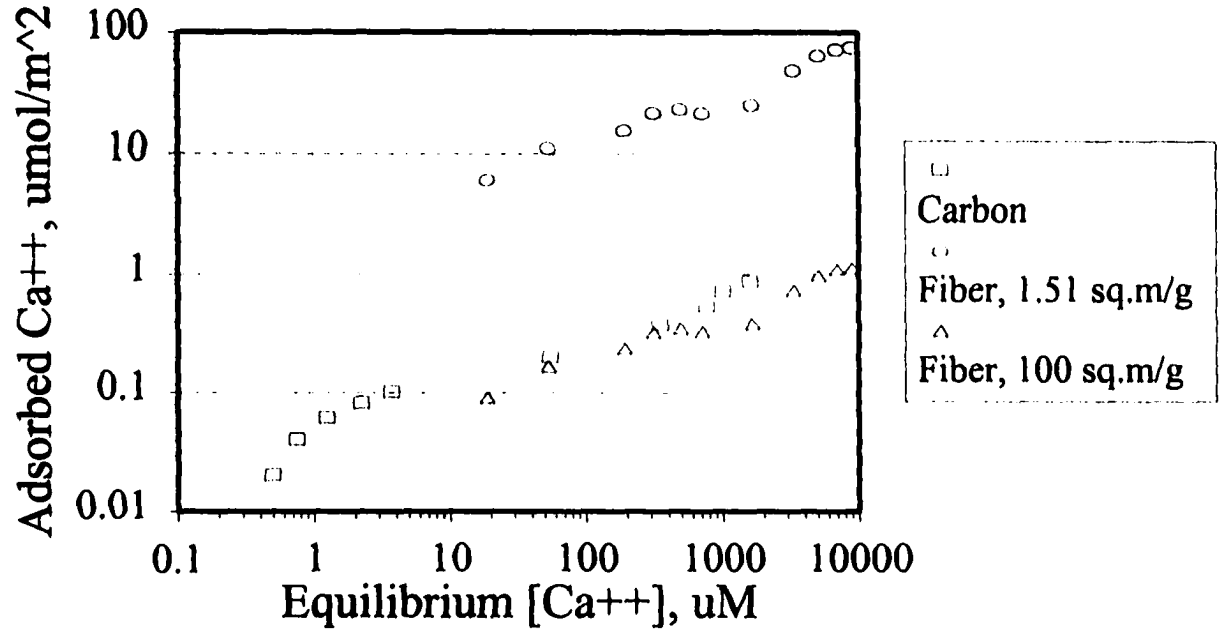

Figure 3.4. C8 Adsorption on Carbon and Fibers. $[Ca^{2+}] = 0$ μM

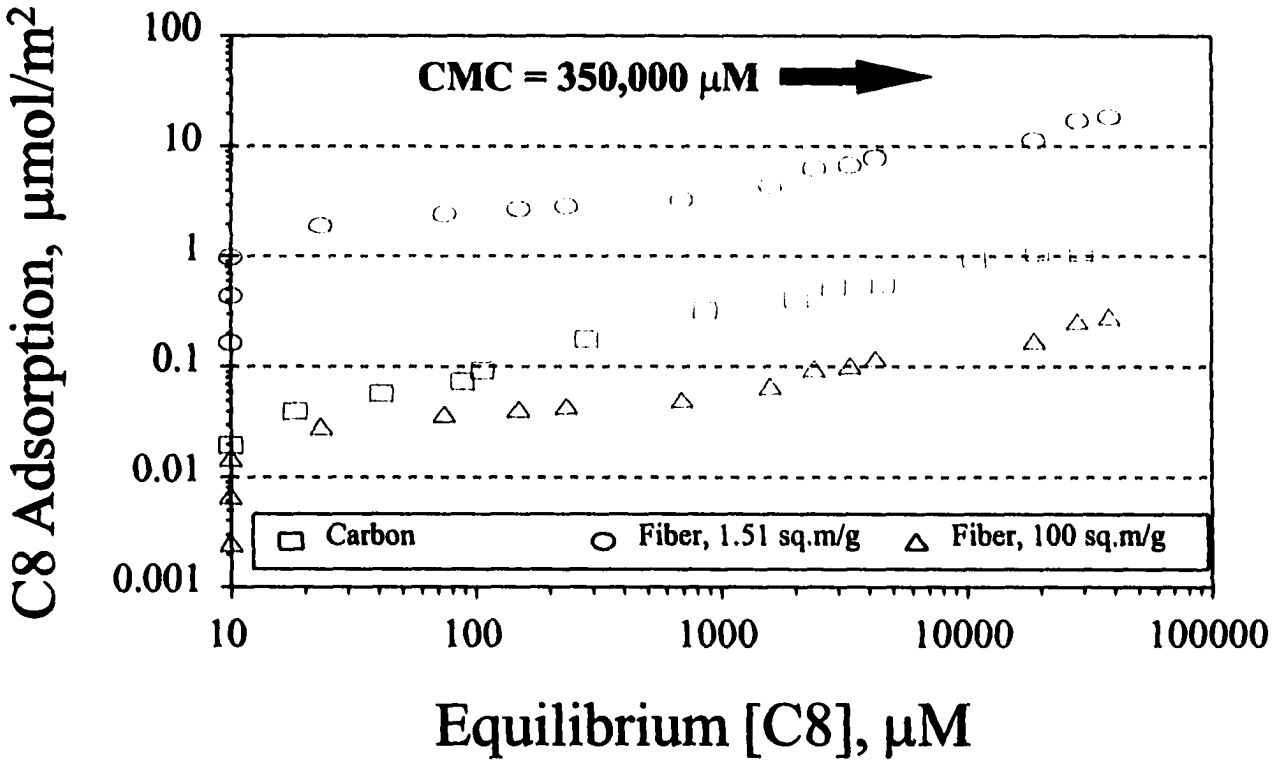

Figure 3.5. SDS Adsorption on Carbon and Fiber; [Ca++]=Variable

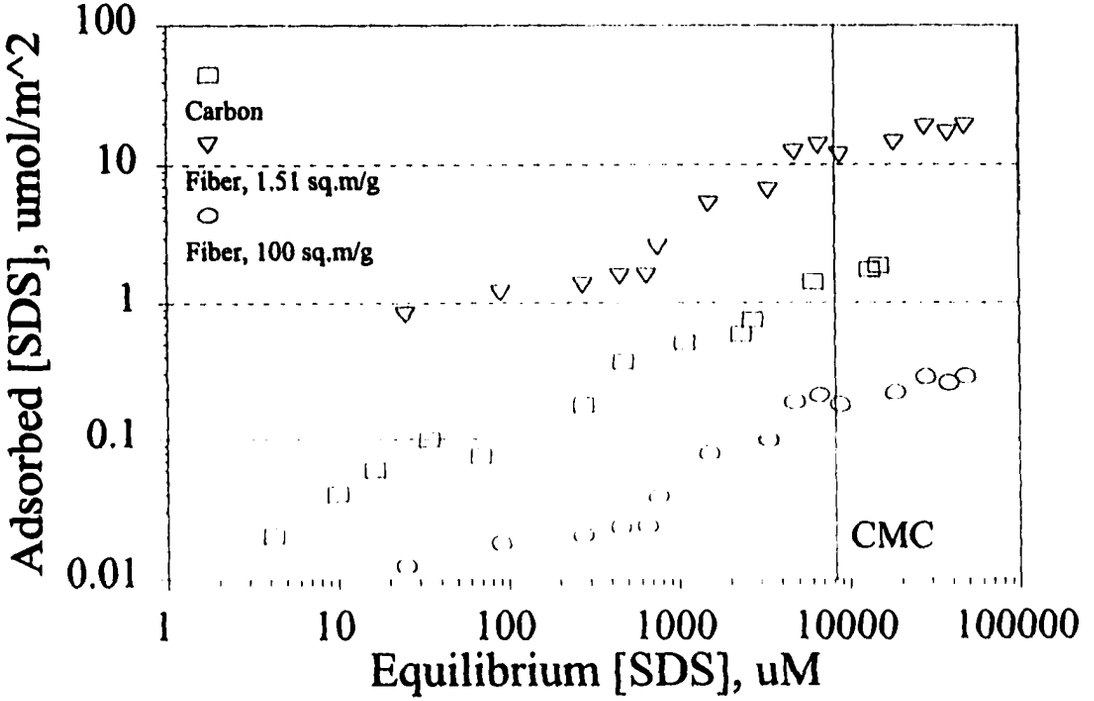

Figure 3.6. C8 Adsorption on Carbon and Fibers. $[Ca^{2+}]$ = Variable. Fiber based on 100 m^2/g

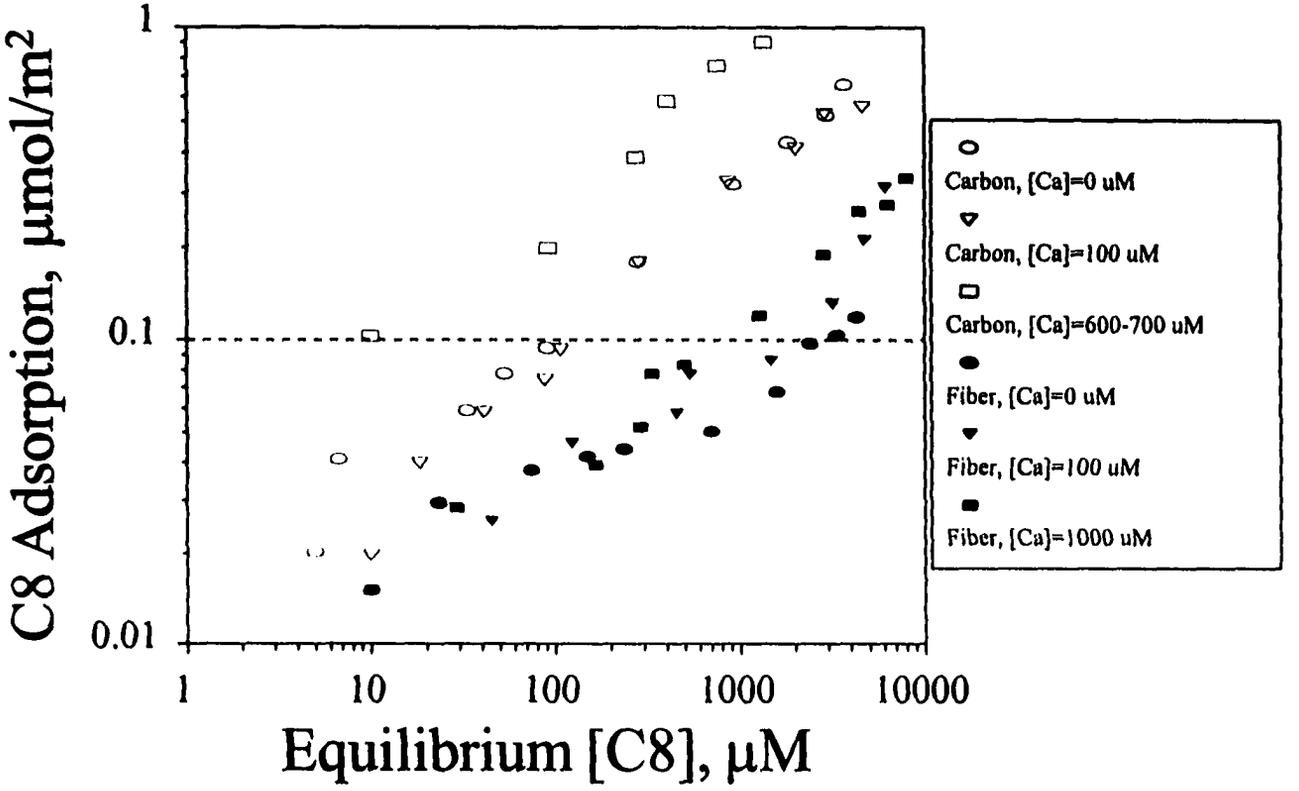

Figure 3.7. SDS Adsorption on Carbon and Fiber; [Ca++]=Variable. Based on 100 sq.m/g

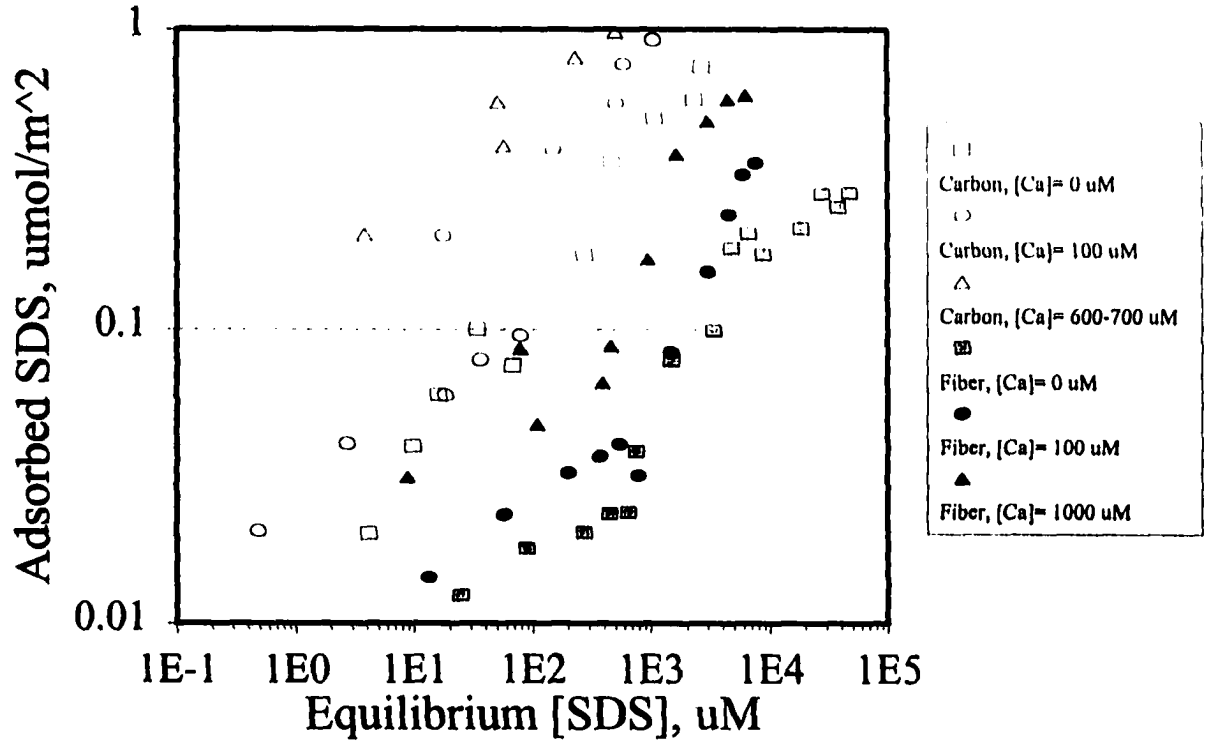

Figure 3.8. Ca++ Adsorption vs. Inital [C8]; Initial [Ca++]=100 uM

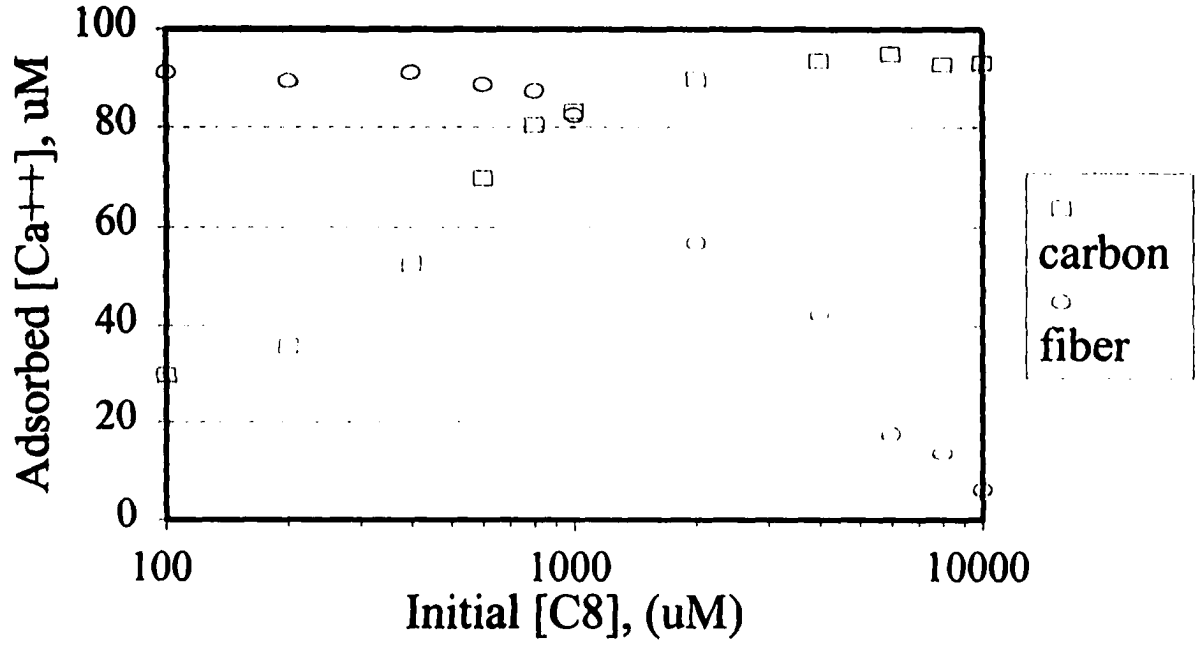

Figure 3.9. Ca++ Adsorption vs. Initial [SDS]; Initial [Ca++]=100 uM

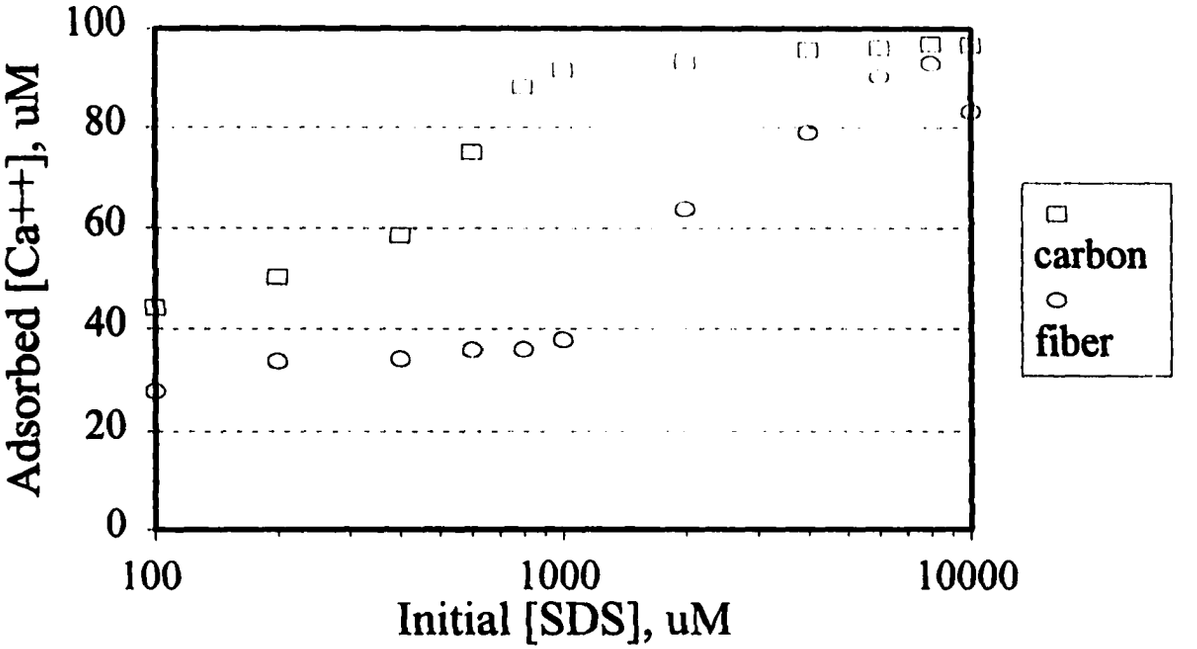

Figure 3.10. Zeta Potential as a Function of Initial [Surfactant]; [Ca++]=0

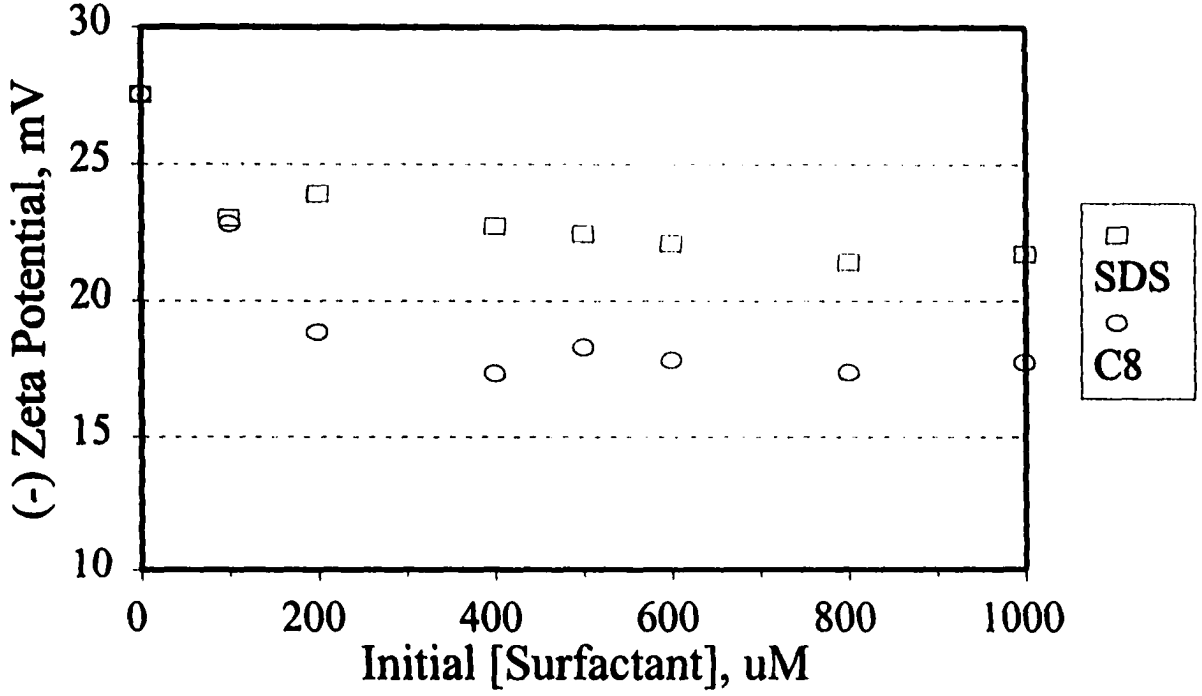

Figure 3.11. Zeta Potential of Fiber vs. [Ca++]; [C8]=Variable

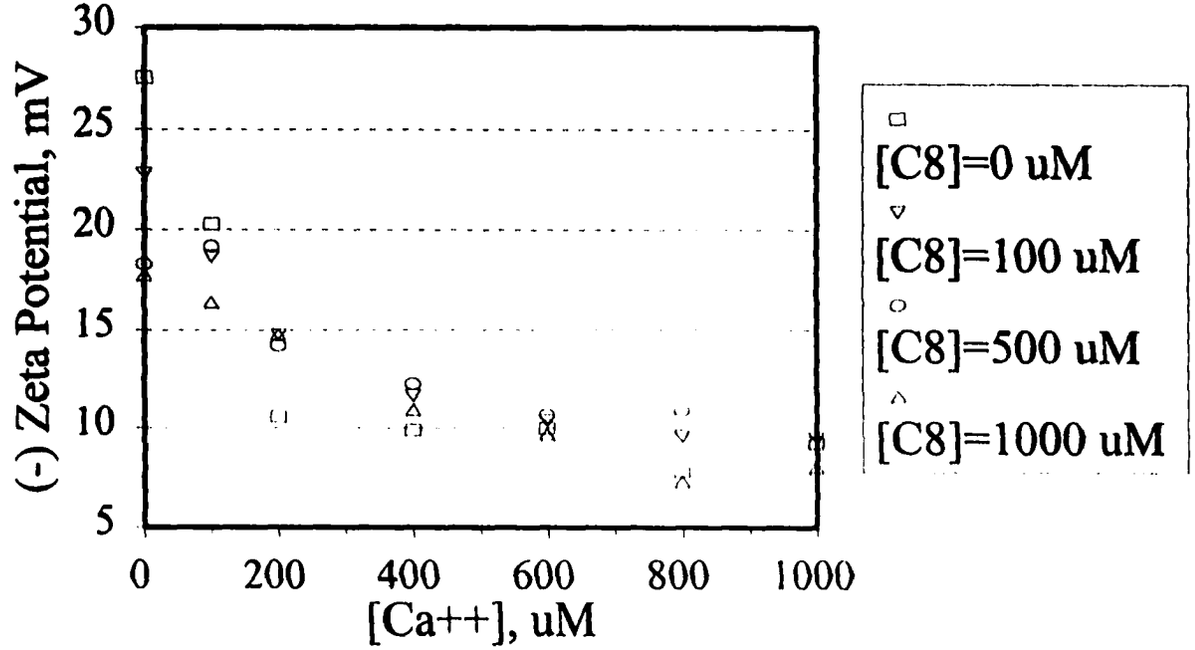

Figure 3.12. Zeta Potential of Fiber vs. [Ca++]; [SDS]=Variable

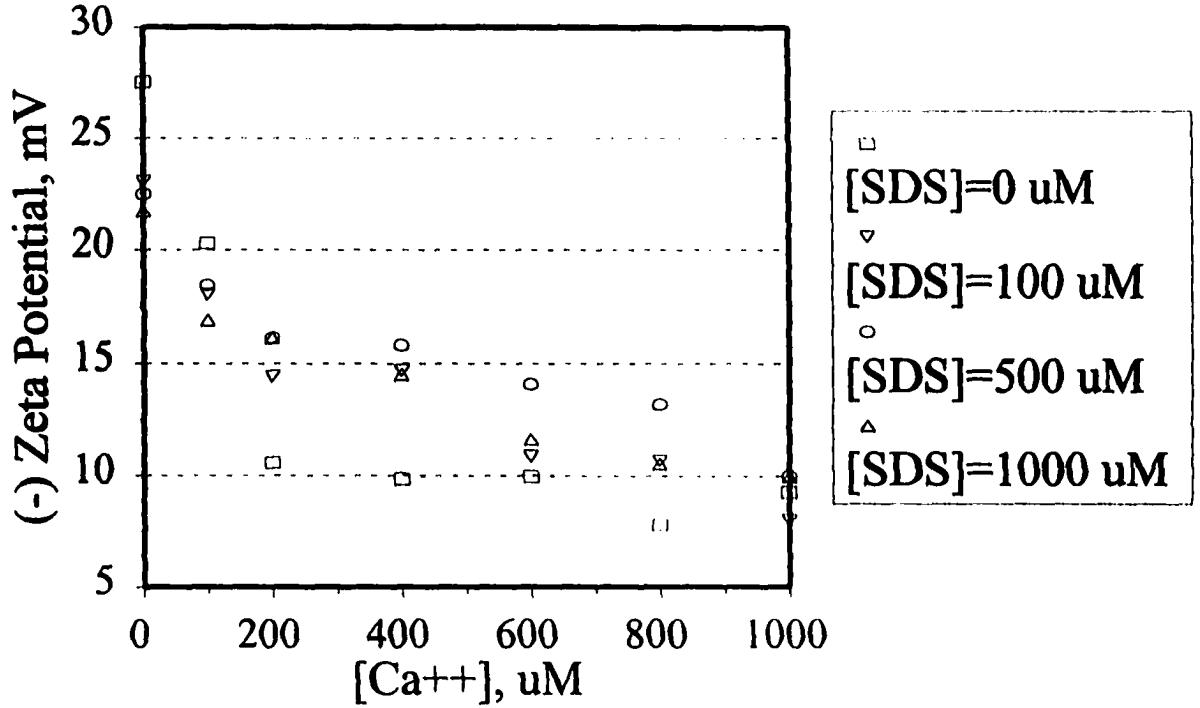

Figure 3.13. Carbon and Fiber Flotations vs. [C8]

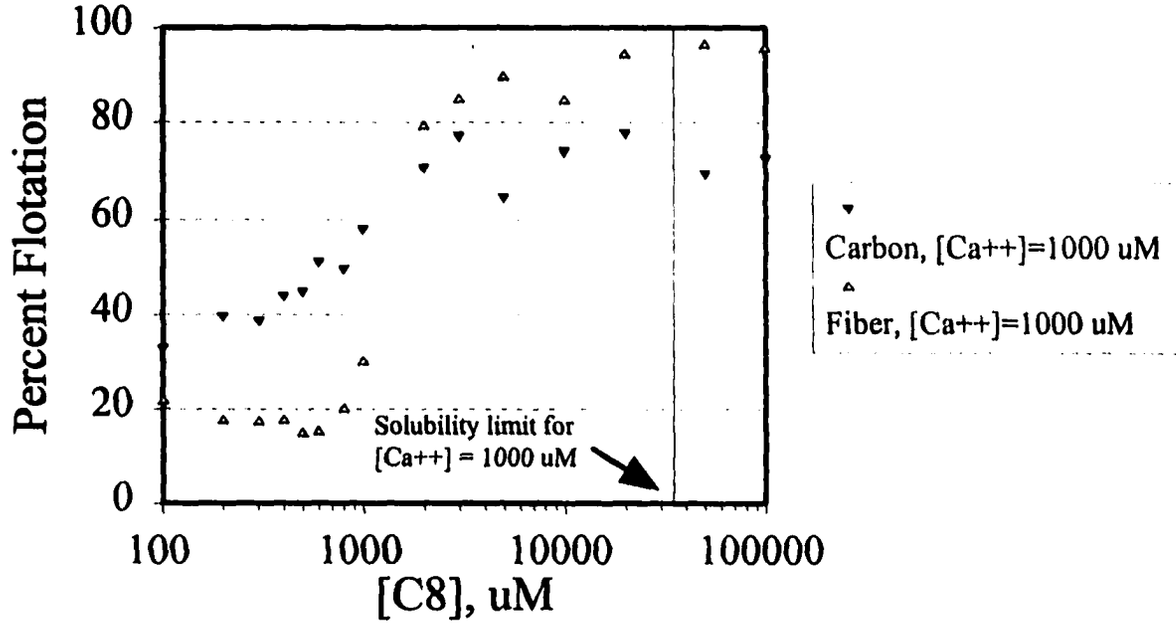

Figure 3.14. Carbon and Fiber Flotation vs. [SDS]

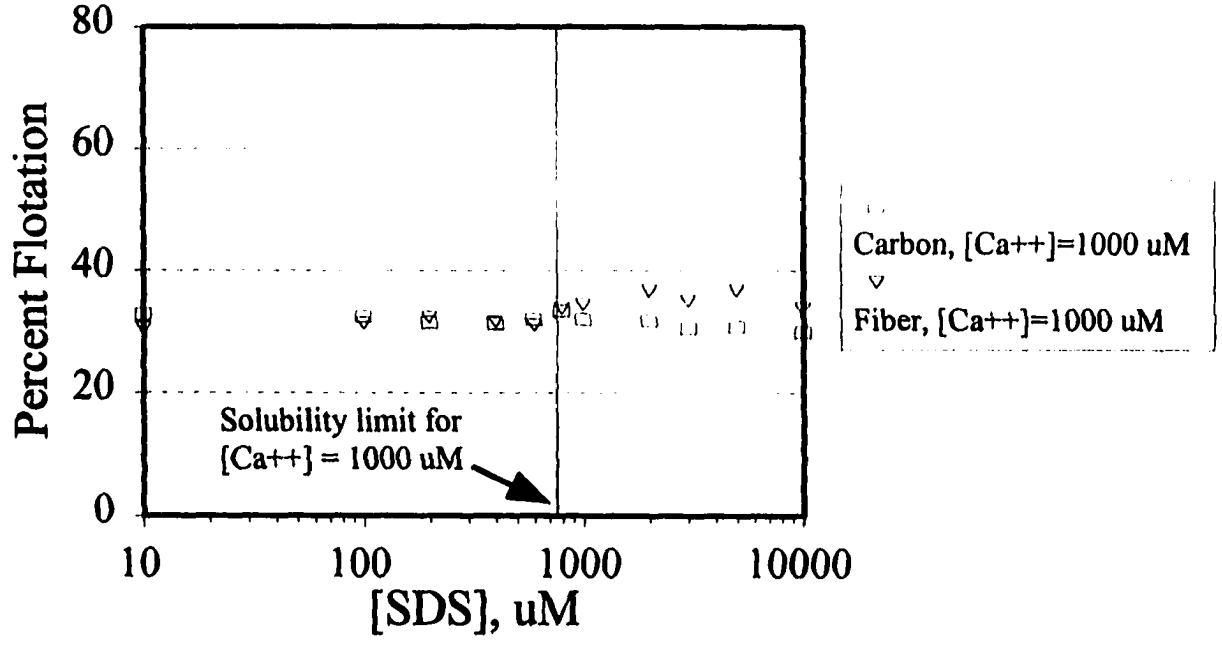

Figure 3.15. % Flotation of Carbon and Fiber vs. [C8]; [Ca++]=1000 uM

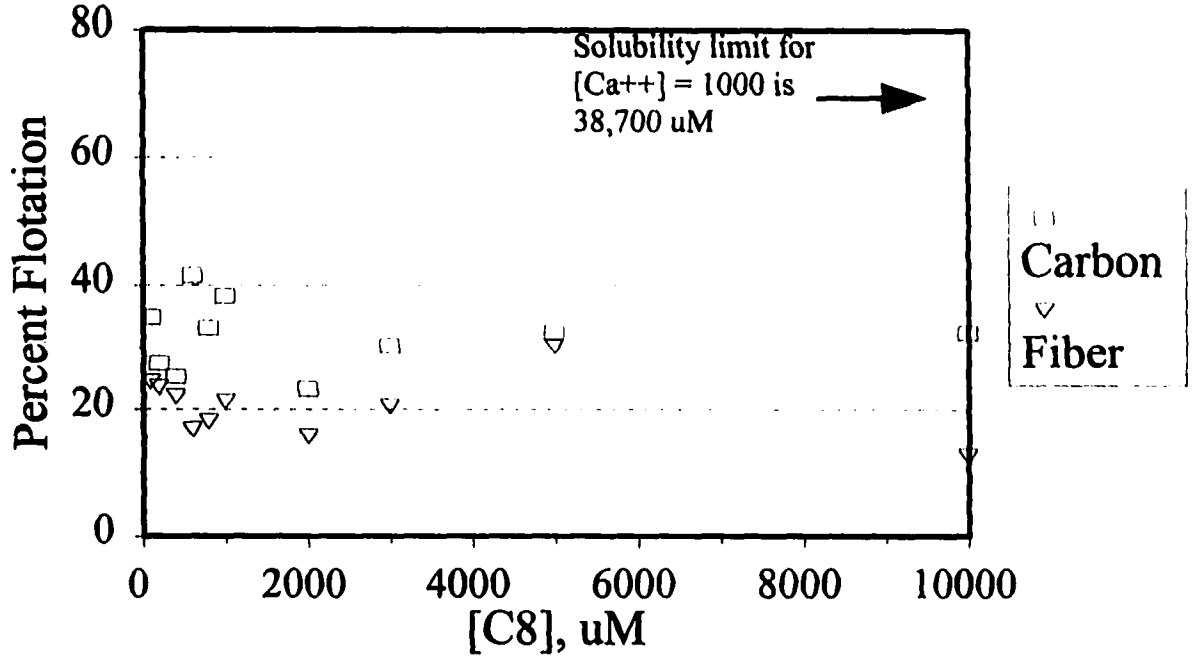

Figure 3.16. % Flotation of Carbon and Fiber vs. [SDS]; [Ca++]=1000 uM

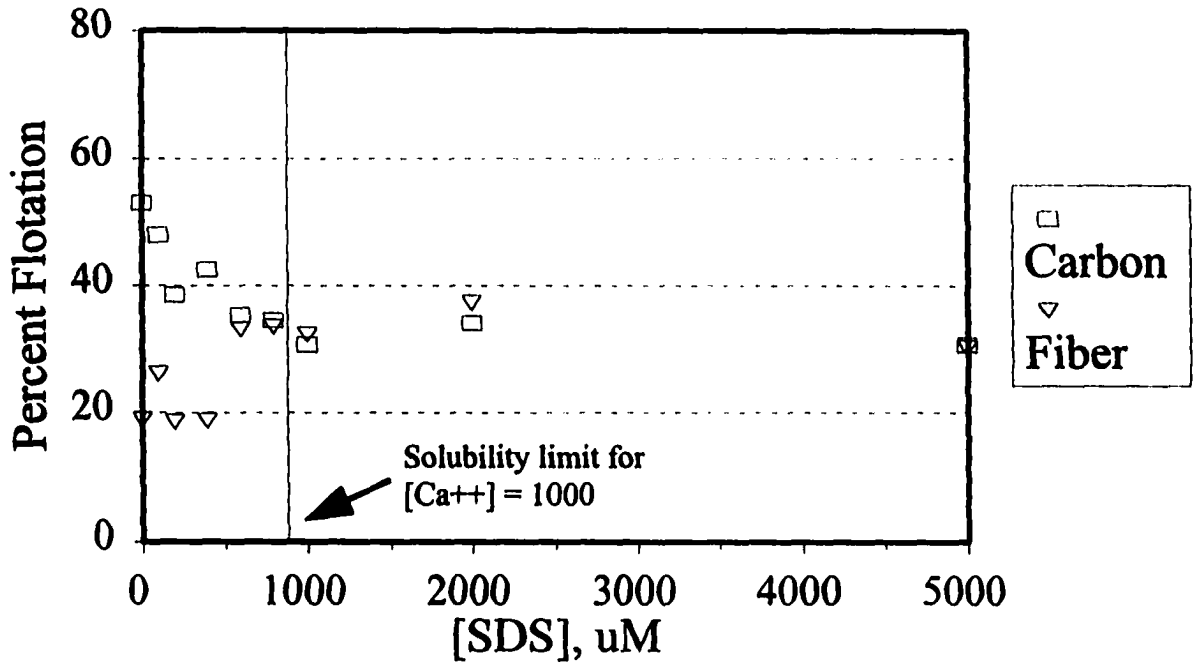

Figure 3.17. Increase in Reflectance Points of Unfloated Pulp; [Ca++]=1000 uM

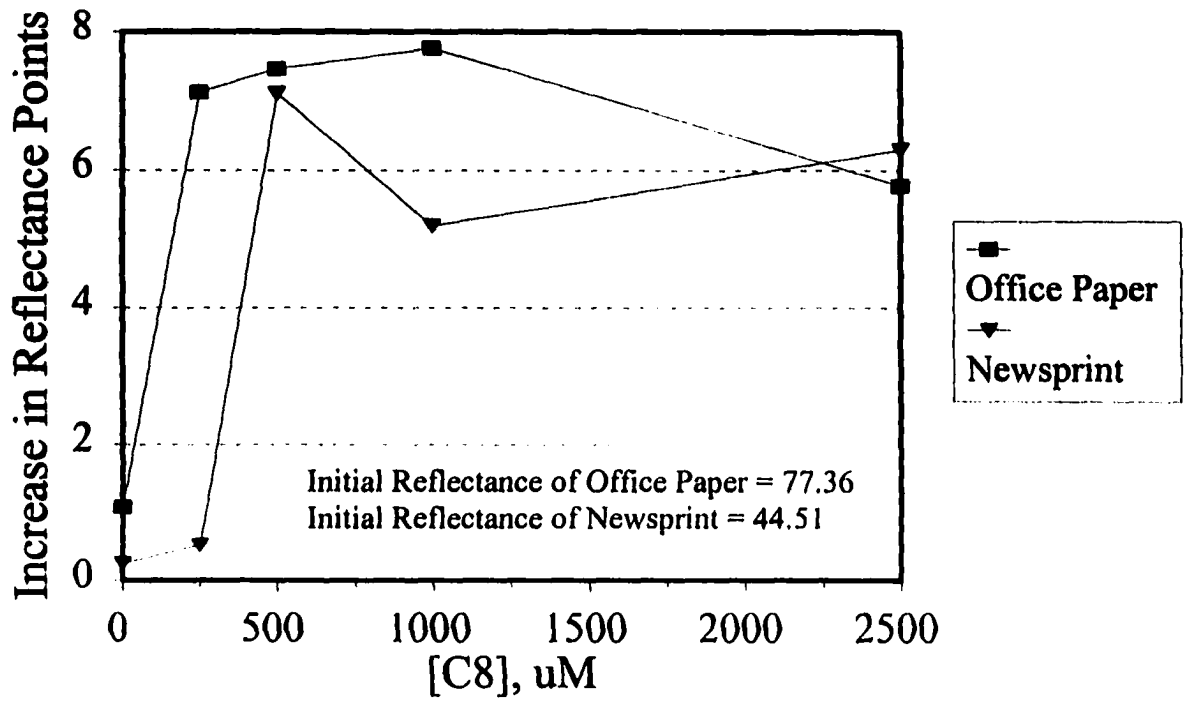

CHAPTER 4

THE USE OF IMAGE ANALYSIS TO MEASURE BRIGHTNESS OF PAPER

The application of image analysis techniques to the measurement of brightness of paper is described. In this application, excellent agreement of the TAPPI and ISO values derived from traditional measuring apparati with the TAPPI and ISO values based on the image analysis were observed. The image analysis-derived brightness values for the TAPPI and ISO scales may not necessarily correlate exactly with those from traditional brightness measuring apparati because the image analysis technique is more objective with respect to accounting for the percentage of ink coverage and the sensitivity of brightness to the particle size. The system represents a significant time savings over individual measuring systems for the determination of TAPPI and ISO brightnesses and ink speck count as well as avoids the expense of three pieces of equipment.

Keywords: Image analysis, brightness, ISO, TAPPI, recycling, ink speck count

4.1 INTRODUCTION

The visual aesthetic quality of paper is one of the most important criteria for consumer use. Therefore, quality control of the optical properties of the paper is essential. This is particularly true when secondary, or recycled, fibers are included in the fiber source. Secondary fiber sources commonly contain a considerably higher population of possible contaminants, such as ink, that may affect the optical properties of the final product. Two of the most important of these properties are the brightness, and the dirt or ink speck count of the paper. "Brightness" of the paper is determined by the fraction of a prescribed wavelength of light that is reflected off a sample, or handsheet, of paper from a designated light source. This parameter has become an industry accepted measurement of paper optical quality despite some shortcomings, as will be discussed in this paper. Opacity, which is essentially a derivative of the brightness measurement, is performed with different backings to the sample paper and with a different bandwidth of reflected light. The traditional dirt or ink speck count of the paper measures the discrete visible contaminant concentration of the handsheet. While standard instrumentation has been available for the brightness and opacity measurements for decades, dirt counts have traditionally been performed manually. However, with the rapid advancement of computer hardware and software, image analysis (IA) apparati are quickly becoming a staple for the contaminant count of the paper.

4.2 BRIGHTNESS MEASUREMENTS

There are two dominant methods for determining the brightness of paper: the TAPPI standard method [1], employed primarily in the United States, and the ISO method [2, 3, 4], used in most other countries. The former method, also referred to as directional brightness, was formerly known as GE brightness after General Electric, the first manufacturer of the instrument used. Both methods are based on the principle of measuring the reflectance of the wavelengths of light in the 457.0 ± 22.0 nm bandwidth from the paper sample. This transmission cutoff is achieved by the use of optical filters in conjunction with the energy response characteristics of the detector. Both methods employ an incident beam of full spectrum light which may or may not include ultraviolet light that can cause fluorescent excitation of additives that may be present. Differences between the two methods arise from the geometry of the incident light as illustrated in Figure 4.1. The directional brightness standard calls for a collimated beam incident at 45° to the sample, with the reflected light being collected perpendicularly to the sample surface. The ISO method (also called diffuse brightness) includes a spherical diffuser that allows the incident light to fall on the sample from a multitude of angles. Jordan et al. [5] have demonstrated that for the measurement of optical properties of paper, the incident angle can have a profound impact upon the results and recommend the use of a 0.0° incident angle to eliminate shadowing or other optical anomalies. The brightness scales are based on the

reflectance of magnesium oxide or barium sulfate being 100.0. Calibration of the instruments with brightness standards, usually tabs of paper pre-evaluated on a master instrument, is required for the determination of brightness values of samples.

The effect of residual ink on the reflectance-based values of brightness has been documented [6], and several shortcomings of the standard brightness measurements have been noted. Problems arise in comparison of results from the two systems because there is no direct correlation between the two scales [7]. Also, brightness, as defined by the standard test methods, is an inherently subjective and possibly misleading measurement [8, 9, 10]. This criticism is based on the fact that brightness does not accurately reflect the contaminant level that may be present in the paper sample [9, 10] because the ink particle size and spacial distribution can affect the reflectance of the paper as a whole. The properties of discete ink particles can affect this average non-discriminatory brightness parameter. These discrepancies are extremely important when one considers ink removal from secondary fiber. Finally, the brightness of the paper samples is evaluated in the blue region of the spectrum. However, it is obvious that the human visual spectrum is not limited to these wavelengths. Therefore, the contributions of varying discolorations of the fibers are essentially skewed [9, 10] when compared to the single-color brightness measurement.

4.3 IMAGE ANALYSIS

Image analysis is the name given to the general technique of employing a computer to acquire an image of a paper sample and determine the number and size of the contaminants (generally ink--hereafter, referred to as such). The image acquisition may be either microscope-based (Figure 4.2) or scanner-based. The latter configuration is able to discern only those specks above the limit of vision (50-60 μm), while microscope-based machines are able to detect particles in the micron-size range. Configurations involving microscopes are also much more flexible, allowing the operator to choose the magnification or manipulate the illumination source, be it reflected (most common) or transmitted. Following the image acquisition, the signal may be sent to an image enhancer that allows image averaging, overlays, and background subtraction. This signal is then transferred to the computer where analysis of the image can be performed. The method of speck detection is based on the assignment of a gray value to each pixel in the field of view. A threshold is set below which all darker portions of the image are then considered as ink specks. Pre-written software or specially written code is employed to extract the histographic information, and accurate and reproducible results are usually achieved, assuming the threshold remains constant.

Several authors [5, 11-13] have investigated the errors associated with image analysis. Zeyer et al. [11] have concluded that if the threshold is held constant,

inadequate sampling is the only source for appreciable error. In a related paper, Zeyer et al. [12] present a mathematical expression for the confidence interval and confidence level of the sampling technique as a function of the average particle size and contaminant population. The evaluation involves the calculation of a confidence interval constant, K_{CI} (%), which relates the area of ink coverage of the paper, the average particle size, and the sampling area to a confidence interval, CI, (%) for a given confidence level. The following equation are specific for a CI of 95%. The relationships are defined by Equations {4.1} and {4.2}:

$$K_{CI} = 3(2*100 / CI)^2 - 1 \qquad \{4.1\}$$

$$A_S = [(10^6 K_{CI} A_M / A_C)] \qquad \{4.2\}$$

where A_S is the area required to be sampled, A_M is the average particle area, and A_c is the concentration of contaminant coverage, expressed in ppm. Equations {4.1} and {4.2} can be combined to yield an explicit function for CI:

$$CI^2 = 120{,}000 \left\{ 1 / \left[\frac{As\ Ac}{(10^6)A_M} + 1 \right] \right\}. \qquad \{4.3\}$$

The confidence interval and level are most easily illustrated by the following example: a 95% confidence *level* is employed to determine the confidence *interval*, meaning that on average, only one out of 20 measurements falls outside the range of this *interval*. This statistical treatment is consistent with TAPPI Test Method T437

om-90 ("Dirt in Paper and Paperboard" [14]) and is employed to determine the confidence intervals in the present study. Thus, the technique of image analysis can be an objective measurement of the contaminant level in the paper sample, providing a representative lot of fields of view are assessed.

4.4 APPLICATION OF IMAGE ANALYSIS TO BRIGHTNESS MEASUREMENTS

Due to the manner in which the image analysis operates, it inherently lends itself very well to the evaluation of brightness parameters, as well as other optical properties measurements, in addition to the determination of residual ink concentration. The image analyzer assigns a gray value to each pixel, by which it discerns the ink particles in the field of vision. It is also possible, however, to compute an overall gray value for the field of vision, which is the essence of the brightness measurement. This combination is, to our knowledge, a novel application of image analysis.

For this technique of image anlaysis-detemined brightness to be successful, the image analyzer must be configured in a manner that resembles a standard design for conventional brightness measuring techniques. The geometry of the ISO brightness standard lends itself particularly well to the unaltered design of the microscope and gives the recommended [5] 0.0° incident angle of the light source to

the reflected beam. However, the diffuse illumination cannot easily be accomplished with a microscope. The 45° incident beam of the TAPPI standard is also difficult to achieve without significant alterations to the viewing stage. However, a combination of the collimated incident beam and 0.0° degree illumination can be employed without modification to any part of the microscope. Optical filters can then be inserted into the path of the reflected beam to narrow the bandwidth to the prescribed standards of the particular testing method. The optics of the microscope do not cause refraction of the light or changes in the wavelengths [15]. Also, the specified dimensions for the light apatures for the traditional instruments are on the order of tens of millimeters [1, 2] and do not lend any significant optical aberrations to the incident or reflected light beams. Therefore, the size of the apertures are not significant to the translation of brightness measurement from the standard machine to the proposed apparatus. Thus, simple physical modifications transform the physical arrangement of the image analyzer to that of a conventional brightness measuring machine.

Standards must be obtained and employed to calibrate the instrument. These standards are readily available from several companies and in several forms. The most common standards are paper tabs that are pre-evaluated for the brightness values. Also recommended by the TAPPI and ISO guidelines are standards manufactured from opal glass. Reflected light microscopy has the limitation,

however, that different surfaces can provide different amounts of reflected light due to the scattering of the light by uneven surfaces such as fibers. Thus, for the image analyzer-based determination of brightness, paper tab standards should be employed. Also, the calibration data obtained from these standards must be reproducible over a wide range of brightness values.

4.5 EXPERIMENTAL

An image analyzer was configured in the previously described manner to measure paper brightnesses. The equipment consisted of a Nikon Optifot II microscope, with reflected and transmitted light capabilities and optical filter slots. Reflected light was chosen for the illumination. A Hamamatsu C2400 CCD monochromatic video camera was mounted on the microscope with the use of an adapter. The image created by the camera was sent to a Hamamatsu Argus 20 image processor/camera controller with image averaging, background subtraction, and overlay capabilities. The video signal was displayed on a Sony Trinitron monitor while simultaneously being sent to a Imaging Technology, Inc. VISION*plus*-AT frame-grabber computer card that controlled the image acquisition. Version 4.1 of the Optimas imaging software was employed to manipulate the image and provide various measurements, which were controlled from the computer (Intel Pentium®, 60 MHz clock speed) CRT. The microscope stage was a worm driven, 3 x 4 inch travel,

motorized stage, manufactured by Prior. Stage movement was controlled by software written for the Optimas package, thus allowing automated sample movement. The IA system, being a microscope-based apparatus, was capable of discerning ink particles in the micron range while a scanner-based system would have a lower detection limit of approximately 60 μm.

The Nikon microscope easily accepted optical filters in the incident and reflected beam paths. All optical filters were manufactured by Andover Corporation except one UV cut-off filter which was supplied by Nikon. For reflected light, the collimated incident beam was passed through a diffuser and two UV filters that combined to yield an effective cutoff for all wavelengths under 450 nm, thus eliminating fluorescent excitation of any brightness enhancers that may have been in the paper sample. The light source, manufactured by Ushio, was a standard halogen lamp with a color temperature of 3300 K. The lamp's spectral output, as well as the transmission characteristics of the 450 nm cutoff filter, are shown in Figure 4.3. An in-line power conditioner (Sola Model CVS) was employed to stabilize the voltage for the reflected light source. As data for the spectral transmissions of the Nikon equipment were unavailable due to its proprietary nature, the overall spectral transmission characteristics for the light paths were assumed to be similar to that of the light source combined with the UV cutoff filter for the bandwidth of interest. A filter closely corresponding to the wavelength distribution prescribed by the standard

TAPPI and ISO test methods for brightness was then inserted in the path of the reflected beam. This filter had the spectral response shown in Figure 4.4; the principal wavelength of the brightness filter was 453.2 nm, and the bandwidth was 35.3 nm.

It must be noted that the neither the incident light nor the optical filters employed conformed exactly to the TAPPI standards. The objective of this study was not to copy the physical design of a brightness/opacity meter but rather to cause the image analysis equipment to function in a similar manner. Due to the manner in which the image analyzer obtains data, the results were expected to deviate somewhat from the brightnesses measured with conventional machines.

For each handsheet in this investigation, brightness measurements were taken in each of the four quadrants of the felt side of the paper using the 5x objective of the microscope-based analysis equipment. The 5x objective was chosen because it afforded a reasonable compromise between the desire for a high magnification and a large area to be examined. With this objective, particles as small as several microns were detectable while the region of interest was large enough to allow representative sampling in a short period of time. A 7x7 grid of frames was acquired and processed, thus totaling 196 total measurements per handsheet-side, with the area of each frame being approximately 1 mm^2. The Optimas software allowed the whole field of view to be included in the region of interest, and the average gray value was then calculated

while *simultaneously* measuring the area of the ink specks and the percentage area of ink coverage of the handsheet. The data was exported to an electronic spreadsheet (Excel) where calculations were performed. The brightness values of the four quadrants were averaged to obtain the overall single-side brightness for the handsheet. The secondary fiber source employed for the manufacture of the handsheets was obtained from Shell Development Company mill trials as well as laboratory studies. Stocks ranged from newsprint to mixed office waste. Brightnesses of the paper samples (standard handsheets) were evaluated by Shell with TAPPI and ISO standard machines (Technidyne S-4 Brightness Meter for the TAPPI scale and Technidyne 950 for the ISO scale). These results were then compared to the brightness values obtained from the image analysis equipment.

The threshold limit was determined by viewing a region of interest and increasing the threshold until all ink specks were marked by the software. These thresholds were set at the beginning of each data gathering session and were not changed. The levels were not necessarily constant from session to session due to small differences in the intensity of the lighting, video image contrasting, and the relative gray values of the paper and the ink specks. The instrument was calibrated with pre-evaluated paper tab brightness standards (supplied by Technidyne Corporation) at the beginning of each data gathering session. A specially designed sample holder was employed to hold the paper samples and their backings flat, thus

allowing nearly completely automated data gathering. Samples were backed in the "infinite sheet" style suggested by TAPPI Test Method T452 om-92 (directional brightness).

This setup offers quite a bit of flexibility in that different optical filters can be employed to gather data in different regions of the spectrum. Such advantages lend applicability not only to brightness, but to other optical properties measurements such as opacity (TAPPI Standards T425 om-91 and T519 om-91) and colourimetry (TAPPI Standards T524 om-94 and T527 om-94). Also, it must be stressed that with this system, not only are these optical properties being determined, but the dirt or ink speck count is also being obtained *at the same time*, leading to savings in analysis time. Typical TAPPI and ISO brightness evaluations each require at least four (4) minutes per handsheet (measuring brightness of each of the four quadrants of the sample). Scanner-based IA ink counts, which are capable of detecting only particles above approximately 60 μm, require an additional four minutes. In this study, the time required to evaluate one handsheet-side was approximately 15 minutes, which is roughly comparable to the sum of the times for traditional measurements. However, this is the same amount of time required for a microscope-based IA ink count (a single measuremnt), while the new system discussed here allows brightnesses to be evaluated simultaneously. Only one machine is required, no sample transfer must be made, and the resultant time savings is roughly 33%.

For this study, the statistical evaluation suggested by Zeyer et al. [12] was employed to calculate the confidence interval associated with a confidence level of 95%. These calculations were made by employing the number average particle area and the percentage area coverage by the ink as determined by the image analysis *during* the measurement of the brightness values.

4.6 RESULTS AND DISCUSSION

The precision or consistency of the data is first addressed. Several authors [11, 12, 16] have discussed the importance of threshold in the determination of contaminant areas. Heintze [16] reported that factors of as high as 20 could be exhibited in the difference in calculated particle area, depending on the user-set threshold. However, threshold can also be affected indirectly by fluctuations in the gray levels detected by the instrument. Such variations can arise from lighting inconsistencies. Figure 4.5 (curve "without line conditioner") illustrates typical variations exhibited by the standard lamp employed in this investigation. The erratic function depicts the overall gray value of a single frame as a function of time for the standard system configuration. Significant variances are seen both during and following the warm-up period of approximately 1.5-2.0 hours. This fluctuation is attributed to small variations in the lamp intensity due to line voltage instability. The "with line conditioner" curve in Figure 4.5 illustrates that an in-line power

conditioner reduced variations in the average gray value to ± 0.5%. The deleterious effect of fluctuating lamp intensity cannot be understated for the overall gray value measurement as well as the particle identification. The latter consequence occurs even though the threshold for particle detection does not change. This is due to the fact that the gray values do change and may cause lighter particles to remain undetected. Error associated with this anomaly can be effectively reduced by the use of the power conditioner. Further reduction could be achieved by installing a second power conditioner in series with the first.

For the calibration of the instrument, pre-evaluated paper tabs were employed. Gray values for a series of both TAPPI and ISO standards were obtained so as to be able to calculate brightnesses of each of the handsheets on both scales. Eight fields of view were taken for each calibration tab, and the overall gray values were averaged. Typical calibration results are depicted in Figure 4.6. The gray value for the zero (0) brightness point was obtained by placing a black felt cloth at a 45° angle in an unfocussed incident light beam. This procedure is similar to the black body backing employed for some opacity measurements [17]. To insure that reproducible calibration results were being obtained, the gray values of six calibration runs were compared to the gray values for a single calibration. For all series, the values of calibration sets scale linearly to the values of the other sets with a minimum square of the coefficient of linearity (R^2) of 0.9988. Similar results were obtained for

the ISO calibration curves. These data imply that the random error associated with the measurements is extremely small. Therefore, instead of a calibration curve, interpolation between the calibration points was used for the calculation of the TAPPI and ISO gray values for the sample handsheets.

Figures 4.7 and 4.8 illustrate the comparison of the TAPPI and ISO brightness values obtained with the image analysis equipment to those from traditional brightness measuring machines. The 45° line represents exact agreement. As the figures demonstrate, while some deviation was observed, the overall agreement between the new method and the standard techniques is excellent. The average of the absolute value of the differences between the standard machine-determined values and those from the image analysis (henceforth referred to as IA brightnesses) was 4.05 points for the TAPPI scale and 3.88 points for the ISO scale (approximately 6%). It is most likely that the IA-ISO brightnesses differed less than the IA-TAPPI brightnesses due to the overall geometry of the apparatus. The 0.0° incident/viewing angle in the new technique is the same as that of the standard ISO measurement technique. However, diffuse light could not be achieved in the IA set-up.

As illustrated by Figures 4.7 and 4.8, the IA brightness values tended to be lower than those of the TAPPI and ISO scales. Since all calibrations were made with paper tabs containing *no* contaminants, this observation would tend to imply that the deviations are a result of the residual ink in the handsheets. Equation {4.3} suggests

that the confidence interval associated with the particle size and coverage area is inversely proportional to the square root of the quotient of the area of ink coverage divided by the average particle area. This relationship, however, does not apply to the IA brightness or the deviation of the IA brightnesses from the standard measurement techniques. The deviations can be correlated using the population function, Ψ:

$$\Psi = \ln\left[\frac{A_W}{A_M}\right] \qquad \{4.4\}$$

where the

$$A_W\,(\%) = \left\{\frac{\sum_i [(100 - B_i) * A_i]}{A_s}\right\}. \qquad \{4.5\}$$

In Equations {4.4} and {4.5}, A_W is the weighted percent area, and, for particle i, B_i is the IA brightness and A_i is the area of that particle. This value is subtracted from 100 in Equation {4.5} because the brightness scales are based on a maximum of 100. This type of area was employed because darker particles contribute more heavily to the decrease in brightness values than do lighter particles of the same size. The calculations were made on the basis of the area of one frame of observation for ease of number handling rather than on the sum of the areas of the 196 regions of observation.

In Figures 4.9 and 4.10, a clear trend of increasing negative deviation of the IA brightness from the traditional brightnesses is illustrated for increasing values of

the population function, Ψ. Jordan and Popson [10] showed that the percent reflectance (brightness) of paper does not decrease linearly as a function of ink concentration. Instead, the reduction in brightness becomes much smaller as the total ink concentration increases. This observation is consistent with our data as shown in Figure 4.11. As the coverage area increases, Ψ also increases, and the negative deviation of the IA brightness from the traditional brightness becomes greater.

Similarly, smaller particle sizes cause traditional brightnesses to decline rapidly [9]. However, as the brightness decreases, as shown in Figure 4.11, the effect of added (smaller) particles diminishes. In fact, Jordan and Popson [10] showed that while 2000 ppm of flexographic ink reduces the reflectance (brightness) of newsprint (original reflectance $\approx$ 60) to 40, a concentration of 4000 ppm of ink reduces the brightness only 5 additional points. Once the small particles diminish the brightness to an extent, an increased density of particles, large or small, have little effect on the brightness. Therefore, for the case in which the average particle size is small, traditional brightness measuring techniques do not reflect the relative ink concentration in the paper well. Applying this principle to the population function, it is seen that as the average particle size decreases, Ψ increases, as should the deviation of the IA brightness from traditional brightnesses as reflected in Figures 4.9 and 4.10.

Analysis of the possible errors associated with this study includes the consideration of random equipment errors, repeatability, and sampling errors. Figure

4.5 suggests that random equipment errors in the gray value intensities are negligible, while the calibration results illustrate that for paper samples with no ink coverage, repeatability is excellent. To investigate the effect of ink particles on repeatability of the brightness, three samples were measured four times during different data gathering sessions. For each trial, the calibration and the portions of sample that were scanned were different. The three samples were chosen to represent the most and the least uniform handsheets. Results of the brightness values are shown in Figure 4.12. For these samples, the standard deviations for the brightnesses ranged from 0.682 (0.99%) to 1.670 (2.00%) points for the TAPPI scale and 0.471 (0.68%) to 2.081 (2.50%) points for the ISO scale. Sample 495-162-2 was the most heterogeneous while sample 085-88-3 was the most homogeneous. Also several handsheets were analyzed twice on traditional brightness measuring machines. The average absolute deviation for the TAPPI and ISO measurements were 1.864 and 1.307 brightness points, respectively, over a range from approximately 48 to 87 brightness units. Finally, the effect of possible random sampling errors was calculated for the coverage and particle areas using the correlations suggested by Zeyer et al. [10, 11]. Table 4.I lists the % area coverage, weighted % areas, average particle area, and CI for all handsheets. The greatest CI for a confidence level of 95% is 11.35%, while the average CI is 4.50%. Using these values of confidence intervals for the recalculation of A_M and A_c in Ψ for Figures 4.9 and 4.10 results in negligible changes; therefore,

Ψ is not a strong function of the sampling error. Also, there is no correlation between the brightness deviations and the CI. Therefore, the effect of sampling error is this study on the IA brightnesses was small. It may be concluded that the precision associated with the IA brightness measuring technique is approximately the same as that exhibited by the traditional brightness measuring apparati. Again, it must be noted that the technique does not mirror the traditional brightness measuring techniques and, thus, does not supply the same values for the brightnesses of the handsheets. However, the IA brightness measurements are more objective than the traditional methods.

4.7 CONCLUSIONS

The application of image analysis to the brightness measurement can be accomplished successfully. The IA brightness values for the TAPPI and ISO scales may not necessarily correlate exactly with those from traditional brightness measuring apparati because the IA technique is more objective with respect to accounting for the percentage of ink coverage and the sensitivity of brightness to the particle size. This technique is extremely flexible and could easily be extended to measurements that are derivatives of reflectance-based optical properties such as opacity and colourimetry. In addition to these advantages, the IA method is capable of obtaining histographic information of the contaminant population while simultaneously gathering the optical

property data. This advantage saves the time required for two independent measurements as well as the expense of a second piece of equipment.

4.8 REFERENCES

1. TAPPI Standard T452 om-92, Brightness of pulp, paper, and paperboard (directional reflectance at 457 nm) in *TAPPI Test Methods* 1995-1995, TAPPI Press, Atlanta (1994).
2. ISO 2469, Paper, board, and pulps--Measurement of diffuse blue reflectance factor (ISO brightness).
3. ISO 2470, Paper, board, and pulps--Measurement of diffuse reflectance factor (ISO brightness).
4. TAPPI Standard T525 om-92, Diffuse brightness of pulp (d/0°) in *TAPPI Test Methods* 1995-1995, TAPPI Press, Atlanta (1994).
5. Jordan, B. D.; Nguyen, N. G.; Trépanier, R. J. R. Measuring the particle-size distribution of residual ink in recycled paper. Tappi J. 76, no. 10: 110 (1993).
6. Larsson, A., Stenius, P., Odberg, L. Surface chemistry in flotation deinking: Part 2. The importance of particle size. Svensk Papperstid. 87, no. 18: R165 (1984).
7. Bristow, J. A. What is ISO brightness? Tappi J. 77, no. 5: 174 (1994).
8. McCool, M. A. Taylor, C. J. Image analysis techniques in recycled fiber. Tappi J., 66, no. 8: 69 (1983).
9. McKinney, R. W. J. Evaluation of deinking performance: A review of test methods. Tappi J. 72, no. 1: 129 (1989).

10. Jordan, B. D.; Popson, S. J. Measuring the concentration of residual ink in recycled newsprint. J. Pulp Pap. Sci., 20, no. 6: J161 (1994).

11. Zeyer, C., Venditti, R. A., Puangchinda, K. W., Heitmann, J. A. The effect of sample size on the confidence inteval for image analysis of impurities in pulp and paper. Tappi J. 78, no. 2: 168 (1995).

12. Zeyer, C., Venditti, R. A., and Heitmann, J. A. The distribution of impurities in pulp and paper: the effects of the random distribution of impurities on image analysis. Tappi J., 78, no. 2: 176 (1995).

13. Moss, C. S. Image analysis standardization. Tappi J. 76 no. 10: 117 (1993).

14. TAPPI Standard 437 om-90, Dirt in paper and paperboard, in *TAPPI Test Methods* 1995-1995, TAPPI Press, Atlanta (1994).

15. Frey, C., Nikon, private communication.

16. Heintze, H. The measurement of dirt in recycled fine papers. Pulp Pap. Can., 93, no. 10: 51 (1992).

17. TAPPI Standard T519 om-91, Diffuse opacity of paper (d/0° paper backing) in *TAPPI Test Methods* 1995-1995, TAPPI Press, Atlanta (1994).

Table 4.I. Data for handsheets

Sample	Area coverage (%)	TAPPI A_w	ISO A_w	Average Particle Area (μm^2)	CI (%)
085-65-1	0.054	1.68	1.66	31.20	6.387
085-65-2	0.023	0.90	0.89	41.97	11.355
495-162-1	3.152	102.48	101.46	970.18	4.662
495-162-2	2.298	76.25	75.53	1414.82	6.594
495-05-6	0.485	19.24	19.16	362.98	7.270
495-36-1	0.781	28.56	28.38	421.13	6.170
085-131-1	3.052	106.35	105.61	465.02	3.280
085-88-1	0.043	1.36	1.35	55.42	9.542
085-91-4	0.084	2.76	2.74	53.03	6.677
085-88-3	0.068	2.15	2.13	49.41	7.163
085-97-3	0.060	1.93	1.92	58.05	8.266
085-91-2	0.131	4.18	4.15	36.05	4.408
85-82-3	0.099	3.26	3.24	52.26	6.105
553-60-1p	1.628	57.25	56.80	118.90	2.271
553-62-1p	1.930	67.97	67.44	112.01	2.024
553-68-1p	1.437	51.39	51.00	100.51	2.222
553-80-1p	1.086	38.87	38.57	80.70	2.290
553-59-1	0.579	24.98	24.92	81.49	3.152
53-69-1f-1	0.621	25.18	25.09	84.44	3.098
53-74-1f-1	0.656	26.40	26.30	105.65	3.372
553-77-1	1.199	46.19	46.03	64.32	1.946
553-66-1	0.481	19.83	19.76	77.63	3.375
553-63-1	0.524	21.47	21.40	76.90	3.219
553-76-1	0.808	28.92	28.88	55.71	2.206
553-76-1P	1.420	54.97	54.92	83.32	2.035
553-61-1P	1.412	51.75	51.71	111.15	2.357
553-59-2P	1.873	60.86	60.81	119.57	2.123
553-69-1P	1.243	47.35	47.31	98.72	2.368

Figure 4.1. Schematics for brightness measuring apparati.

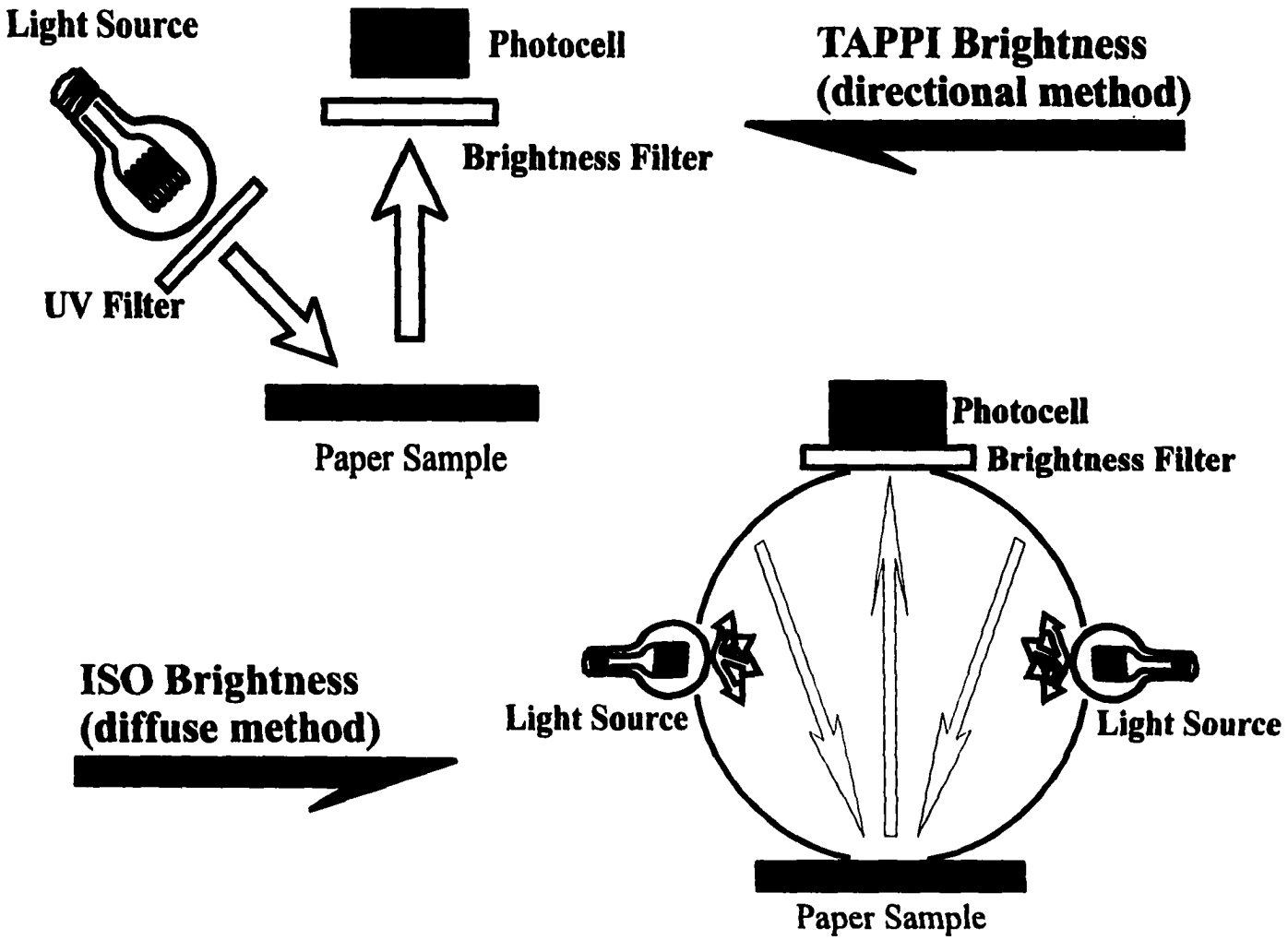

Figure 4.2. Schematic representation of the image analysis system.

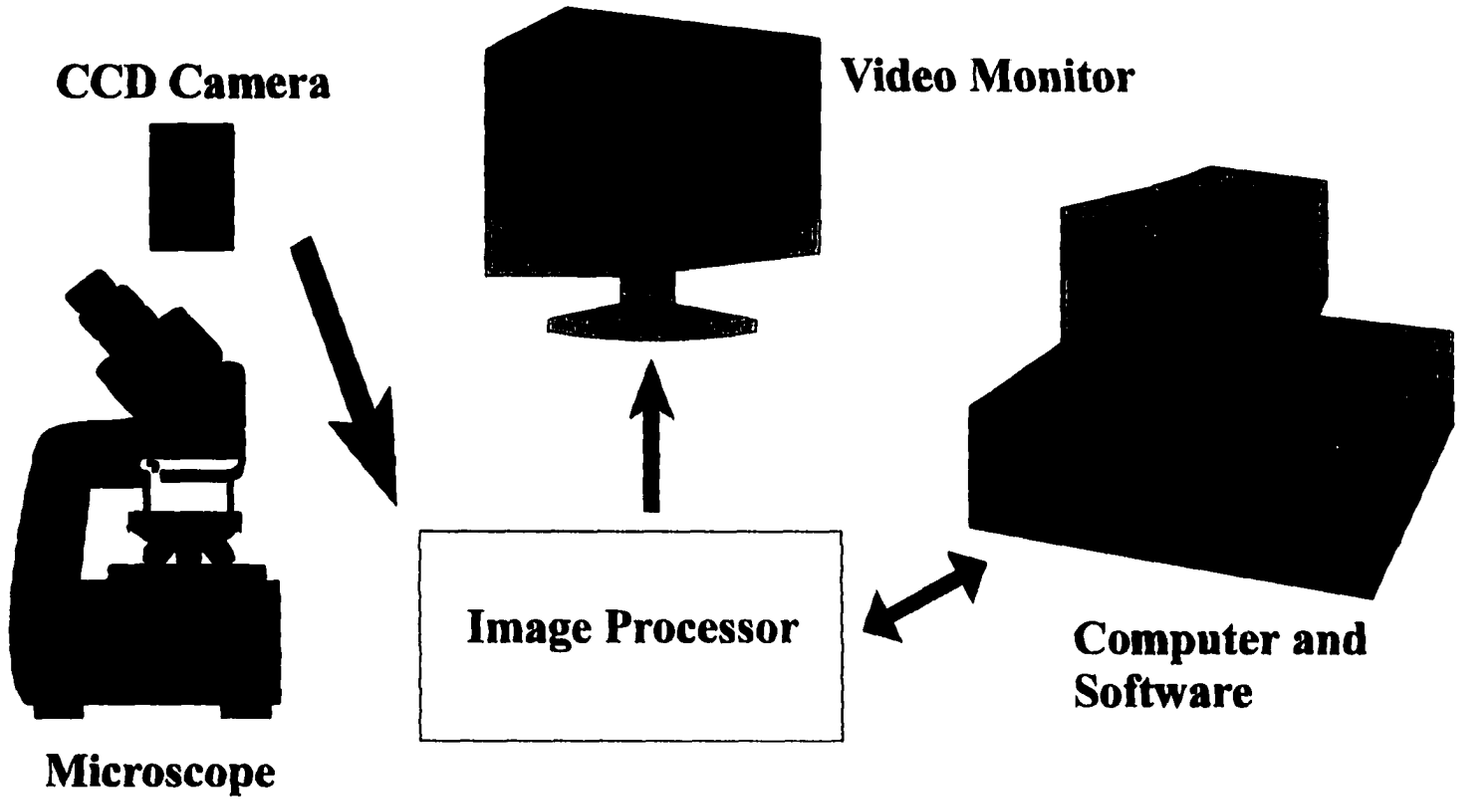

Figure 4.3. Spectral output for the reflected light lamp and the transmission curve for the UV cutoff filter.

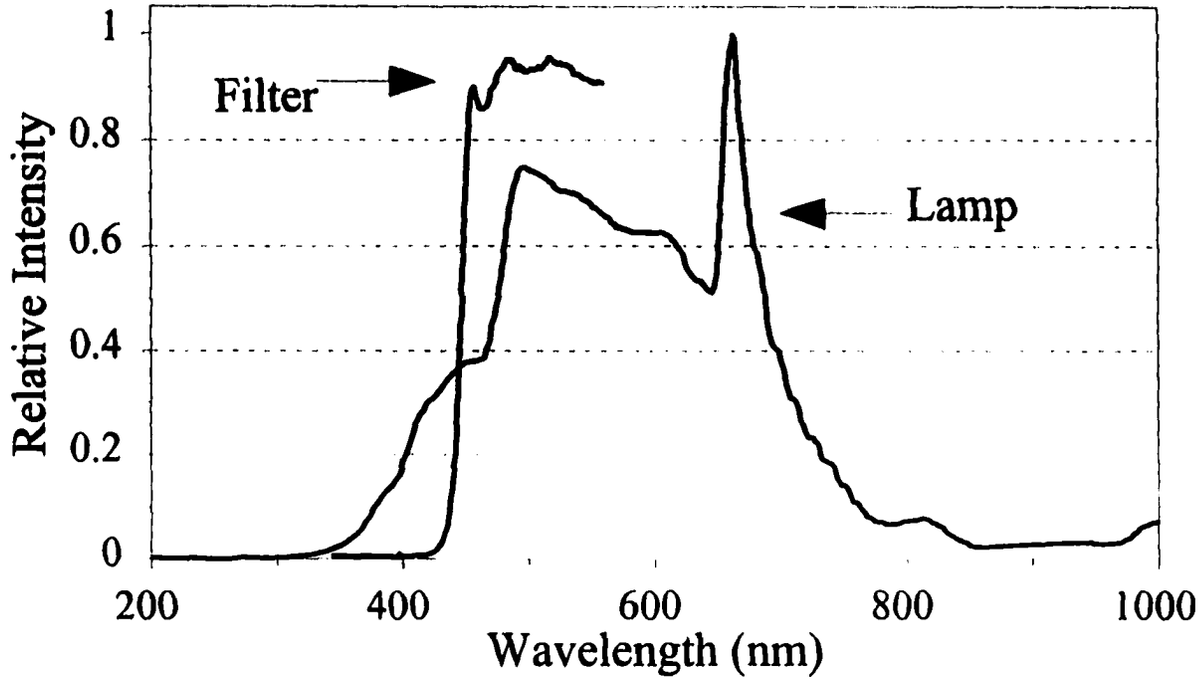

Figure 4.4. Spectral transmittance for Brightness Filter

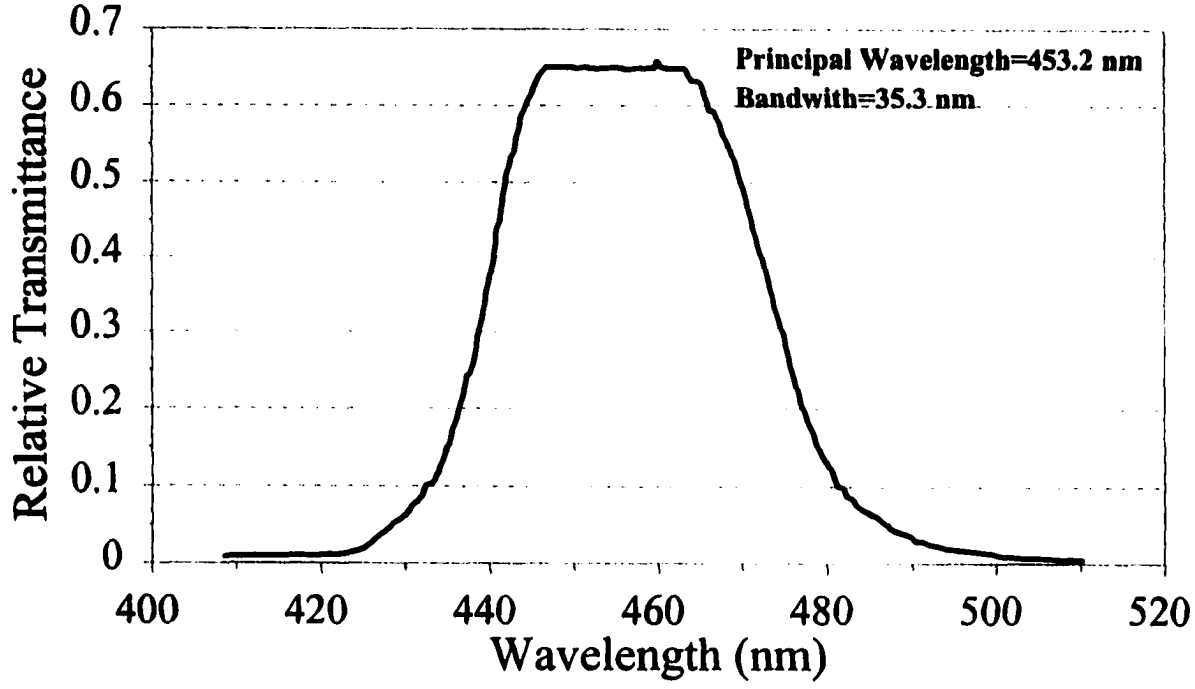

Figure 4.5. The effect of an in-line voltage conditioner on the average grey level.

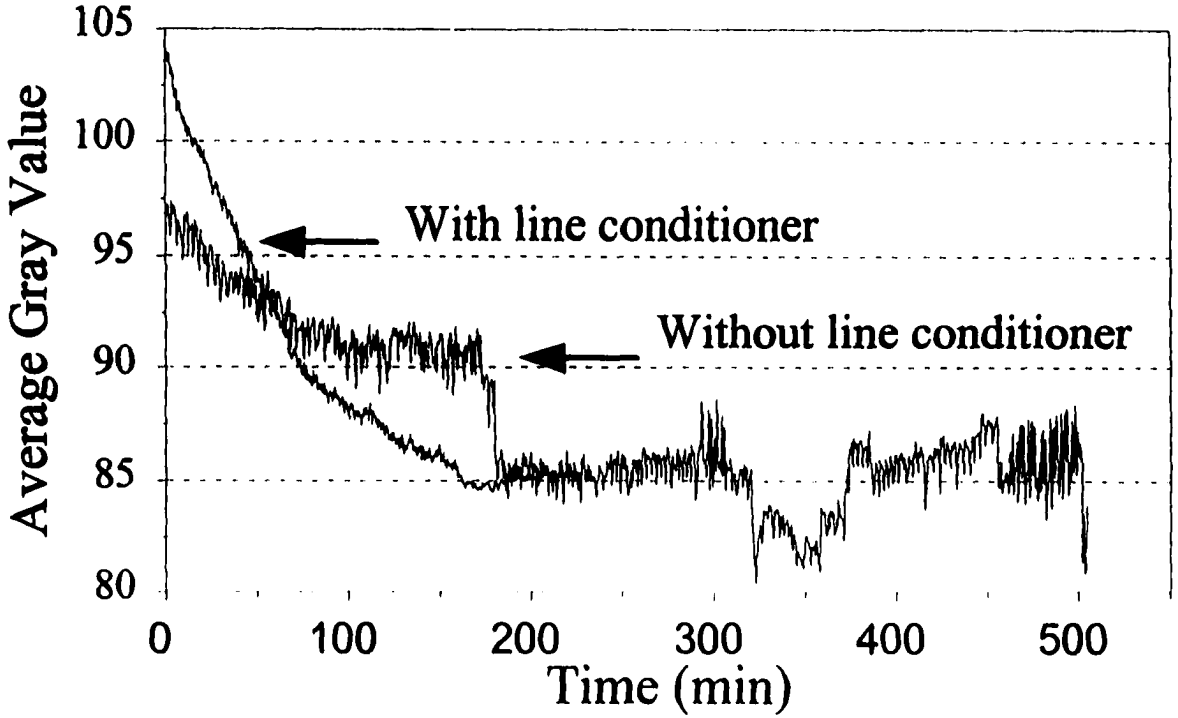

Figure 4.6. Typical calibration curves for TAPPI and ISO standard scales.

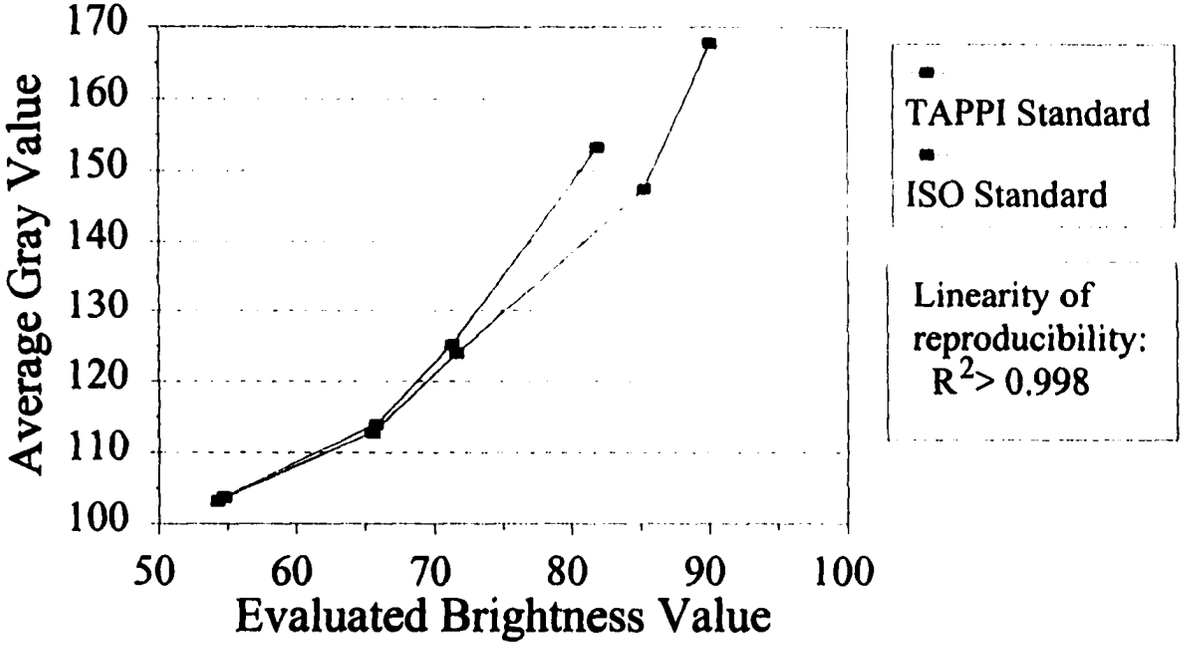

Figure 4.7. IA-TAPPI brightness compared to traditional TAPPI brightness.

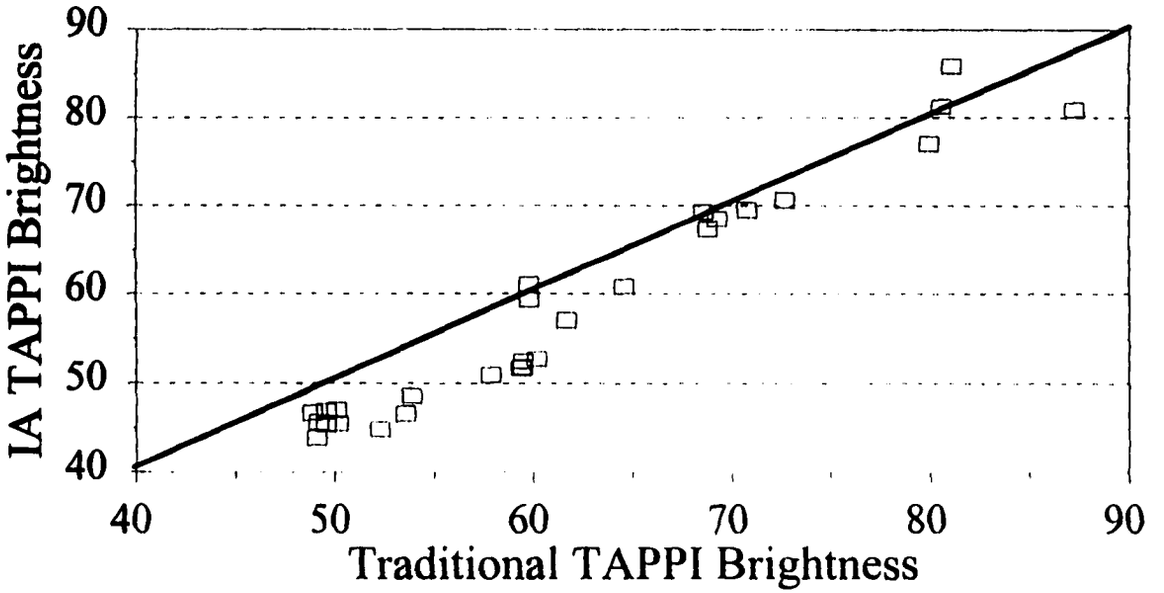

Figure 4.8. IA-ISO brightness compared to traditional ISO brightness.

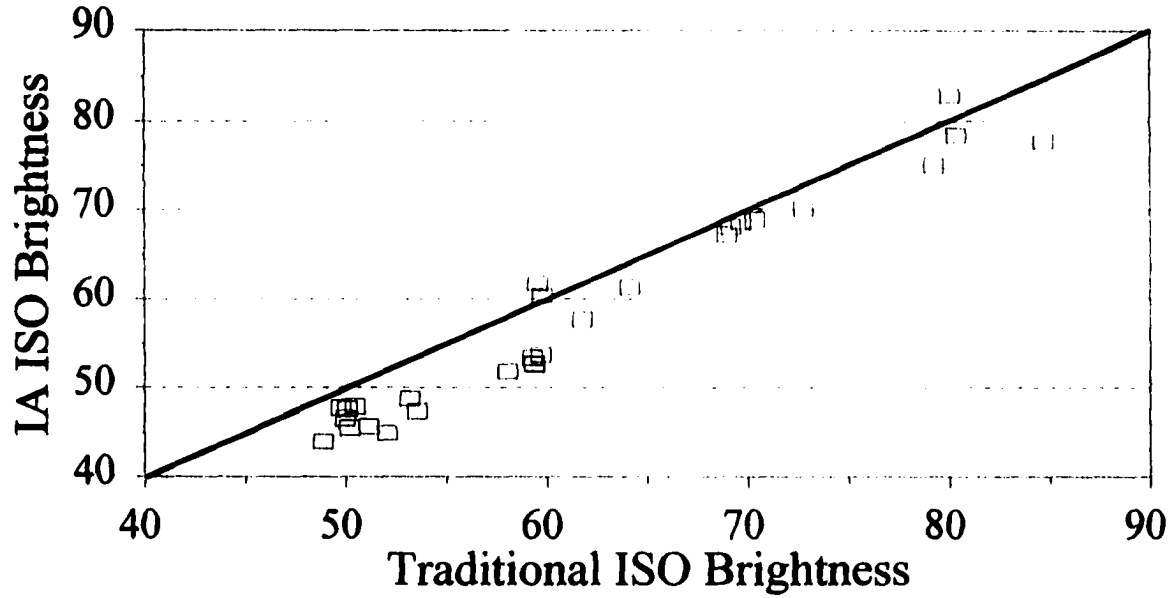

Figure 4.9. Percent deviation of the IA-TAPPI brightness from traditional TAPPI brightness as a function of the population function.

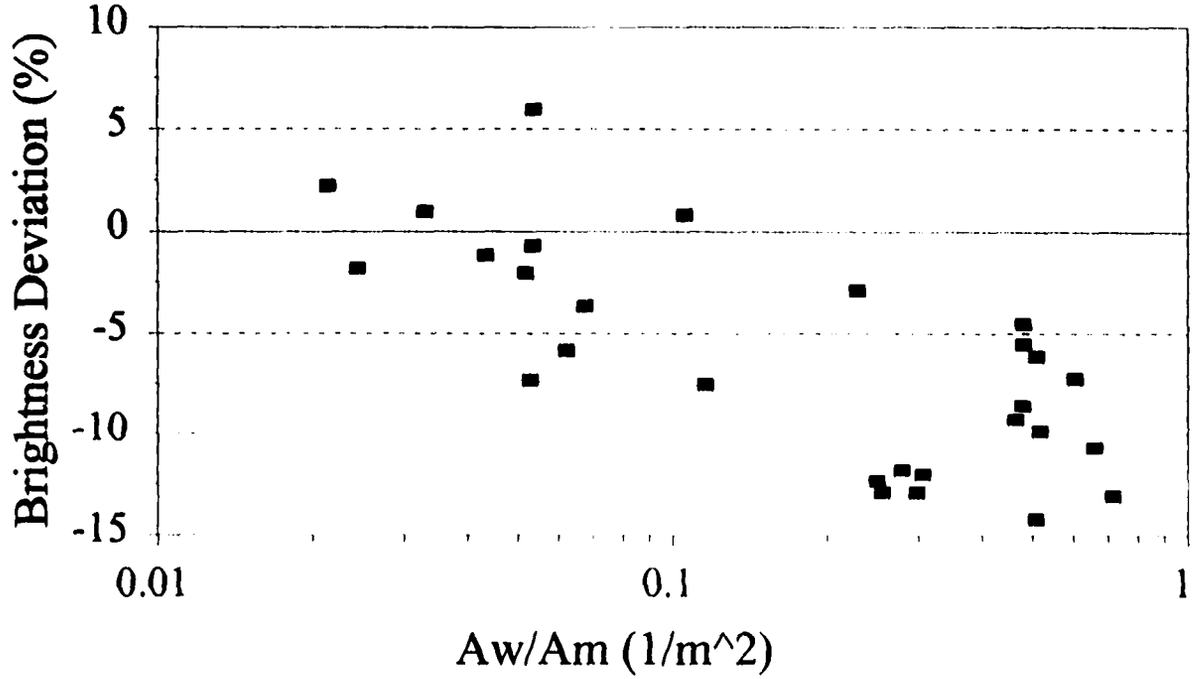

Figure 4.10. Percent deviation of the IA-ISO brightness from traditional ISO brightness as a function of the population function.

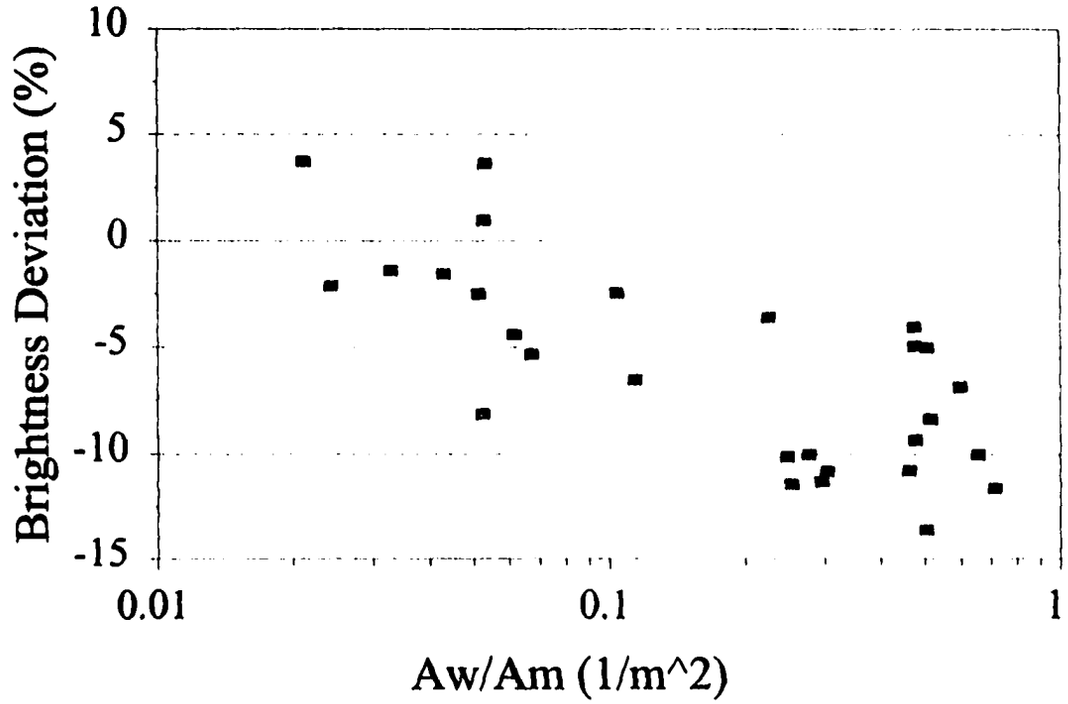

Figure 4.11. Brightness as a function of the area coverage.

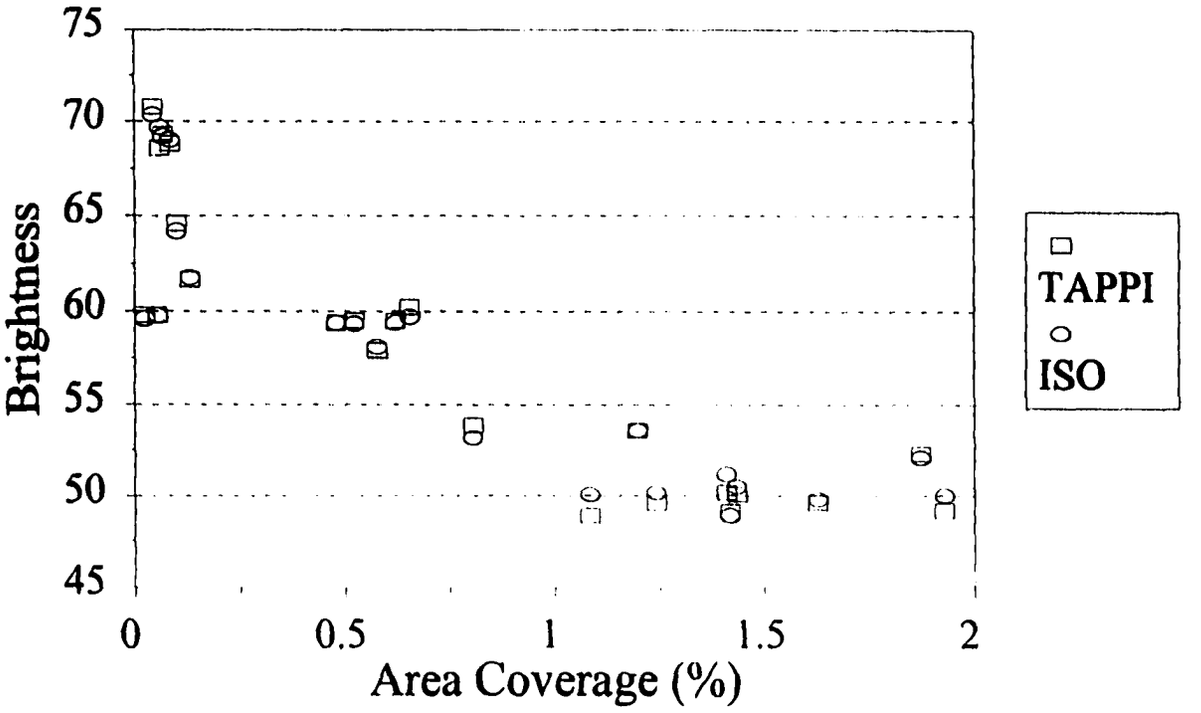

Figure 4.12. Repeatability of IA Brightness Measurements.

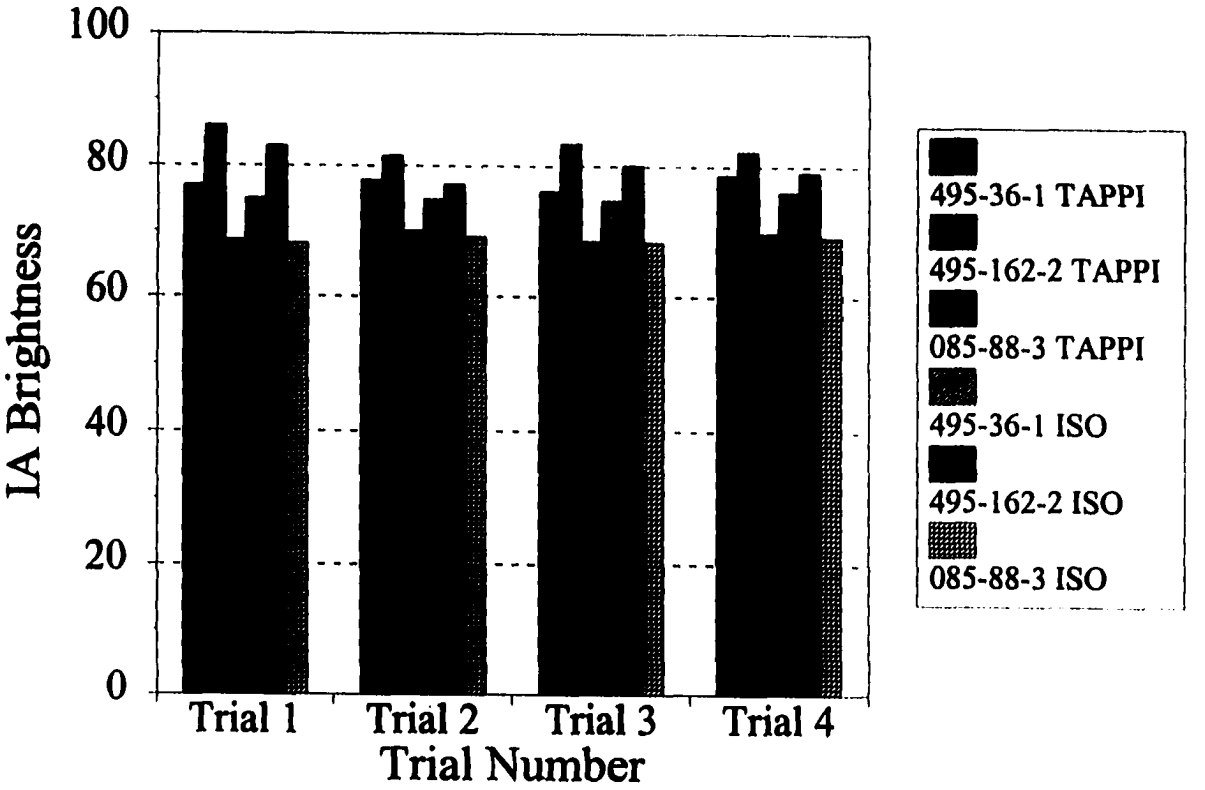

CHAPTER 5

A NOVEL TECHNIQUE FOR THE PRODUCTION OF CUSTOMIZED HPLC PACKINGS

A method for the production of a novel high performance liquid chromatography (HPLC) packing is described. As an example of the synthesis, a packing capable of separating medium chain-length sodium carboxylates, such as sodium octanoate, from solutions of high ionic strength at neutral pH is detailed. The technique involved the synthesis of a patchwise polymer film on the surface of commercially available HPLC-grade silica using admicellar polymerization techniques. For the analysis of underivitized sodium octanoate on the poly(lauryl methacrylate)/silica (PLM) packing that was produced in this manner, the partition coefficient and the effective plate number approached infinity and the retention ratio approached zero in distilled, deionized water at a neutral pH. While traditional packings such as bonded octyl and octadecyl reverse phases were not capable of separating the octanoate from highly ionic solutions, the PLM packing easily resolved the analyte peak from the salt peak with a simple bicratic mobile phase system.

Characterization of the polymer and packing using TGA/MS, GPC, and AFM revealed low molecular weight poly(lauryl methacrylate) on the surface of the silica with a weight percentage of approximately 8.5%. Extension of the technique to the production of other customized HPLC silica packings is anticipated to be simple and straightforward.

Keywords: HPLC, reverse phase, carboxylate, polymer, admicellar polymerization

5.1 INTRODUCTION

The selection of a high performance liquid chromatography (HPLC) packing for the separation of compounds whose molecular weights and solubilities do not lend themselves well to gas chromatography or straightforward liquid chromatography can be very difficult. Examples include the analysis of the medium chain-length carboxylate salts, particularly sodium octanoate ($C_7H_{15}COONa$), in the presence of high concentrations of ionic species. The water solubility of the octanoate is extremely high due to its relatively short carbon tail length and the very polar carboxylate head group. The combination of these two features makes the carboxylate difficult to analyze using traditional HPLC packings such as octadecyl (C18) or octyl (C8) reverse phase silica with aqueous solvents at a neutral pH. The hydrophilicity of the medium-length carbon chain allows little interaction with these common stationary phases and results in extremely small retention times, unresolved peaks, and significant peak asymmetry. In addition, sensitivity can be a factor depending on the detector employed. UV detectors are not useful for underivatized fatty acids at low concentrations because the extinction coefficient of the carboxylate functional group at the wavelengths where the adsorption is maxium (200-210 nm.) is very small-on the order of 1000 times less that that of aromatic compounds such as benzene [1]. Electrical conductivity detectors (ECDs) are very sensitive to ionic compounds, but the analytes must be resolved from the salt peaks, and the

background ionic concentration must not be so high as to swamp out analytes of low concentrations, such as may be the case when an acidic mobile phase is used to fully protonate these carboxylates ($pK_a \approx 4.5$).

HPLC techniques for medium-length chain carboxylates usually involve derivatization of the analyte. This scheme accomplishes two objectives. First, the derivatizing reactant usually contains one or more phenyl rings, thus allowing UV detection of the product at extremely low levels without interference from the ionic character of the mobile phase. Second, the analyte is converted to a compound of higher molecular weight that is easily retained by standard reverse phase C18 or C8 stationary phases. Many reactions schemes for such derivatizations have been proposed. The most common compounds employed for these reactions are phenacyl [2,3], nitrobenzyl [3] and 2-naphthacyl esters [4]. A method involving p-bromo-phenacyl was refined by Korte et. al [5], while Jeungling and Kammermeier [6] developed a single-step procedure for the conversion of fatty acids to fluorescent coumarin esters for HPLC analysis. Another approach was taken by Quilliam and Yaraskavitch [7] in which the t-butyldiphenylsilyl derivatization was produced for the purpose of UV and/or mass spectrometric detection. A catalog of derivatization options can be found elsewhere [8].

Non-derivatization techniques for carboxylate analysis have also been published. Manning and Maskarinec [9] proposed a novel scheme to eliminate salt

peaks and, therefore, both greatly reduce the need for retention of the carboxylate on the stationary phase and allow an electrical conductivity detector to be employed. In the study involving the analysis of low molecular weight (formic to octanoic) carboxylic acids from sour water generated from coal liquefaction, the investigators protonated the carboxylates with 1.0 N sulfuric acid and extracted them from the ionically-laden aqueous phase using diethyl ether. The ether containing the carboxylic acids was then combined with a known volume of doubly-distilled water and was allowed to evaporate, thus depositing the analyte into the aqueous phase. This solution was then analyzed with HPLC using a C18 reverse phase column. The technique, however, allows many opportunities for experimental error to be introduced, and the investigators reported an average precision of 13%.

In another scheme [10], octanoic and decanoic acids were extracted from brain tissue and plasma using acetonitrile. Two HPLC stages employing two different variations of C18 reverse phase columns and a mobile phase of acetonitrile/50 mM sulfuric acid/water (5:3:2) were employed for the analysis. Detection was accomplished with a UV spectrophotometer. In this case, protonation of the carboxylic acids by the sulfuric acid in the mobile phase allowed sufficient residence time on the column for the peaks to be resolved. The UV detection allowed the use of such a mobile phase, while a more sensitive conductivity detector could encounter difficulties because of the high background level associated with the 16.7 mM

concentration of ionizable sulfuric acid.

Since the inception of the idea to combine a polar mobile phase with a nonpolar stationary phase for liquid chromatography by Boscott [11] in 1947, extensive research has been conducted into the production of novel "reverse phase" packings, leading from benzene-saturated, moderately vulcanized rubber [12] to silane-bonded "anchored phases" [13]. Recent developments in "admicellar polymerization" [14-17] now allow tailored polymeric films to be produced on the surface of HPLC silica, thus forming a new class of stationary phase.

Admicellar polymerization is the general term referring to the polymerization of a monomer that has been solubilized in a patchwise surfactant bilayer at a solid-solution interface. Harwell [18] first coined the term "admicelle" to describe the micellar-like, physically adsorbed surfactant bilayer structure that can form on charged solid substrates surfaces such as metal oxides. In a similar manner to that in which micelles solubilize, or incorporate, other molecules into their structure, admicelles are capable of "adsolubilizing" molecules to form a structured heterogeneous bilayer. Wu et al. [14, 16, 17] demonstrated that in monomeric form, a polymerizable species could be solubilized into the admicelle, and a subsequent polymerization reaction could be initiated to create a patchwise thin polymer film on the surface of alumina and silica (see Figure 5.1). The formation of several polymer films, including polystyrene [14, 16, 17, 19-22], polyisoprene, polybutadiene,

copolymers of the three [21], and poly(tetrafluoroethylene) [23] has been described in the literature.

The technique is a four step process in which, first, an ionic surfactant having a head group of opposite charge to that of the substrate is allowed to adsorb and equilibrate into the admicellar structure on the substrate. The monomer then partitions into the favorable hydrophobic interior of the admicelle. It is necessary that at this point the concentration of the surfactant in the bulk solution not exceed the critical micelle concentration (CMC) so as to avoid solubilization and subsequent polymerization in micelles at the expense of the admicelles. Following this equilibration, the polymerization reaction is initiated by a free radical scheme, usually by the thermal decomposition of 2,2'-azobis(2-methylpropionitrile) (AIBN) or a similar compound. This free radical initiator is virtually insoluble in water and also partitions into the hydrophobic interior of the admicelle. During the reaction period, excess monomer from the bulk solution is drawn into the reaction proximity by diffusion [17]. If the reaction is allowed to proceed for a sufficient duration, virtually all of the monomer is incorporated into the polymer. The final step involves washing the surfactant from the silica/polymer surface to expose the polymer film.

Application of this admicellar polymerization technique to the production of custom HPLC stationary phases is straightforward. In a similar manner to that in which traditional reverse-phase packings allow analytes to adsorb or partition from

the mobile phase, a polymer film with pendant groups and a backbone structure compatible with the analyte also would promotes adsorption. For the alkali salts of medium chain-length carboxylic acids such as sodium octanoate, a polymer with a structure having not only a moderately hydrophobic character to accommodate the carbon tails, but, and more importantly, also a moderately polar region for carboxylate head group compatibility, must be produced. The monomer must also contain a terminal unsaturated bond for efficient free-radical polymerization. Finally, the polymer must not be readily soluble in the mobile phases to be employed for the HPLC separation. The methacrylate class of compounds, specifically lauryl methacrylate, lends itself well to this application. The twelve carbon pendant group provides sufficient affinity for the carbon tails and results in low solubility in methanol and water, while the ester linkage in the backbone of the poly(lauryl methacrylate) (PLM) is sufficiently polar to accommodate the carboxylate group.

The surfactant employed for admicelle formation and adsolubilization of the monomer must be ionic in nature and must have a charge opposite to that of the silica surface. For silica, the potential determining ions are the H^+ and OH^- ions, and the point of zero charge (PZC), the pH at which the net surface charge is zero in its transition from net positive to net negative, lies at approximately 4.0 [24]. At a pH of 8, the surface of the silica is sufficiently negative to provide a strong driving force for the adsorption of a cationic surfactant such as cetyltrimethylammonium bromide

(CTAB). More basic conditions cannot be employed due to the increased solubility of silica in alkaline solutions [24].

5.2 EXPERIMENTAL

In this investigation, the objective was to demonstrate the utility of the novelly-produced HPLC packings by separating a medium chain-length carboxylate from high concentration of other ions in the test solutions. To test this analysis, the sodium salt ofoctanoic acid (sodium octanoate) was selected as the analyte, and the added electrolyte employed was sodium chloride. The sodium octanoate was purchased from Sigma Chemical Company with a purity of greater than 99%. The sodium chloride was obtained from Fisher Scientific, and the monomeric lauryl methacrylate purchased from Haven Chemical. The n-hexadecyltrimethylammonium bromide (CTAB) was provided by Aldrich Chemical Company, and the free radical initiator, 2,2'-Azobis[2-(2-imidazolin-2-yl) propane] dihydrochloride (henceforth referred to by its trade-name, VA-044) was supplied by Wako Pure Chemical Ind., Ltd. The silica was purchased from Rainin Instrument Company and had a supplier-provided diameter of 5 μm, a BET surface area of 190 m^2/g, and an average pore size of 100 Å. The HPLC-grade methanol employed in the analysis was purchased from Mallinkrodt Chemicals and was 99.9% pure. The pH adjustments were made with Fisher-Brand N/20 NaOH. All of the above materials were used without further

purification. The water used for the experiments was distilled and deionized.

For the admicellar polymerization of the lauryl methacrylate on the silica surface, a 45 ml. Pyrex glass vial was charged with 3.0 grams of silica, 0.371 g (0.001018 moles) of CTAB, 0.259 g (0.001018 moles) of lauryl methacrylate, 0.045 g (0.000139 moles) of VA-044, and 40 ml of water at pH 8. This pH was chosen to be high enough to insure the net negative surface charge of the silica provided sufficient driving force for the surfactant adsorption while not being so basic so as to be in a region of unacceptably high solubility of silica. The quantities of reactants were derived from recommendations given in the literature [19-21] and are based on CTAB adsorption isotherms and solubility of the lauryl methacrylate in the admicelle. The mixture was stirred with a magnetic stirrer for one day to allow equilibration of the admicelle on the silica and the adsolubilization of the monomer and initiator. The vial was then placed in a thermostatted water bath at 70° C for 12 hours to allow the reaction to proceed. Following this reaction period, the contents of the vial were centrifuged and washed five times successively with distilled-deionized water. The complete procedure was then repeated to increase the amount of polymer film on the silica surface.

The C18 HPLC column used for comparison was 105 mm long and 3.0 mm in inner diameter and was packed with 10 μm ODS-3 reverse phase silica packing from Whatman. The C8 column was of the same dimensions and was packed with Maxsil

10 μm 10C8 reverse phase silica procured from Phenomenex, while the column for the PLM-treated silica was 115 mm long and 3.0 mm in inner diameter. All columns were constructed of stainless steel. A slurry-type HPLC column packing apparatus manufactured by Micromeritics Instrument Company was employed to pack the columns. The packing solvent was a 1:1 mixture of methanol and propanol. Following packing, each column was flushed alternately with water and methanol solutions until no ionic species were detected by the ECD. As CTAB is extremely soluble in alchohols, the majority of the residual CTAB was removed from the PLM column in the packing step. However, the methanol washing ensured that any remaining non-PLM-associated CTAB was removed and did not interfere with partitioning during the separations. The conductivity detector was a Wescan model 213-505, and a 100 μl. sample loop was employed for injection of the analytes into the columns.

A Dupont Model 951 thermal gravimetric analyzer interfaced to a Hewlett Packard 5985 quadrapole mass spectrometer (TGA/MS) was used to determine the weight percent of polymer on the silica. The connection, a model MCVT-1-50 variable splitting valve manufactured by Scientific Glass Engineering, Inc., was maintained at 200 °C. The carrier gas was helium and had a flow rate was 50 mL/min. All heating rates were 10 °C/min. The mass spectra were acquired using 70 eV electron bombardment ionization and scanning from m/z = 10 to 500.

Gel permeation chromatography (GPC) was employed for the determination of the polymer molecular weight. Samples of the PLM were extracted from treated silica with tetrahydrofuran (THF) in a Soxlet extraction apparatus under reflux conditions for 18 hours. The resulting solutions were evaporated in a vacuum oven at 60°C, and the residue was dissolved in freshly distilled N,N-dimethylformamide (DMF). Polystyrene molecular weight standards were obtained from Aldrich, and freshly distilled DMF at a flowrate of 0.5 ml./min. was used for as the solvent. A PLGel 5 μm Mixed-C GPC column and a Shodex RI-71 refractive index detector were also employed for the analysis.

The atomic force microscope (AFM) employed to obtain micrographs of the silica was a Nanoscope III manufactured by Digital Instruments. Tapping-mode scanning was used to acquire the AFM micrographs.

5.3 RESULTS AND DISCUSSION

In order to confirm successful polymerization of the lauryl methacrylate on the silica, GPC was used to determine the molecular weight distribution of the resulting PLM. Employing the polystyrene standards and DMF as the mobile phase, a calibration curve relating the number average molecular weight of the polymer to its retention time on the column was obtained. Monomeric lauryl methacrylate was then analyzed, and the calculated molecular weight (252.5) agreed with the actual

molecular weight (254.42) within 1%. From this result, it was concluded that the conformation of the PLM in the DMF was similar to that of the polystyrene and that DMF was an acceptable solvent for molecular weight determination. Samples of the extracted PLM were then analyzed, and molecular weight peaks were observed at approximately 9800, 5850, 3100, 2540, and 1430, with the 5850 being the dominant peak. This multi-modal molecular weight distribution does not correspond to standard kinetic models for polymerization and is most likely due to oxidative cleavage of the PLM by the THF during the extraction process. Though the number-average and mass-average molecular weights could not be calculated due to this breakdown, the GPC results confirm the admicellar polymerization of the lauryl methacrylate monomer on the surface of the silica.

In order to evaluate the quantity of PLM on the surface of the silica, a sample of the treated silica was combusted in a TGA, and the effluent was analyzed by MS. Figure 5.2 depicts both the TGA and the overall (m/z = 10 to 500) MS response traces for the treated silica. During combustion to 650 °C in the helium purge, two distinct weight loss events, the first at approximately 282 °C and the second at approximately 378 °C, occurred for a total mass loss of 11.03%. To determine the identity of the TGA peaks, pure CTAB was combusted (Figure 5.3). The MS analysis of this combustion revealed that greater than 99% the elutant from the TGA was a species with an m/z of 58. In light of this evidence, the MS response specific to the m/z

equal to 58 for the PLM treated silica was plotted (Figure 5.4). Comparison of Figure 5.4 to the original PLM treated silica trace (Figure 5.2) reveals that the decomposition of the CTAB from the PLM treated silica is the first weight loss event. The peak tailing was most likely due to holdup at the interface between the TGA and the MS. Therefore, the decomposition of the PLM occured at approximately 378 °C. From Figure 5.2, the weight percentage of the PLM on the silica is calculated to be 8.57%.

Atomic force microscopy was employed to visually inspect the surface of the treated and untreated silica particles. Figures 5.5 and 5.7 depict the silica prior to and following, respectively, the admicellar polymerization. In Figure 5.5, the surface of the untreated silica is observed to be very regular and mostly smooth. Figure 5.6 illustrates a depth profile of the detailed view of the untreated surface and reveals no abrupt or significant height changes. However, the micrograph of the surface following treatment (Figure 5.7) shows the formation of patchwise PLM agglomerates on the substrate surface. The depth profile of the detailed view of the treated surface (Figure 5.8) reveals abrupt and significant height changes of approximately 3.66 nm that correspond to the PLM patch.

Having confirmed the presence of the PLM on the surface of the silica, an HPLC column was packed with the treated stationary phase, and its performance was evaluated in relation to commercially available C8 and C18 reverse phase packings. The bicratic solvent flushes of methanol and water that were performed following the

packing of the columns ensured that no residual species remained on the silica. This washing was particularly important in the case of the PLM column because residual non-PLM-assciated CTAB remaining adsorbed to the silica could contribute to mixed mode partitioning and skew the chromatographic results. The analyte for the comparison was sodium octanoate with and without 0.200 M sodium chloride. For the C8 and C18 columns, an isocratic system was employed with the mobile phase being distilled, deionized water. This mobile phase was chosen in an attempt to impart maximum retention time of the sodium octanoate on the columns while remaining at a neutral pH. Figure 5.9 illustrates chromatograms for 0.020 M sodium octanoate (2.0×10^{-6} moles injected) with no added salt analyzed on the C8, C18 and PLM columns with a 2.0 ml constant flowrate and employing an ECD. The small peaks at the beginning of the chromatograms were due to the salt counterions from the dissolution of the analyte. While the water mobile phase employed for the C8 and C18 columns very quickly eluted the analyte, it was necessary to switch the mobile phase to a methanol rich solution to elute the carboxylate from the PLM column in a reasonable amount of time. Without the change in mobile phases, the carboxylate did not elute from the PLM column even after 120 minutes. Therefore, a bicratic solvent scheme of water and methanol/water (80/20) was employed for the PLM column. In Figure 5.9, significant peak tailing is observed for the C18 column (Chromatogram A) while a sharp but nearly immediate peak is eluted from the C8 column

(Chromatogram B). The PLM column, however, delayed the elution of the octanoate until the methanol rich solvent is introduced into the column at 4.00 minutes after the start of the run.

From the elution (retention) times of the peaks, the partition ratio or capacity factor, k' [1], and the retention ratio, R, [25] can be calculated for each column with respect to the analyte in question. These results are presented in Table 5.I. The partition ratio is significant in column chromatography as it relates the time the analyte spends on or in the stationary phase to that spent in the mobile phase. k' is defined by the following equations:

$$k' = \frac{t_R - t_M}{t_M} = \frac{t'_R}{t_M} \qquad \{5.1\},$$

where t_M is the transit time of a non-retained solute, t_R is the retention time of the analyte, and t'_R is the adjusted retention time. Some authors [25] prefer the retention ratio, R, to k' due to its ease of use in chromatographic equations and its direct proportionality to peak migration velocity. The retention ratio is related to the partition ratio by the following equations:

$$k' = \frac{c^*_s V_s}{c^*_m V_m} = \frac{1-R}{R} \qquad \{5.2\},$$

where c^*_s and c^*_m are the concentrations of the solute in the stationary phase and in the mobile phase, respectively, and V_s and V_m are the respective volumes of the stationary and mobile phases within the column. The effective plate number, N_{eff} [1],

which is a measure of the number of times the solute partitions between the stationary and mobile phase, and the effective plate height, H, were also computed for the test columns. For the case of the C18 and C8 columns, the equation

$$N_{eff} = \frac{41.7(t'_R / W_{0.1})}{(a/b) + 1.25} \qquad \{5.3\},$$

derived by Foley and Dorsey [26] specifically for asymmetric peaks, was employed to calculate N_{eff}. In Equation {5.3}, $W_{0.1}$ is the time width of the peak at one tenth of the peak height, and a and b are the time distances from the peak center to the peak edge measured at one tenth of the peak height. N_{eff} is related to the H by the following equation:

$$H = \frac{L}{N_{eff}} \qquad \{5.4\},$$

where L is the length of the column. H is a necessary parameter when comparing columns of different lenghts. In the case in which an analyte resides solely in the stationary phase and cannot be eluted without changing the mobile phase, the partition ratio and effective plate number approach infinity and the retention ratio and effective plate height approach zero.

As is evident from Table 5.I, the sodium octanoate had a significantly greater affinity for the PLM treated column. Due to the fact that a bicratic solvent scheme was necessary to elute the octanoate from the PLM column, the k' and N_{eff} values approached infinity and R and H values approached zero with the aqueous mobile

phase. This strong interaction was due to the ester linkages in the backbone of the PLM with the carboxyl head group of the octanoate as well as the twelve carbon pendant groups providing a suitable environment for the seven carbon tail. This mechanism allowed the partitioning of the octanoate anion into the stationary phase. The highly hydrophobic C8 and C18 bound phases did not provide this combination of head/tail interactions and resulted in low k' and high H values. It is interesting to note that while the partition coefficient of the C18 column was greater than that of the C8 column, the effective plate height was also greater. This effect was due to the greater peak broadening of the C18 column.

While HPLC/ECD analysis of sodium ocatanoate dissolved in distilled deionized water is quite possible using the C18 and C8 columns, a different situation arises when the ionic concentration is high. Figures 5.10 and 5.11 illustrate the chromatograms for 0.020 M (2.0×10^{-6} moles injected) and 0.0020 M (2.0×10^{-7} moles injected) sodium octanoate, respectively, in a 0.200 M NaCl solution (2.0×10^{-5} moles injected) from the C18, C8, and PLM columns. The resolution, R_s, of the two peaks can be calculated from the equation

$$R_s = \left\{ \frac{t_{R,2} - t_{R,1}}{0.5(W_2 + W_1)} \right\} \qquad \{5.5\},$$

where $t_{R,2}$ and $t_{R,1}$ are the retention times of the two peaks and W_2 and W_1 are the average time widths of the peaks [1]. A value of R_s equal to 1.0 represents a peak

area overlap of approximately 3.0% and is generally considered the lower limit of completely resolved peaks.

The calculated R_s values of the analyte peaks from the salt peak appear in Table 5.II. For the 0.020 M sodium octanoate concentrations, the C18 column achieved an R_s of 1.38 but again causes peak tailing, while the C8 packing nearly resolved the two peaks with an R_s of 1.23. The bicratic solvent scheme employed with the PLM column allowed complete retention of the octanoate with elution following the 4.00 minute run-time solvent switch. Complete resolution is achieved. However, for the cases in which the analyte concentration was reduced to 0.002 M, R_s values dropped significantly for the conventional packings. Figure 5.11 illustrates this result by showing the chromatogram traces. The R_s for the C18 column decreased to 0.75, while the analyte peak from the C8 column was completely obscured by the salt peak, and calculation a resolution value was not possible. On the other hand, by employing the PLM column, it was possible to retain the analyte until the detector returned to the baseline, and again complete resolution was achieved with the switch to the methanol-rich mobile phase at 26.50 minutes (Figure 5.11, Chromatogram C). The negative peak that followed the carboxylate peak is due to the lower conductivity of the methanol-rich solvent with respect to distilled, deionized water. The return to the original baseline occured when the mobile phase is returned to the distilled, deionized water. Therefore, the PLM column was capable of

achieving resolution of the analyte peak even in the presence of high concentrations of other electrolytes in solution.

Due to the polymeric nature of the PLM stationary phase, questions arise as to the solubility of the polymer film in the mobile phases. The PLM column was subjected to multiple cycles of solvent switching between the aforementioned mobile phases, and only after several hundred cycles was there a noticeable loss of column capacity. This performance degradation was presumably due to sparing solubility of the PLM in the methanol, but no such degradation was observed after extended water flushing. While this study did not concern itself with different polymerization initiation and reaction schemes and the resulting polymer molecular weights, further studies with respect to this variable most probably would allow the manufacture of packings with much greater column life.

In this investigation, the comparison of the PLM packing to traditional C8 and C18 reverse phase packings demonstrates that the technique of admicellar polymerization for the production of novel HPLC packings can be easily customized to fill analytical voids existing in the capabilities of the traditional chromatographic packings. This success suggests that a wide variety of analyte-specific packings could be manufactured employing this technique. The criteria for selection of a potential stationary phase are simple. First, the monomeric organic compound must have a structure that would provide a suitable chemical environment for analyte

partitioning . Also, the organic compound must be polymerizable, preferably with terminally unsaturation. Finally, the resultant polymer must be sparingly soluble or insoluble and resistant to significant swelling in the proposed mobile phases so as to allow long column life and minimize sustained and swing pressures in the column. These simple considerations could allow for the generation of multiple analyte-specific packings.

5.4 CONCLUSIONS

The study demonstrated the applicability of admicellar polymerization to the production of novel HPLC packings. The technique involved the synthesis of a patchwise polymer film on the surface of commercially available HPLC silica using admicellar polymerization techniques. In this example, a simple bicratic mobile phase scheme with the specially prepared packing allowed resolution of the analyte from highly ionic solutions without complex solution schemes, derivitization, or expensive polymeric packings. Also, a standard electrical conductivity detector, capable of detection of the compounds into the micromolar concentration region, was employed for the analysis. The method is easily extendible to other systems to allow the production of analyte-specific HPLC packings.

5.5 REFERENCES

1. *H. H. Hobart, L. L. Merritt, Jr., J. A Dean, and F. A Settle, Jr.*, Instrumental Methods of Analysis-Seventh Edition, Wadsworth, Belmont, California, 1988.
2. *S. Lam and E. Grushka*, J. Chromatogr., **15**, 234 (1977).
3. *E. Grushka, H. D. Durst, and E. J. Kikta, Jr.*, J. Chromatogr., **112**, 673 (1975).
4. *W. Distler*, J. Chromatogr., **192**, 240 (1980).
5. *K. Korte, K. R. Chien, and M. L. Casey, J.* Chromatogr., **469**, 261 (1989).
6. *E. Juengling and H. Kammermeier*, Anal. Biochem., **171**, 309 (1988).
7. *M. A. Quilliam and J. M. Yaraskavitch*, J. Liq. Chromatogr., **8**, 449 (1985).
8. *Karl Blau and Graham S. King*, eds., Handbook of Derivatives for Chromatography, Heyden & Sons, Ltd., London, 1978.
9. *D. L. Manning and M. P. Maskarinec*, J. Liq. Chromatogr., **4**, 705 (1983).
10. *H. G. Dean, J. C. Bosner, and J. P. Gent*, Clin. Chem., **35**, 1945 (1989).
11. *R. J. Boscott*, Nautre (London), **139**, 342 (1947).
12. *J. Boldingh*, Experientia, **4**, 270 (1948).
13. *H. N. M. Stewart and S.G. Perry*, J. Chromatogr., **37**, 97 (1968).
14. *J. Wu, J. H. Harwell, and E. A. O'Rear*, Langmuir, **3**, 531 (1987).
15. *J. H. Harwell and E. A. O'Rear*, U. S. Patent No. 4,770,906 (1988).
16. *J. Wu, J. H. Harwell, E. A. O'Rear, and S. D. Christian*, AIChE J., **34**, 1511 (1988),.

17. *J. Wu, J. H. Harwell, and E. A. O'Rear*, J. Phys. Chem., **91**, 623 (1987).

18. *J. H. Harwell*, Ph.D. Dissertation, The University of Texas at Austin, 1983.

19. *J. H. O'Haver, J. H. Harwell, E. A. O'Rear, W. H. Waddell, L. J. Snodgrass, and* 20. *J. R. Parker*, Mat. Res. Soc. Symp. Proc., **304**, 161 (1993).

21. *J. H. O'Haver, J. H. Harwell, E. A. O'Rear, L. J. Snodgrass, and W. H. Waddell*, Langmuir, **10**, 2587 (1994).

22. *W. H. Waddell, J. H. O'Haver, L. R. Evans, and J. H. Harwell*, J. Appl. Polymer Sci., **55**, 1627 (1995).

23. *H. Chen*, Masters' Thesis, The University of Oklahoma, 1992.

24. *C. Lai*, Masters' Thesis, The University of Oklahoma, 1992.

25. *R. K. Iler*, The Chemistry of Silica, John Wiley and Sons, New York, 1979.

26. *J. C. Giddings*, Unified Separation Science, John Wiley and Sons, New York, 1991.

27. *J. P. Foley and J. G. Dorsey*, Anal. Chem., **55**, 730 (1983).

Table 5.I. Column parameters for 2.0 X 10^{-6} moles sodium octanoate with 100% water mobile phase. Detector: ECD.

Column	k'	R	N_{eff}	H (mm)
C18	6.075	0.141	19.41	5.31
C8	2.975	0.252	28.52	3.61
PLM	$\rightarrow \infty$	$\rightarrow 0$	$\rightarrow \infty$	$\rightarrow 0$

Table 5.II. Column resolutions for 2.0 X 10^{-6} and 2.0 X 10^{-7} moles sodium octanoate from 2 X 10^{-5} moles NaCl with 100% water mobile phase. Detector: ECD.

	R_s	
Column	2.0 X 10^{-6} moles $C_7H_{15}COONa$	2.0 X 10^{-7} moles $C_7H_{15}COONa$
C18	1.39	0.75
C8	1.23	$\rightarrow 0$
PLM	$\rightarrow \infty$	$\rightarrow \infty$

Figure 5.1. The four step admicellar polymerization process.

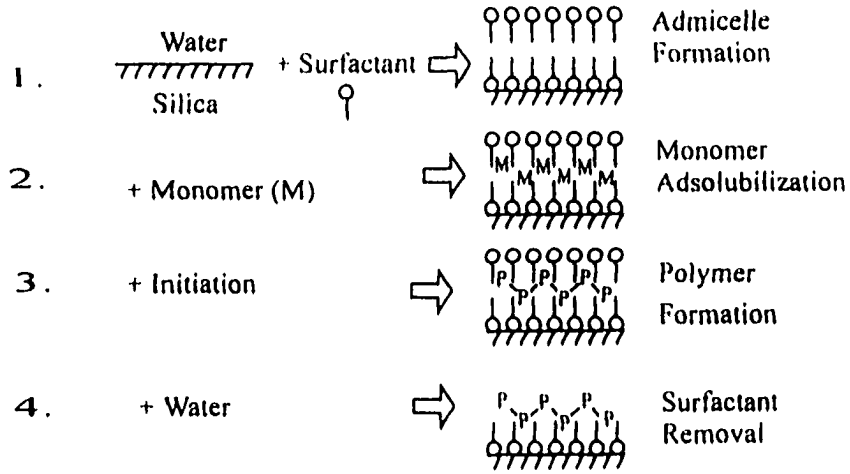

Figure 5.2 TGA and overall MS responses for the combustion of the PLM treated silica.

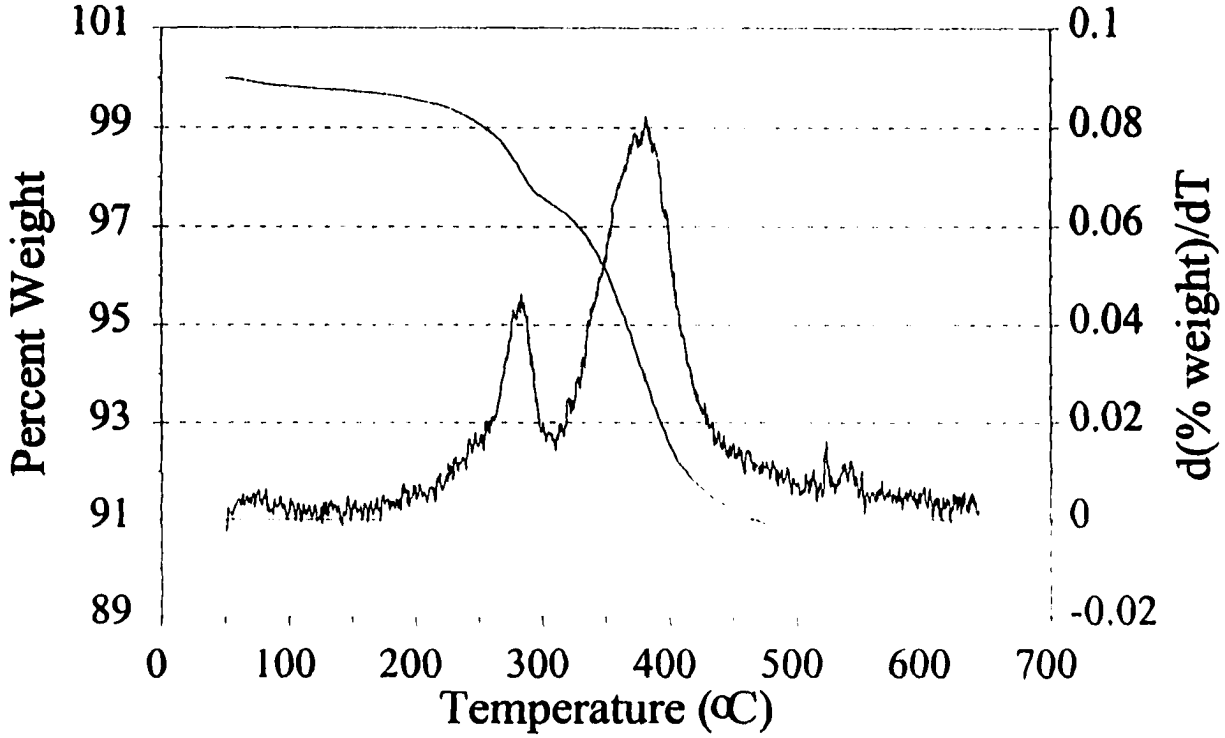

Figure 5.3. TGA/MS responses for the combustion of CTAB.

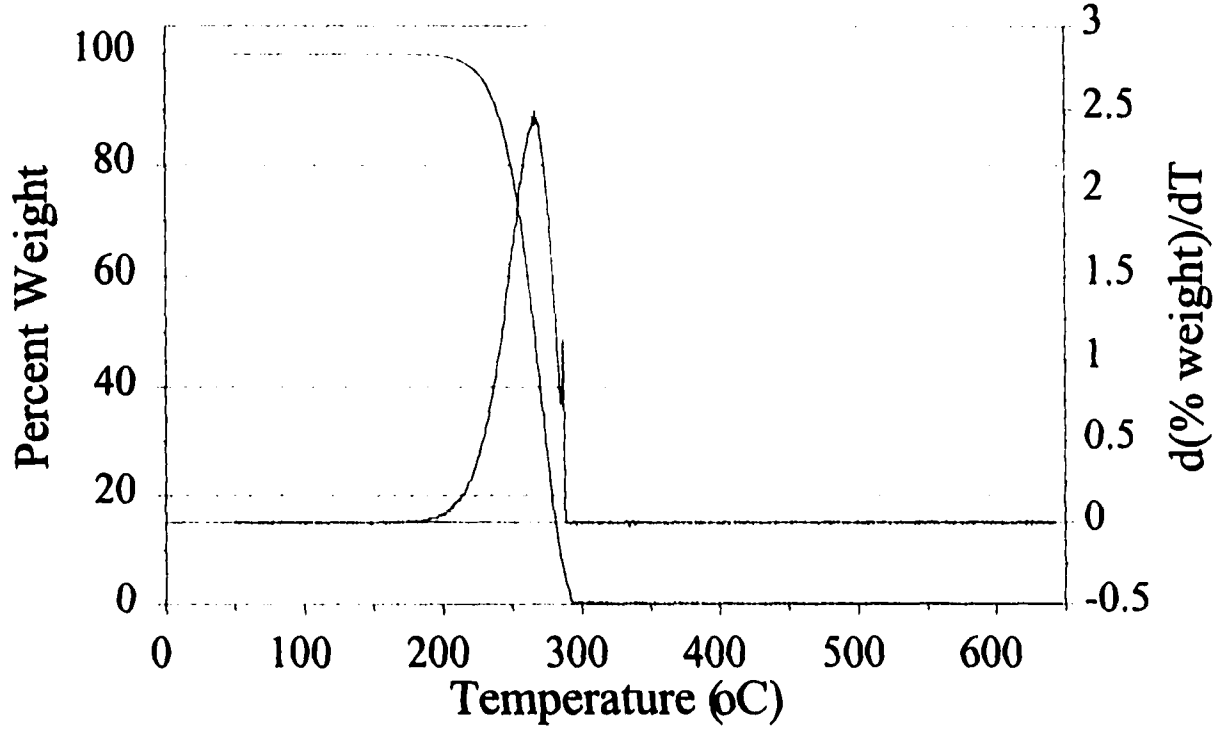

Figure 5.4. MS response at m/z = 58 for the combustion of the PLM treated

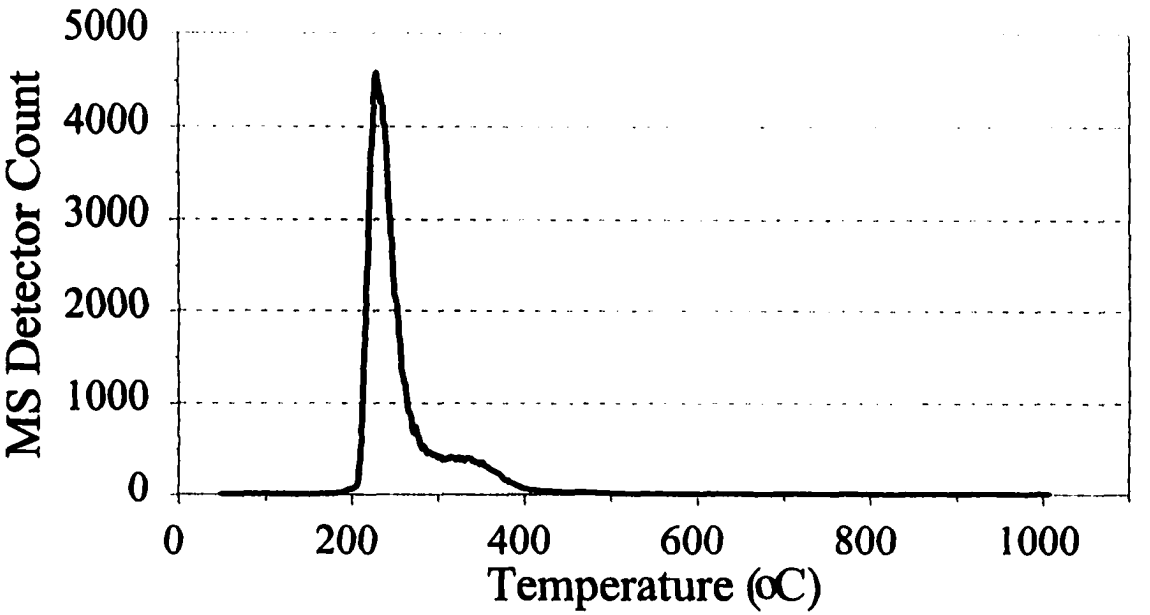

Figure 5.5. AFM of untreated silica particle surface

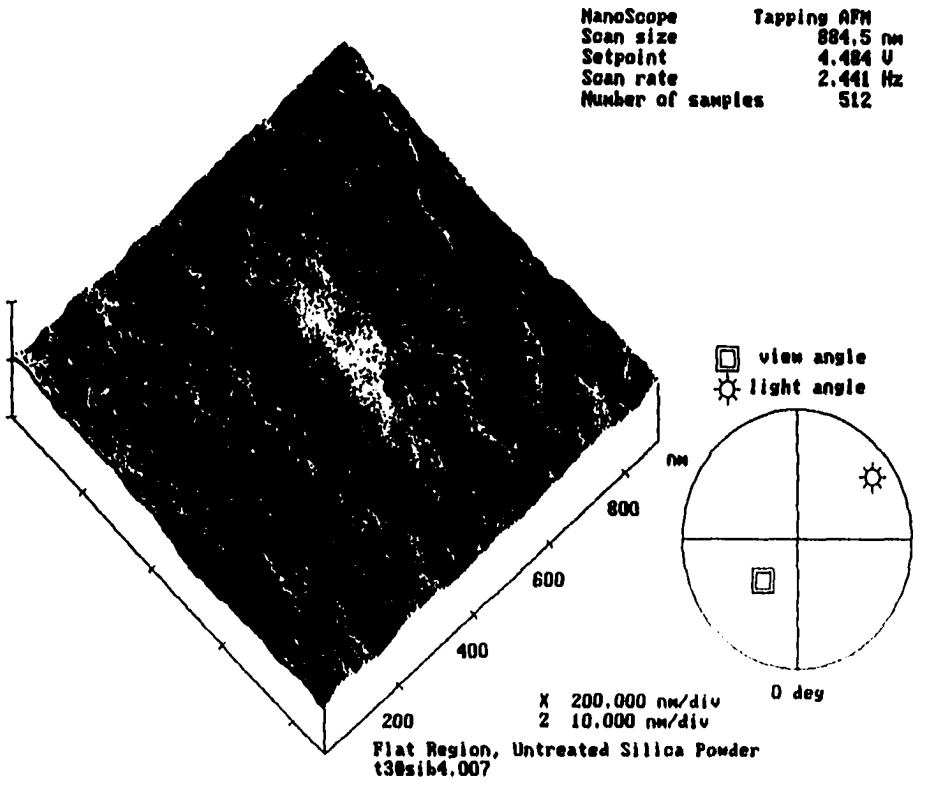

Figure 5.6. AFM depth profile of untreated silica particle surface

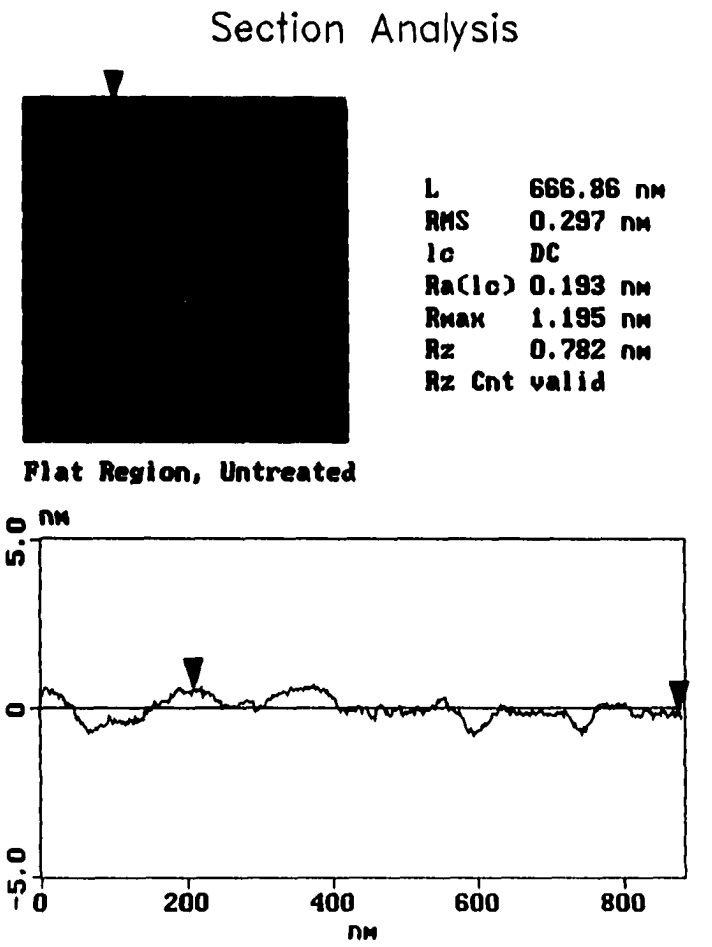

Figure 5.7. Detailed AFM of PLM-treated silica surface.

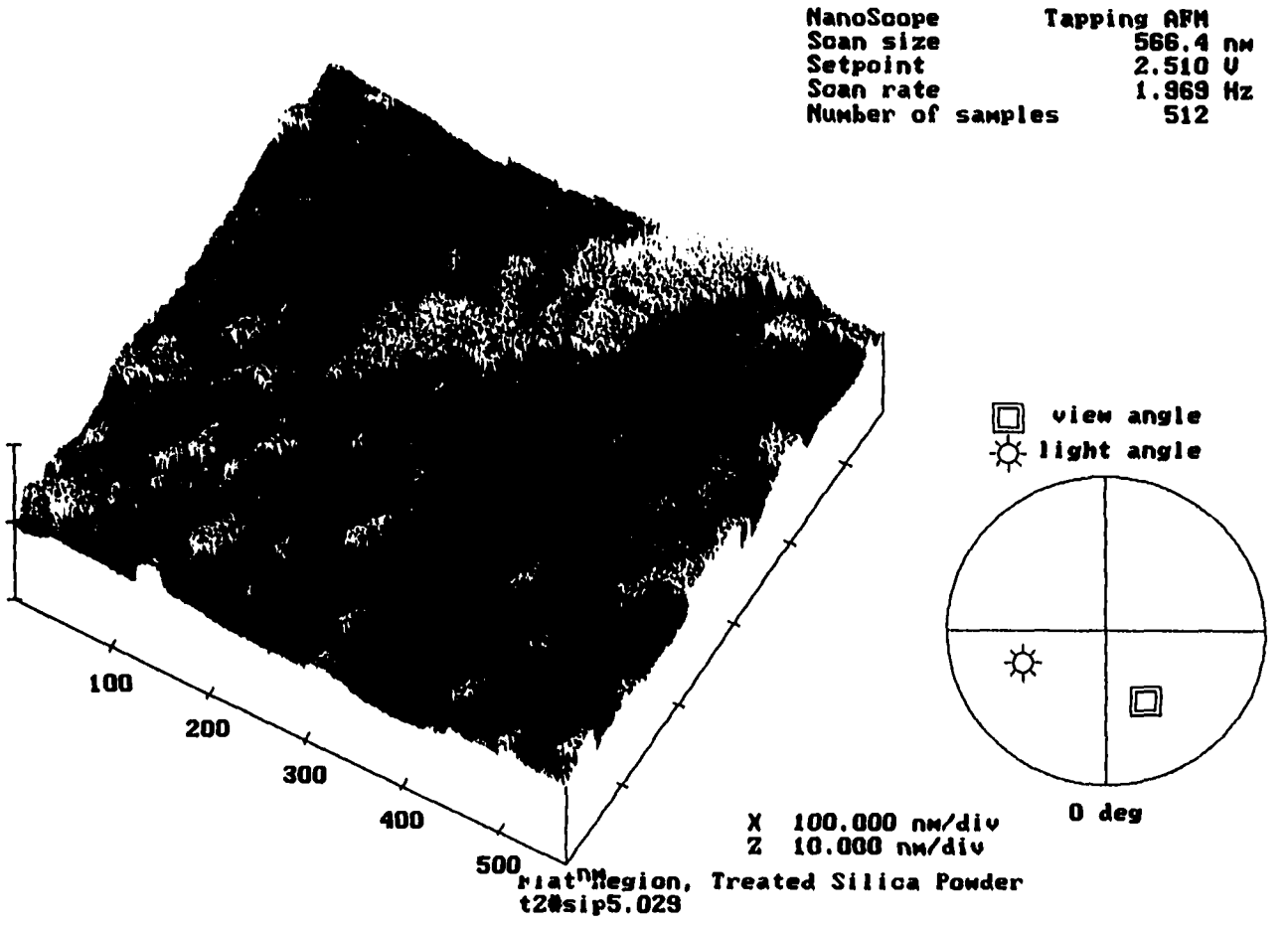

Figure 5.8. AFM Depth Profile of PLM-treated silica particle surface

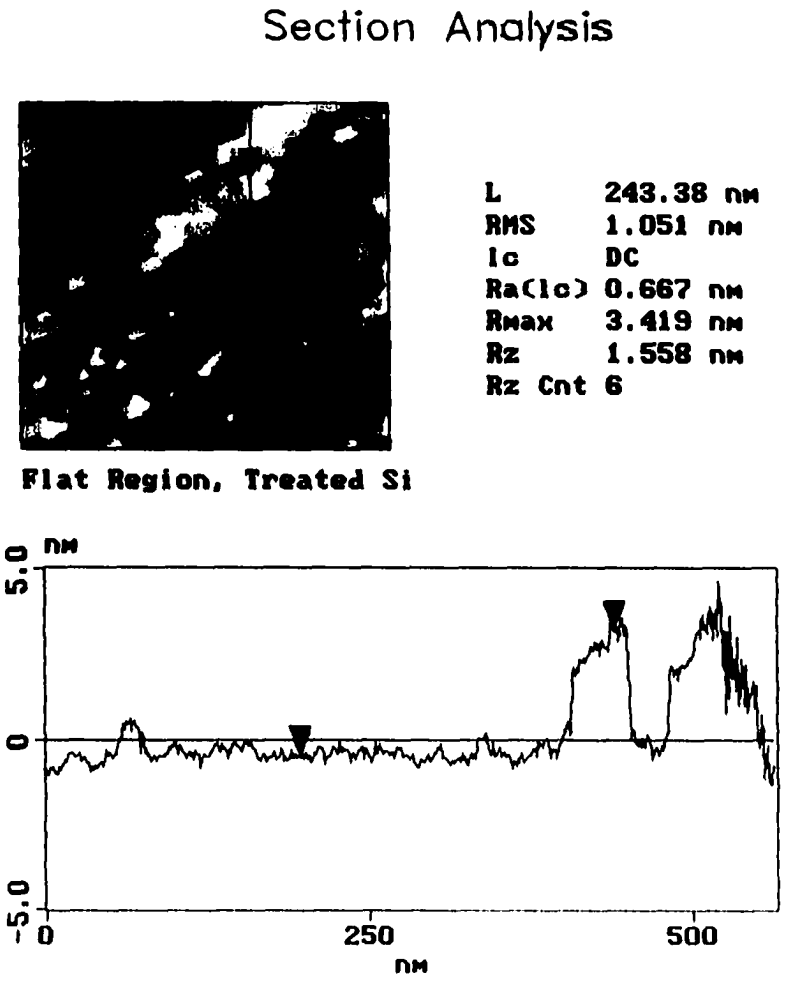

Figure 5.9. Chromatogram traces for 2.0×10^{-6} moles $C_7H_{15}COONa$. A) C18 column with water mobile phase. B) C8 column with water mobile phase. C) PLM column with mobile phase switching from water to methanol/water (80/20) at 4.00 minutes.

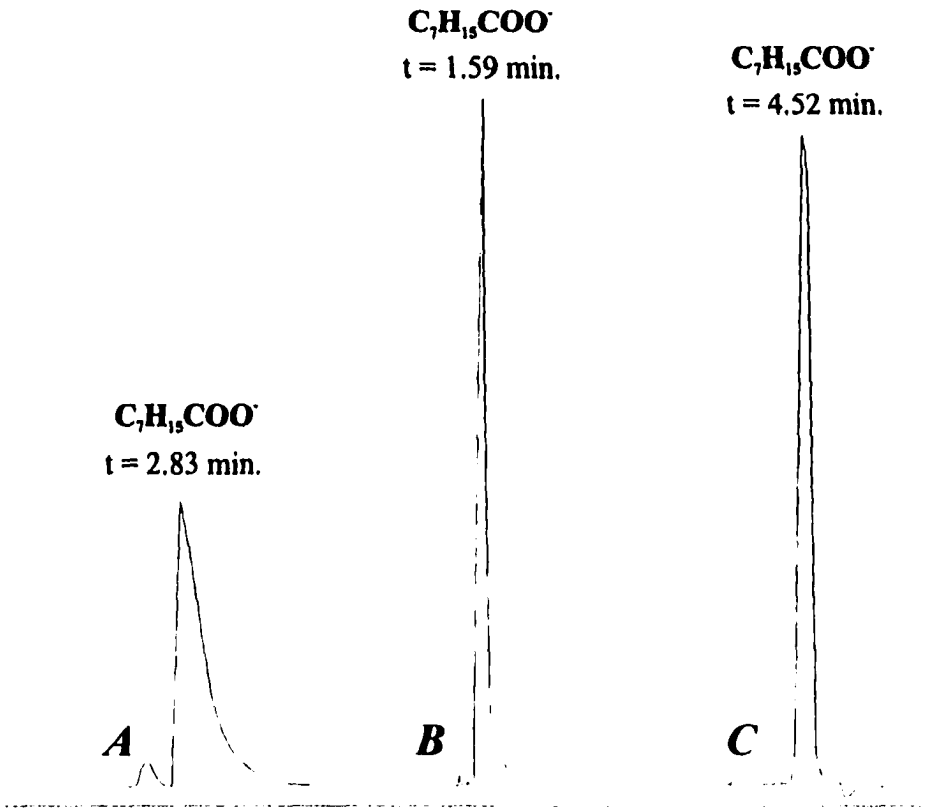

Figure 5.10. Chromatogram traces for 2.0×10^{-6} moles $C_7H_{15}COONa$ with 2.0×10^{-5} moles NaCl. A) C18 column with water mobile phase. B) C8 column with water mobile phase. C) PLM column with mobile phase switching from water to methanol/water (80/20) at 4.00 minutes.

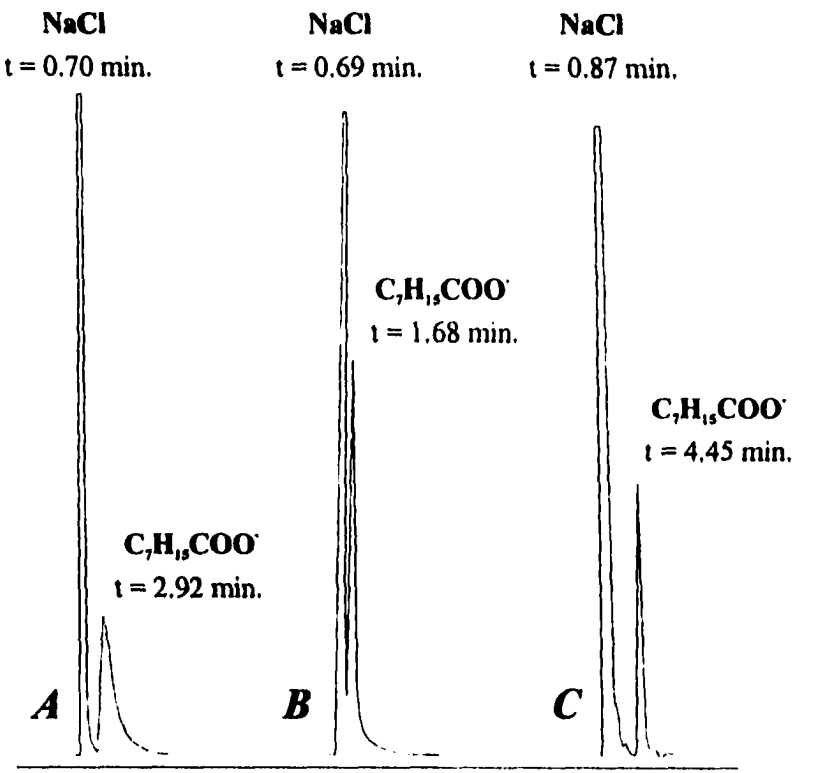

Figure 5.11. Chromatogram traces for 2.0×10^{-7} moles $C_7H_{15}COONa$ with 2.0×10^{-5} moles NaCl. A) C18 column with water mobile phase. B) C8 column with water mobile phase. C) PLM column with mobile phase switching from water to methanol/water (80/20) at 26.50 minutes.

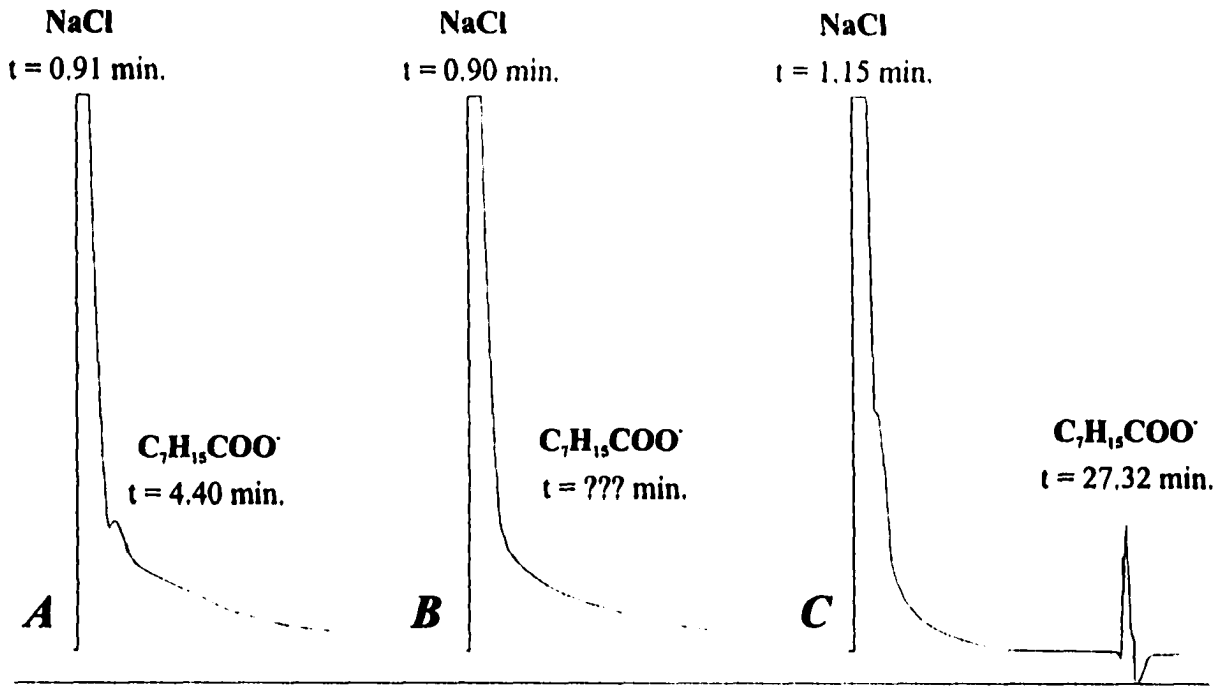

APPENDIX A

Data from pH=11 experiments

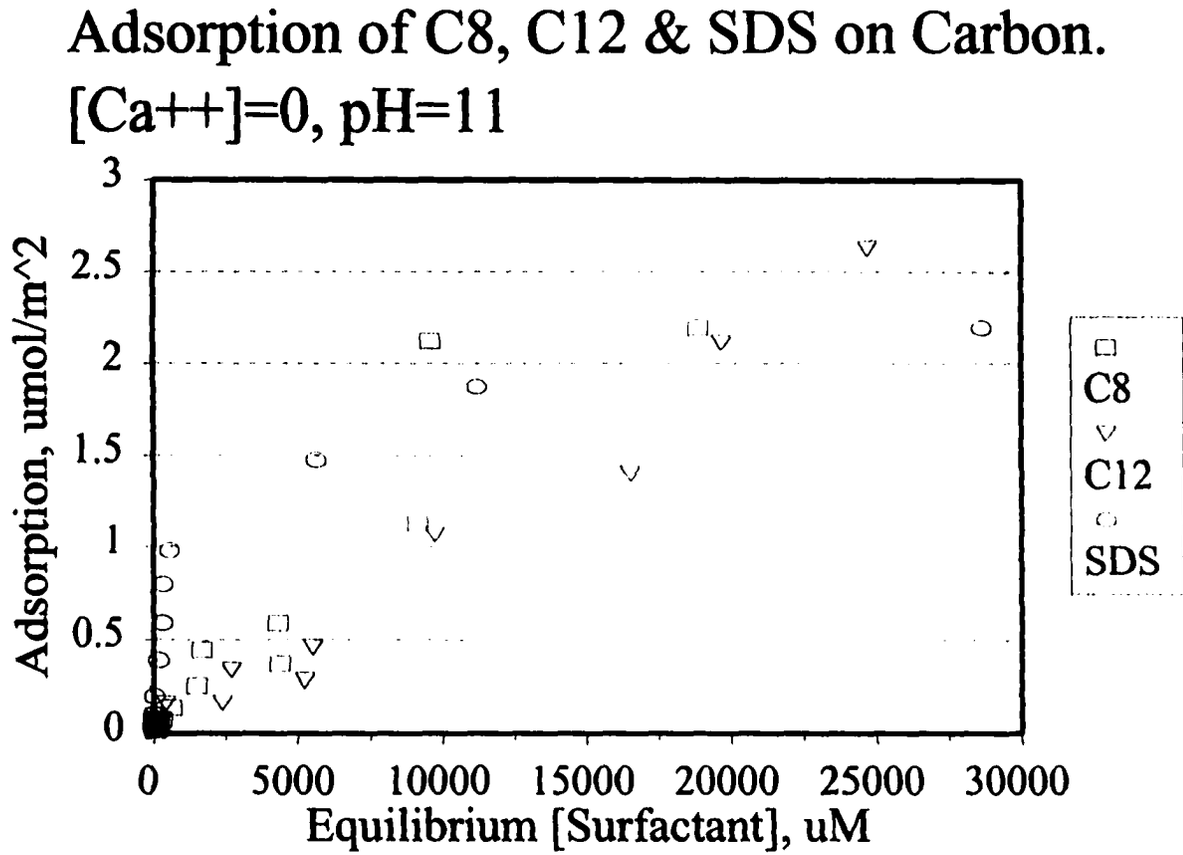
Adsorption of C8, C12 & SDS on Carbon.
[Ca++]=0, pH=11
Adsorption, umol/m^2
3
2.5
2
1.5
1
0.5
0
0
5000
10000
15000
20000
25000
30000
Equilibrium [Surfactant], uM
C8
C12
SDS

Adsorption on Carbon; pH=11.

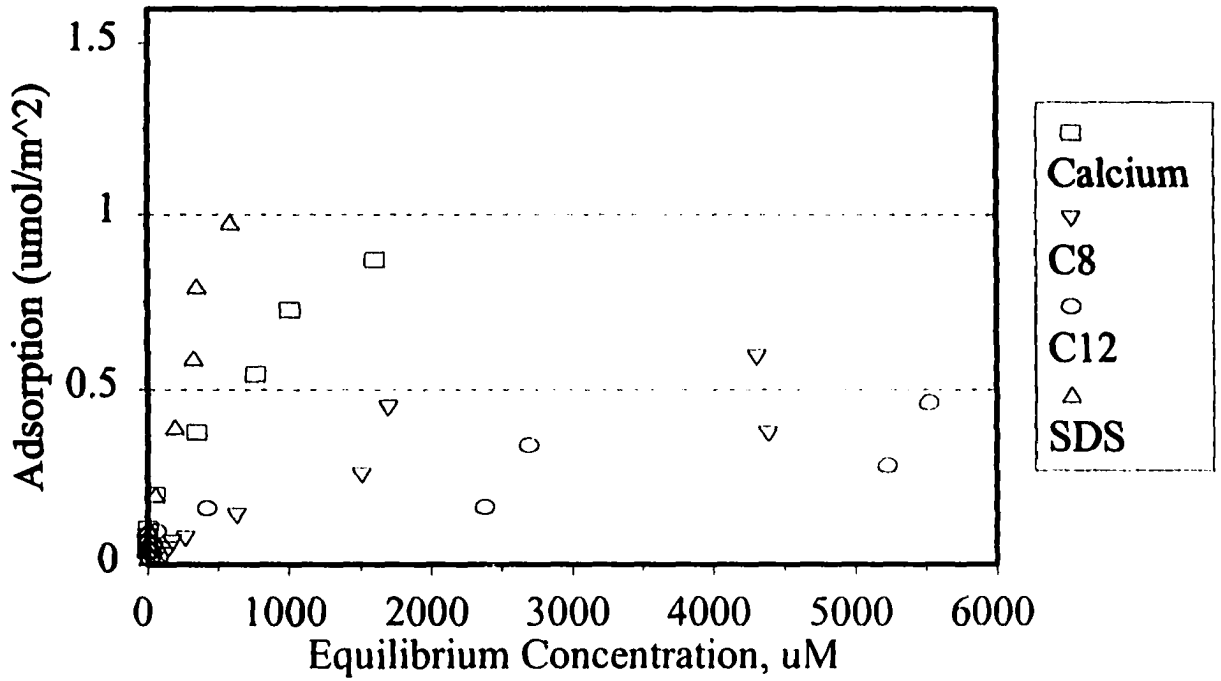

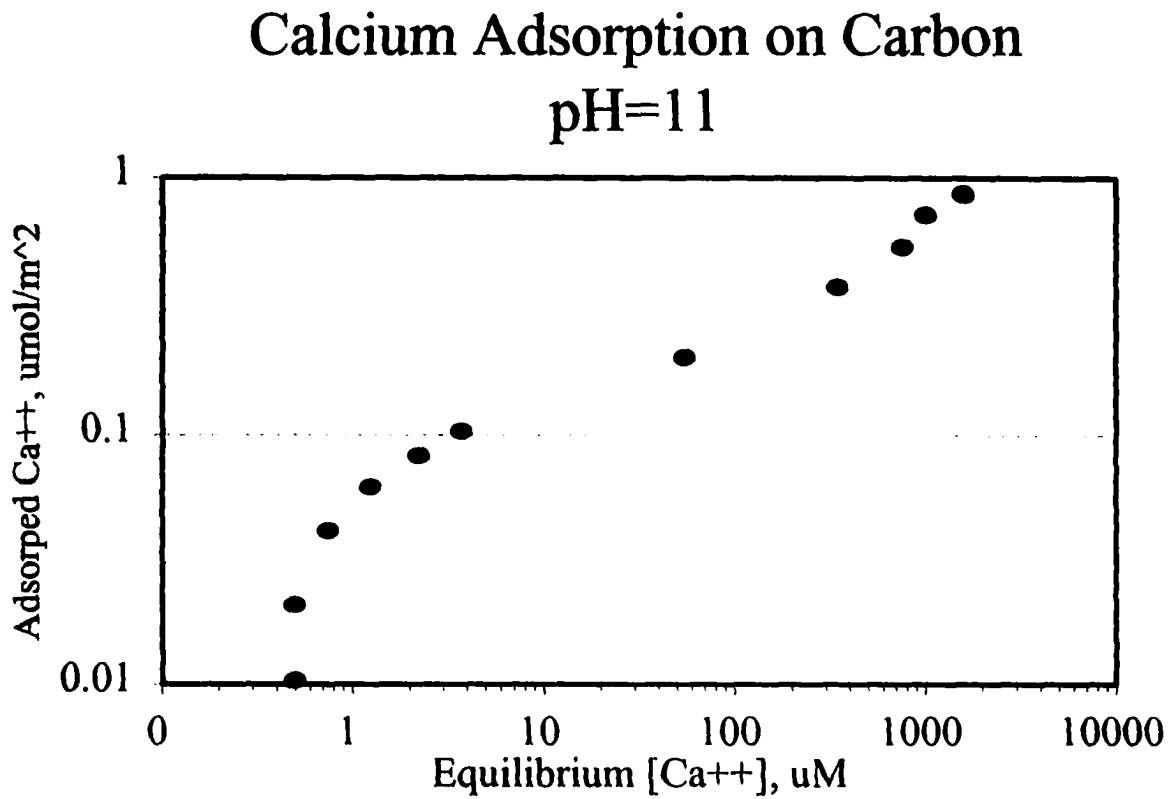
Calcium Adsorption on Carbon
pH=11
Adsorped Ca++, umol/m^2
1
0.1
0.01
0
1
10
100
1000
10000
Equilibrium [Ca++], uM

C8 Adsorption on Carbon

[Ca++]=Variable; pH=11

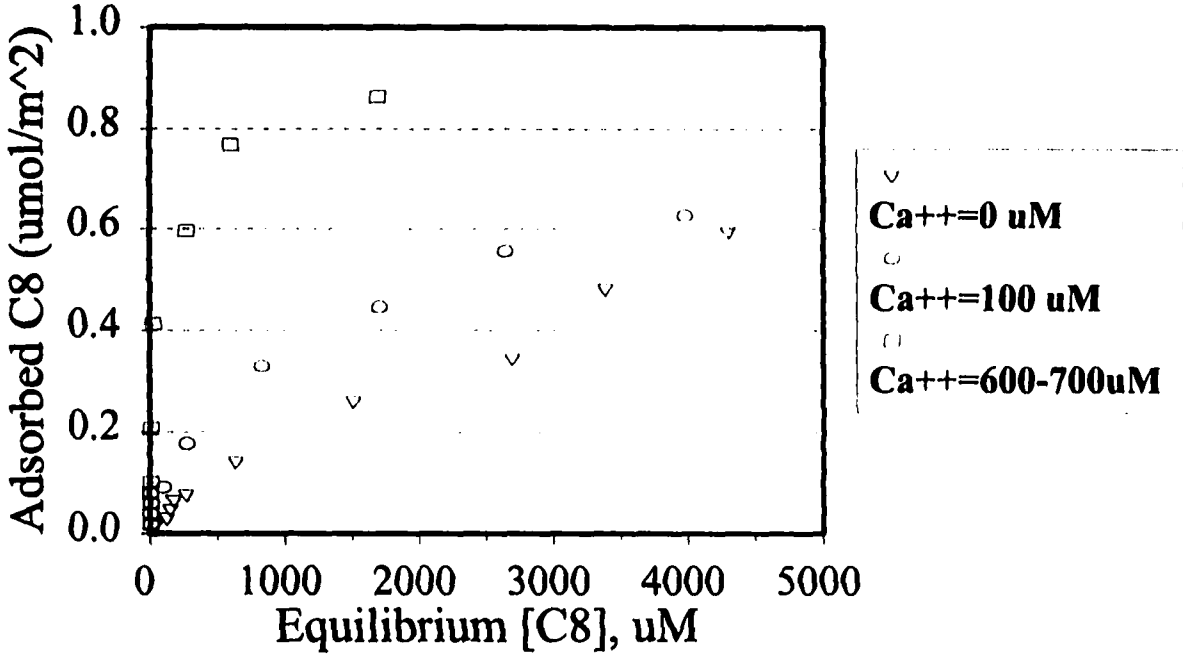

C12 Adsorption on Carbon
[Ca++]=Variable; pH=11

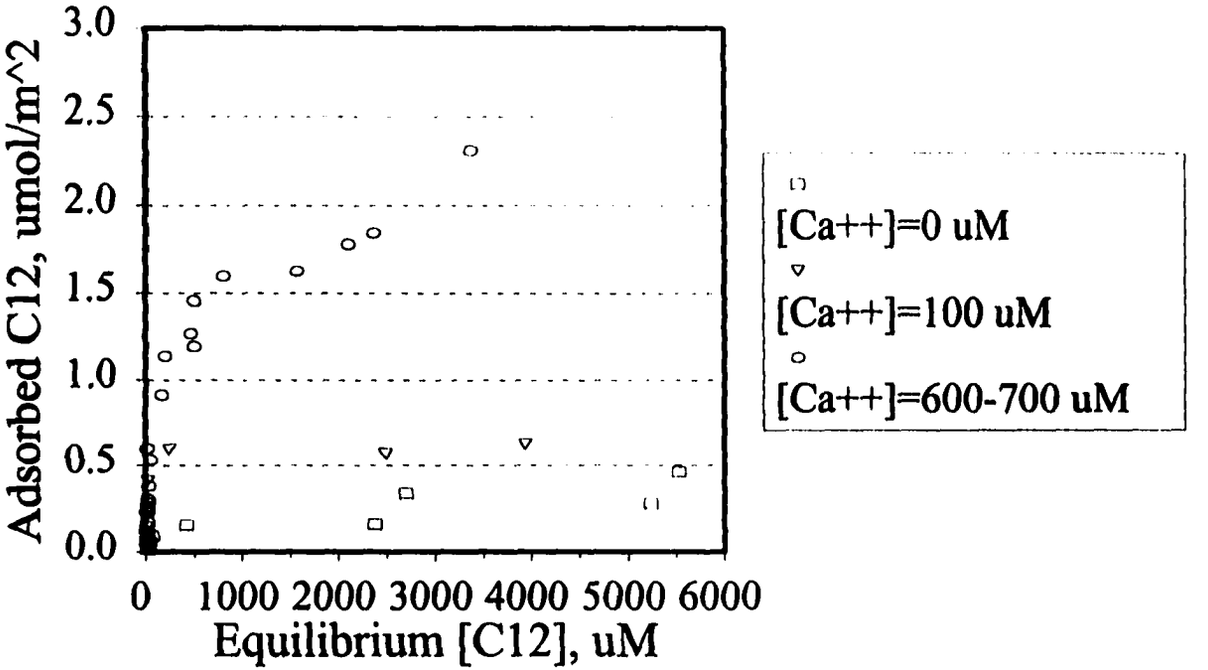

SDS Adsorption on Carbon
[Ca++]=variable; pH=11

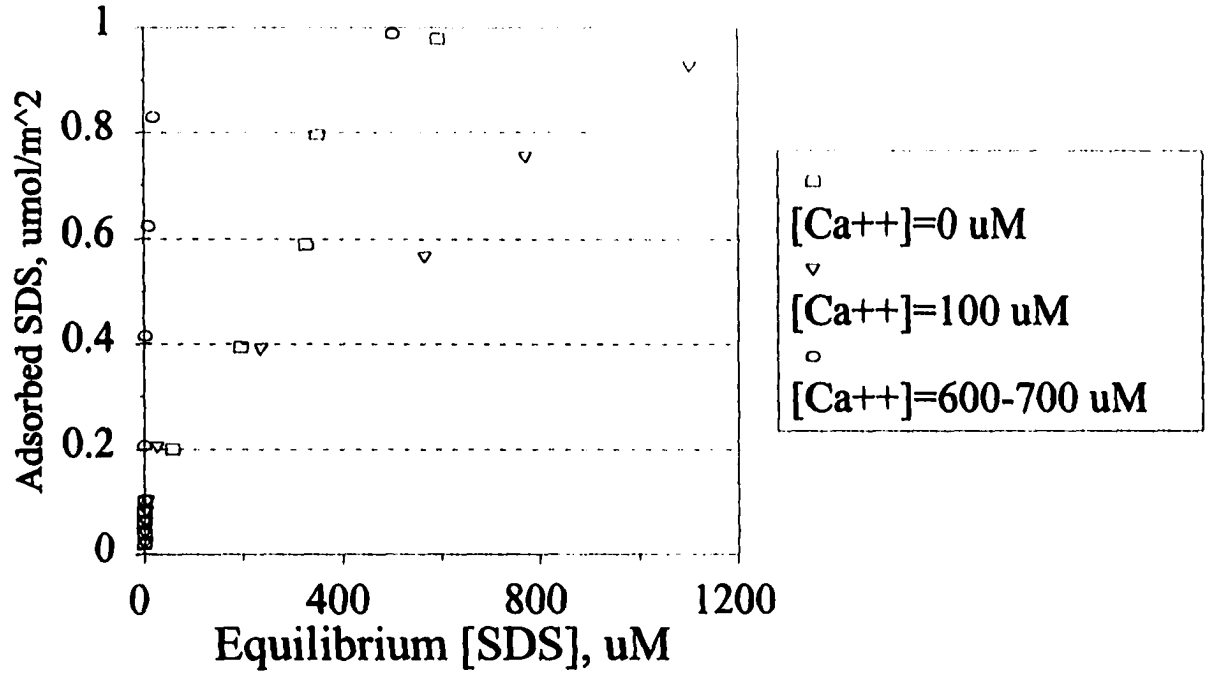

Calcium Adsorption on Carbon Black vs. Initial [C8]; pH=11

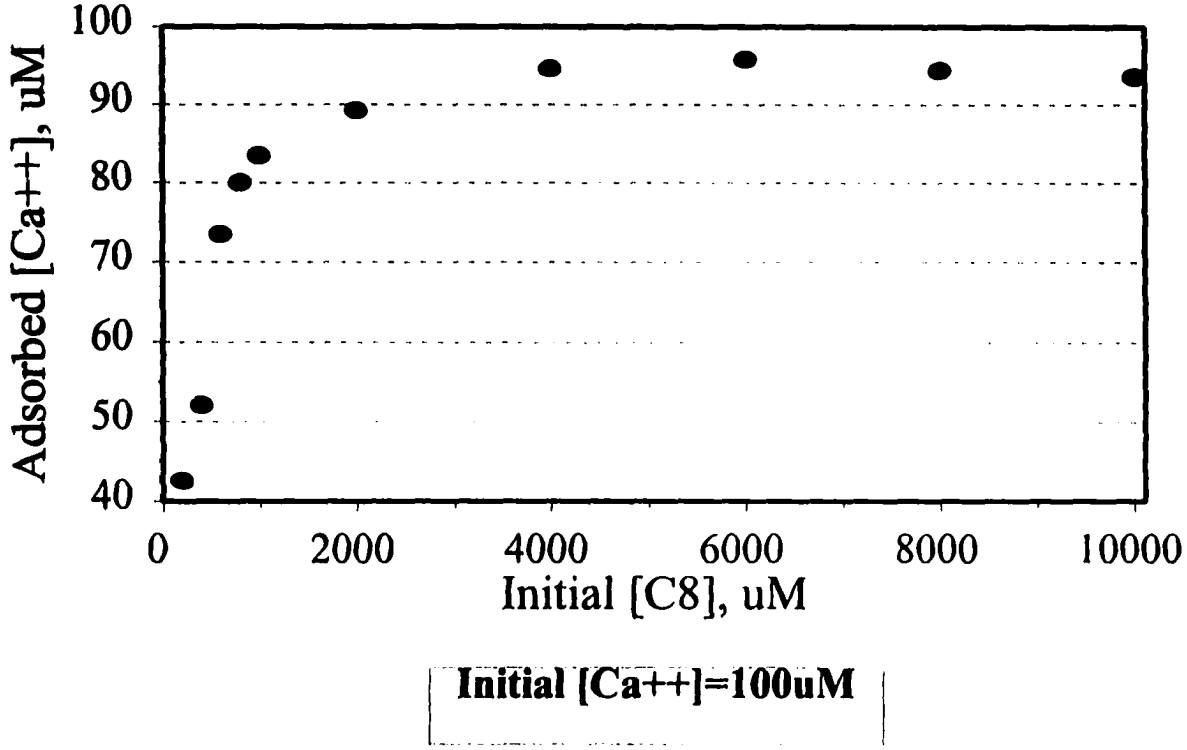

(-) Zeta Potential of Carbon Black vs. Surfanctant Concentration; pH=11

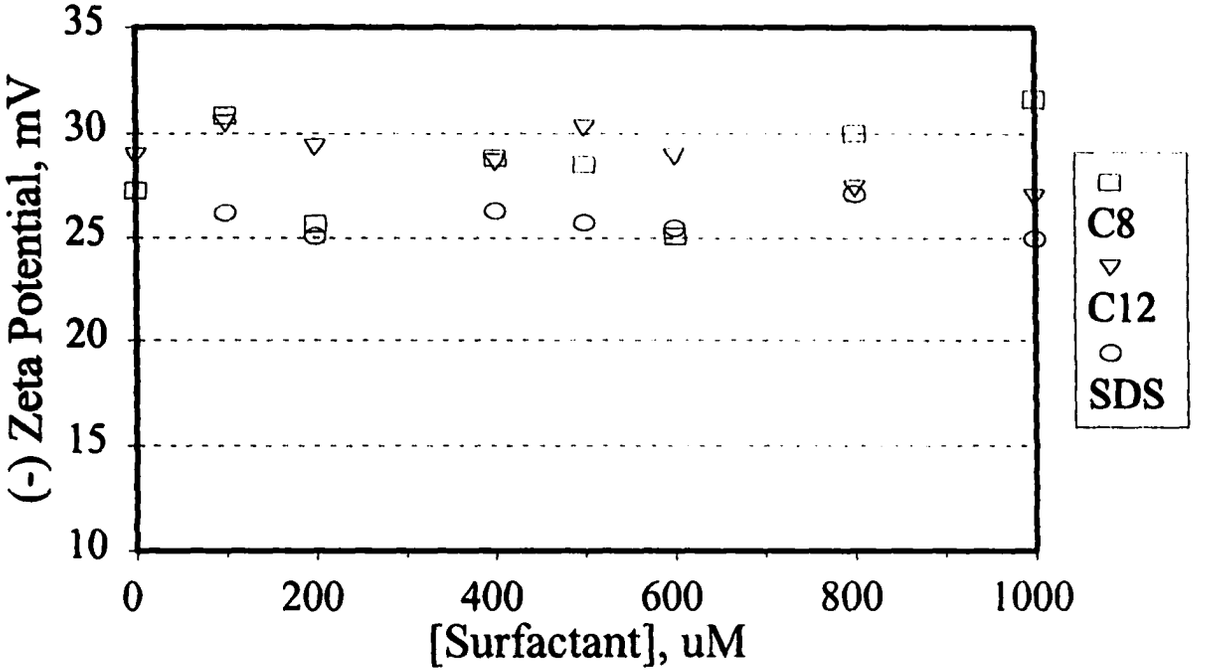

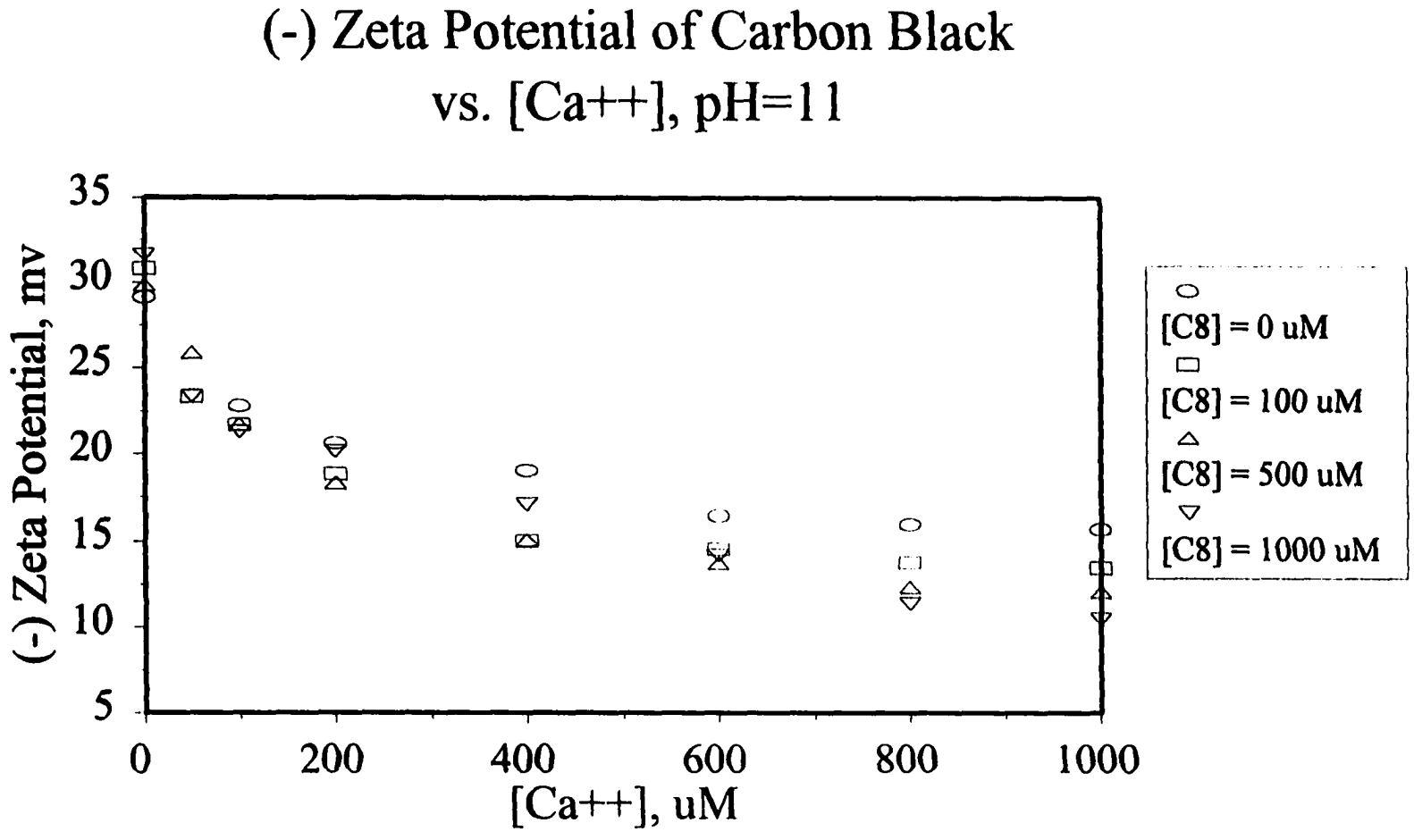
(-) Zeta Potential of Carbon Black
vs. [Ca++], pH=11
(-) Zeta Potential, mv
35
30
25
20
15
10
5
0
200
400
600
800
1000
[Ca++], uM
[C8] = 0 uM
[C8] = 100 uM
[C8] = 500 uM
[C8] = 1000 uM

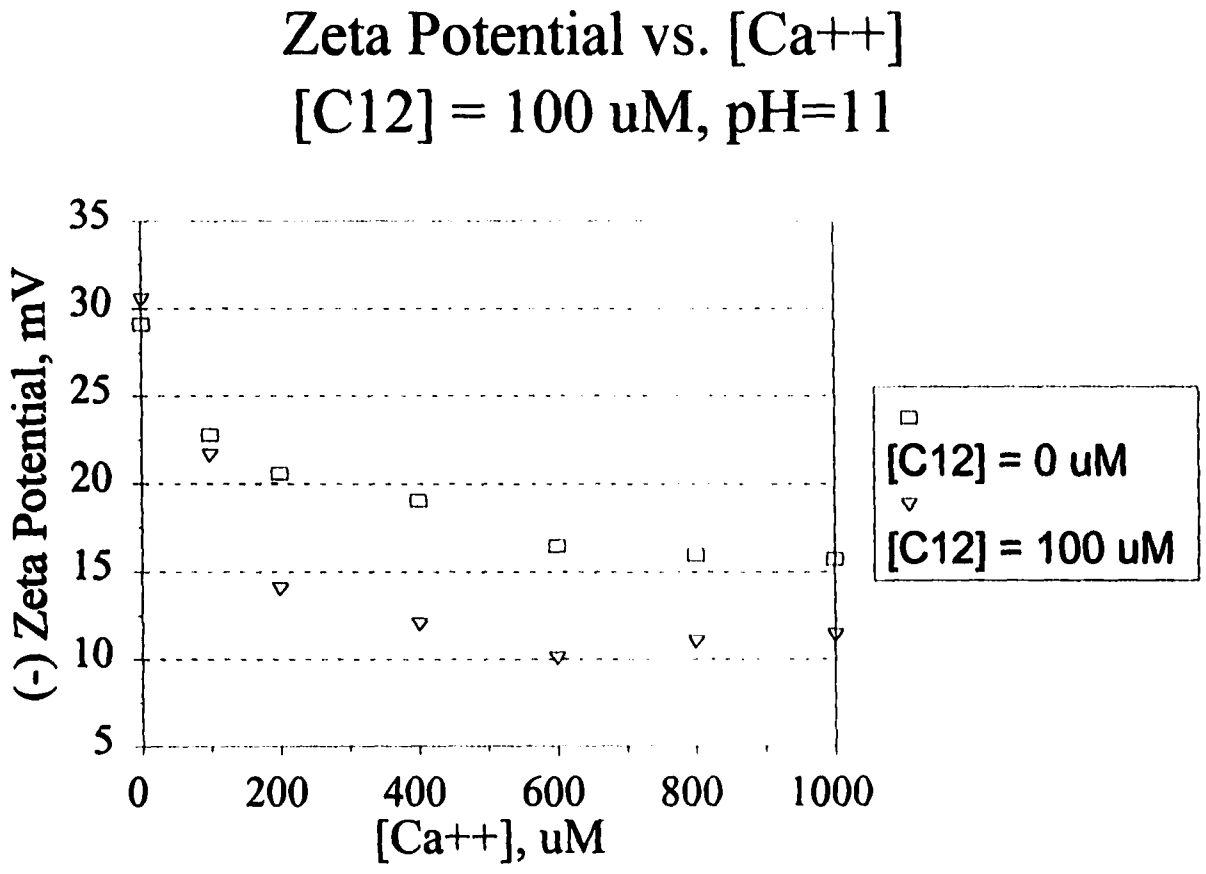
Zeta Potential vs. [Ca++]
[C12] = 100 uM, pH=11
(-) Zeta Potential, mV
35
30
25
20
15
10
5
0
200
400
600
800
1000
[Ca++], uM
[C12] = 0 uM
[C12] = 100 uM

Zeta Potential of Carbon vs. [Ca++]
[SDS]=Variable; pH=11

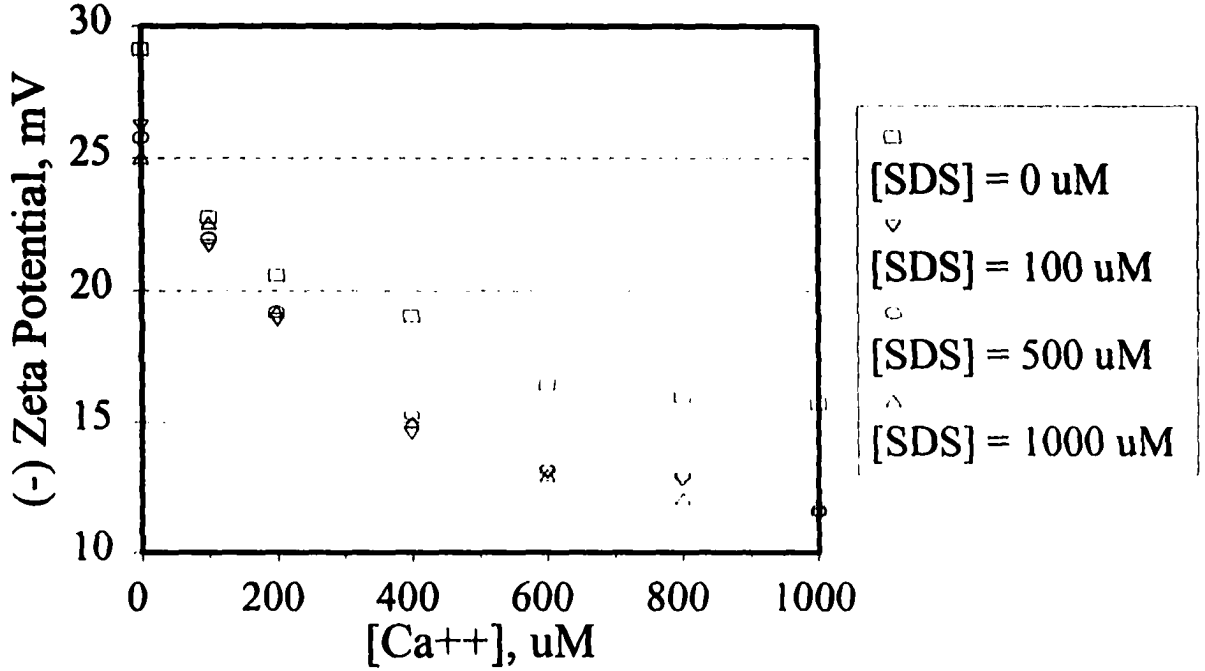

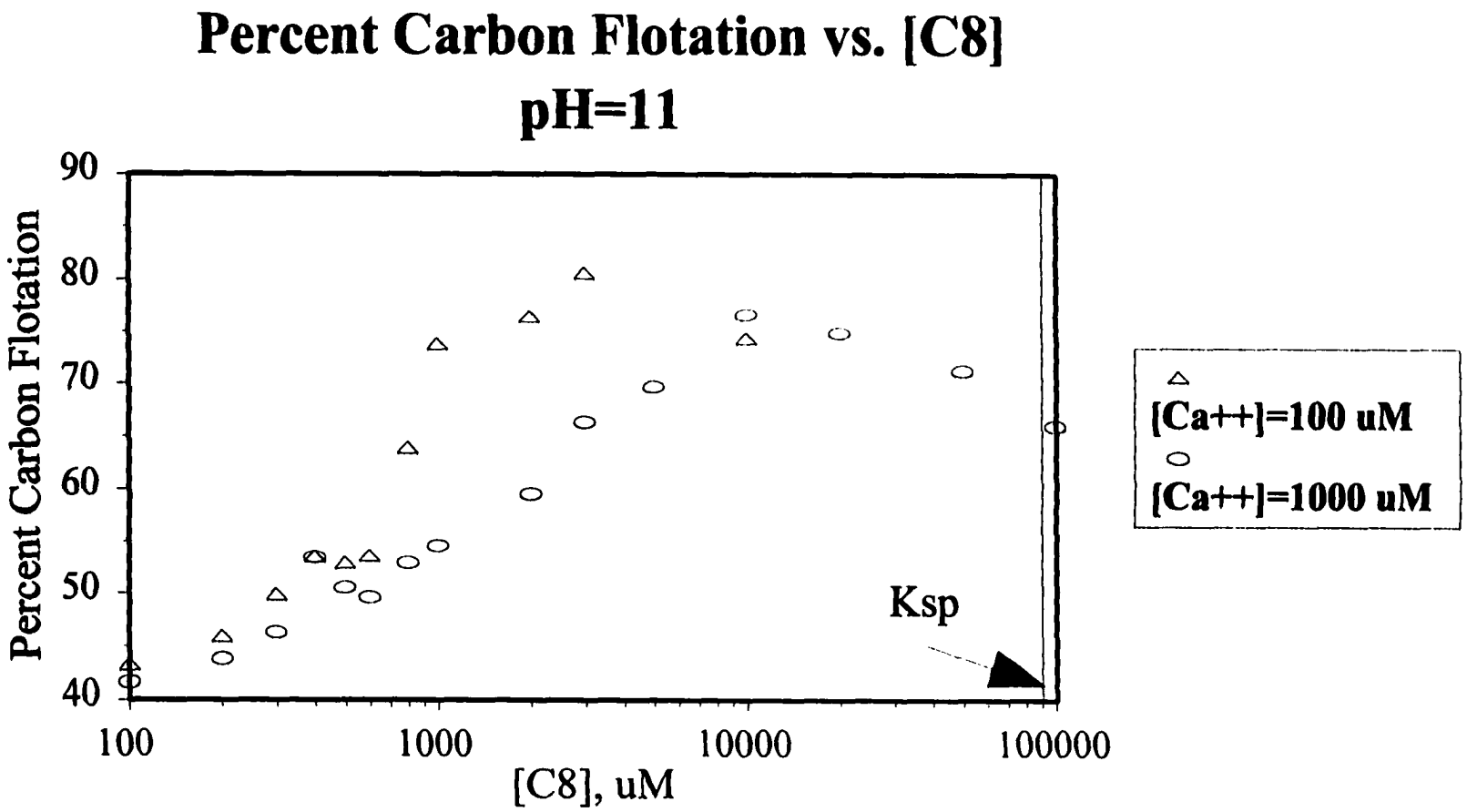
Percent Carbon Flotation vs. [C8]
pH=11
Percent Carbon Flotation
90
80
70
60
50
40
100
1000
10000
100000
[C8], uM
Ksp
[Ca++]=100 uM
[Ca++]=1000 uM

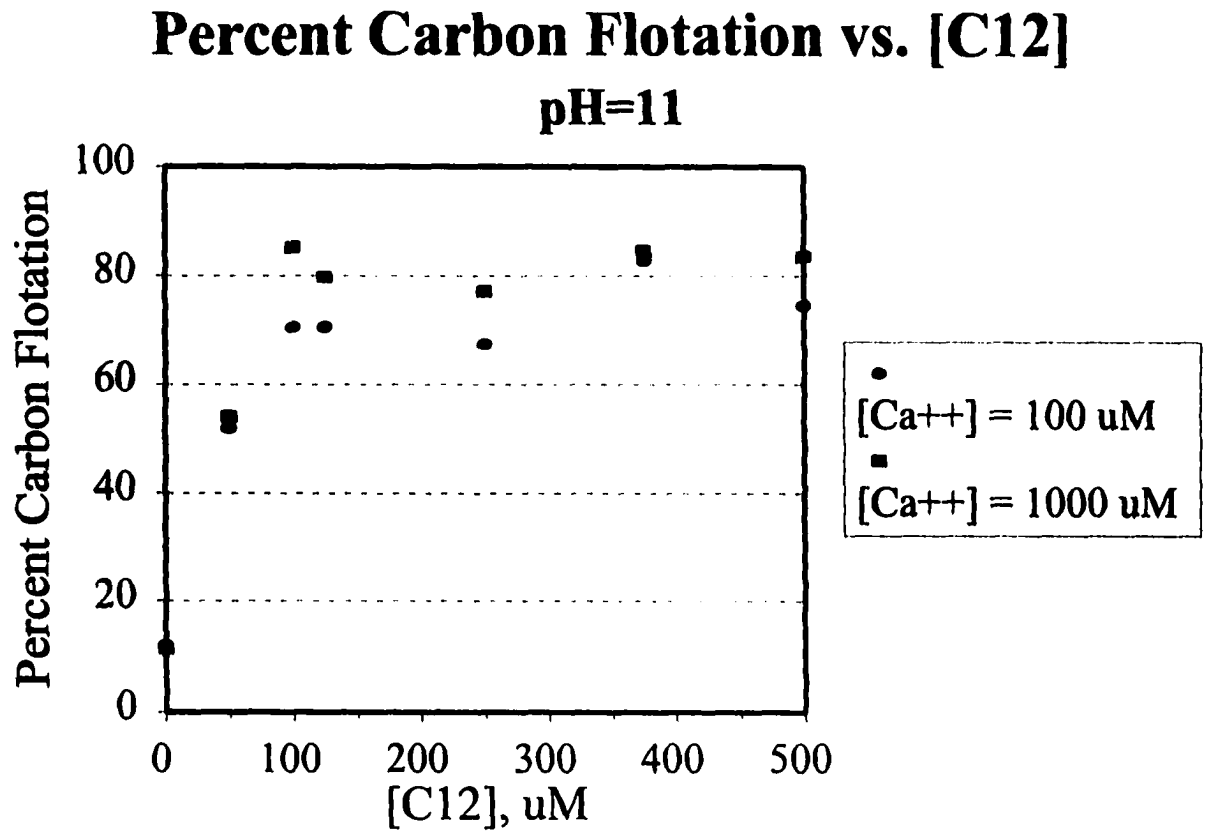
Percent Carbon Flotation vs. [C12]
pH=11
Percent Carbon Flotation
100
80
60
40
20
0
0
100
200
300
400
500
[C12], uM
[Ca++] = 100 uM
[Ca++] = 1000 uM

Percent Flotation of Carbon vs [SDS]; [Ca++]=Variable; pH=11

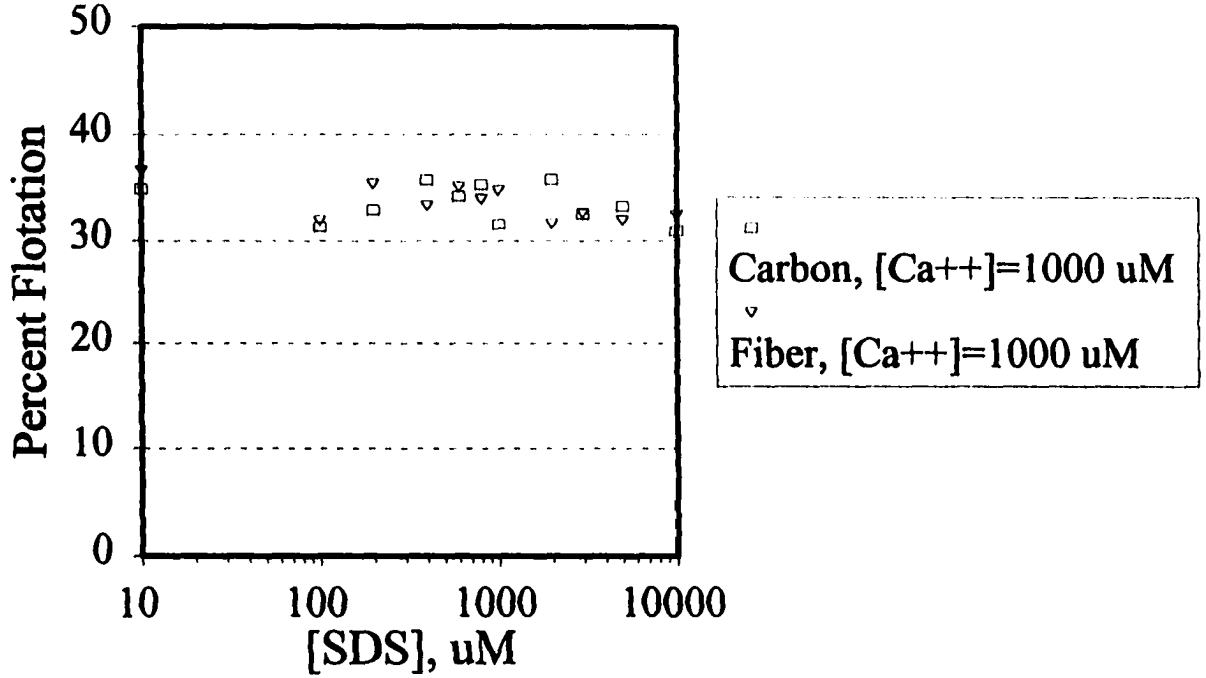

Ca++ Adsorption on Carbon and Fibers
pH=11

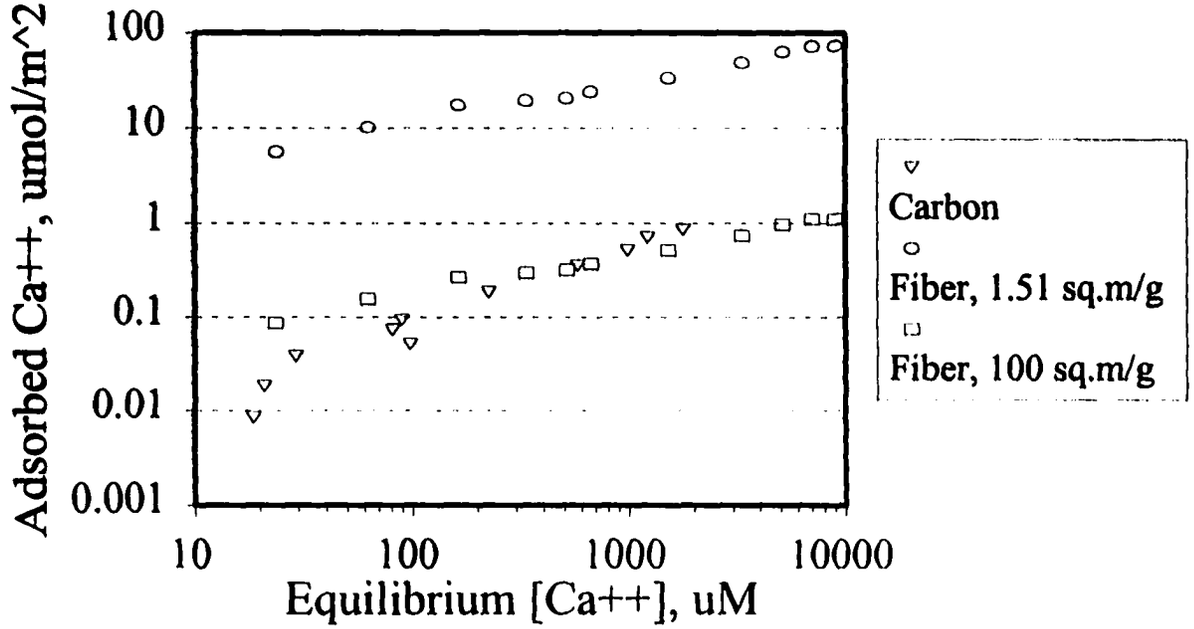

C8 Adsorption on Fiber
[Ca++]=Variable; pH=11

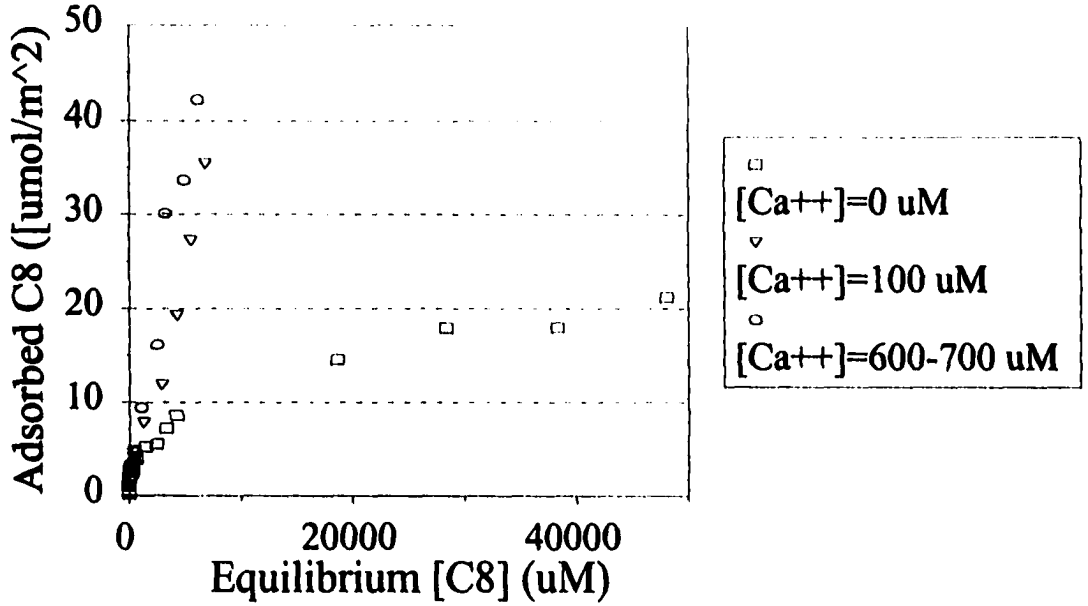

SDS Adsorption on Carbon and Fiber
[Ca++]=0 uM; pH=11

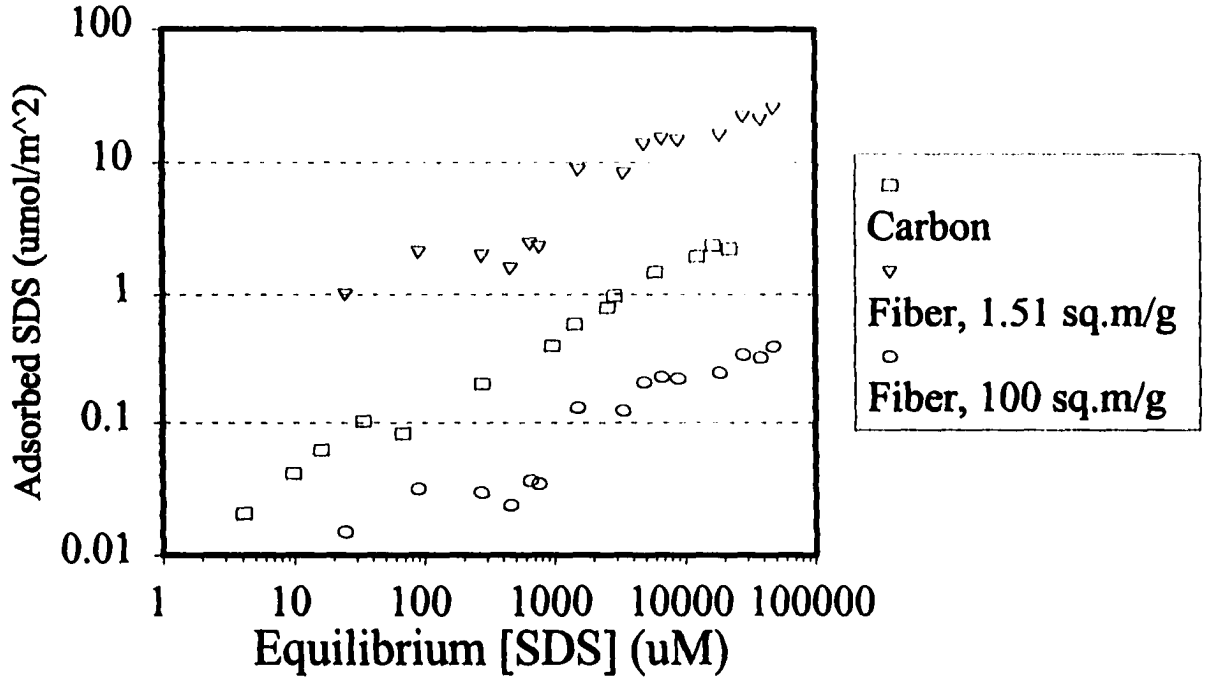

SDS Adsorption on Fiber
[Ca++]=Variable; pH=11

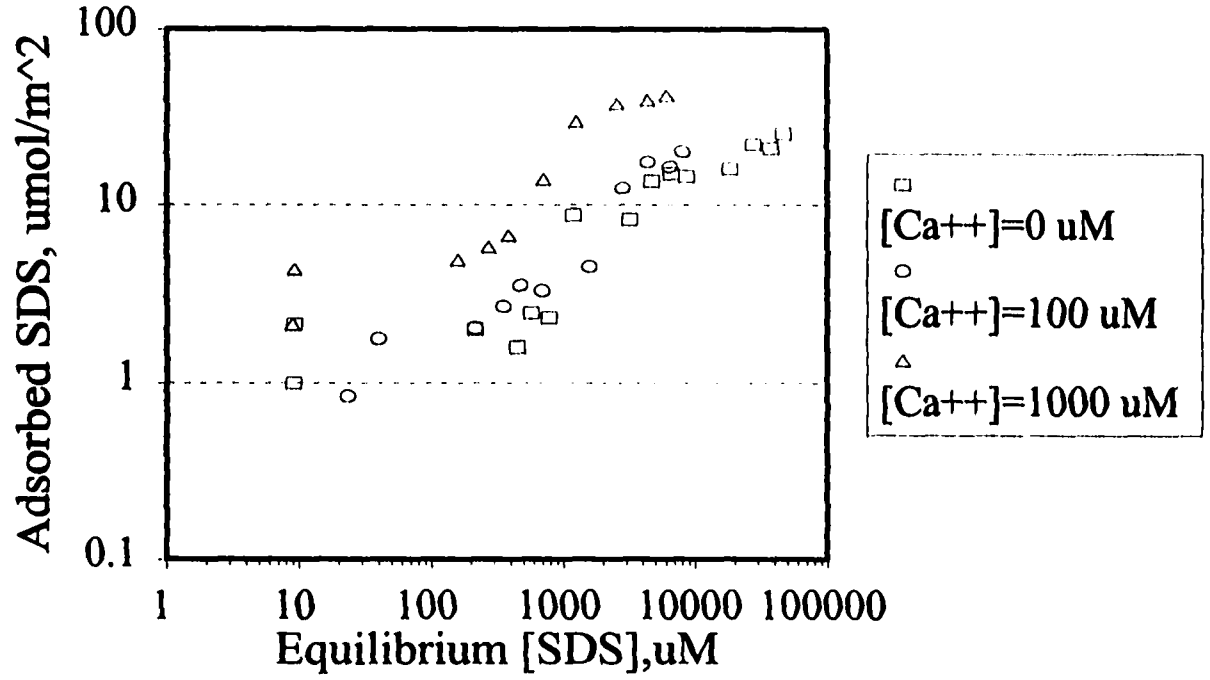

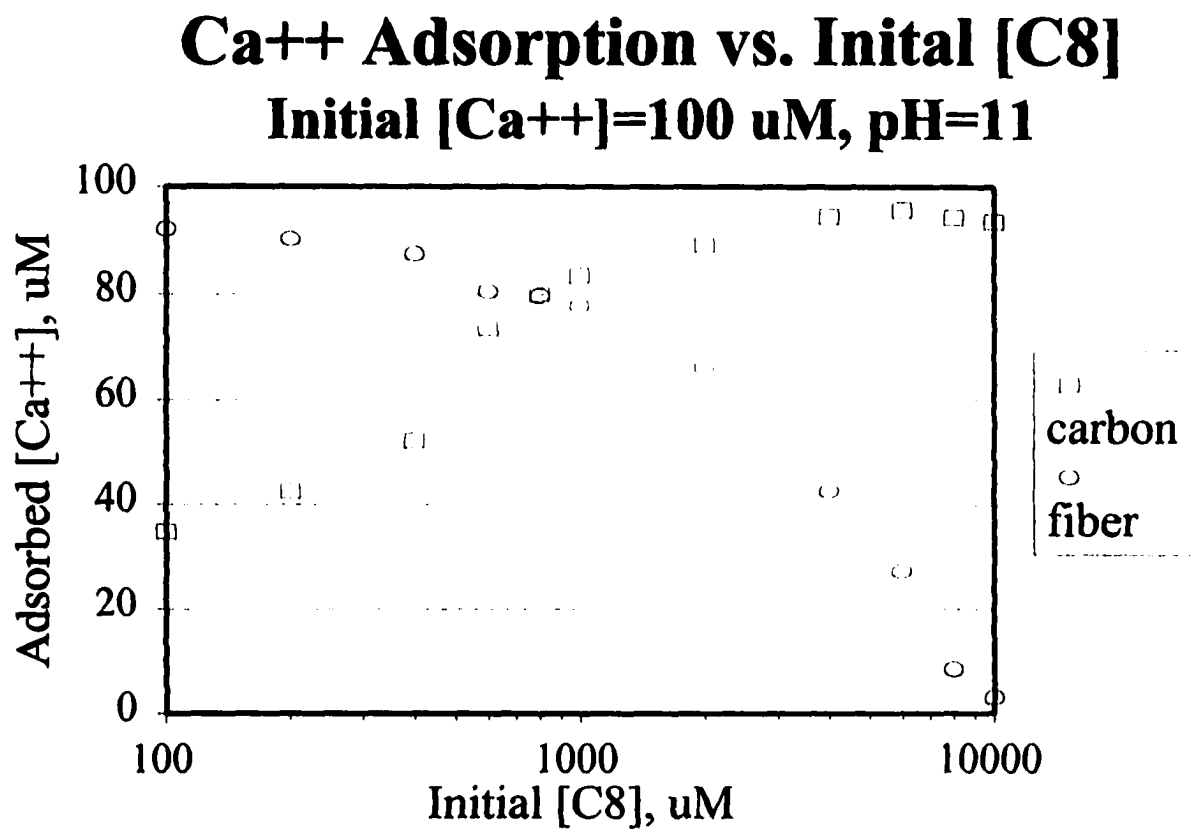
Ca++ Adsorption vs. Inital [C8]
Initial [Ca++]=100 uM, pH=11
Adsorbed [Ca++], uM
100
80
60
40
20
0
100
1000
10000
Initial [C8], uM
carbon
fiber

Ca++ Adsorption vs. Inital [C8]
pH=9, Initial [Ca++]=1000 uM

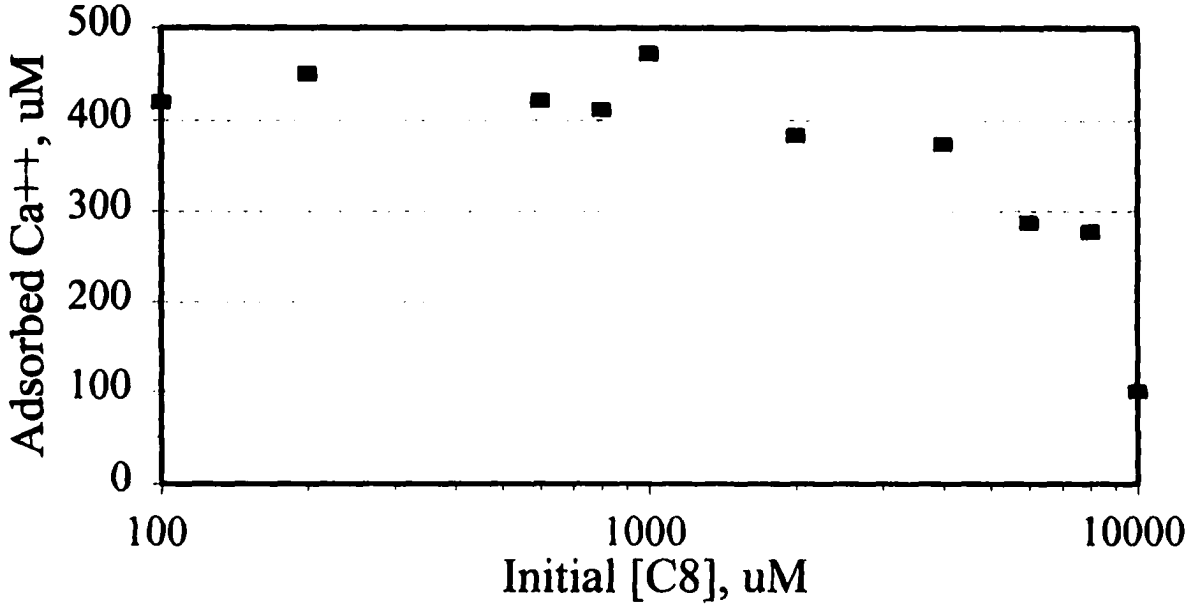

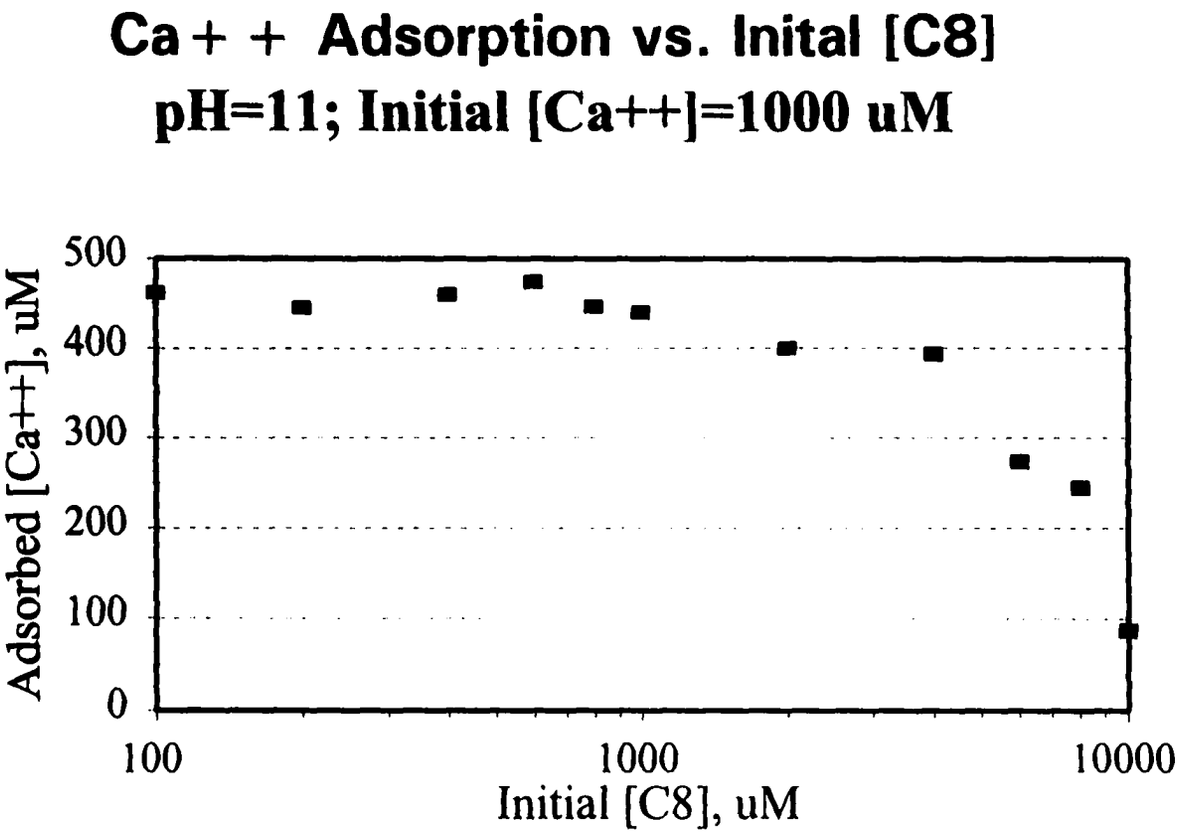
Ca + + Adsorption vs. Inital [C8]
pH=11; Initial [Ca++]=1000 uM
Adsorbed [Ca++], uM
500
400
300
200
100
0
100
1000
10000
Initial [C8], uM

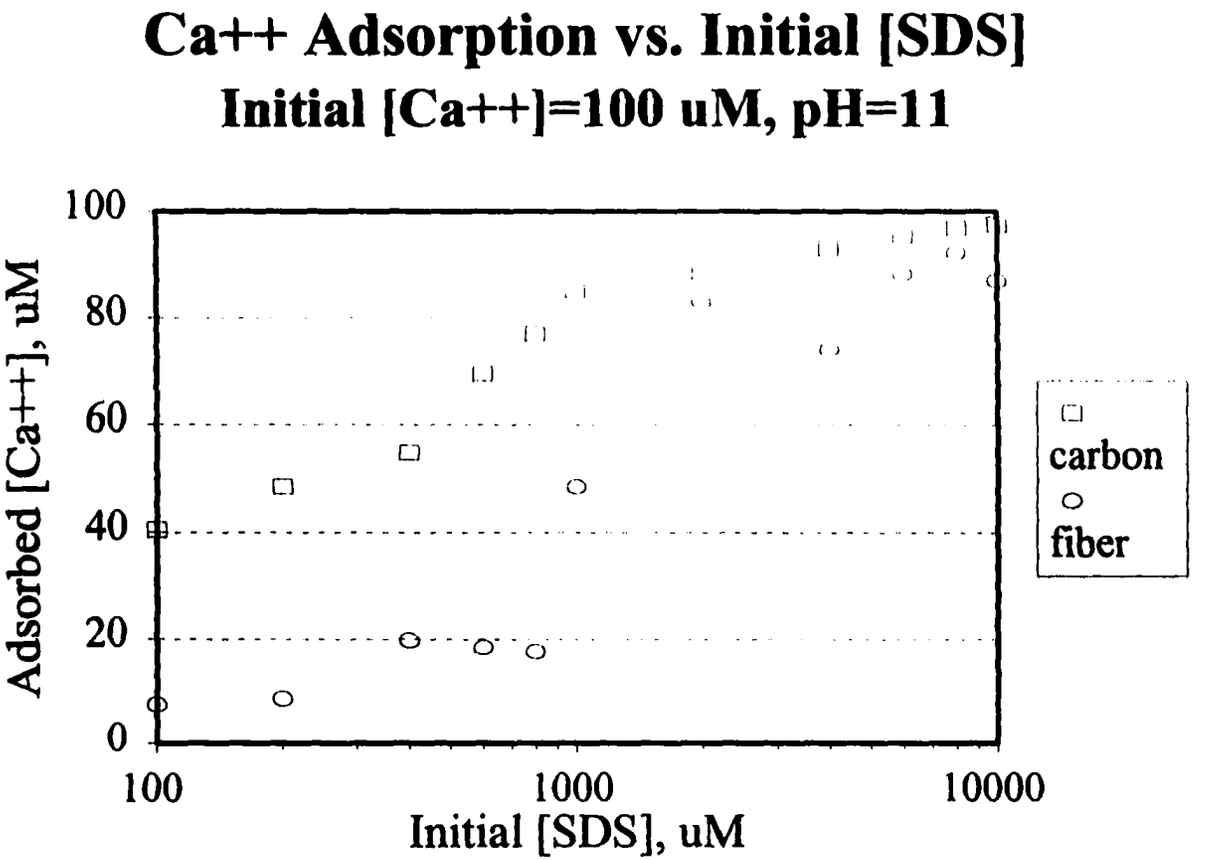
Ca++ Adsorption vs. Initial [SDS]
Initial [Ca++]=100 uM, pH=11
Adsorbed [Ca++], uM
100
80
60
40
20
0
100
1000
10000
Initial [SDS], uM
carbon
fiber

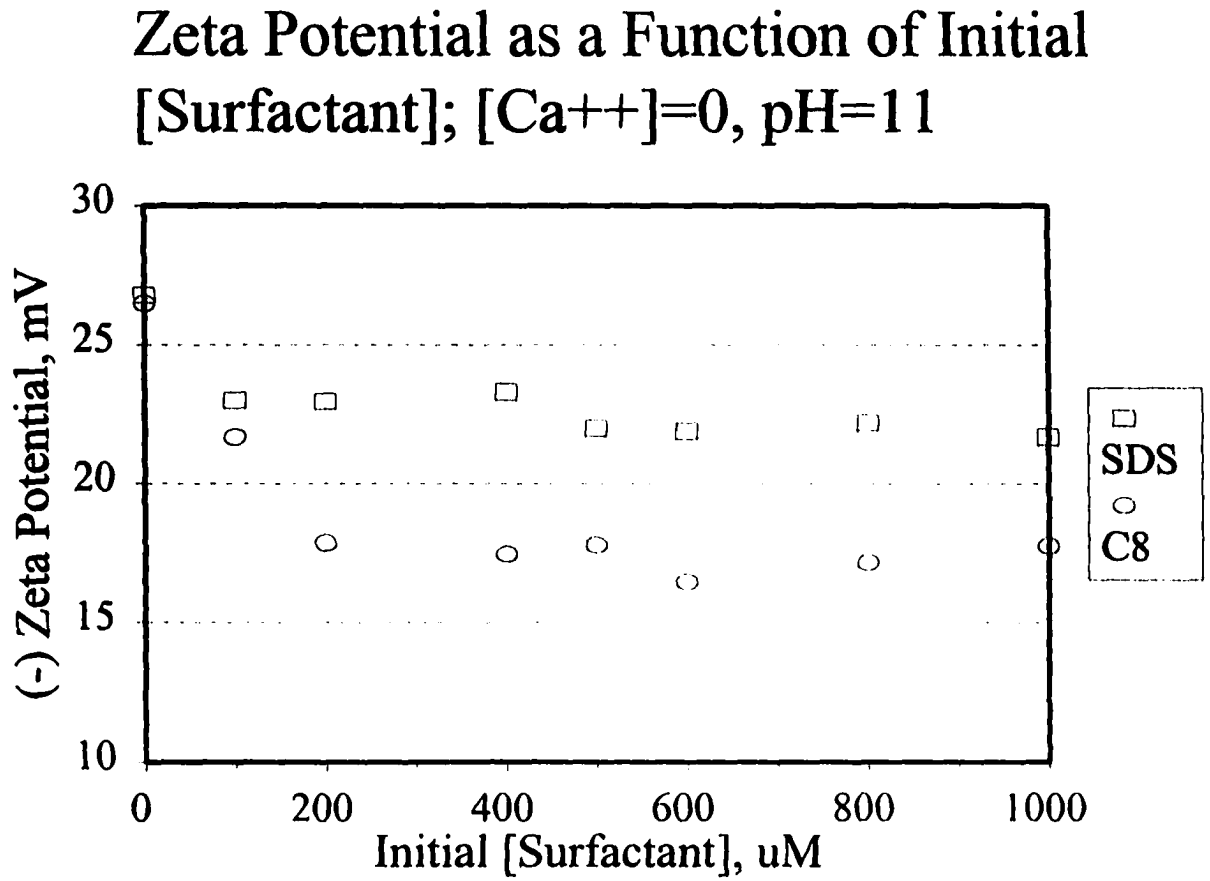
Zeta Potential as a Function of Initial [Surfactant]; [Ca++]=0, pH=11
(-) Zeta Potential, mV
30
25
20
15
10
0
200
400
600
800
1000
Initial [Surfactant], uM
SDS
C8

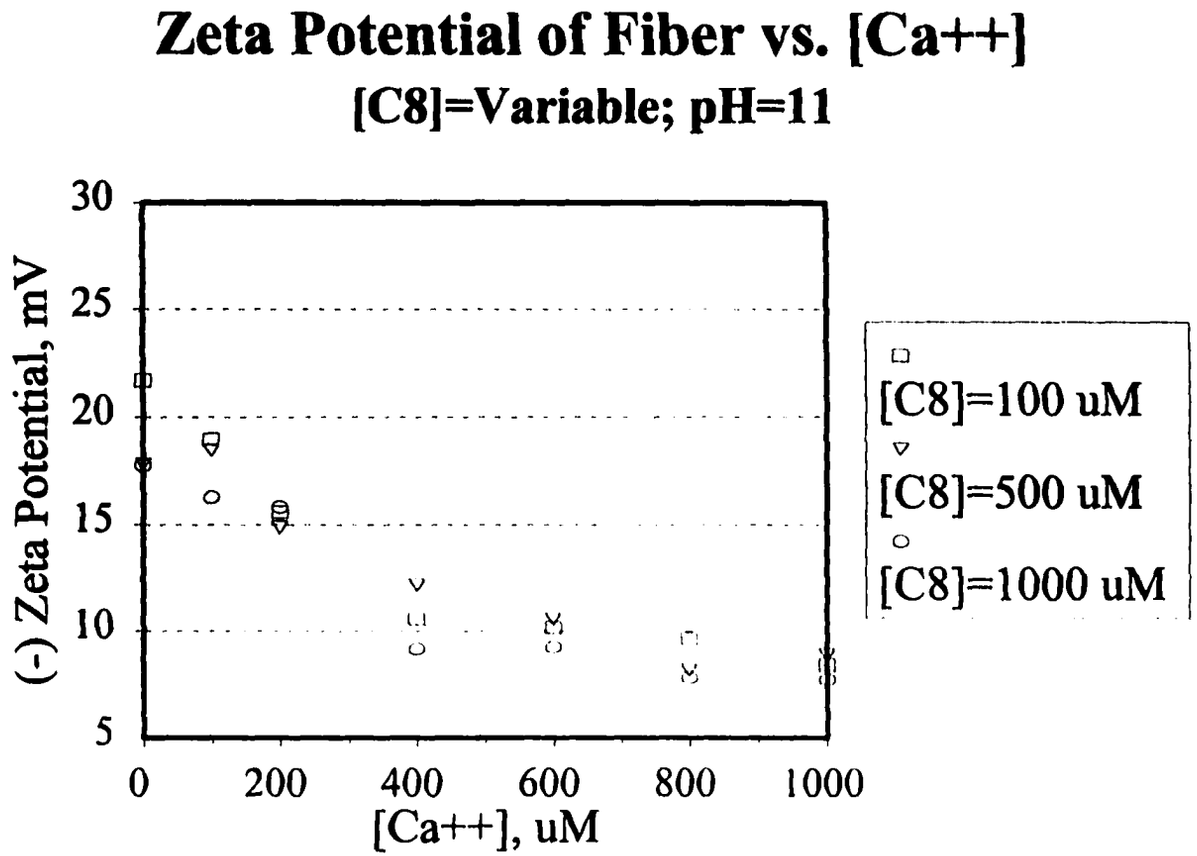
Zeta Potential of Fiber vs. [Ca++]
[C8]=Variable; pH=11
(-) Zeta Potential, mV
30
25
20
15
10
5
0
200
400
600
800
1000
[Ca++], uM
[C8]=100 uM
[C8]=500 uM
[C8]=1000 uM

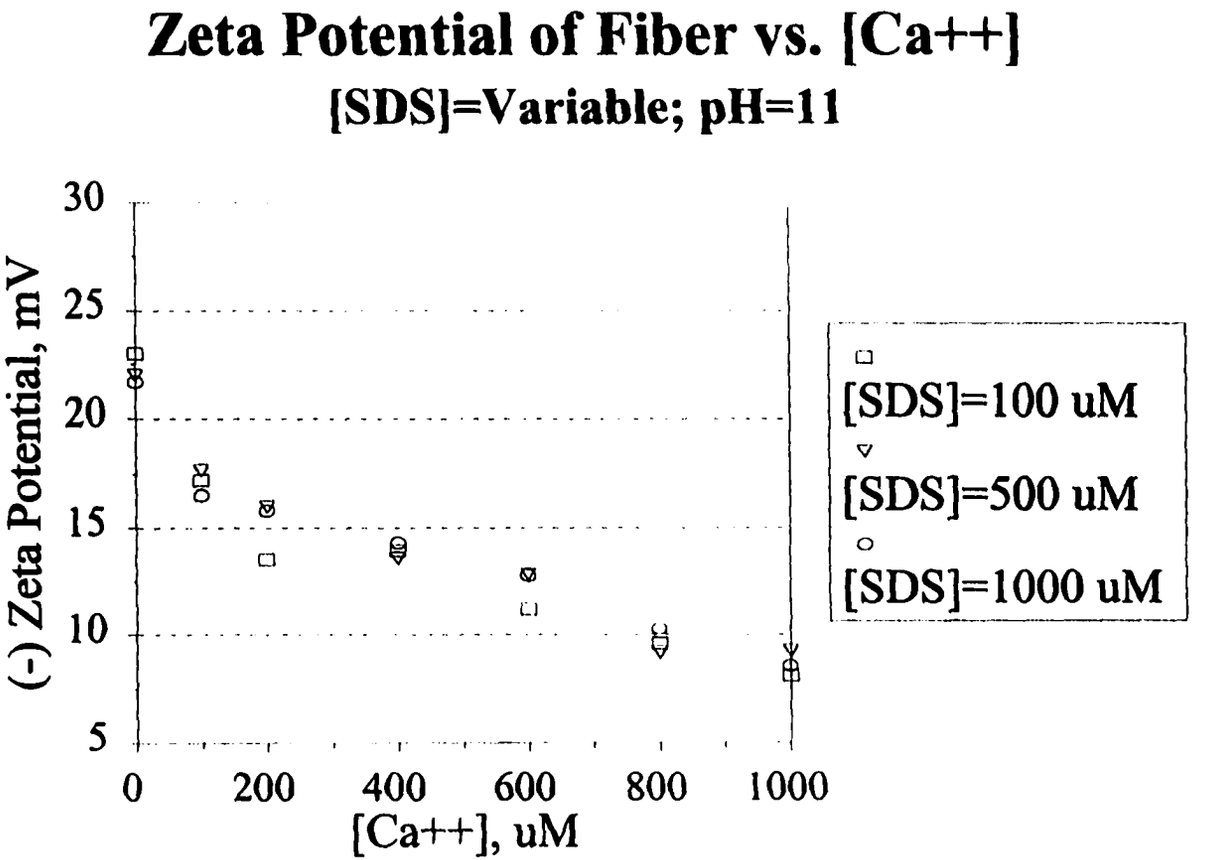
Zeta Potential of Fiber vs. [Ca++]
[SDS]=Variable; pH=11
(-) Zeta Potential, mV
30
25
20
15
10
5
0
200
400
600
800
1000
[Ca++], uM
[SDS]=100 uM
[SDS]=500 uM
[SDS]=1000 uM

Carbon and Fiber Flotation vs. [C8]
pH=11

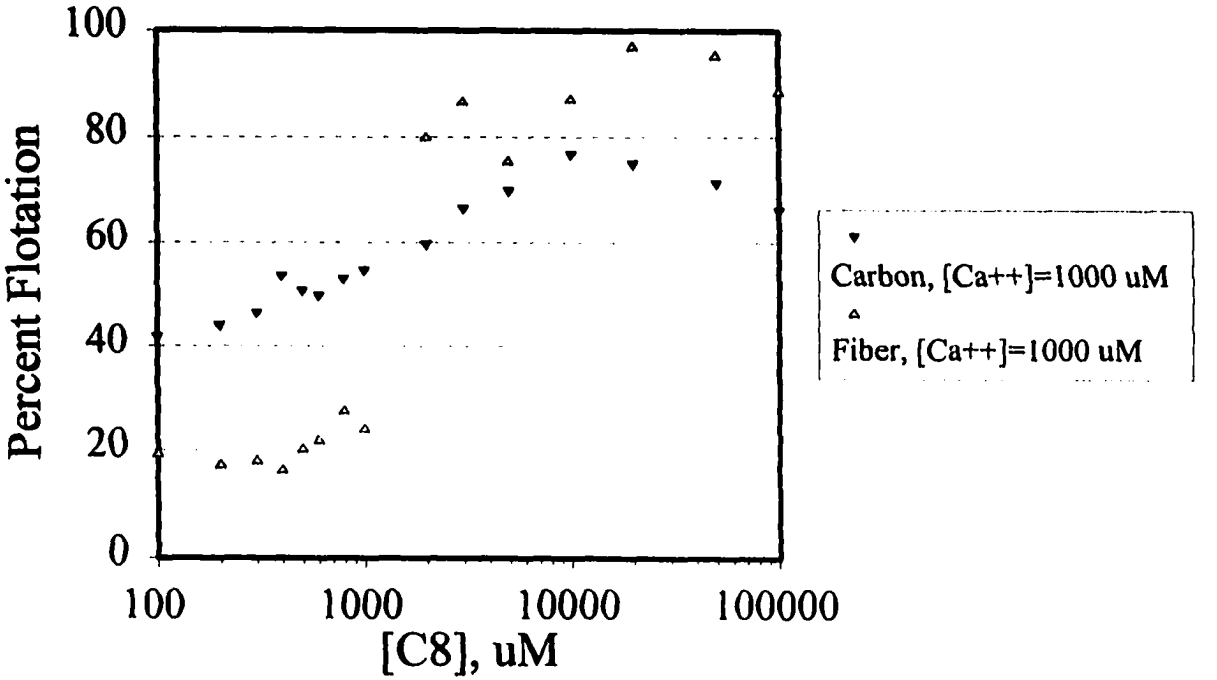

Carbon and Fiber Flotation vs. [SDS], pH=11

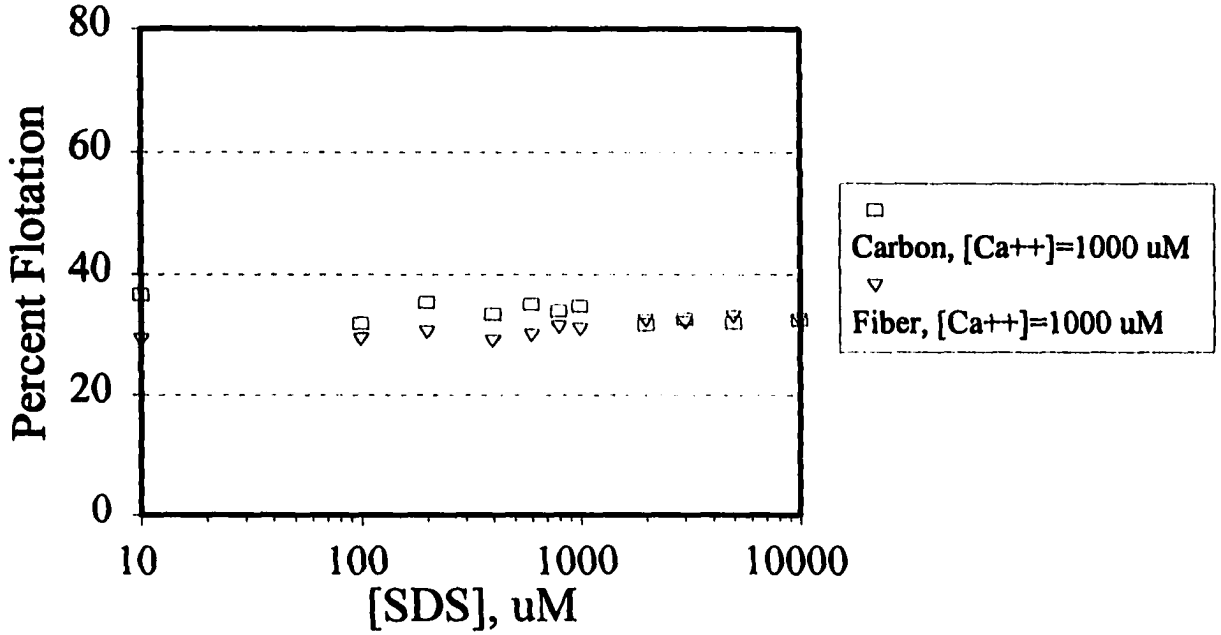

Carbon and Fiber Flotation vs. [SDS], pH=9

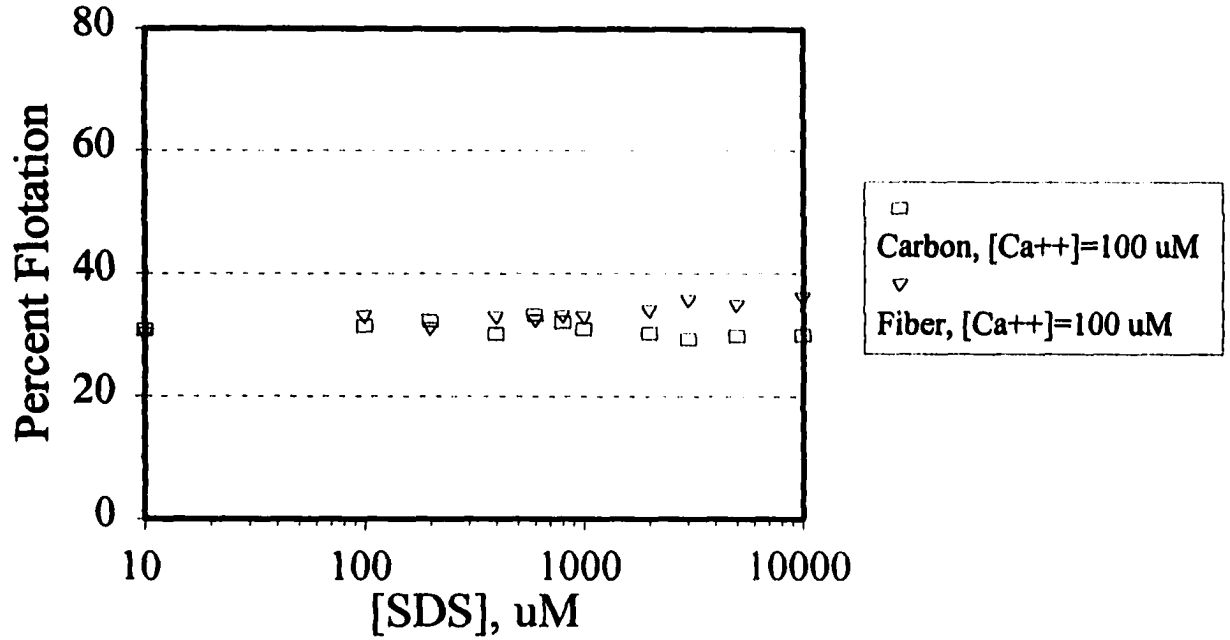

Carbon and Fiber Flotation vs. [SDS], pH=11

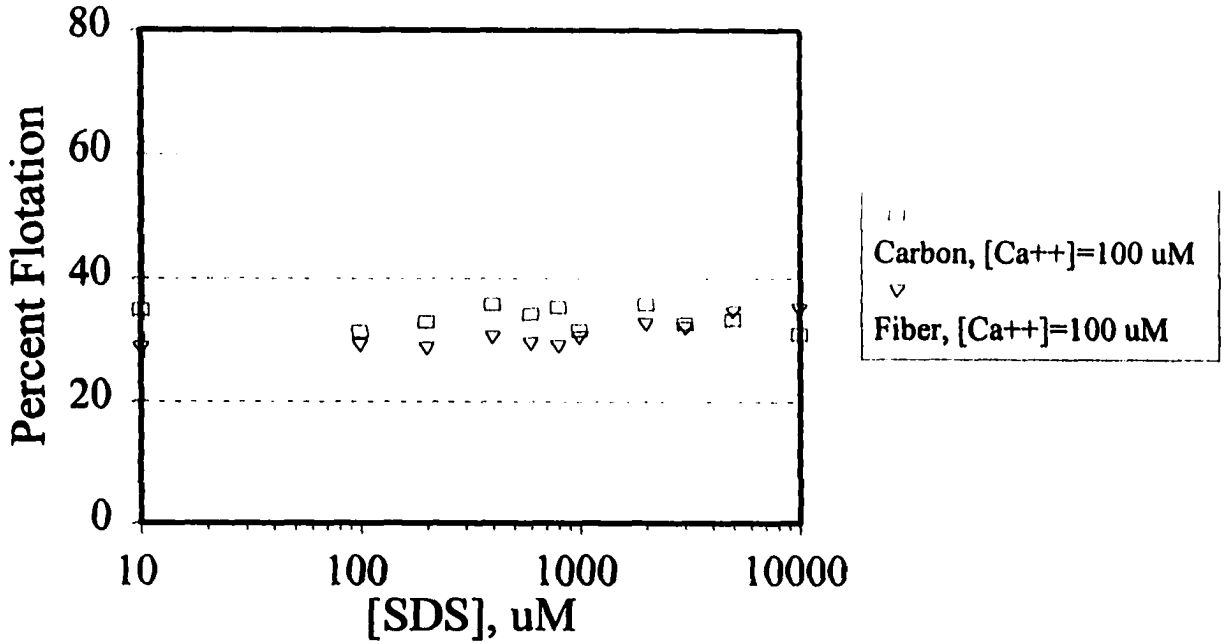

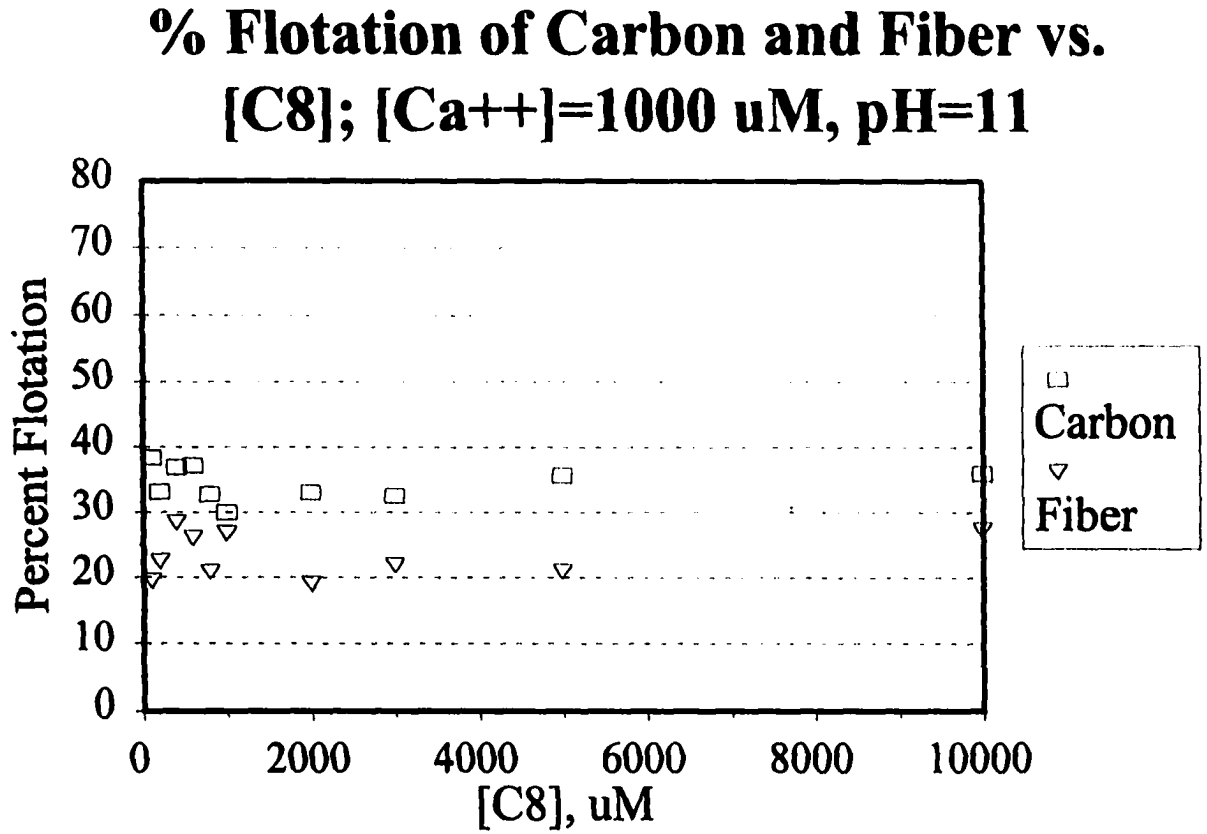
% Flotation of Carbon and Fiber vs. [C8]; [Ca++]=1000 uM, pH=11
Percent Flotation
80
70
60
50
40
30
20
10
0
0
2000
4000
6000
8000
10000
[C8], uM
Carbon
Fiber

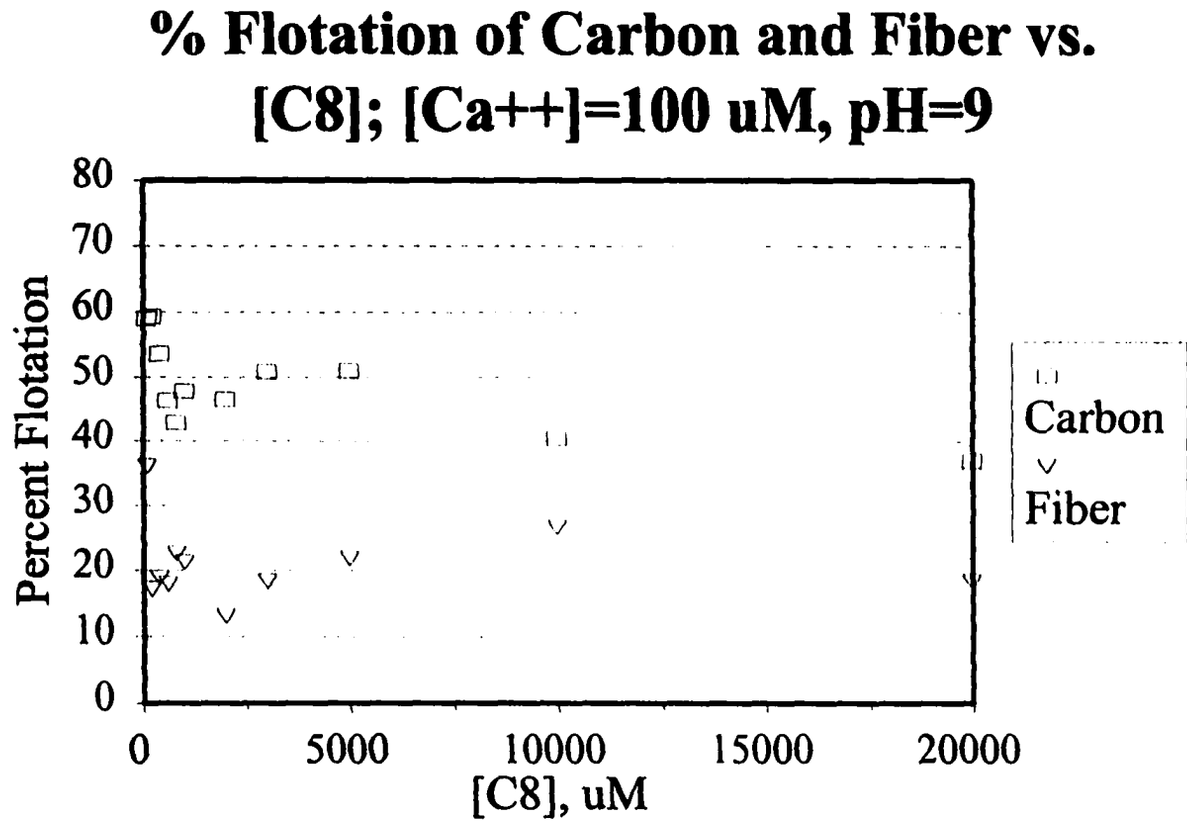
% Flotation of Carbon and Fiber vs. [C8]; [Ca++]=100 uM, pH=9
Percent Flotation
80
70
60
50
40
30
20
10
0
0
5000
10000
15000
20000
[C8], uM
Carbon
Fiber

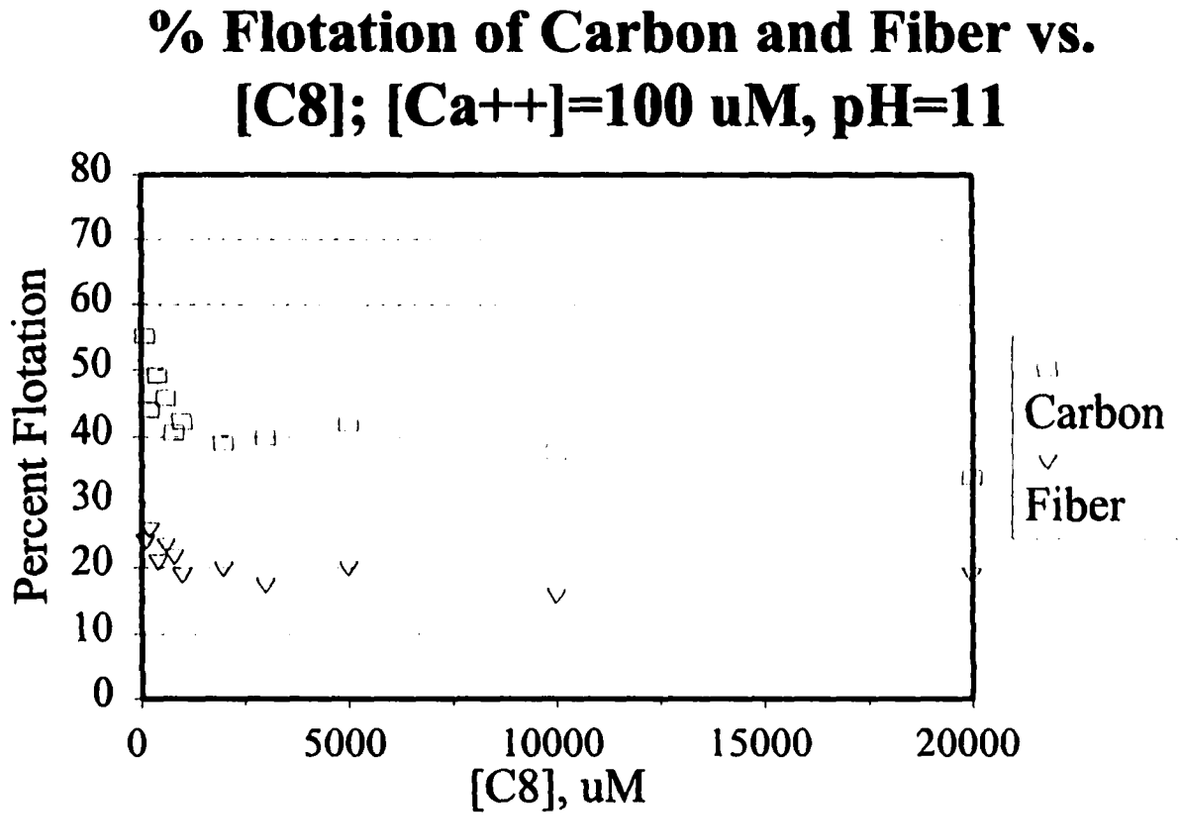
% Flotation of Carbon and Fiber vs. [C8]; [Ca++]=100 uM, pH=11
Percent Flotation
80
70
60
50
40
30
20
10
0
0
5000
10000
15000
20000
[C8], uM
Carbon
Fiber

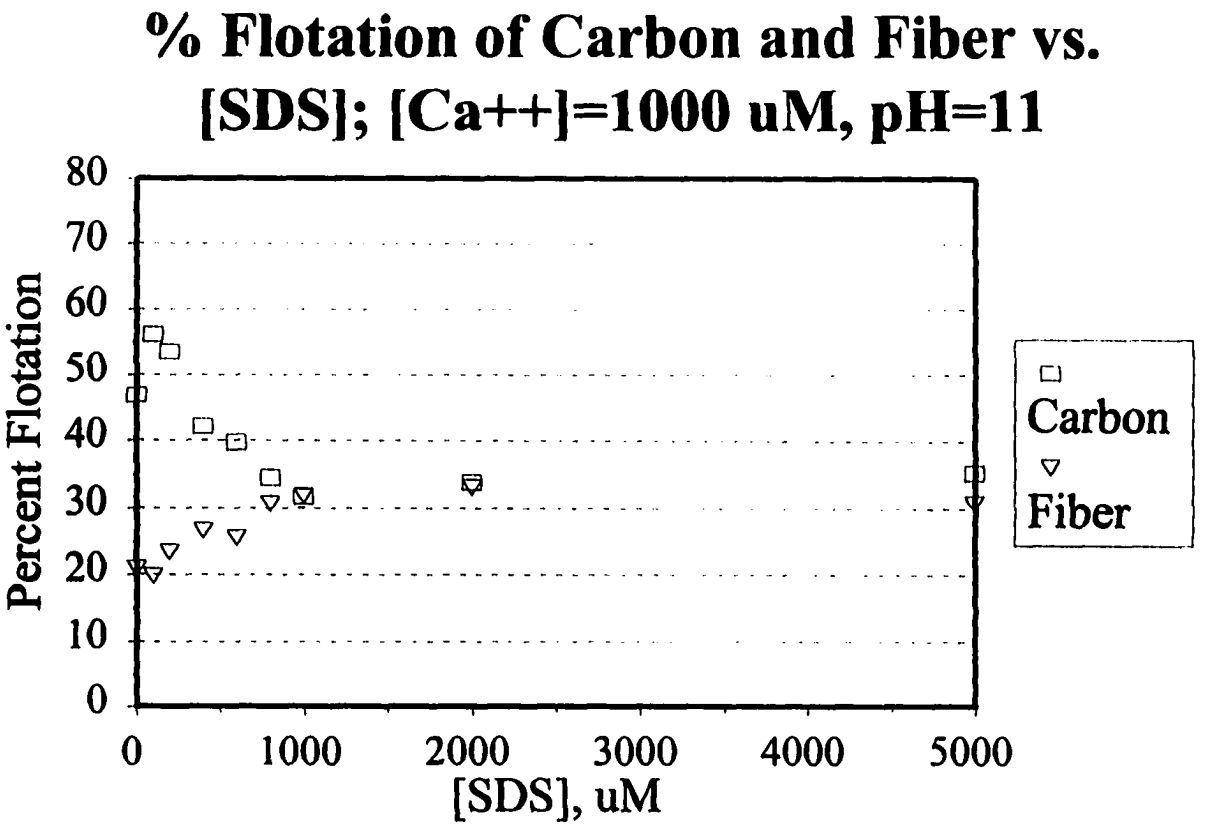
% Flotation of Carbon and Fiber vs. [SDS]; [Ca++]=1000 uM, pH=11
Percent Flotation
80
70
60
50
40
30
20
10
0
0
1000
2000
3000
4000
5000
[SDS], uM
Carbon
Fiber

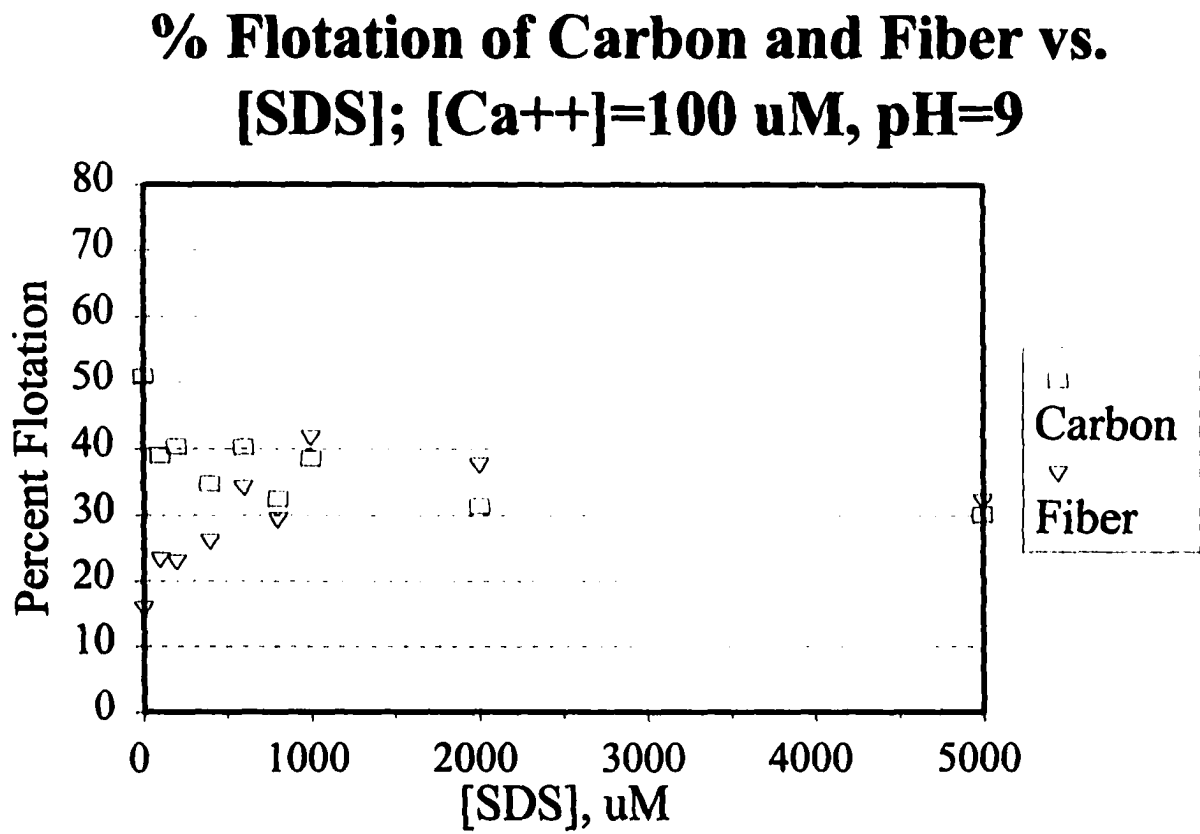
% Flotation of Carbon and Fiber vs. [SDS]; [Ca++]=100 uM, pH=9
Percent Flotation
80
70
60
50
40
30
20
10
0
0
1000
2000
3000
4000
5000
[SDS], uM
Carbon
Fiber

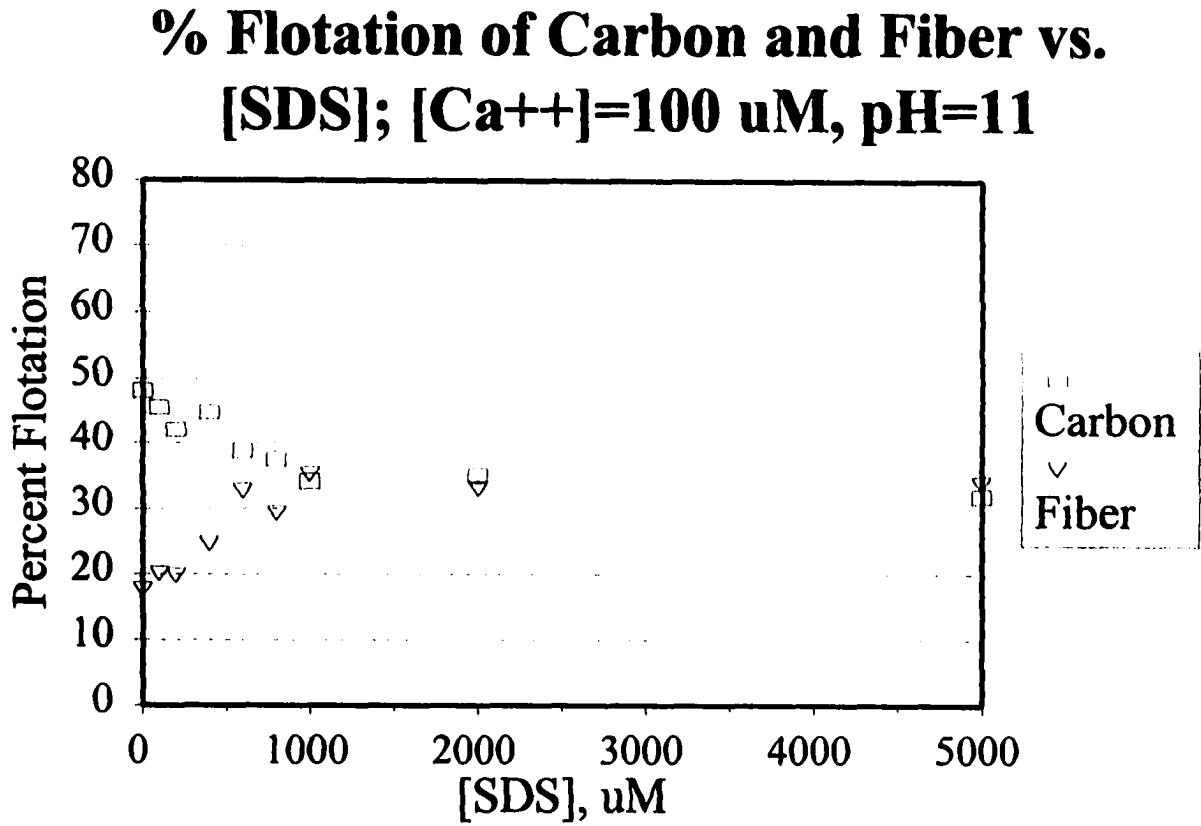
% Flotation of Carbon and Fiber vs. [SDS]; [Ca++]=100 uM, pH=11
Percent Flotation
80
70
60
50
40
30
20
10
0
0
1000
2000
3000
4000
5000
[SDS], uM
Carbon
Fiber